ANALYSIS OF DRUG RESISTANCE AND THE ROLE OF THE STEM CELL NICHE IN LEUKAEMIA

EMYR YOSEF BAKKER

Biomedical Research Centre, School of Environment and Life Sciences
University of Salford, Salford, M5 4WT.

Submitted in Partial Fulfilment of the Requirements for the Degree of
Doctor of Philosophy, 2017.

Table of Contents

List of Tables

List of Figures

Acknowledgments

Declaration

This thesis represents approximately three and a half years of research for the award of the degree of Doctor of Philosophy, commencing in October 2013 and funded by a Graduate Teaching Studentship from the University of Salford. Results within this thesis have been published in conference proceedings over the course of the PhD, and also now are utilised as part of papers that have been published or submitted to peer-reviewed journals. No portion of this thesis has been used as part of a submission for another qualification at Salford University or any other institution.

Although the author carried out the majority of experiments and analysis for the results of this thesis, part of the work is as a result of collaboration with a former PhD student colleague, Dr Malak Qattan (King Saud University, Saudi Arabia). The immunoblot results in Figure 3.3.1 (Page 109) are the work of the author, whilst the densitometric analyses presented in Figure 3.3.2 (Page 110), Figure 3.3.3 (Page 111) and Figure 3.3.4 (Page 113) are a result of combining densitometric analysis of immunoblot data generated by the author of this thesis with densitometric analysis (performed by the author) on immunoblot data generated by Dr Qattan. Similarly, the immunoblotting data shown in Figure 3.4.3 (Page 116) were all the work of the author, but the densitometric analyses in Figure 3.4.5 (Page 118) and Figure 3.4.6 (Page 119) are a result of combining densitometric analysis of immunoblot data generated by the author of this thesis with densitometric analysis (performed by the author) on immunoblot data generated by Dr Qattan.

Lastly, the flow cytometry data presented in Figure 3.7.2 (Page 134) represents the combined work of experiments carried out both by the author and Dr Qattan, with data being pooled to get the most representative effect. These experiments have been included as part of a publication in PLOS ONE, for which the author and Dr Qattan are equal-contributing co-first authors (Qattan et al., 2017). Thus, for the sake of consistency between the paper and this thesis the densitometric data for the figures stated previously and flow cytometry data for Figure 3.7.2 represent pooling of the data generated by the author of this thesis and Dr Qattan.

List of Abbreviations

11beta-HSD	11β-HydroxySteroid Dehydrogenase
ABCA1	ATP Binding Cassette Subfamily A Member 1
ACTH	Adrenocorticotropic Hormone
AF-1	Activation Function 1
AFP	Alpha Fetoprotein
ALL	Acute Lymphoblastic Leukaemia
AML	Acute Myelogenous Leukaemia
ATG5	Autophagy Protein 5
ATG7	Autophagy Protein 7
AP-1	Activator Protein 1
APAF-1	Apoptotic Protease Activating Factor 1
APS	Ammonium Persulfate
AR	Androgen Receptor
ARHGAP35	Rho GTPase Activating Protein 35
BAG1	BCL2 Associated Athanogene 1
BAX	BCL2 Associated X, apoptosis regulator
BCL2L11	BCL-2-Like Protein 11
BECN1	Beclin-1
BID	BH3 Interacting-Domain death agonist
BIRC3	Baculoviral IAP Repeat-Containing Protein 3
BMF	Bcl2 Modifying Factor
CAD	Caspase-Activated DNase
CASP8	Caspase-8
CD2	CD2 Molecule
CD40LG	CD40 Ligand
CFLAR	CASP8 and FADD-Like Apoptosis Regulator
ChIP	Chromatin Immunoprecipitation
CLL	Chronic Lymphocytic Leukaemia
CM	Conditioned Media
CML	Chronic Myelogenous Leukaemia

CNA	CellNetAnalyzer
COPASI	COmplex PAthway SImulator
CPN	Coloured Petri Nets
CREB1	cAMP Responsive Element Binding Protein 1
CREBBP/EP300	CREB Binding Protein/E1A Binding Protein P300
CRH	Corticotropin-Releasing Hormone
CXCL12	Chemokine (C-X-C motif) Ligand 12)
DAP3	Death Associated Protein 3
DAXX	Death Domain Associated Protein
DBD	Deoxyribonucleic Acid (DNA) Binding Domain
DCC-FBS	Dextran-Coated Charcoal Treated Foetal Bovine Serum
DMSO	Dimethyl Sulphoxide
DNA	Deoxyribonucleic Acid
EDTA	Diaminoethanetetra-Acetic Acid Disodium Salt
EGTA	Ethylene Glycol-Bis(B-Aminoethyl Ether)-N,N,N',N'-Tetraacetic Acid
ERα	Oestrogen Receptor Alpha
ERβ	Oestrogen Receptor Beta
FACS	Fluorescence Activated Cell Sorting
FADD	Fas-Associated protein with Death Domain
FasL	FAS Ligand
FasR	FAS Receptor
FBS	Foetal Bovine Serum
FSCN1	Fascin Actin-Bundling Protein 1
GC	Glucocorticoid
GEB052	Glucocorticoid Receptor Model By Emyr Bakker, Consisting Of 52 Nodes
GEO	Gene Expression Omnibus
GILZ	Glucocorticoid-Induced Leucine Zipper
GLUL	Glutamate-Ammonia Ligase
GO	Gene Ontology
GR	Glucocorticoid Receptor

GRE	Glucocorticoid Response Element
GRU	Glucocorticoid Response Unit
HAT	Histone Acetyletransferase
HDAC	Histone Deacetylase
HDAC1	Histone Deacetylase 1
HDAC6	Histone Deacetylase 6
HPA	Hypothalamic-Pituitary-Adrenal
HSC	Haematopoietic Stem Cell
HSLB	High Salt Lysis Buffer
HSP70	Heat Shock Protein 70
HSP90	Heat Shock Protein 90
IAP	Inhibitor of Apoptosis
IL10	Interleukin 10
IL6	Interleukin 6
IP	Immunoprecipitation
JNK	C-Jun N-Terminal Kinase
kDa	Kilodaltons
LBD	Ligand Binding Domain
LC3	Microtubule-associated protein Light Chain 3
LIF	Leukaemia Inhibitory Factor
LSC	Leukaemic Stem Cell
LSSA	Logical Steady State Analysis
MAPK	Mitogen-Activated Protein Kinase
MED1	Mediator Complex Subunit 1
MLKL	Mixed Lineage Kinase Domain Like Pseudokinase
MOMP	Mitochondrial Outer Membrane Permeabilisation
MRD	Minimal Residual Disease
mRNA	Messenger RNA
MTOR	Mechanistic Target of Rapamycin
MTS	[3-(4,5-dimethylthiazol-2-yl)-5-(3-carboxymethoxyphenyl)-2-(4-sulfophenyl)-2H-tetrazolium, inner salt; MTS]
NCOA1	Nuclear Receptor Coactivator 1

NCOA2	Nuclear Receptor Coactivator 2
NCOA3	Nuclear Receptor Coactivator 3
NCOA6	Nuclear Receptor Coactivator 6
NCOR1	Nuclear Receptor Corepressor 1
NCOR2	Nuclear Receptor Corepressor 2
NFKB	Nuclear Factor Kappa-Light-Chain-Enhancer Of Activated B Cells
NF-κB	Nuclear Factor Kappa-Light-Chain-Enhancer Of Activated B Cells
nGRE	Negative Glucocorticoid Response Element
NLS	Nuclear Localisation Signal
NR1I3	Nuclear Receptor Subfamily 1 Group I Member 3
NR2F2	Nuclear Receptor Subfamily 2 Group F Member 2
NRIP1	Nuclear Receptor Interacting Protein 1
NTD	N-Terminal Domain
ODE	Ordinary Differential Equation
PBS	Phosphate Buffered Saline
PBST	Phosphate Buffered Saline + 0.1% Tween
PI	1µg/ml Protease Inhibitors (Leupeptin, Pepstin, And Aprotinin)
PI3KIII	Class III Phosphatidylinositol 3-Kinase
PIK3C2B	Phosphatidylinositol-4-Phosphate 3-Kinase Catalytic Subunit Type 2 Beta
PKA	Cyclic AMP-Dependent Protein Kinase
PML	Promyelocytic Leukemia Protein
PMS	Phenazine Methosulfate
PMSF	Phenylmethanesulfonyl Fluoride
POU2F1	Pou Class 2 Homeobox 1
POU2F2	Pou Class 2 Homeobox 2
PRKDC	Protein Kinase, Dna-Activated, Catalytic Polypeptide
PTGES3	Prostaglandin E Synthase 3
RIPK1	Receptor Interacting serine/threonine Kinase 1
RIPK3	Receptor Interacting serine/threonine Kinase 3

RMA	Robust Multi-Array Average
RNAP	RNA Polymerase
RPM	Revolutions Per Minute
S134	Serine 134
S203	Serine 203
S211	Serine 211
S226	Serine 226
S404	Serine 404
SCAP	SREBF Chaperone
SCF	Stem Cell Factor
SD	Standard Deviation
SDF1	Stromal cell-Derived Factor 1
SDS	Sodium Dodecyl Sulfate
SDS-PAGE	Sodium Dodecyl Sulfate Polyacrylamide Gel Electrophoresis
SEM	Standard Error Of The Mean
SGK1	Serum/Glucocorticoid Regulated Kinase 1
SMAD3	SMAD Family Member 3
SMARCA4	SWI/SNF Related, Matrix Associated, Actin Dependent Regulator Of Chromatin, Subfamily A, Member 4
STAT3	Signal Transducer And Activator Of Transcription 3
STAT5B	Signal Transducer And Activator Of Transcription 5B
STRING	Search Tool For The Retrieval Of Interacting Genes/Proteins
STSFA	Signal Transduction Score Flow Algorithm
SUMO	Small Ubiquitin-Like Modifier
TBP	TATA-Binding Protein
TBS	Tris Buffered Saline
T-GR	Total GR
TNF	Tumour Necrosis Factor
TP53	Tumor Protein p53
TRADD	TNF Receptor superfamily member 1A Associated via Death Domain
TSC22D3	TSC22 Domain Family Member 3

TSG101	Tumor Susceptibility 101
UBC	Ubiquitin C
USCS	University of California Santa Cruz

Abstract

Glucocorticoids and etoposide are used to treat acute lymphoblastic leukaemia (ALL) as they induce death in lymphoblasts through the glucocorticoid receptor (GR) and p53. However, glucocorticoid resistance, cell death mechanisms and the contribution of the bone marrow microenvironment to drug response/resistance all require investigation.

Using microenvironment-mimicking conditioned media (CM), dexamethasone (a synthetic glucocorticoid) and etoposide to treat glucocorticoid-sensitive (C7-14) and glucocorticoid-resistant (C1-15) cells, pathways by which the microenvironment exerts its chemoprotective effect have been investigated. CM reduced caspase-3/8 activation, downregulated RIPK1 (necroptotic marker), and limited chemotherapy-induced BECN1 downregulation, suggesting protective effects of CM. Glucocorticoids upregulated BIRC3 (which ubiquitinates RIPK1), whilst CM altered GR phosphorylation. GR occupancy was observed on the RIPK1, BECN1 and BIRC3 promoters and changed depending on its phosphorylation. High-molecular weight proteins reacting with the RIPK1 antibody increased with CM, and reduced following AT406 BIRC3 inhibitor treatment suggesting they represent ubiquitinated RIPK1. These results suggest mechanisms by which CM promotes survival, as well as indicating novel glucocorticoid-regulated pathways.

Complementing laboratory investigation is the construction of a Boolean model of the GR interaction network (GEB052, GR "interactome") containing 52 nodes (proteins, inputs/outputs) connected by 241 interactions. *In silico* mutations and analyses have generated predictions that were subsequently validated on a genome-wide scale via comparison to microarray data. GEB052 demonstrated high prediction accuracy, consistently achieving a better prediction rate than a randomised model. Quantitative algorithmic analysis via microarray superimposition has also been performed, and lastly the model has been preliminarily validated as a clinical tool via superimposition of patient microarray data and comparing model predictions to clinical data.

In summary, this thesis provides novel insight into the effects of the microenvironment, and identifies new glucocorticoid-regulated pathways. The GEB052 model of GR signalling represents the novel application of this modelling approach to GR research, and generates accurate predictions.

Chapter 1 Introduction

1.1   Introduction to Cancer

Healthy cells in the body have a variety of mechanisms in place to ensure that they do not replicate beyond a certain point, or continue to grow despite mutations that they may have acquired. Such fine control of cell numbers is obviously essential to the healthy functioning of an organism, and yet in diseases such as cancer this control is disrupted (Donley and Thayer, 2013). Cancer is a broad term that incorporates a variety of different diseases but they share similar features, including the description that cancer is uncontrolled cell growth. Cancerous cells are those that have bypassed normal cellular mechanisms controlling cell fate and thus divide much more rapidly than their healthy counterparts. In advanced cases of cancer, the tumour (cancerous cell mass) can spread to other parts of the body and form secondary tumours in a process known as metastasis (Bashyam, 2002).

The need to develop treatments for cancer, based both on humanitarian values as well as the impact of cancer to the economy, is self-evident. In 2014, there were 356,860 new cases of cancer across the UK whilst 163,444 individuals in the UK died from cancer in the same year. Incidence rates are also projected to increase by 2% between 2014 and 2035 (CRUK, 2015b). In 2012, worldwide, there were approximately 14 million new cases of cancer, and approximately 8.2 million cancer-related deaths in the same year (WHO, 2015).

In terms of the economic impact of cancer, it has been estimated that in 2008, cancer cost the economy approximately $895 billion. Importantly, this figure does not include the direct costs of treating cancer. It is thought that this economic impact is due to both premature death and disability, among other factors (ACS, 2010). Combined with the incidence and mortality statistics, there is an obvious need to improve therapeutics to improve clinical outcomes for the sake of patients and reduce the economical stain that cancer causes.

1.2   The Hallmarks of Cancer

Decades of research into different types of cancer has unveiled similar mechanisms of disease progression across different types of cancer. These common mechanisms that change healthy cell populations to cancerous cell populations have been referred to as the "hallmarks of cancer" and have been described in multiple papers (Hanahan and Weinberg, 2000; Hanahan and Weinberg, 2011). Initially, there were six hallmarks of cancer that were described: sustaining proliferative signalling; limitless replicative potential; evading growth suppressors; resisting cell death; sustained angiogenesis and tissue invasion and metastasis (Hanahan and Weinberg, 2000). Hanahan and Weinberg (2000) described these as "acquired characteristics", reflecting the idea that healthy cells will obtain these characteristics and thus develop into cancerous cells.

Although different cancers may all acquire the hallmarks of cancer, they may acquire these features in different ways. For example, sustaining proliferative signalling may be achieved through autonomous production of growth factor ligands, which cancer cells then respond to through their cognate receptor. As an alternative, it is possible that cancer cells could signal to healthy cells in the periphery and be supplied with growth factors in that way (Hanahan and Weinberg, 2011). Thus, although cancers may share the characteristic hallmarks, it is possible that they acquire them in a different way thus complicating treatment and options to reduce chemoresistance, as well as explaining the complexity behind understanding cancer development.

Genomic instability was also identified as an "enabling characteristic" of cancer progression (Hanahan and Weinberg, 2000). In reality mutation is a rare phenomenon and there are checkpoints in place (such as cell cycle checkpoints) to ensure that cells with mutations do not replicate – and yet the acquired hallmarks require some genetic mutation prior to their emergence. The amount of mutations required to accumulate the hallmarks of cancer would require a length of time that exceeds the normal human lifespan and thus pre-existing genomic instability facilities the acquisition of mutations that allow the hallmarks of cancer to be developed (Hanahan and Weinberg, 2000).

More than a decade after the first hallmarks of cancer paper, an update was released (Hanahan and Weinberg, 2011). Following new discoveries and an increased understanding of cancer aetiology, two additional acquired characteristics (described as "emerging hallmarks") and one additional enabling characteristic were described. The two additional acquired characteristics were the reprogramming of metabolic processes and evasion of the immune system. It is increasingly evident that cancer cells reprogram their metabolism to fuel their high proliferative rate and this appears to be as common to different cancers as the other six previously-established hallmarks.

Evasion of the immune system relates to the idea that the immune system can play a role in tumour suppression. It has been shown that tumour transplants from immunocompromised mice to immunocompetent mice were inefficient at forming secondary tumours, indicating a role for the immune system in tumour regulation (Hanahan and Weinberg, 2011). In cases where tumours from immunocompetent mice were transferred to immunocompromised mice, there was no loss of efficiency in the formation of secondary tumours (Hanahan and Weinberg, 2011). This provides further evidence for tumour regulation by the immune system. Furthermore, it has been hypothesised that evasion of immune surveillance is a mechanism by which leukaemia cells can survive (Bakker et al., 2016). Thus, the ability to evade immune detection is one that may also be a characteristic of cancer progression.

The additional enabling characteristic described in the second paper was classified as tumour-promoting inflammation. Although immune evasion is described as a hallmark of cancer, inflammation may be pro-tumourigenic; for example, the inflammatory response may supply the cancer cells with bioactive molecules, including factors such as anti-apoptotic signalling and enzymes that aid in angiogenesis (Hanahan and Weinberg, 2011).

The identification of common features across different cancers facilitates the development of novel therapeutics and thus is hugely important to study. The factors identified by Hanahan and Weinberg (Hanahan and Weinberg, 2000; Hanahan and

Weinberg, 2011) are useful in this regard, though it is of course important to study individual cancers and isolate the specifics of individual tumour types.

1.3   Types of Cancer and Types of Leukaemia

Although different cancers may share hallmarks of development and some clinical features, cancer is not one disease that occurs in different parts of the body but rather is a group of diseases that share similar properties. Further complicating the issue is that even for the same cancer, there can be both inter- and intra-tumoural heterogeneity, which makes it harder to both diagnose and successfully treat. Furthermore, because many different cell in the body could become cancerous, it has been estimated that there are over 200 different types of cancer (CRUK, 2015d).

Despite this, cancer may be classified based on its characteristics such as the origin point of the tumour: sarcomas (originating from supporting cells such as bone and fat); carcinomas (cellular lining of external and internal body surfaces); lymphomas/myeloma (lymph nodes and immune cells); leukaemia (immature blood cells that grow in the bone marrow and spread through the bloodstream in high numbers) and brain/spinal cord cancers (CRUK, 2014b). Detail regarding incidence rates of different cancer types within the UK can be seen in Figure 1.3.1:
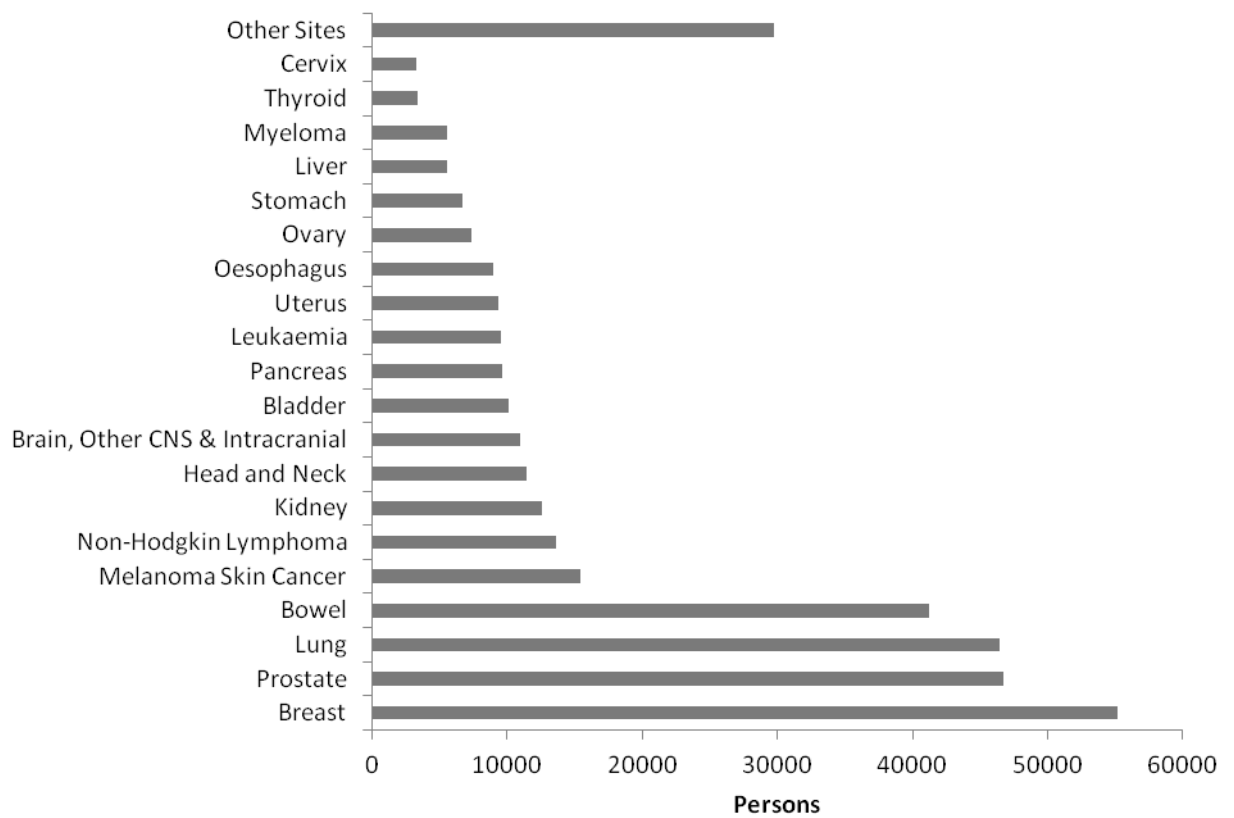
Figure 1.3.1: Incidence rates of different cancers.

Types of cancer are shown on the y-axis whilst the number of persons are shown on the x-axis. Adapted from Cancer Research UK (CRUK, 2016).

In addition to Figure 1.3.1 above, Figure 1.3.2 shows survival rates for different types of common cancers:
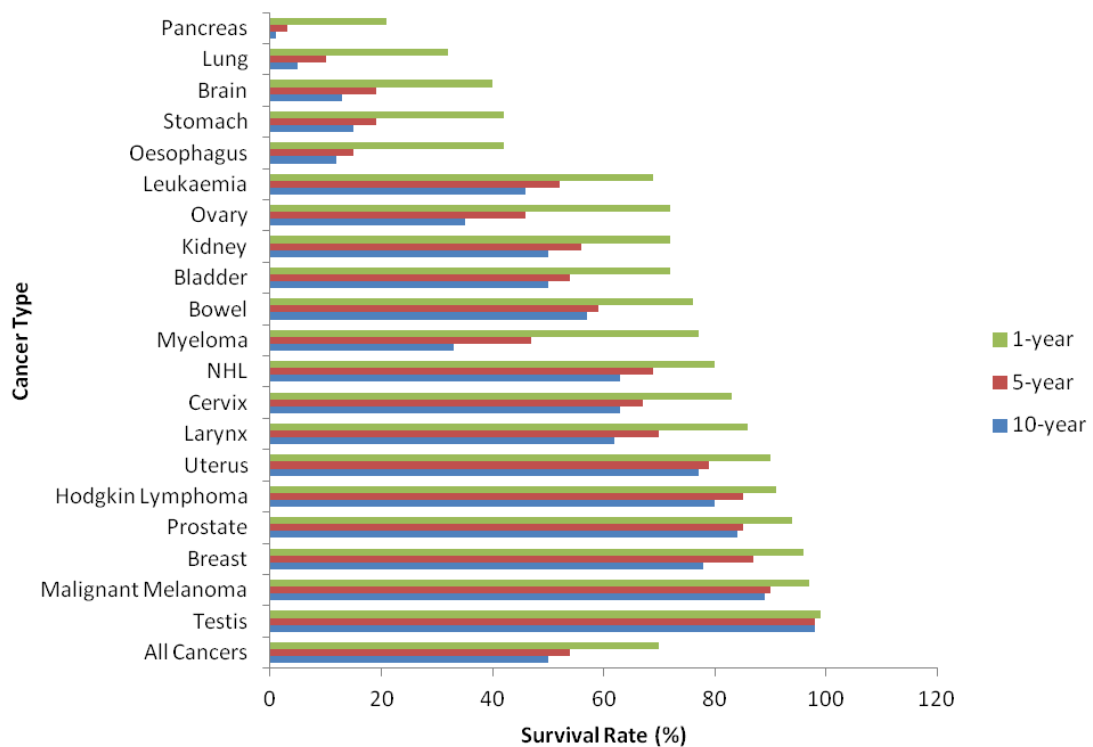
Figure 1.3.2: Survival rates for common cancers at one, five, and ten years.

Cancer types are shown on the y-axis whilst the survival rate is shown on the x-axis. Green, red and blue bars indicate one, five and ten-year survival respectively. Adapted from Cancer Research UK (CRUK, 2014a).

As is clear from Figure 1.3.2, cancer mortality is still an issue. Projected ten-year survival for all cancer types is only 50%, indicating an urgent need to develop novel therapeutics and uncover the mechanisms behind cancer development.

Although there are broad different types of cancer listed above in Figure 1.3.1 and Figure 1.3.2, within each type there are multiple sub-types and classifications within one type of cancer. With regard to leukaemia, it can be split into two broad classifications: acute and chronic. Acute leukaemia develops very quickly, and requires immediate treatment (ASH, 2008; Hoffbrand and Moss, 2011). On the other hand, chronic leukaemia develops much more slowly, can be asymptomatic for a great length of time, for months or even years (CRUK, 2015a).

Leukaemia can be further classified depending on the cell type from which the cancer originates. Leukaemia may thus be classified into one of four broad types: chronic lymphocytic leukaemia; chronic myelogenous leukaemia; acute lymphocytic leukaemia and acute myelogenous leukaemia. Myelogenous leukaemia refers to cancer of cells that will develop into blood cells such as erythrocytes and platelets, whilst lymphocytic leukaemia refers to cancer originating from cells that will become lymphocytes (ASH, 2008; Hoffbrand and Moss, 2011).

1.4   Acute Lymphoblastic Leukaemia

Acute lymphoblastic leukaemia (ALL) is the most common form of childhood cancer (Cardoso et al., 2008; NCI, 2016b). As a cancer of lymphoblasts, immature immune cells, ALL may be of either early pre-B, pre-B-, B-cell or T-cell origin (Pui et al., 1990) with approximately 15% being T-ALL (Cardoso et al., 2008). Although paediatric patients with T-ALL generally have a poorer prognosis than the B-ALL counterparts, this difference can be corrected for by appropriately intensive treatment (NCI, 2016a; Pui et al., 1990).

There are approximately four hundred diagnoses of paediatric ALL per year in the UK, and half of these diagnoses occur in children under five (Macmillan, 2016). Boys are affected at a slightly higher rate than girls, and the peak age of incidence for paediatric ALL is between 2-5 years old (Swensen et al., 1997). Symptoms of the disease include: pale skin; general fatigue and bone and joint pain; feeling breathless; repeated infections; weight loss; abdominal pain (due to a swollen liver or spleen); easily bruised skin; high temperature; night sweats and unusual, frequent bleeding (such as nosebleeds) (NHS, 2016). In cases of disease spread to the central nervous system, additional symptoms can include dizziness, vomiting, blurred vision, seizures and headaches (NHS, 2016).

The exact aetiology and underpinnings of ALL development remains unclear, despite decades of research (Wiemels, 2012). Despite this, several factors have been implicated as a risk factor for ALL development, such as exposure to household chemicals; one

analysis found that ALL susceptibility may be linked to the use of solvents in paints (Freedman et al., 2001). Other environmental factors such as birth order in families and whether or not the child attends day-care have also been implicated (Chang et al., 2011). Day-care attendance is thought to decrease the probability of developing ALL through early exposure to common infectious agents. Risk factors that have been demonstrated for other cancer types such as ionising radiation and parental smoking have been identified for ALL (Wiemels, 2012).

Unlike for other cancer types such as chronic myeloid leukaemia where there is a clear genetic causal factor, ALL has no such identified root cause. However, several genetic aberrations appear to occur at a higher rate in ALL patients than healthy individuals such as trisomy 21 (Watson et al., 1993) and translocations such as t(12;21) and t(9;22) which form the oncogenic fusion proteins *TEL/AML-1* and *BCR-ABL* respectively (Velders et al., 2001).

Curiously, there is a difference in the relative occurrence of different translocations between childhood and adulthood ALL; the Philadelphia chromosome (t(9;22)) is implicated in only 2-6% of childhood ALL cases, but approximately 25% of adult ALL cases (Velders et al., 2001). The opposite is true for the t(12;21) translocation; while present in only 2% of adult cases, it is present in 30% of childhood cases. These genetic differences between adult and paediatric cases of ALL could potentially provide a partial explanation for the different clinical outcomes that are observed between adult and child groups.

For children, ALL is one of the most survivable cancers, with a successful treatment rate of approximately 80%. Adults, however, have a much poorer prognosis, with only 30% cured; thus the difference between child and adult ALL in terms of prospects is substantial (Velders et al., 2001). This difference is potentially explained by the different trends in genetic mutations between adult and child cases, which in turn complicate the underlying aberrant molecular pathways, which may be altered both between adult and children, as well as inter- and intra-tumoural variation between individuals of the same group.

Treatment for ALL consists of multimodality therapy, with possible treatment options including approaches such as radiotherapy and chemotherapy. Radiotherapy employs the use of high-energy waves to induce cancer cell death and stop their growth, and may be used in conjunction with high-dosage chemotherapy in cases where ALL has metastasised to the brain and spinal cord, as chemotherapy is typically insufficient at reaching those areas (NCI, 2016b). However, radiotherapy in general is avoided where possible due to side-effects and the possibilities of long-term issues such as blindness (Margileth et al., 1977).

1.5   Chemotherapy for ALL

Chemotherapy treatment for ALL consists of a variety of drugs that are utilised in combination to exert an anti-cancer effect. Chemotherapy itself is of several phases: induction phase; consolidation phase; interim maintenance phase; delayed intensification phase; and maintenance phase (AboutKidsHealth, 2010; Cooper and Brown, 2015). Induction chemotherapy is the first stage of chemotherapeutic treatment and aims to eliminate cancerous lymphoblasts and induce remission. Multiple drugs are used at the induction phase such as asparaginase, vincristine, dexamethasone and methotrexate (Esterhay et al., 1982). Induction typically lasts 29 days, followed by a week of rest from chemotherapy (AboutKidsHealth, 2010).

Following induction, an MRD (minimal residual disease) test is carried out; if negative, then no lymphoblasts are detected. However, if the test is positive then leukaemic cells are detected, and the child is placed into either very-high or high-risk, and may receive a bone marrow transplant or undergo more intensive chemotherapy (AboutKidsHealth, 2010).

Consolidation is the second phase of chemotherapy, which is performed as there may still be circulating lymphoblasts that are undetectable by the MRD test. Consolidation typically lasts between four to eight weeks and the same drugs from the induction phase may be utilised, or other new drugs such as etoposide added (AboutKidsHealth, 2010;

Pinkerton et al., 1987). The third phase of chemotherapy, the interim maintenance phase, lasts for eight weeks and servers a similar function to the consolidation phase. Vincristine, mercaptopurine, as well as methotrexate are examples of drugs utilised at this stage.

The fourth stage of chemotherapy, delayed intensification phase, serves as another induction and consolidation phase and lasts for approximately eight weeks. Drugs such as vincristine are again utilised, but other drugs such as doxorubicin may also be prescribed. The final stage of chemotherapy, maintenance phase, lasts for two to three years, and is the point at which leukaemic cells are no longer detectable. Cancer cells may however still be present so this stage serves to prevent relapse (AboutKidsHealth, 2010).

1.6   Glucocorticoid Steroid Hormones

One key class of chemotherapy drugs utilised in the treatment of ALL are glucocorticoid steroid hormones (GCs), utilised both for their immunosuppressive and anti-inflammatory properties as well as their ability to induce apoptosis in lymphoid malignancies (Schmidt et al., 2004; Piovan et al., 2013). Glucocorticoids are one of the most important drugs for ALL therapy, and are included in virtually all chemotherapy regimens for lymphoid malignancies (Schmidt et al., 2004). Rather than the natural glucocorticoid cortisol, synthetic glucocorticoids such as prednisolone and dexamethasone are utilised, due to the fact that synthetic glucocorticoids are both more stable and more potent than their natural counterparts (Inaba and Pui, 2010; Mokra and Mokry, 2011). Glucocorticoid use in chemotherapy for ALL previously utilised primarily prednisolone, though dexamethasone has seen increasing use recently, potentially due to its ability to penetrate the central nervous system and longer half-life, as well as its higher potency (Inaba and Pui, 2010).
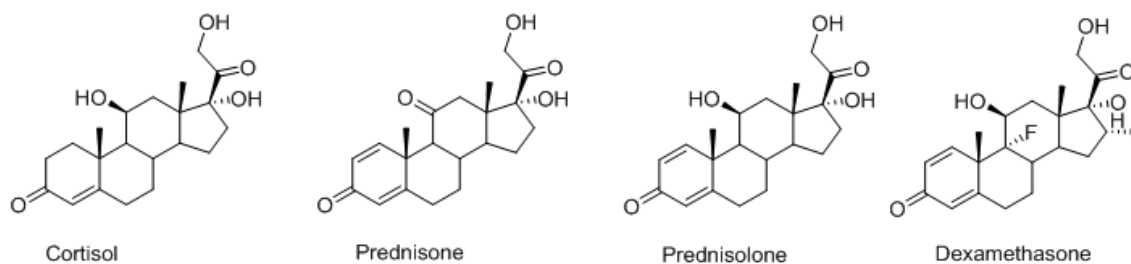
Figure 1.6.1: Chemical structures of various glucocorticoids.

Cortisol (far left) is the natural corticosteroid within the body, whilst prednisone (second left), prednisolone (first right) and dexamethasone (far right) are synthetic glucocorticoids with higher potency and stability than cortisol. Adapted from Inaba and Pui (2010).

Glucocorticoids are prescribed for their treatment of ALL for their ability to induce cell death in white blood cells, though as stated earlier this is not their sole role. Within healthy individuals glucocorticoids are involved in a variety of bodily functions such as metabolism, the stress response, and growth and development. The other main use of glucocorticoids clinically is their prescription as anti-inflammatory agents (Zhou and Cidlowski, 2005). A common problem with the use of glucocorticoids in the clinic is that due to their diverse range of effects in the body, they often have numerous side-effects in patients, such as weight gain (and potentially Cushing's syndrome), fragile skin (leading to easy bruising), impaired wound healing, cardiovascular problems and potentially even behavioural issues (Stanbury and Graham, 1998). For children, the two main side effects that are a cause for concern are suppression of the immune response (leading to infection) and suppression of growth (Deshmukh, 2007).

1.7   The Hypothalamic-Pituitary-Adrenal (HPA) Axis
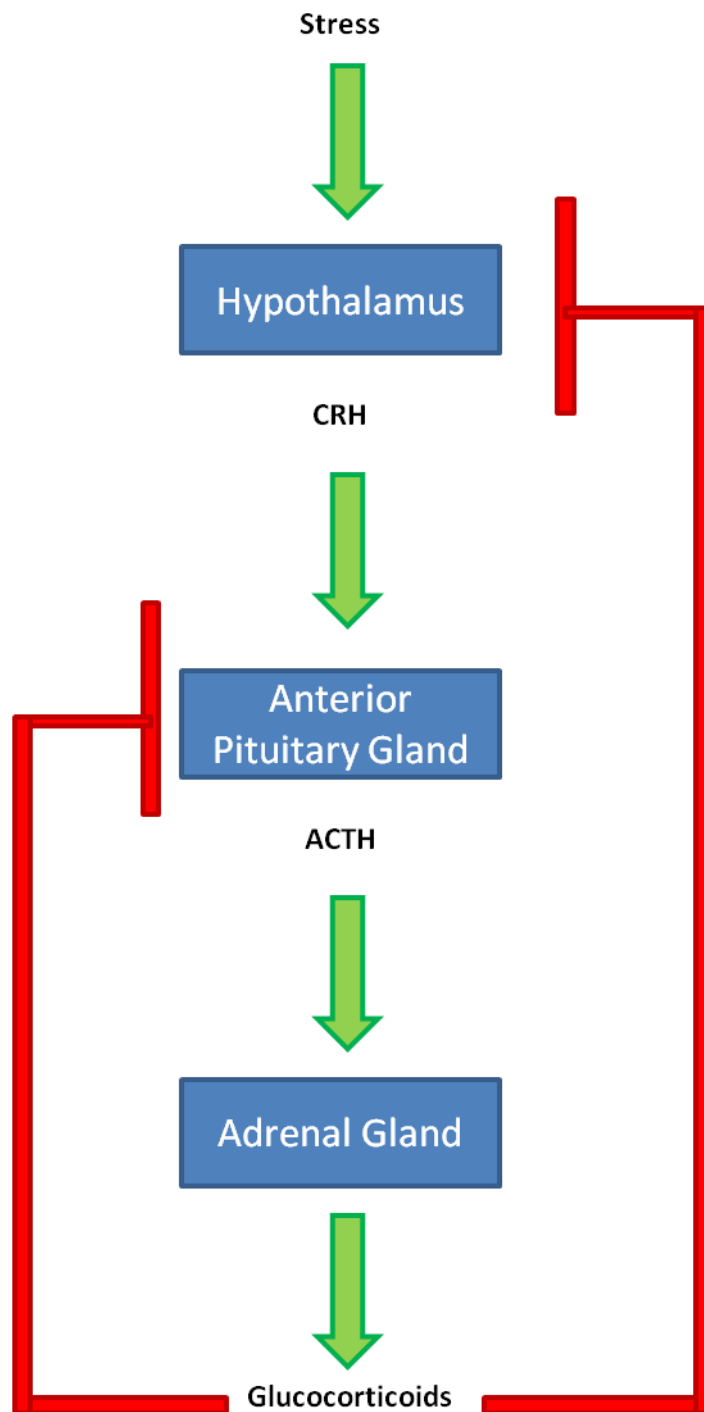
Figure 1.7.1: Schematic representation of the HPA axis.

In addition to circadian rhythm, stress triggers the release of corticotropin-releasing hormone (CRH) from the hypothalamus which promotes the release of adrenocorticotropic hormone (ACTH). ACTH in turn stimulates the adrenal gland to release glucocorticoids, which self-limit their own production through two negative feedback loops targeting both the anterior pituitary gland and the hypothalamus.

Glucocorticoid production in the body is controlled by the hypothalamic-pituitary-adrenal (HPA) axis within the body. As summarised in Figure 1.7.1, following a trigger such as a stress signal, corticotropin-releasing hormone (CRH) is released by the hypothalamus, which stimulates the pituitary gland to release adrenocorticotropic hormone (ACTH) (Kadmiel and Cidlowski, 2013). ACTH then travels through the blood to the adrenal gland and stimulates the release of cortisol from the zona fasciculata of the adrenal cortex (O'Connor et al., 2000). Cortisol then self-regulates its own production through two negative feedback loops targeting both the pituitary gland and the hypothalamus (Kadmiel and Cidlowski, 2013). Cortisol itself is the active form of the hormone, which is converted from inactive cortisone by 11β-Hydroxysteroid dehydrogenase (11beta-HSD). Two forms of 11beta-HSD exist, 11beta-HSD1 and 11beta-HSD2, the former of which converts cortisone to cortisol whilst the latter converts cortisol to inactive cortisone (Tomlinson and Stewart, 2001).

1.8   The Glucocorticoid Receptor

Regardless of whether the glucocorticoid in question is natural or synthetic, it is commonly accepted that most if not all of the actions of glucocorticoids are mediated through its intracellular receptor, the glucocorticoid receptor (GR) (Zhou and Cidlowski, 2005). The GR is a member of the steroid hormone receptor family (Khan et al., 2011) and a member of the nuclear receptor superfamily (Mangelsdorf et al., 1995).

The nuclear receptor superfamily is divided into four broad types based on dimerisation and DNA-binding properties. Steroid hormone receptors are Type I, and are ligand-dependent receptors that form homodimers and translocate from the cytoplasm to the nucleus following activation. Type II receptors include ligand-dependent receptors that are not steroid hormone receptors and are distinguished from Type I receptors by virtue of the fact that they reside in the nucleus bound to their DNA regions even in the absence of a ligand, in addition to the fact that they form heterodimers with retinoid X receptor. Type III nuclear receptors are similar to Type I except that their DNA response elements exhibit a different organisation (direct repeat instead of an inverted

repeat) whilst Type IV nuclear receptors bind as monomers to half-site response elements (Mangelsdorf et al., 1995; Sever and Glass, 2013)

As with other members of the nuclear receptor superfamily, and as detailed in Figure 1.8.1, the GR has features such as a central DNA-binding domain (DBD) consisting of two zinc fingers, and a ligand-binding domain (LBD) which controls hormone recognition and response selectivity (Mangelsdorf et al., 1995).
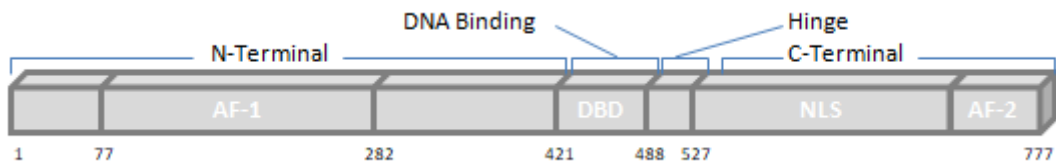
Figure 1.8.1: Structure and relative location of human GRα domains.
GR has numerous domains including the N-terminal domain, the DNA binding domain (DBD), and the C-terminal domain. The hinge region, nuclear localisation signal (NLS) and activation functions 1 and 2 (AF-1 and AF-2) are important determinants of GR activity. Adapted from Kadmiel and Cidlowski (2013).

The gene for the GR is located on chromosome five, more specifically 5q31-32 and the full-length GR protein is approximately 94 kilodaltons (kDa), consisting of several domains as detailed above in Figure 1.8.1 (Gehring et al., 1985; Quax et al., 2013; Japiassu et al., 2009). Domains for the GR include the N-terminal domain (NTD), the DNA-binding domain (DBD), the hinge region, and the C-terminal region, which contains the ligand-binding domain (LBD) (Zhou and Cidlowski, 2005).

The N-terminal region of the GR contains the AF-1 (activation function 1) region, which is important for the interaction of the GR with its cofactors (Kadmiel and Cidlowski, 2013). The N-terminal region also contains important sites for post-translational modifications such as phosphorylation which can have positive or negative effects on its activity depending on the site and type of modification (Oakley and Cidlowski, 2011).

The DBD of the GR allows it to interact with and bind to specific DNA sequences within genes called glucocorticoid response elements (GREs). The consensus GRE is a palindromic sequence consisting of two active half-sites (underlined): AGAACANNNTGTTCT (Del Monaco et al., 1997). However, because this is only a consensus sequence, the GR may regulate genes whose putative GREs do not closely match the consensus GRE (Le et al., 2005), and the GR may regulate genes without binding to a GRE, for example through the recruitment of cofactors or processes such as tethering (Teurich and Angel, 1995). This is expanded upon in the subsequent section "Mode of Action of Glucocorticoids" (Page 36).

The hinge region of the GR has been shown to play a role in GR dimerisation (Savory et al., 2001) and is located between DBD and LBD. The first nuclear localisation signal (NLS1) is located in the hinge region (Carrigan et al., 2007) and it has been suggested that the hinge region allows the GR to have structural flexibility, which allows a single GR protein to contact multiple GREs (Nicolaides et al., 2010).

As stated earlier, the C-terminus of the GR contains the ligand-binding domain, whose crystal structure contains twelve alpha helices and four beta sheets (Nicolaides et al., 2010). The LBD also contains a section activation function region (AF-2) and a second nuclear localisation signal (NLS2) (Duma et al., 2006). As the name implies, the LBD is crucial to the ligand-dependent response of the GR and plays a role in cofactor interaction (Nicolaides et al., 2010).

Alternative splicing of GR messenger RNA (mRNA) can lead to multiple protein isoforms of the protein, with the two most common being GRα (the classical GR) and GRβ (Duma et al., 2006). Though GRβ can exert a dominant-negative effect when overexpressed (Duma et al., 2006), it appears to be transcriptionally inactive (Oakley et al., 1999). Both of these effects may be due to its inability to bind to the GC hormone, and the dominant negative effect may also be due to the fact that GRα and GRβ can form heterodimers (Oakley et al., 1999). However, it has also been hypothesised that the dominant-negative effect of GRβ is explained through its competition to bind cofactors (Charmandari et al., 2005). An important point is that the ratio between GRα and GRβ

has been determined for different cell types, and this ratio is a key determinant of GR activity and hormone response (Schaaf and Cidlowski, 2002). GRγ, GR-A and GR-P are other splicing isoforms and each has been implicated in glucocorticoid resistance (Oakley and Cidlowski, 2011; Moalli et al., 1993). In addition to mRNA splicing forms leading to GR protein isoforms, alternative translation (use of different start codons) has also been identified for GR, leading to numerous forms in total. These alternatively translated GR proteins also play a role in glucocorticoid response (Lu and Cidlowski, 2005).

1.9   Mode of Action of Glucocorticoids
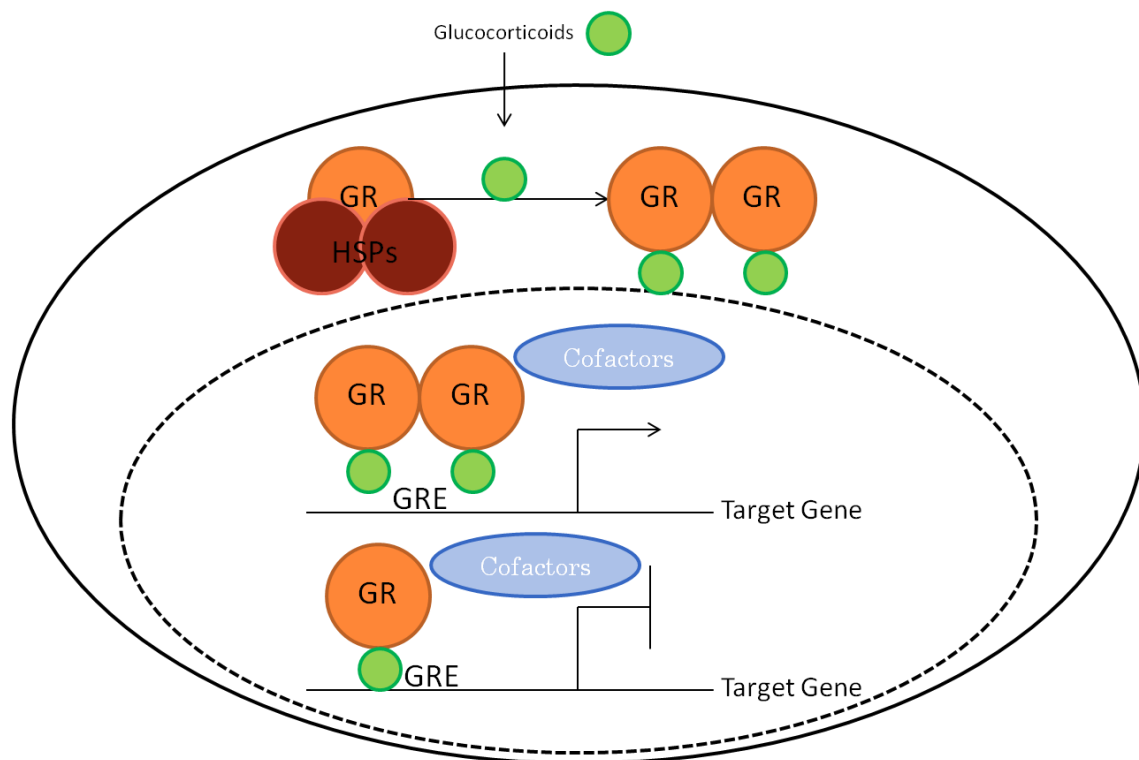
Figure 1.9.1: Classical mode of action of glucocorticoids.

The classical model for the activation of the glucocorticoid receptor (GR) is that in the absence of a ligand, the GR exists in the cytoplasm bound to chaperones such as heat-shock proteins (HSPs). Following ligand binding, these chaperones dissociate and, for transactivation, the GR would dimerise, translocate to the nucleus, and bind to a glucocorticoid response element (GRE) and facilitate target gene activation through the recruitment of cofactors. Transrepression under the classical model occurred via GR monomers.

A summary of the classical model for the control of the glucocorticoid receptor is summarised in Figure 1.9.1. The classical model states that in the absence of a ligand the GR is maintained in a stable state in the cytoplasm through interaction with chaperones such as heat-shock protein 90 (HSP90), heat-shock protein 70 (HSP70), PTGES3 (prostaglandin E synthase 3) and other chaperones. This complex stabilises the GR protein and prevents its degradation (Echeverría et al., 2009). Activation of the GR occurs following the entry of a glucocorticoid into the cell. It was originally hypothesised that ligand binding of the GC to the GR would cause dissociation of the chaperones such as HSP90, expose the nuclear localisation signal of the GR and cause its translocation into the nucleus, where it would affect its target genes (Vandevyver et al., 2012). However, this view has been challenged, as some studies have shown that HSP90 does not dissociate from the GR during translocation, rather it is instead required for nuclear import (Galigniana et al., 1998; Echeverría et al., 2009).

Once in the nucleus, the GR will affect its target genes either by transactivation or transrepression. During transactivation the GR will bind to a GRE on the DNA of the target gene (consensus GRE sequence AGAACANNNTGTTCT). This binding will stimulate transcription of the gene either through direct interaction with transcription machinery or recruitment of chromatin remodelling complexes. During transrepression, the GR will bind to a negative GRE (nGRE), the consensus sequence of which is less well-defined than for GREs; though a potential sequence described is ATYACNNTNTGATCN (Schoneveld et al., 2004). Following binding to the nGRE the GR will inhibit the expression of that gene either by direct inhibition or prevention of the binding of general transcription factors (Schoneveld et al., 2004).

It is possible for the GR to regulate genes by binding as a monomer to GRE half-sites (Segard-Maurel et al., 1996). Typically, the GR requires additional factors to regulate genes containing a GRE half-site, however if multiple GRE half sites are present the gene may be rendered glucocorticoid-inducible (Schoneveld et al., 2004). In addition to GREs, there are GRUs (glucocorticoid response units), which are composite regulatory elements containing not only GREs, but also binding sites for other transcription factors. GRUs may typically exhibit a stronger response to induction than GREs, though

this may not always be the case (Schoneveld et al., 2004; Scott et al., 1998). Lastly, the GR may also regulate genes through a process known as tethering; transcription factors other than the GR will bind to the DNA of their target gene, and recruit the GR to serve as a co-regulator independent of the GR binding to a GRE (Stocklin et al., 1996). Tethering may affect the target gene in a positive or a negative manner (Schoneveld et al., 2004).

Because both transactivation and transrepression are facilitated through binding to a GRE, a question often arises as to how the GR can "decide" to repress or activate. Understanding this difference could lead to improved therapeutics as the side-effects of glucocorticoids detailed earlier can often arise from the opposite molecular pathway that cause the therapeutic effect – for example transrepression may be useful therapeutically (i.e. anti-inflammatory effect) whilst transactivation pathways cause the side-effects (Sedwick, 2014). A currently explored approach in research is investigating what is called "dissociated" glucocorticoid receptor ligands that are capable of transrepression or transactivation but not transactivation or transrepression respectively. A currently investigated compound is Compound A (Liberman et al., 2012). It is envisaged that dissociated glucocorticoid receptor ligands could improve therapy by reducing side-effects.

It was originally thought that when undertaking transactivation, the GR would dimerise, whilst GR monomers would undertake transrepression. This was thought due to several experiments conducted on a mutated GR protein (GRdim) which was thought to be unable to dimerise and could carry out transrepression but not transactivation. However, this view has recently been challenged as it has been shown that GRdim can in fact dimerise *in vivo* and a study found no difference between dimerisation state and transcriptional activity (Presman et al., 2014). Thus, further research into glucocorticoid function is necessary to fully understand its molecular effects and signalling mechanisms.
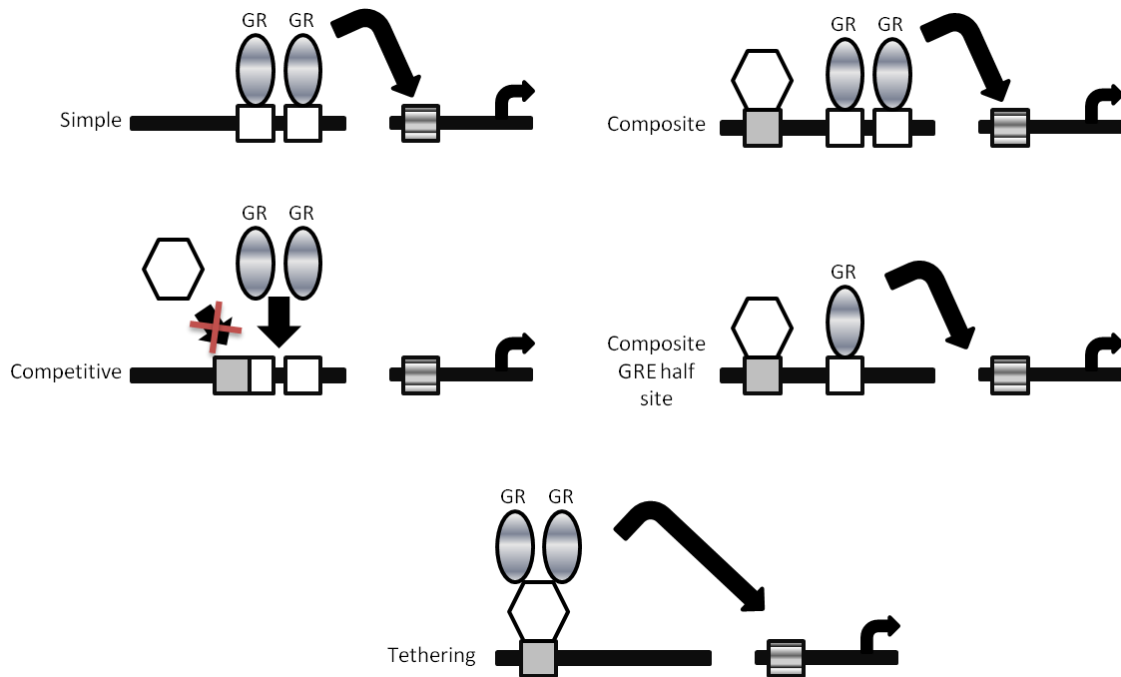
Figure 1.9.2: Summary of different mechanisms of GR action.

The glucocorticoid receptor (GR) may regulate genes directly or indirectly through various mechanisms such as direct binding, binding with an additional cofactor, competitive binding, binding to a GRE (glucocorticoid response element) half-site or tethering. Figure adapted from Schoneveld et al. (2004).

1.10   Glucocorticoid Receptor Post-Translational Modifications

There are numerous ways in which the activity of a protein can be modified. In addition to regulation at the level of gene transcription, genes are also regulated at the mRNA level and when translated as proteins. Post-translational modifications occur by the addition of chemicals or small proteins to specific amino acid residues of the protein sequence. Numerous post-translational modifications exist, such as phosphorylation, ubiquitination and sumoylation, with each of these having different effects on the protein's activity and function.

Ubiquitination is the covalent attachment of a small protein (ubiquitin) to the modified protein. Ubiquitinated proteins are generally targeted toward the ubiquitin/proteasome-dependent degradation pathway; thus, ubiquitination of the GR is linked to decreased activity through its degradation (Wang and DeFranco, 2005). However, ubiquitination

for other proteins has been shown to be important for maintenance of part of their activity (de Almagro et al., 2017), thus it should not be assumed that ubiquitination is equal to degradation.

A similar process to ubiquitination is sumoylation, as it also involves the addition of a small protein to the modified protein. It has been established that the GR has three sumoylation sites: two in its N-terminal domain and one in the ligand-binding domain. Sumoylation involves the covalent attachment of SUMO (small ubiquitin-like modifier), a small protein, to the GR. Sumoylation of the GR typically has a repressive effect on its transcriptional capacity. However some studies have recently shown that sumoylation of the SUMO site within the ligand-binding domain can affect the GR positively (Druker et al., 2013). Moreover, it has been identified that phosphorylation of the GR at S246, which is the rat ortholog of human S226 (Lukic et al., 2015), can potentiate sumoylation of the GR, and that loss of S246 phosphorylation corresponded to loss of GR sumoylation (Davies et al., 2008)

The most well-studied post-translational modification of the glucocorticoid receptor is phosphorylation, which is a post-translational modification that adds a phosphate group to specific amino acids such as serine or tyrosine. The GR contains many known phosphorylation sites as well as several putative ones, but the most well-studied in humans are serine 226 (S226), serine 211 (S211) and serine 203 (S203) and serine 404 (S404). Phosphorylation at S203 and S404 correlate with reduced GR activity, whilst phosphorylation at S211 is correlated with increased transcriptional activity of the GR in leukaemia cells. However, phosphorylation at S226 correlates with a reduced hormone response, due to increased nuclear export of the GR (Galliher-Beckley and Cidlowski, 2009).

The phosphorylation status of the GR is dependent upon kinases such as cyclin-dependent kinases (such as CDK2) and ERK/p38 MAPK (mitogen-activated protein kinase), which modulate phosphorylation at S211, whilst phosphorylation at S226 is affected by JNK (c-Jun N-terminal kinase) and CDK5 (Lynch et al., 2010; Galliher-Beckley and Cidlowski, 2009; Krstic et al., 1997). CDK5 is interesting as its function is

restricted to cells of the nervous system and it appears to phosphorylate the GR at multiple residues including S203, S211 and S226 (Galliher-Beckley and Cidlowski, 2009). Phosphorylation also modulates the activity of other steroid receptors and is in fact one of the most well-studied post-translational modifications of steroid receptors (Faus and Haendler, 2006; Rochette-Egly, 2003). For several steroid receptors including the androgen receptor (AR), oestrogen receptor alpha (ERα) and oestrogen receptor beta (ERβ) phosphorylation within the N-terminal (A/B) region by kinases such as MAPK or Akt facilitates coactivator recruitment, thus exerting a positive effect on the receptor's activity (Rochette-Egly, 2003). Phosphorylation may also exert a negative effect on the activity of other steroid receptors, such as phosphorylation of ERα within its DNA binding domain by PKA (Protein Kinase A/ Cyclic AMP-dependent protein kinase) (Rochette-Egly, 2003). Phosphorylation sites for different steroid receptors are shown in Figure 1.10.1:
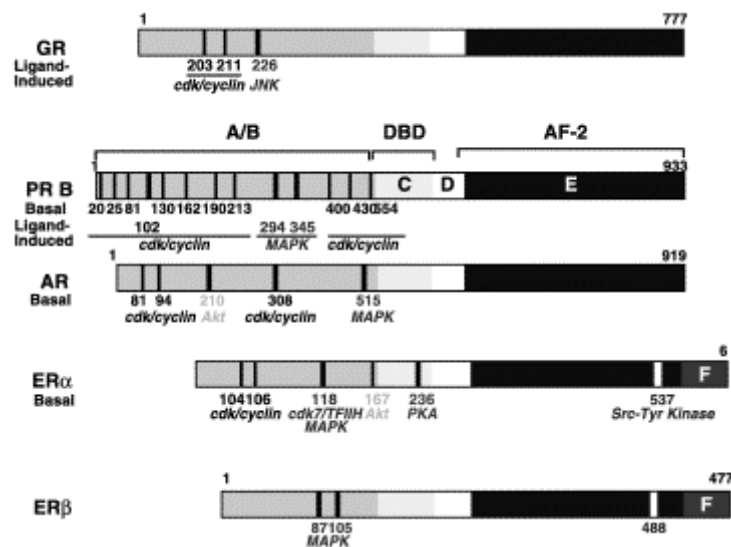
Figure 1.10.1: Phosphorylation sites in steroid nuclear receptors.

Different nuclear receptors have similar structures including the glucocorticoid receptor (GR, top) progesterone receptor (PR, second), androgen receptor (AR, middle) and oestrogen receptor alpha and beta (ERα and ERβ, bottom). Phosphorylation and post-translational modifications in general are key determinants of nuclear receptor activity. Figure adapted from Rochette-Egly (2003).

It is crucial to have a detailed understanding of the post-translational modifications of the GR, as it is important towards improving therapies. For example it has been shown

that GC-resistant leukaemia exhibit defective S211 phosphorylation; if this phosphorylation aberration could be ameliorated then GC resistance may be overcome, allowing for improved therapeutics.

1.11 Cofactors of the Glucocorticoid Receptor

When bound to the DNA of its target genes, the GR will recruit cofactors that may be coactivators or corepressors. Coactivators are recruited and may act as a "bridge" between transcription machinery and the DNA-bound GR to begin transcription (Endler et al., 2014). In addition, coactivators may promote nucleosomal remodelling to make the DNA into a more accessible form to allow for activation, as described below (Kumar and Thompson, 2005). One common type of coactivator for nuclear receptors is histone acetyltransferases (HATs), which via histone acetylation promote unwinding of DNA and access of RNA polymerase II (Adcock, 2001). The GR is known to recruit HATs such as EP300 to facilitate the activation of target genes (Amat et al., 2007). Another type of coactivator for the GR include chromatin remodelers such as SMARCA4 (ATPase subunit of the SWI/SNF chromatin remodelling complex), which act via remodelling chromatin into a more accessible position for transcriptional machinery, exposing the GRE (Fryer and Archer, 1998).

Corepressors may reduce transcription through for example the recruitment of histone deacetylases (HDACs), which induce a conformational change in the chromatin and makes it less accessible, thus reducing transcription (Gelmetti et al., 1998). HDACs serve as the opposite of HATs, as they deacetylate histones rather than acetylate. HDACs known to serve as corepressors for the GR include HDAC1 and HDAC6 (Govindan, 2010; Jee et al., 2005). Other corepressors include NCOR1 and NCOR2, which are thought to achieve their repressive effects via recruitment of HDACs (Szapary et al., 1999; Ramamoorthy and Cidlowski, 2013).

1.12 Overview of Transcription

The central dogma of molecular biology follows the logic that DNA is transcribed to RNA which is then translated to protein. Transcription itself is an essential process to both prokaryotic and eukaryotic cells, though the process is considerably more complex in eukaryotes (Cooper, 2000). Transcription is a process that is dependent upon RNA polymerase (RNAP). There are multiple types of RNAP, each regulating the transcription of different cellular components; for example RNAP I primarily transcribes ribosomal RNA whilst RNAP II is responsible for transcribing protein-coding DNA to mRNA (Cooper, 2000).

Transcription in eukaryotes is dependent not only upon RNAP, but also upon transcription factors. Transcription factors are broadly of two kinds: general transcription factors (those that are required for RNAP function and thus are relatively ubiquitous) and sequence-specific (such as the GR binding only to its target genes). Transcription by RNAP II is dependent upon binding to promoter regions, with the most common recognition sequence being an A-T rich sequence commonly called "TATA box" which is typically thirty nucleotides upstream of the transcription start site. An early event is RNAP II transcription is the binding of the general transcription factor TFIID (comprised of subunits TBP (TATA-binding protein) and TBP-associated factors) to the TATA box, which is facilitated by transcription factors TFIIA and TFIIB (Imbalzano et al., 1994). TFIIB proceeds to bind RNAP II, and the transcription preinitiation complex is ultimately comprised of the aforementioned transcription factors in addition to others such as TFIIE, TFIIF and TFIIH (Cooper, 2000).

The transcription cycle as a whole consists largely of three steps: initiation, elongation and termination. Initiation, which involves promoter binding, DNA melting and short RNA transcript synthesis, proceeds to elongation via a transition known as "promoter escape" (Conaway and Conaway, 2004). Following promoter escape and during elongation RNAP II traverses along the coding region towards the 3' end of the gene, synthesising the RNA strand (Shandilya and Roberts, 2012). Lastly, termination occurs following mRNA synthesis when RNAP II dissociates from the DNA. Termination for protein-coding genes in eukaryotes commonly occurs through a poly-A site due to what is commonly referred to as the cleavage and polyadenylation complex recognising the

poly-A site and then cleaving the transcript (Shandilya and Roberts, 2012; Grzechnik et al., 2014).

1.13   The Role of the Bone Marrow Microenvironment in Chemoresistance

Although glucocorticoids are utilised as part of many treatment regimens for lymphoid malignancies, GC resistance and disease relapse remain a problem. Microenvironments (also called stem cell niches) have been defined as "local tissue microenvironments that maintain and regulate stem cells" (Morrison and Spradling, 2008). Within healthy adults, the microenvironment plays a crucial role in the maintenance of multipotent stem cells. In the case of the bone marrow microenvironment, haematopoietic stem cells (HSCs) are maintained in a quiescent state through interaction with the niche (see Figure 1.13.1). HSCs themselves differentiate into a variety of blood cell types such as leukocytes, erythrocytes, and platelets, indicating their importance (Bakker et al., 2016).

The bone marrow microenvironment was classically said to consist of two parts: the endosteal niche and the vascular niche. The endosteal niche, also called the osteoblastic niche, comprises the inner surface of the bone cavity and is lined with cells that are involved in osteogenesis such as osteoclasts and osteoblasts. The vascular niche, also called the sinusoidal niche, is comprised of several structures including sinusoids, which are thin-walled blood vessels that serve as an interface between the circulating blood and marrow cavity (Bakker et al., 2016). As stated above and summarised in Figure 1.13.1, the bone marrow microenvironment contributes to the maintenance of HSCs. A variety of factors are crucial to HSC maintenance, in particular CXCL12 (chemokine (C-X-C motif) ligand 12, also known as stromal cell-derived factor 1 (SDF1)) which is thought to be an important attractant for HSCs (Bakker et al., 2016)
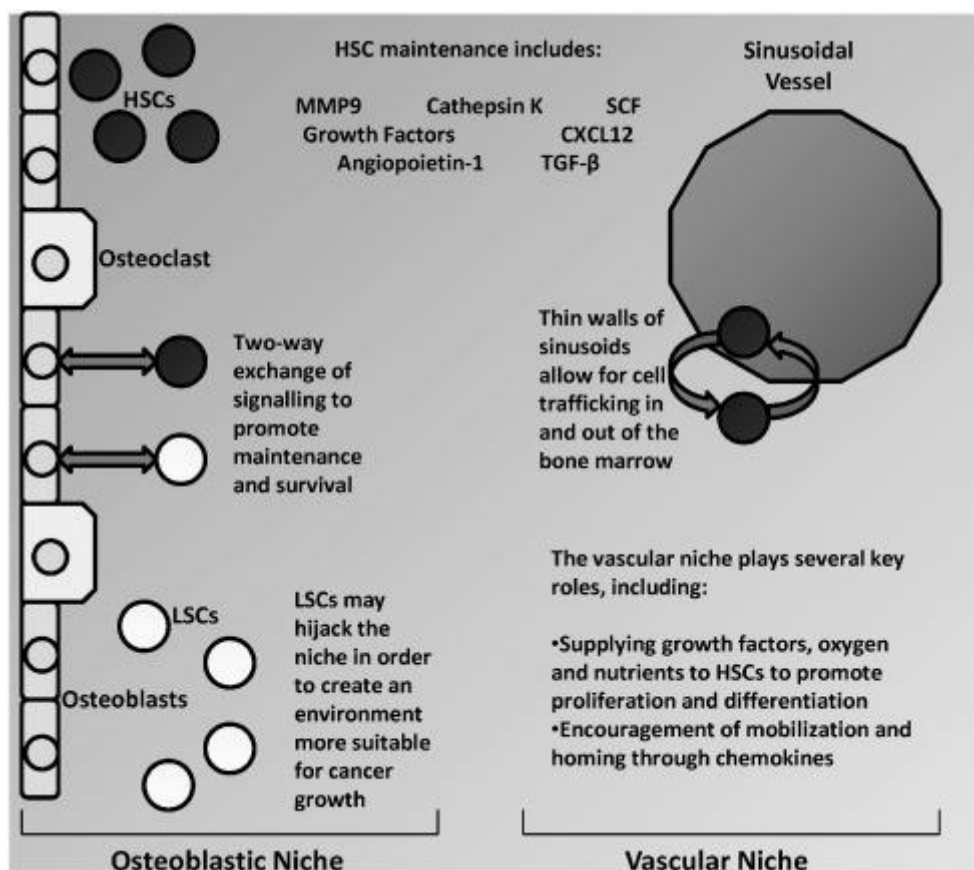
Figure 1.13.1: Summary of the bone marrow microenvironment.

Numerous signalling pathways between the microenvironment and haematopoietic stem cells (HSCs) and leukaemic stem cells (LSCs) may exist. Factors important for HSC maintenance include matrix metalloproteinase 9 (MMP9), stem cell factor (SCF), Chemokine (C-X-C motif) ligand 12 (CXCL12), and transforming growth factor beta (TGF-β). The bone marrow microenvironment is said to comprise of two components: the osteoblastic (endosteal) niche and the vascular (sinusoidal) niche. Figure taken from Bakker et al (2016).

Understanding the maintenance of HSCs is crucial as it links to the concept of cancer stem cells (CSCs). CSCs are a sub-type of tumour that exhibit stem-like properties, such as the fact that they are capable of self renewal. CSCs have been identified in a variety of cancers, including leukaemia. Although the microenvironment is crucial for HSC maintenance in healthy individuals, it is also well-established that these niches may undergo a two-way exchange of information with circulating cancer cells that creates an environment suitable for cancer progression and tumour growth (Bakker et al., 2016). A summary of the different ways in which the microenvironment and cancer cells can communicate are shown in Figure 1.13.2:
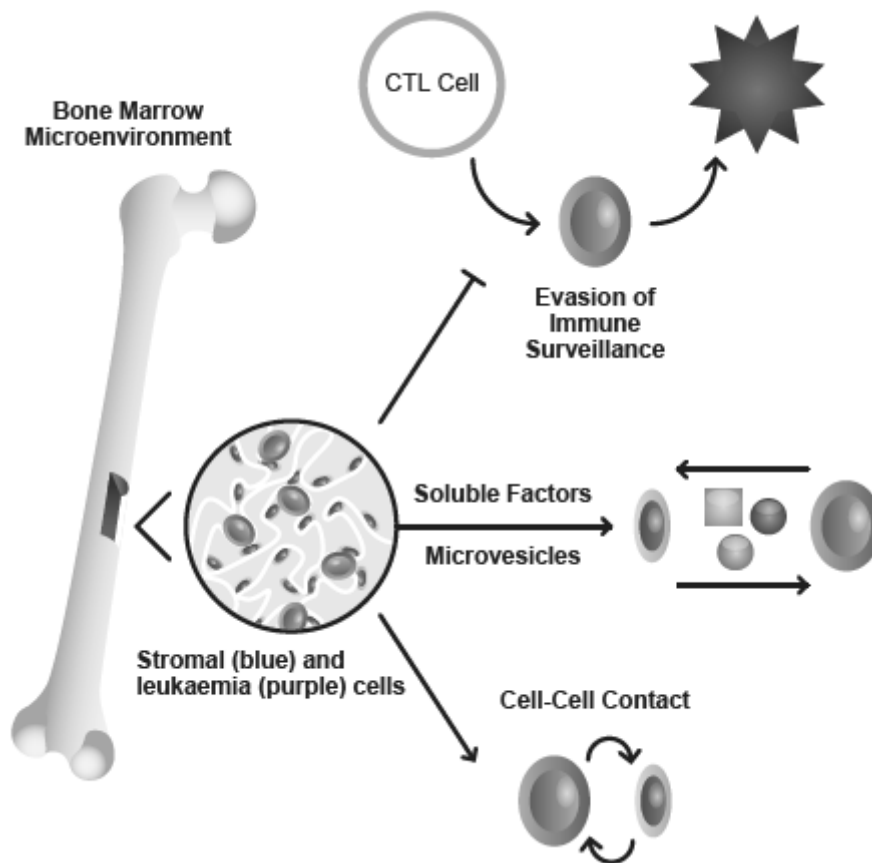
Figure 1.13.2: Summary of microenvironment-leukaemia interactions.

The microenvironment may communicate in a variety of ways such as cell-cell contact, secreted factors such as microvesicles, and modulation of the immune system to allow escape from immune detection. Figure taken from Bakker et al (2016).

As is clear in Figure 1.13.2 above, there are numerous ways by which the microenvironment may nurture chemoresistance. Cell-cell contact between leukaemic cells and stromal cells is one method of communication, as are soluble factors as well as microenvironment-mediated immune evasion. Soluble factors include substances secreted by constituents of the microenvironment such as microvesicles (exosomes), which are small lipid vesicles that are conserved throughout evolution and contain substances such as microRNAs that can alter gene expression and cell fate (Bakker et al., 2016). An example of altered signalling by leukaemic cells and the microenvironment is the aforementioned CXCL12; though important for HSC maintenance and attraction, leukaemic stem cells (LSCs) are also attracted by CXCL12,

though they alter the niche via stem cell factor (SCF) which is important for haematopoiesis (Bakker et al., 2016).

Ultimately leukaemia cells may have a two-way exchange with the niche, be affected by secreted factors such as cytokines, and acquire a chemoresistant phenotype (Konopleva et al., 2009). Although the microenvironment may nurture chemoresistance, it is possible for this to be overcome through targeted therapy aimed at eliminating the factors that promote a drug-resistant phenotype (Sison et al., 2013). Thus, an increased understanding of the microenvironment and how it can contribute to leukaemic chemoresistance is important towards improving therapies and clinical outcomes.

Research has made it possible to simulate certain properties of the microenvironment *in vitro*. This approach utilises what is called "conditioned media" – that is, cell growth media that has been incubated with (for example) bone cells for a set period of time. After incubation, and after which the bone cells should have secreted factors into the media, this media is collected, processed and ultimately utilised as part of the media used to grow leukaemia cells. It has been demonstrated that this conditioned media can also exert a chemoprotective effect on leukaemia cells (Gordon et al., 2014; Liu et al., 2012; Liu et al., 2015).

Previous analysis has utilised the approach of conditioned media to investigate glucocorticoid resistance. As part of this a microarray experiment was carried out, treating glucocorticoid-sensitive cells with dexamethasone in the presence and absence of conditioned media (Qattan, 2014). The microarray revealed that conditioned media modulated the expression of numerous genes, but one gene that was significantly repressed by conditioned media was *RIPK1* (receptor interacting serine/threonine kinase 1), shown by the microarray to be significantly repressed at the mRNA level. RIPK1 is an interesting target as it is a key mediator of necroptosis, a form of cell death (see the next section, "Autophagy, Apoptosis, Necrosis and Necroptosis") (Huang et al., 2013). It also plays a role in apoptosis (Loder et al., 2012), has been implicated in glucocorticoid-induced cell death (Belz, 2014), and its induction of necroptosis can be

reduced through autophagy (Bray et al., 2012). Combined, these highlight RIPK1 as an interesting target for future research.

1.14   Autophagy, Apoptosis, Necrosis and Necroptosis

Cells, both within the body and cultured *in vitro*, may survive and die through different processes and mechanisms. In summary there are four pathways to be considered: autophagy, apoptosis, necrosis, and necroptosis. Of these, apoptosis ("programmed cell death") is the most well-characterised and studied, with key morphological features such as nuclear condensation, fragmentation and cleavage of chromosomal DNA and packaging of the cell into apoptotic bodies (Edinger and Thompson, 2004). This is contrasted with necrosis and necroptosis, where morphological features are less well-defined. However necrotic/necroptotic cells can be distinguished from apoptotic cells by their ruptured membrane and cytoplasmic vacuolation, and similarly autophagy, which is generally a pro-survival process, is characterised by the formation of autophagic vesicles (Edinger and Thompson, 2004). Healthy, apoptotic, autophagic and necrotic cell morphologies are shown in Figure 1.14.1:
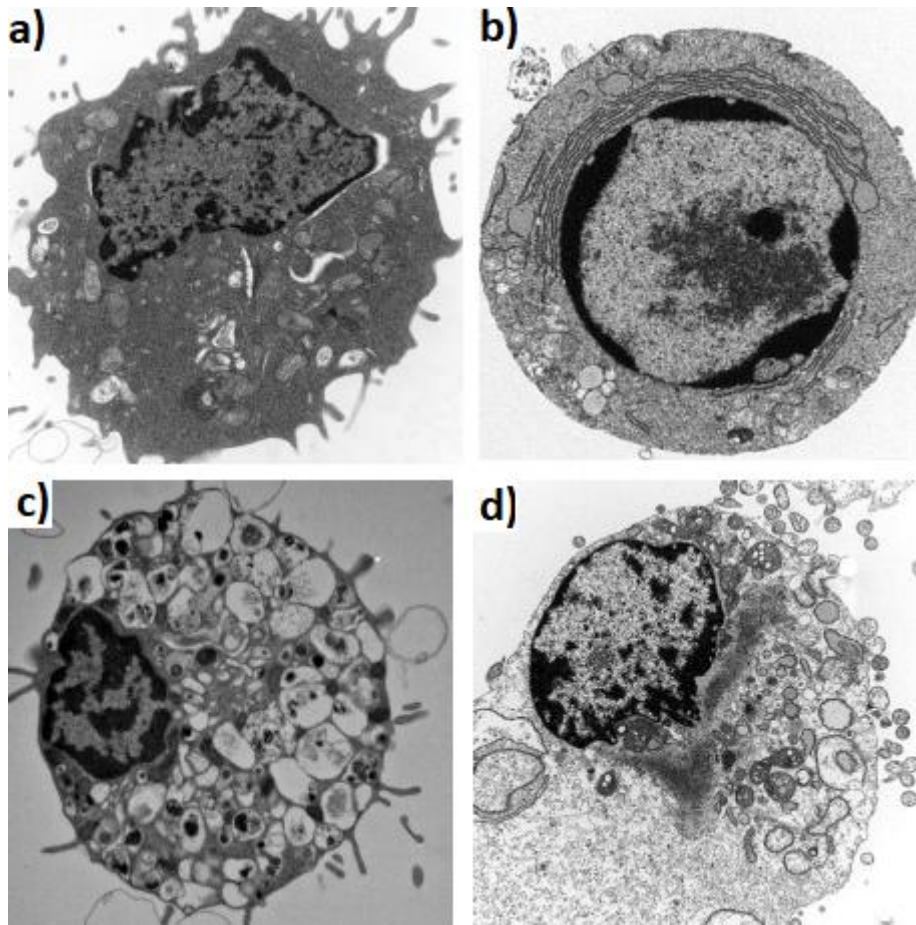
Figure 1.14.1: Healthy (a), apoptotic (b), autophagic (c) and necrotic (d) cells.

Cell morphology differs significantly between the four cell types, with features such as nuclear condensation for apoptotic cells (b), the formation of autophagic vesicles for autophagic cells (c) and ruptured membrane (d) for necrotic cells. Figure adapted from Edinger and Thompson (2004).

The study of apoptosis has a long history. Initial apoptotic mechanisms were identified previously (Kerr, 1965) but the term apoptosis was not used until 1972 (Kerr et al., 1972). Since then, a highly significant amount of research has been carried out to investigate the detailed mechanisms that underlie apoptosis. Apoptosis is characterised by multiple important steps: nuclear condensation and fragmentation; fragmentation of chromosomal DNA; and packing of deceased cell into apoptotic bodies to avoid immune detection (Edinger and Thompson, 2004). The overall signalling behind apoptosis is highly complicated, but two main pathways are recognised: the intrinsic pathway and the extrinsic pathway (Lawen, 2003; Chipuk and Green, 2006).

Intrinsic Pathway
Stress (i.e. DNA Damage)
↓
BCL-2 protein regulation
↓

Mitochondrial Outer Membrane Permeabilisation

Release of Cytochrome C

BID Cleavage ← Caspase-8 Activation

Caspase-3 and Caspase-7 Activation
↓
Cell Death

Extrinsic Pathway
Death Receptors
↓
Ligation of death receptors
↓
Recruitment of adaptors
↓
Recruitment of pro-caspase-8
↓
Caspase-8 Activation
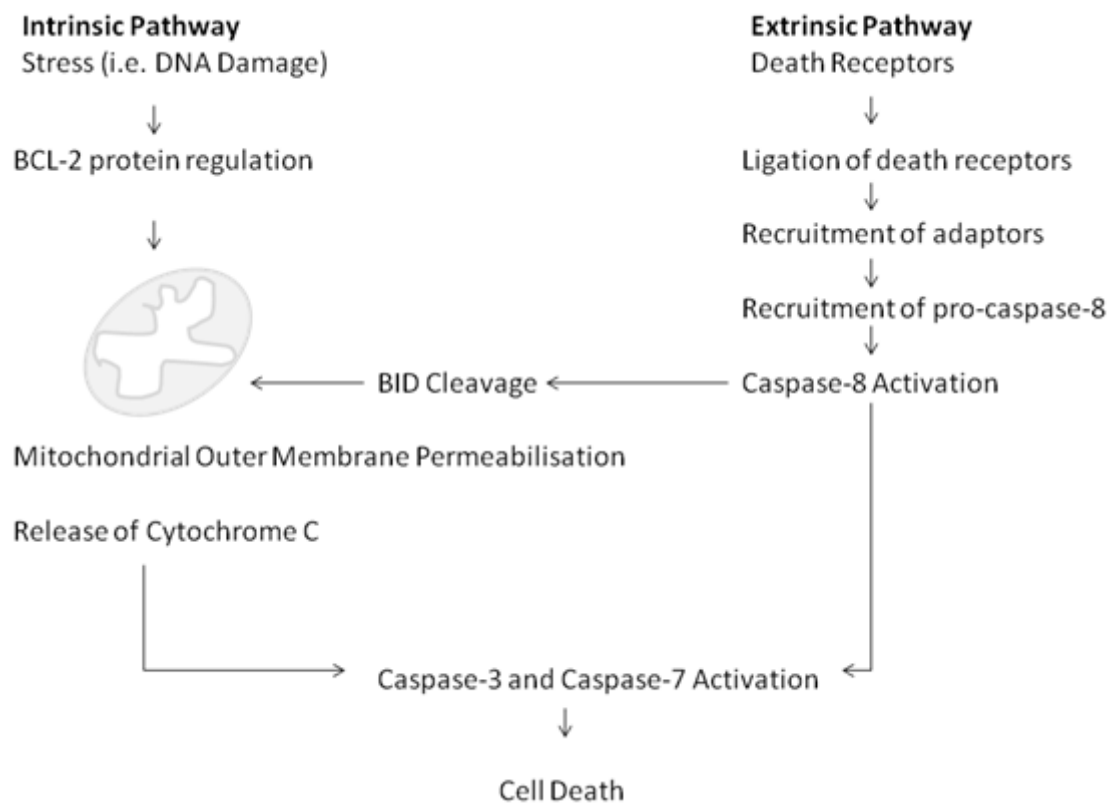
Figure 1.14.2: Intrinsic and extrinsic apoptosis.

Two major apoptotic pathways exist, the intrinsic apoptotic pathway (left) and the extrinsic apoptotic pathway (right). The intrinsic pathway is characterised by the regulation of the BCL-2 family, and there is crosstalk between the two pathways following caspase-8 activation which leads to cleavage of BID (BH3 interacting-domain death agonist). Adapted from Chipuk and Green (2006).

The intrinsic apoptotic pathway is the more complex of the two and is characterised by the use of mitochondria; a key event in the intrinsic apoptotic pathway is the mitochondrial outer membrane permeabilisation (MOMP), which ultimately promotes the release of mitochondrial proteins (Spierings et al., 2005). The intrinsic apoptotic pathway occurs in response to a cellular stress such as DNA damage which triggers the regulation of BCL-2 family, a family of proteins that contain pro- and anti-apoptotic members (Ploner et al., 2008). BCL-2 proteins form what is called the BCL-2 rheostat whereby the switch to apoptosis or survival is regulated by the balance between relative activation of pro- and anti-apoptotic BLC-2 family members (Schlossmacher et al., 2011). Activation of pro-apoptotic BCL-2 family members leads to MOMP, which releases of mitochondrial proteins such as cytochrome c into the cytosol, leading to the activation of APAF-1 (apoptotic protease activating factor 1), which induces a caspase

50

activation cascade beginning with pro-caspase-9 (Spierings et al., 2005). Mitochondrial proteins may also act as caspase-independent death effectors within the cell (Fulda and Debatin, 2006).

Caspases are the main executors of apoptosis, cleaving important cellular entities such as actin to ultimately cause the migration of CAD (caspase-activated DNase) to the nucleus, which cleaves nuclear DNA, in turn leading to cell death (Lawen, 2003).

The extrinsic apoptosis pathway is stimulated through ligand binding to death receptors of the tumour necrosis factor (TNF) superfamily (Fulda and Debatin, 2006). The TNF superfamily share common structural features, most importantly a cytoplasmic domain of approximately eighty amino acids called the "death domain" which plays a key role in transferring the apoptotic signal from the cell's surface to intracellular pathways (Elmore, 2007). As there are numerous death receptors each have been studied to a different degree, with the most well-characterised ligand-receptor pathways being FasL (FAS ligand)/FasR (FAS receptor) and TNF-α/TNFR1 pathways. Under these, ligand binding to the receptor induces recruitment of factors such as FADD (Fas-associated protein with death domain), TRADD (TNF receptor superfamily member 1A associated via death domain) and RIPK1 (Elmore, 2007). FADD then associates with pro-caspase-8, which is activated by the formation of a death-inducing signalling complex (DISC).

The activation of pro-caspase-8 leads to the execution of downstream caspases such as caspase-3 and caspase-7 (Elmore, 2007). The extrinsic apoptotic pathway exhibits crosstalk with the intrinsic pathway through its cleavage of BID (BH3-interacting-domain death agonist) which beings a process that ultimately induces MOMP (Chipuk and Green, 2006). The extrinsic apoptotic pathway can be blocked by CFLAR (CASP8 (caspase-8) and FADD-like apoptosis regulator, also called c-FLIP) which binds FADD and caspase-8 to render them ineffective (Elmore, 2007).

Autophagy is a cellular process that is linked to both cell death and cell survival (Gump and Thorburn, 2011). Autophagy is a term that refers to the "degradation of cytoplasmic components within lysosomes" (Mizushima, 2007) and is essentially a pro-survival

process, where autophagosome assembly leads to clearance of pathogens, proteins, and damaged organelles. Autophagy also helps cells to survive during periods of starvation (Gump and Thorburn, 2011). Despite this, autophagy has also been shown to influence apoptosis, as inhibition of key autophagic molecules lead to a reduction in mortality in one study (Yu et al., 2006), and inhibition of Beclin-1 (BECN1), previously demonstrated to be important for autophagy, resulted in inhibition of dexamethasone-induced apoptosis in leukaemic cells (Laane et al., 2009). Thus, autophagy is a highly interesting process due to its complex nature.
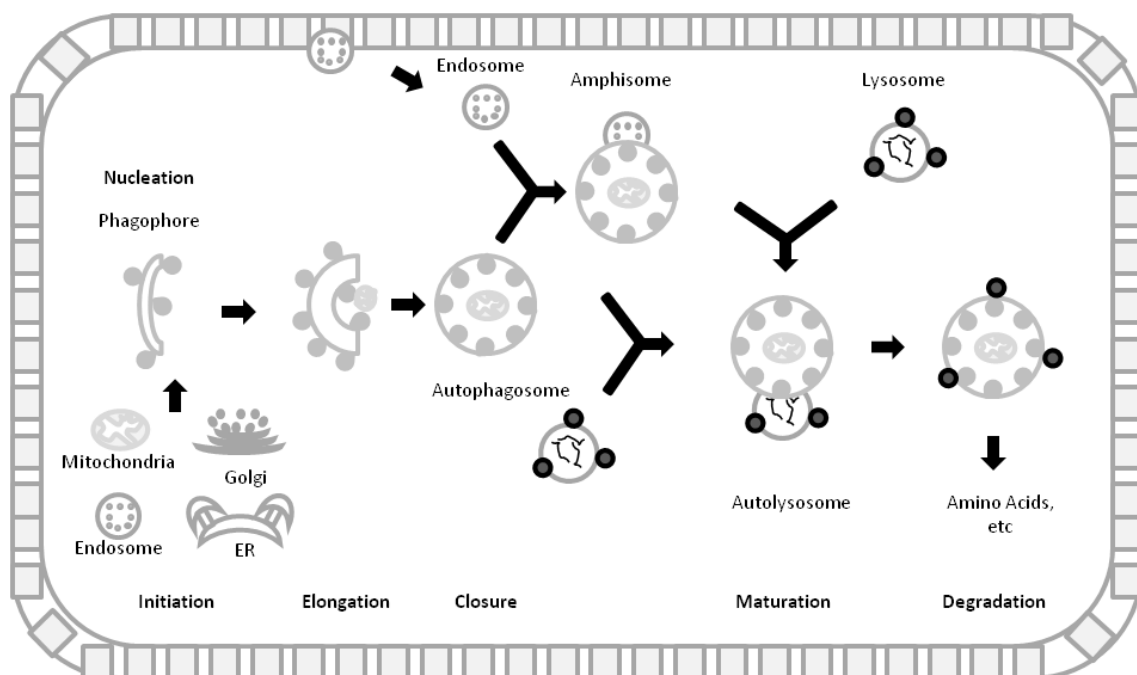
Figure 1.14.3: Overview of autophagy.

Autophagy consists of several steps including initiation, nucleation, elongation, closure, maturation and degradation. Phagophore formation may be around various organelles including the endoplasmic reticulum (ER) and mitochondria, whilst the phagophore ultimately undergoes a stepwise maturation process. Figure adapted from Kang et al. (2011).

Autophagy itself is mediated by autophagosomes, consists of several steps such as sequestration, degradation, and amino acid/peptide generation and is typically triggered due to factors such as starvation (Mizushima, 2007). The first step of autophagosome formation involves the sequestration of the cytoplasmic contents by the phagophore (or isolation membrane) which may be generated by sources such as the Golgi apparatus,

the endoplasmic reticulum or mitochondria (Kang et al., 2011). These membranes are then fused at their edges to create autophagosomes, double-membrane vesicles. Autophagosomes undergo a maturation process involving fusion with acidified vesicles, and eventually deliver the cytoplasmic contents to the lysosomal components, where contents are degraded and recycled (Kang et al., 2011). Key genes for the function of autophagy include *ATG5* (autophagy protein 5), *ATG7* (autophagy protein 7), *LC3* (microtubule-associated protein light chain 3), and *BECN1* has also been shown to be highly important for its process (Kang et al., 2011). The complexity of autophagy signalling indicates the need for further research as increased understanding of molecular pathways may improve therapeutics.

Necrosis is what has been described as a "passive" form of cell death as it typically forms in response to an injury and is usually detrimental to the host organism (Berghe et al., 2010). However, it is now known that there are distinct programmed cell death approaches that differ morphologically from apoptosis; "necroptosis" is called such due to its morphological resemblance to necrosis. Necroptosis is characterised *in vitro* by cytoplasmic swelling, rounding of the cell, absence of chromatin condensation and dilated organelles (Berghe et al., 2010).

TNF stimulation is widely used to study necroptosis, due to the fact that RIPK1 (one of its key effectors) is known to be recruited and activated by receptors such as FasR. RIPK1 may activate RIPK3 (receptor interacting serine/threonine kinase 3) and subsequently necroptosis (Oberst, 2016). A summary of TNF-driven necroptosis is shown in Figure 1.14.4:
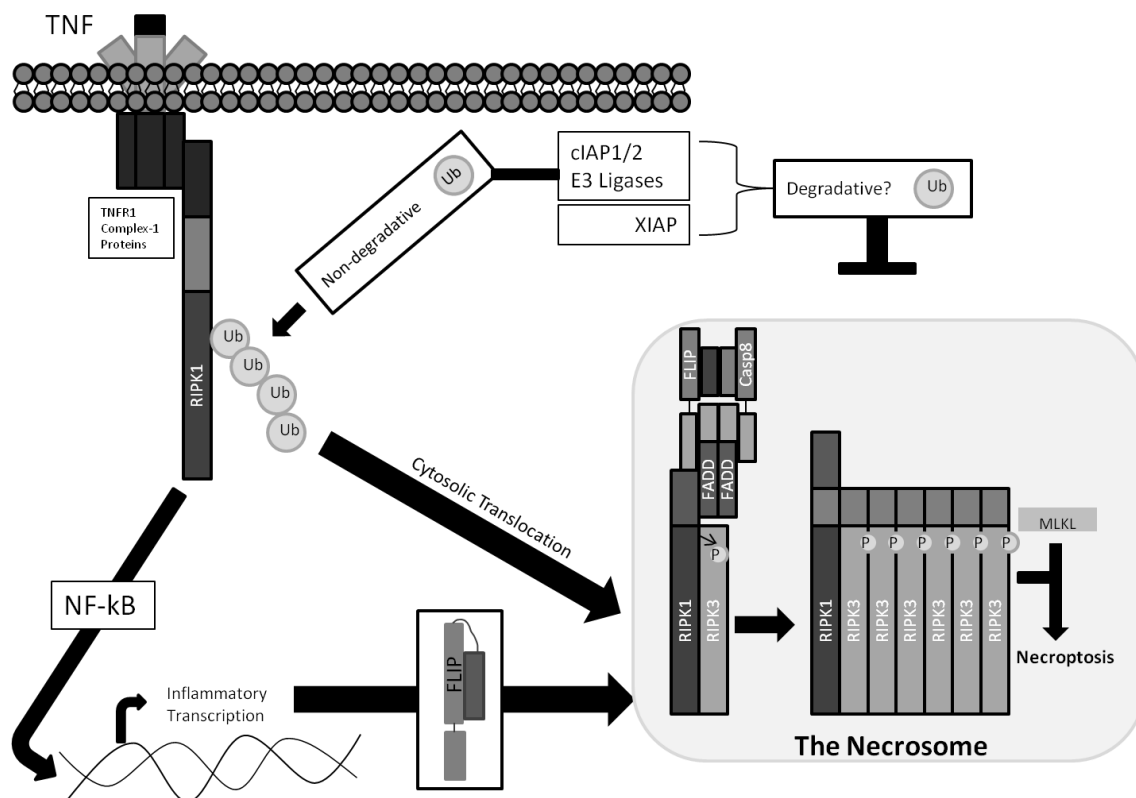
Figure 1.14.4: Overview of TNF-driven necroptosis.

Necroptosis consists of numerous steps and has crosstalk between multiple pathways and proteins/complexes such as the cellular inhibitors of apoptosis (CIAP1/2), caspase-8 (casp8), MLKL (mixed lineage kinase domain like pseudokinase) and nuclear factor kappa b (NF-kB). Ubiquitination (Ub) and phosphorylation (P) statuses are important determinants of which signalling pathway is undertaken. Other important proteins in this pathway include FLIP (Cellular FLICE (FADD-like IL-1β-converting enzyme)-inhibitory protein). Figure adapted from Oberst (2016).

RIPK1 is established as a key mediator of necroptosis, as inhibition of RIPK1 through Necrostatin-1 (a RIPK1 inhibitor) lead to inhibition of necroptosis, and RIPK3 is another key mediator of necroptosis. MLKL (mixed lineage kinase domain like pseudokinase) is another key player of necroptosis, and is activated and phosphorylated by RIPK3, which ultimately leads to the morphological features of necroptosis such as swelling and rupture (Oberst, 2016). Activated MLKL translocates to the cellular membrane, where it interacts with phospholipids to trigger permeabilisation and swelling, which is markedly different to the mechanisms of apoptosis (Oberst, 2016). However, the exact details regarding how MLKL exerts its effects and indeed necroptosis as a whole remain unclear. The key necroptotic mediator RIPK1 represents an interesting target due to its apparent connectedness with multiple cellular pathways

such as the extrinsic apoptotic pathway and caspase-8 (Elmore, 2007), key role in necroptosis (Berghe et al., 2010), and potential link to the activation of NF-κB (Oberst, 2016).

Although these forms of cell death and survival have been identified, the full details of the signalling pathways through which their effects are mediated are not yet completely established; this is particularly true for necroptosis. Furthermore, though many drugs are used in the clinic to treat leukaemia, how they induce cell death is not fully understood, nor is potential crosstalk between their mechanism of cell death and other cellular processes.

Dexamethasone and etoposide are two of the most common drugs used to treat leukaemia, and act via the GR and tumour protein p53 (*TP53*, involved in the DNA damage response) respectively. Both are known to affect mediators of cell death and survival in multiple ways. Mechanisms behind glucocorticoid-induced cell death remain unclear, though several factors such as low expression of the GR and overexpression of the anti-apoptotic Bcl-2 protein have been indicated as resistance factors (Schlossmacher et al., 2011; Bakker et al., 2016).

Glucocorticoid-induced cell death is thought to work primarily through the intrinsic apoptotic pathway via induction of pro-apoptotic BCL-2 family members such as *BCL2L11* (Bcl-2-like protein 11, also known as BIM) or repression of anti-apoptotic BCL-2 family members such as the Bcl-2 protein (Schlossmacher et al., 2011). Evidence corroborating this is that knockout of pro-apoptotic BCL-2 family members confers resistance to glucocorticoid-induced apoptosis in thymocytes (Rathmell et al., 2002), whilst a microarray analysis unveiled that several pro-apoptotic BCL-2 family members were induced by glucocorticoid treatment, whilst other anti-apoptotic BCL-2 family members were repressed (Lynch et al., 2010). Thus, the GR appears to modulate BCL-2 family members to promote apoptosis via the intrinsic pathway.

However, there has also been some evidence of glucocorticoids affecting the extrinsic apoptotic pathway, such as glucocorticoid treatment inducing FasL in mouse

thymocytes (Schmidt et al., 2004), which indicates potentially indicates cell type-specific differences and the need for further research. There is further crosstalk between the GR and cell death pathways such as autophagy and necroptosis. For instance, it has been indicated that autophagy may be important for glucocorticoid-induced cell death through the key autophagy mediator BECN1 (Laane et al., 2009), and there is also a link to necroptosis as it has previously been demonstrated that glucocorticoid resistance can be overcome by autophagy-dependent necroptosis (Bonapace et al., 2010). Bonapace et al. (2010) demonstrated the necessity of RIPK1 to overcome glucocorticoid resistance, further demonstrating the crosstalk between these pathways.

Etoposide induces apoptosis via DNA damage activation of *TP53*, which following activation accumulates in the nucleus to control the expression of numerous pro-apoptotic genes including *BAX* (BCL2 associated X, apoptosis regulator) and *BID* (BH3 interacting-domain death agonist) (Chipuk and Green, 2006). In the case of these genes being silenced, partial resistance to TP53-induced apoptosis was seen, providing further evidence for the idea that TP53/DNA damage-induced apoptosis occurs primarily through the intrinsic apoptotic pathway (Chipuk and Green, 2006).

1.15   Computational approaches to glucocorticoid signalling

High-throughput research methodologies, where the aim is to generate findings on thousands of genes or proteins as opposed to traditional laboratory methodologies which focus on a small subset of genes at a time, are changing the field of biological and biomedical research. These high-throughput techniques apply to a variety of fields and are informally referred to as "omics" (i.e. genomics, transcriptomics, proteomics). Although it is only natural that research methodologies evolve over time, be it due to changing resources, technology or knowledge, the quantity of information generated by these omics approaches presents a daunting task for analysis, generally requiring the use of computers to analyse the large datasets in both a more efficient and more integrated manner (Wang, 2010).

The terms "bioinformatics" and "computational biology" are often used interchangeably, but they are arguably two distinct fields, albeit with overlapping and similar aims. The NIH (2000) has defined computational biology as "[t]he development and application of data-analytical and theoretical methods, mathematical modeling and computational simulation techniques to the study of biological, behavioral, and social systems", whilst bioinformatics was defined as "[r]esearch, development, or application of computational tools and approaches for expanding the use of biological, medical, behavioral or health data, including those to acquire, store, organize, archive, analyze, or visualize such data" (NIH, 2010). Thus, although similar, the NIH highlights a difference between the two terms, with computational biology referring to the use of computers to study biological data whilst bioinformatics largely refers to the development of tools to analyse data (NIH, 2010).

In order to integrate the large data generated by omics fields, effectively analyse them and elucidate relationships between constituents of the dataset in question, it is necessary to employ mathematical theory and computation to the data, as traditional laboratory-based approaches cannot carry out this task (Wang, 2010). Many approaches are utilised within bioinformatics and computational biology, with one subspecialty being Systems Biology.

1.16   Systems Biology

Systems biology is a field that aims to integrate different sources of omics data and analyse them effectively (Wang, 2010). It is interesting to observe the fact that since the early 2000s, there has been a steadily rising and ultimately exponential increase in the number of publications relating to systems biology, as summarised in Figure 1.16.1:
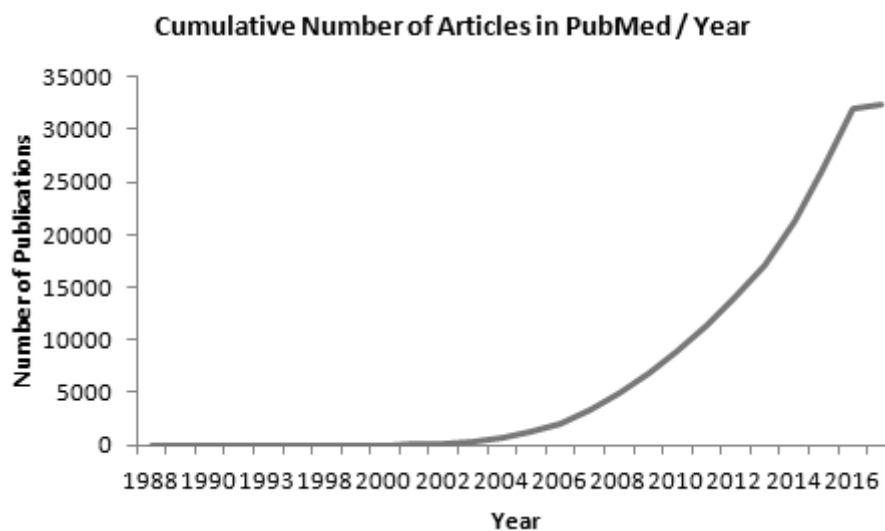
Figure 1.16.1: Cumulative PubMed entries containing "Systems Biology" per year.

The x-axis shows the year whilst the y-axis shows the number of publications. Data extracted from PubMed "Results by Year" and processed into a cumulative form.

It is clear from Figure 1.16.1 that there has been a dramatic increase in the number of publications relating to systems biology in recent years, most notably after 2010. Such a significant increase in the number of publications relating to the field indicates quite clearly the interest in its methodologies, its importance in the field, as well as the fact that it is capable of generating publishable-quality data at a relatively rapid rate.

The goal of computational biology is to generate models that are a good fit to *in vivo* behaviour and thus provide accurate predictions to aberrations in the network. Modelling offers several advantages over traditional laboratory-based research. One key advantage of computational modelling is its cost-effectiveness; other than requiring dedicated hours from the researcher, models can be constructed, analysed, and even validated at little or no monetary cost; this is made possible through the use of open-source software and public databases.

Furthermore, once a model has been constructed, numerous analyses can be undertaken (such as different *in silico* knockout scenarios compared to wild-type) again at no extra cost other than time and computation power. There are other advantages, such as that during construction of the model gaps in the knowledge of a signalling network (for example) may be uncovered – and in fact, once the model is built it may provide an

answer or insight into this gap through network analysis (Klipp et al., 2009). Lastly, computational modelling may drive research forward through predictions; if a model is sufficiently large and accurate, it will generate predictions as to how the system behaves following a perturbation to the network. These predictions may then be validated in the laboratory and provide novel insights, thus driving the field and research forward.

However, as stated earlier and despite the advantages offered by computational approaches, modelling is not without its own problems. The statement by statistician George Box – "essentially, all models are wrong but some are useful" – is worth remembering. There are several key issues to acknowledge during model building. The first is that the initial construction of a model is limited to the currently available knowledge, which in turn is dependent on the quality of the experiments used to generate that knowledge. Another limitation of modelling is that by the very nature of the approach models will only encapsulate a small portion of the whole system, meaning that other aspects, which may be crucially important for network regulation, are by necessity simplified or omitted (Klipp et al., 2009). Ultimately, however, a combined approach of modelling and wet laboratory investigation would provide more insight than either approach alone.

1.17   Approaches to Computational Modelling

There are numerous approaches to modelling depending on the size and scope of the model, in addition to the aims that the research hopes to address. As a whole, modelling can be generally split into two different categories: top-down and bottom-up (Edwards and Thiele, 2013).

The top-down approach adopts a holistic method to modelling, aiming to generate a model of an entire system that can be a good overall fit to *in vivo* behaviour (Klipp et al., 2009). By starting at the "top", such as genome-wide data or a model of the entire signalling network in question, the top-down approach aims to uncover relationships closer to the "bottom" (Bruggeman and Westerhoff, 2007). Top-down modelling has been described as "phenomenological": model interactions are not based on exact

mathematical modelling of the kinetics of reactions, but rather are based on an overall approach of i.e. Protein 1 activates Protein 2 (Bruggeman and Westerhoff, 2007).

Contrasting with top-down modelling is its opposite, bottom-up modelling. Bottom-up modelling studies elementary processes in isolation and applies them to a model (Klipp et al., 2009). Such a modelling approach requires detailed knowledge of the exact mechanisms of reactions such as enzyme kinetics and diffusion properties (Bruggeman and Westerhoff, 2007). Thus, a bottom-up model accurately models a small portion of the whole, with accurate mechanisms and reaction rates. One aim of bottom-up modelling is to combine several small-scale models of different process in isolation to form the whole, thus reaching the "top" (Bruggeman and Westerhoff, 2007). Bottom-up modelling has been applied to a variety of fields within biological science, such as a model of *E. coli* metabolism based on a plethora of factors such as transcription factor kinetics (Bettenbrock et al., 2006) and modelling of glycolysis in yeast based on enzyme properties (Teusink et al., 2000). As a whole, bottom-up modelling can be described as "mechanism-based", reflective of the fact that the modelling approach aims to accurately model biological phenomena by using exact detailed knowledge of the reactions underpinning the network.

It is clear from the above paragraphs that there are various modelling approaches that may be used in biological research; the type chosen depends largely on the aims of the study and scope of the modelling practice. There are many different types of modelling approaches, but specific examples include ordinary differential equation (ODE) modelling, Petri nets, and Boolean logical modelling, all expanded upon in the following sections.

1.18   ODE Modelling

ODE modelling is one of the most common modelling approaches within systems biology, and has been extensively applied to biological research (Klipp et al., 2009). ODE modelling employs numerical values (such as transcription rates) to smaller-scale models to study the underlying interaction phenomena of a system in a quantitative

manner (Baker et al., 2013). The state of a node (model constituent such as protein or mRNA) is dependent on a variable; a typical variable utilised for ODE modelling is time (de Jong, 2002). A simple example is that the change in the mRNA levels of a protein could be measured experimentally over time, following a drug treatment. This data (combined with others such as protein levels and biological outputs) could then be used to generate an ODE model of the system.

The detailed biological data required prior to model generation represents a limitation of ODE models, as although these values may be obtained through *in vitro* experiments, this is often difficult, time-consuming, and may not even be possible (Lillacci and Khammash, 2010). The application of ODE models to systems biology is thus limited due to the requirement for several kinds of initial parameters (such as basal mRNA/protein concentrations), as well as the fact that ODE models on a larger scale necessitates a large computational demand (Khan et al., 2014; Akman et al., 2012).

Despite this, there are numerous advantages to ODE modelling, most particularly that they retain the quantitative nature and inherent causality of biological systems (Chen et al., 2012). Another advantage to ODE modelling is that many different programs have been developed to handle ODE simulations, which can handle the complex mathematical processes without a significant amount of user input. One example of such software is COPASI (Complex Pathway Simulator), which is a freely-available program that requires only the details of (for example) protein interactions and related kinetic data, whilst not requiring an in-depth understanding of the mathematical processes underlying model analysis (Tindall, 2012). Thus with software such as COPASI it is possible to generate models and analyse them without detailed knowledge of how the models are solved; this can thus increase the pace at which research can be carried out as it is accessible to more users.

1.19   Petri Net Modelling

In addition to ODE modelling as a way to measure time-dependent processes is the use of another modelling technique known as Petri Net modelling (Klipp et al., 2009). Petri

Net models consist of three components: places, transitions and arcs, which connect places to transitions (Chaouiya, 2007). A place is an object, such as a metabolite or protein, which represents the resources of the network, which contains either zero or a positive number of "tokens", which represent factors such as the amount of that particular place. Transitions represent events that can change the state of resources, whilst arcs connect places and transitions and thus depict the relationship between a place and a transition (Klipp et al., 2009; Chaouiya, 2007). Thus, transitions determine how and when an interaction (arc) will proceed.

A transition will become active ("fire") if its input place has at least the minimum tokens required by the weight of the arc. Tokens will then appear at the output place connected to the transition, with the number of tokens being determined by the weight of the arc. The distribution of tokens within the Petri Net is called a mark, and determines the state of the model at any given point. The starting distribution, the initial marking, is referred to M_0. Any transitions that can fire (due to having sufficient tokens from their input places) will do so, leading to a new distribution of tokens within the model. This thus changes the marking to M_1, and any new transitions will fire (leading to the sequential marking M_2, and so on). This process has been described as a "token game" (Chaouiya, 2007; Klipp et al., 2009). Very simple examples of Petri Nets are shown in Figure 1.19.1 to clarify and summarise the process:
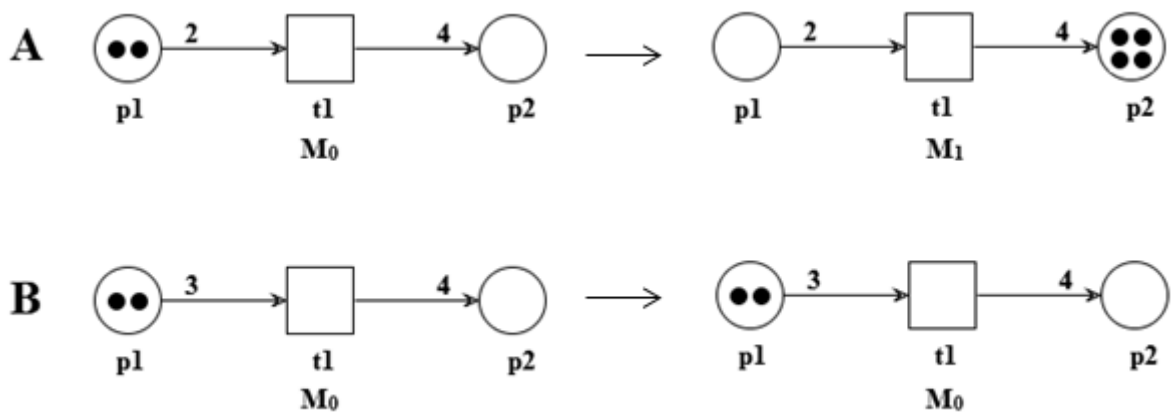
Figure 1.19.1: Examples of Petri Nets.

Places are represented by circles, transitions are represented by squares, and arcs are represented by directed arrows. Small black circles represent tokens, whilst the number above an arc refers to its weight. "M" refers to "marking"; "p" to place; and "t" to transition.

In Figure 1.19.1A above, the arc connecting p1 to t1 has a weight of two, whilst p1 has two tokens. This thus allows t1 to fire, thus transitioning from M_0 to M_1, whilst p2 has four tokens due to the output arc from t1 having a weight of four. However, in Figure 1.19.1B the input arc for t1 has a weight of 3, whilst p1 still only has two tokens. Thus t1 does not fire, and the marking for the Petri Net remains the same. This is of course a very simple example of how Petri Nets can operate, though in reality they are capable of modelling more complex interactions. For example multiple places can be connected to a single transition element, using a logical operator such as "AND". This can for instance be used in cases where, biologically, two proteins are required to cooperatively activate another.

Although classical Petri Nets do not contain time as a variable (Chaouiya, 2007), since their inception researchers have developed extensions to Petri Nets which allow for more in-depth analysis to be carried out. One example is Coloured Petri Nets (CPNs) which, among other things, permit data values to be assigned to tokens, and allow for timed transitions (Chaouiya, 2007). Timed Petri Nets have been successfully applied to biological research, for instance modelling apoptotic signalling events (Chen et al., 2007).

Petri Nets are a promising modelling approach due to their relative simplicity in terms of understanding, as well as the fact that they can be easily described graphically as well as mathematically. Furthermore, the extensions that have been developed since their inception allows for their usage in systems biology (Klipp et al., 2009). However, they are not without issue as there is a lack of graphical tools to visualise large (>100 nodes) models and there is little modularity support for Petri net models (Krepska et al., 2008)

1.20   Modelling Larger Networks: Boolean Modelling

Although small networks may be modelled using quantitative approaches, this is generally less feasible for larger networks. Due to the high computational demand of quantitative approaches and due to the need for detailed kinetic data for the network constituents, for larger networks discrete modelling may be adopted. Discrete modelling simplifies the modelling process by removing the need for parameters such as initial concentrations and kinetic data such as rate constants. Thus analysis of discrete models is not quantitative, but instead is qualitative, relying primarily on network structure and topology (Khan et al., 2014).

Network modelling for larger networks can be applied to a variety of biological phenomena such as metabolic networks (Feist et al., 2007) and protein-protein interaction networks (Jeong et al., 2001). Mathematical graphs are utilised to formalise and represent the networks, with the nodes of the graphs representing biological entities such as proteins or genes, whilst the edges of the graph represent (for example) the interactions between the nodes of the network (Klipp et al., 2009). The edges of the graph may be directed or undirected; for directed edges the interaction consists of ordered node pairs (linked by a directed arrow) whilst undirected edges are represented by unordered node pairs linked by an edge, represented by a line (Klipp et al., 2009). Analysis can be undertaken in both directed and undirected graphs, though analysis of undirected graphs is limited in that you may only see node connectivity. For analysis of gene regulatory networks, directed graphs are most suitable as they show which node is affected in any particular interaction (Liu et al., 2014).

The simplest form of discrete modelling is Boolean modelling (Saadatpour and Albert, 2012). Boolean modelling utilises the principles of Boolean logic: everything is either true (1, ON) or false (0, OFF). Logical operators such as AND, OR and NOT may be used alone or in combination to modify statements/interactions. Under a Boolean model every network constituent will have a value/state of either 1 (ON) or 0 (OFF). Although this is of course not as quantitatively precise as ODE models, such logic is a good representation of certain processes such as gene regulatory networks, since many genes or proteins exhibit ON/OFF styles of function (Khan et al., 2014).

Boolean modelling utilises mathematical graph theory to represent the network. Nodes can represent biological entities such as proteins, whilst edges represent the interactions between those proteins. Interactions within a Boolean model may be represented with different formalisms such as interaction graphs and interaction hypergraphs (Klamt et al., 2006). The difference between an interaction graph and interaction hypergraph is that interaction hypergraphs are capable of connecting more than one node to a downstream node simultaneously. A simple example is clarified in Figure 1.20.1:
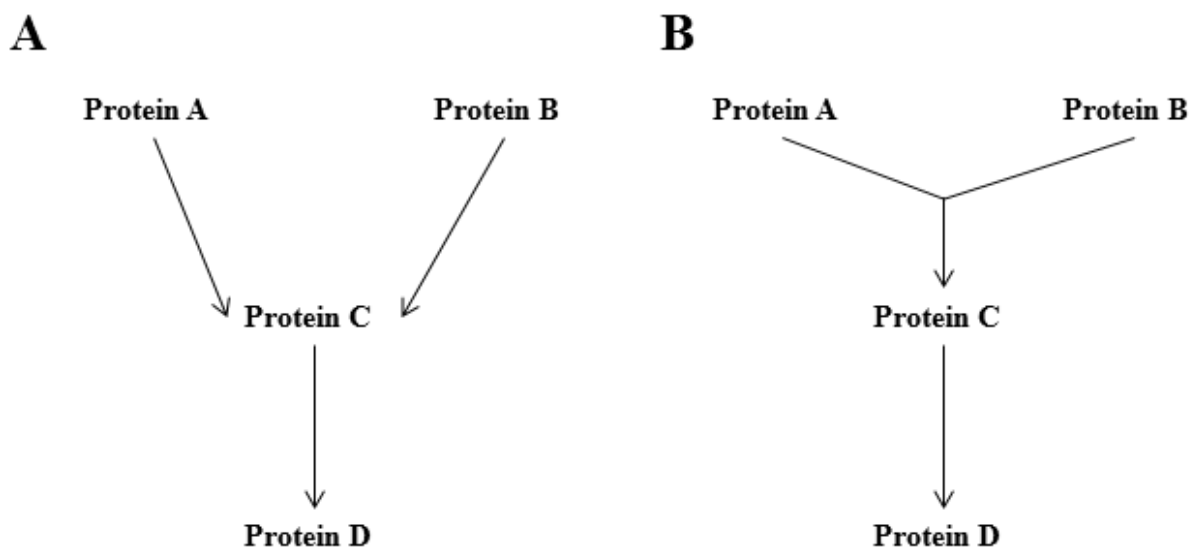
Figure 1.20.1: An interaction graph compared to an interaction hypergraph.
Figure 1.20.1A represents the interaction graph whilst Figure 1.20.1B represents the interaction hypergraph. Adapted from a similar example in Klamt et al. (2006).

In the hypothetical example above in Figure 1.20.1, the biological effect that is intended to be modelled is that both Protein A and Protein B are required for the activation of Protein C, which subsequently activates Protein D. As is clear, the interaction hypergraph (Figure 1.20.1B) represents this interaction more accurately, as it allows for simultaneous interactions of upstream nodes. The interaction graph, however, in Figure 1.20.1A does not present this as accurately and would allow for the activation of Protein C with Protein A or Protein B alone. Thus, Klamt et al. (2006) argued that the interaction hypergraph makes for a more accurate simulation of cellular networks due to the biological reality that proteins often work in tandem with each other to exert their

effects. The allowance of logical operators such as "AND", "OR" and "NOT" further improves model simulation and analysis (Klamt et al., 2006).

Klamt et al. (2007) introduced a MATLAB package called CellNetAnalyzer (CNA), which can be used to create and analyse Boolean models. Two types of models can be created within CNA: mass-flow (suitable to metabolic network) and signal-flow (suitable for gene regulatory networks). Interaction graphs and interaction hypergraphs are accepted into CNA as are logical operators such as AND, OR and NOT which allows for more complex models to be constructed. CNA has been successfully applied to cancer research, for instance a model on the TP53 protein interaction network was generated and analysed in CNA by Tian et al. (2013). Several analyses were undertaken in CNA for this model, such as logical steady state analysis (LSSA), dependency matrix generation, *in silico* knockouts, in addition to wet laboratory verification of model predictions (Tian et al., 2013). Approaches such as LSSA are described in detail in Chapter 2 (Materials and Methods).

The model constructed by Tian et al. (2013) showed high accuracy (up to 71%), demonstrating the power and usefulness of CNA. A semi-quantitative algorithm (called the signal transduction score flow algorithm, STSFA) that superimposes microarray and/or ChIP-seq onto a network model (Isik et al., 2012) was later applied to the TP53 model generated by Tian et al. (2013), and demonstrated improved predictive power over LSSA (Hussain et al., 2014). The TP53 model was later expanded to consider 260 nodes and 980 interactions, with this expanded model again showing accuracy of up to 71% when compared to microarray data (Hussain et al., 2015).

Boolean modelling as a whole offers many advantages. The simplification of interactions (down to a simple ON or OFF as opposed to exact kinetic mechanisms) requires only a low level of computational demand, which in turn allows for the modelling of much larger networks than is generally feasible for ODE models. Though not as quantitatively precise as ODE models, the advantage of Boolean models through the ability to capture large networks and the possibility of semi-quantitative analysis

through the use of algorithms such as the STSFA highlights their strengths and usefulness (Albert and Othmer, 2003).

1.21 Steps of Model Development

Regardless of the modelling approach used, there are several key steps towards model development that are undertaken within systems biology: network construction and visualisation, network analysis, and wet laboratory validation of model predictions (Wang, 2010). Model construction refers to collating the known signalling dynamics of the target system in question. This may be carried out through multiple approaches such as integration of high-throughput datasets, reverse engineering of genome-wide studies, or use of curated databases (Wang, 2010; Ross et al., 2013).

Model visualisation employs various different programs to visualise the network once it has been constructed. Model visualisation is useful not only for providing an overview of the network, but also for the fact that the human mind is capable of leaps of intuition (Woolley and Kostopoulou, 2013). When a network is visualised, rather than held as an abstract thought, it can aid in analysis through pattern recognition and identification of overarching themes and trends.

Visualisation of the network can be carried out in different ways, depending on the nature of the model and goals of the visualisation. Small networks can be visualised in in-depth detail, allowing for detailed examination of individual interactions. Larger networks, however, are generally only seen on a larger scale, seeing overall trends within the model. Networks are generally depicted in a static manner, though there is an increasing drive to develop dynamic visualisations of models. For example, a model consisting of multiple interactions between two nodes depending on an outside variable such as time or cell type may have colour-coded interactions (Wang, 2010). A versatile, popular and open-source program used to visualise models is Cytoscape (Cytoscape, 2016), not only for its visualisation capabilities but also its plug-ins that allow for extension of its function and different types of analysis to be performed such as

algorithm application (Shannon et al., 2003). Cytoscape was used to visualise the TP53 models discussed previously (Hussain et al., 2015; Tian et al., 2013).

Model analysis employs the use of various mathematical and computational testing to the model. Algorithms, logical analysis, and *in silico* knockouts can be performed, which will all generate predictions as to how the system would behave *in vivo* and thus provide a series of potential experiments upon which the model could be validated. Ultimately validation of these predictions would assess the reliability, accuracy, and predictive power of the model, which may in turn lead to the identification of novel therapeutic targets, assuming the model is linked to disease.

1.22   Applications of Computational Modelling to Cancer Research

The use of computational modelling in cancer research is a recently established practice. With increasing knowledge of protein signalling networks, the complexity underlying drug response and diverse patient responses to treatment, computational biology is increasingly required to integrate this data and provide novel insight into improving therapy.

The tumour suppressor protein TP53 is widely recognised as one of the most important proteins in cancer research. The "guardian of the genome" plays a crucial role in suppressing overproliferation of cells, and with its pathways represents a major target for the development of novel therapeutics. However, the complexity of its signalling provides complications to understanding its network dynamics and development of therapies. To this end, computational approaches to understand TP53 have been developed, such as an integrated interactome model that aimed to encapsulate its signalling dynamics (Tian et al., 2013).

The work by Tian et al. (2013) generated a large-scale model consisting of 203 nodes representing genes or proteins, in addition to an input node of DNA damage, and two output nodes of apoptosis and cellular senescence. Within this model a variety of analyses could be employed such as analysis of the relationships between all model

constituents (and how these relationships change followed perturbations such as an *in silico* TP53 knockout) in addition to genome-wide validation of model predictions through comparison to microarray data. This model ultimately showed accurate prediction rates (as stated previously, up to 71%) and provided several potentially novel predictions as to how the network would change following the loss of TP53. Thus, with the laboratory validation of these predictions novel insight into TP53 signalling was obtained.

Computational modelling has also been applied to the glucocorticoid receptor and its signalling. Numerous approaches have been carried out to understand glucocorticoid signalling, including expression profiling of leukaemia patients, microarray analysis on a genome-wide scale, and transcriptional studies (Chen et al., 2010). Chen et al. (2010) identified a gap in the application of computational biology to GR research and thus developed a small-scale kinetic model of glucocorticoid-induced gene regulation. Two types of models were developed: a direct model (for genes that are transcriptional targets of GR) and an indirect model (for genes indirectly regulated by GR).

Due to the fact that these models were kinetic models, detailed information of the mechanisms underlying the regulation and knowledge of parameters such as transcription rates were required. Thus Chen et al. (2010) first performed detailed molecular analysis on the mRNA and protein levels of glucocorticoid-target genes under investigation at various time points. Following this, parameters were estimated to create integrated models of both direct and indirect regulation, and for glucocorticoid-sensitive and glucocorticoid-resistant cells. Model simulations generally displayed agreement with experimental data, thus demonstrating the reliability of the models. The models ultimately identified BMF (Bcl2 modifying factor) as a novel direct target for GR modulation, as the wet laboratory results had a closer fit to the direct model simulation results than the indirect model simulation results. This identification was confirmed by a preliminary chromatin immunoprecipitation experiment, which identified occupancy of the GR on the BMF gene.

The paper by Chen et al. (2010) is just one example of many of the application of computational biology to cancer research and glucocorticoids/nuclear receptors. Other examples include computational screening of potential ligands for nuclear receptors, structural simulations to elucidate mechanisms behind cofactor interactions or particularly important amino acid residues, and *in silico* methods to identify toxicity levels of nuclear receptor modulators (Ai et al., 2009). Another approach utilised microarray data generated from rats following treatment with methylprednisolone, and built on previous work to generate mechanistic models of the pharmacokinetic/pharmacodynamic properties of corticosteroid-responsive genes (Jin et al., 2003). Different models were developed for the type of regulation (such as induction and repression), and the approach by Jin et al. (2003) provided insight into the mechanics of the global effects of corticosteroids.

However, despite the applications above, to date no detailed model of the glucocorticoid receptor protein interaction network (similar to the TP53 network described previously) has been developed. Given the high predictive power demonstrated by both TP53 models mentioned previously (Hussain et al., 2015; Tian et al., 2013), as well as the possibility of semi-quantitative analysis via the STSFA, herein an initial GR interactome model has been developed using a similar approach to that used to generate the TP53 models.

1.23   Hypothesis and Aims of Research

The overarching aim of this research is to provide insights into the routes by which the microenvironment may exert its chemoprotective effects, and also to increase current understanding of glucocorticoid receptor signalling. This will be investigated through a branched approach of wet laboratory experiments and computational modelling.

Specifically, a global approach of interactome generation similar to Tian et al. (2013) will be undertaken, with the model being analysed through qualitative and semi-quantitative approaches and validated using laboratory and clinical data.

This global modelling approach will be complemented by a detailed molecular analysis of the effects of the microenvironment (simulated by bone marrow cell-conditioned media (CM)) and the chemotherapeutic drugs dexamethasone and etoposide on glucocorticoid-sensitive (C7-14) and glucocorticoid-resistant (C1-15) ALL cell lines. The effect of these treatments will be analysed at the molecular level through approaches such as western blotting, chromatin immunoprecipitation and cell viability assays, investigating pathways linked to cellular processes such as apoptosis, autophagy and necroptosis, with the overall effect on cells being validated at the functional level through approaches such as flow cytometry.

Ultimately, it is envisaged that this branched approach will provide increased insight into the role of the microenvironment in nurturing chemoresistance, and that an increased understanding of glucocorticoid receptor signalling will be obtained.

Chapter 2   Materials and Methods

2.1   Wet Laboratory Approaches

2.1.1   Table of Materials

Numerous materials from various companies have been utilised throughout the production of this thesis:

Table 2.1.1: Reagents and consumables utilised throughout research.

Product Name	Supplier	Catalogue Number
Bio-Rad Protein Assay Kit	Bio-Rad	500-0001
BioScript™ Reverse Transcriptase Kit	Bioline	BIO-27036
CellTiter 96® Aqueous MTS Reagent Powder	Promega	G1112
Dexamethasone	Sigma-Aldrich	D1756
Dextran Coated Charcoal FBS	Hyclone	SH30068.03
Diaminoethanetetra-acetic acid disodium salt (EDTA)	Fisher Scientific	10020140
Dynabeads® Protein A for Immunoprecipitation	ThermoFisher Scientific	10002D
Dynabeads® Protein G for Immunoprecipitation	ThermoFisher Scientific	10004D
Etoposide	Sigma-Aldrich	E1383
Foetal Bovine Serum (FBS)	Labtech	FB-1090/500
PageRuler Prestained Protein Ladder	ThermoFisher Scientific	26616
Penicillin/Streptomycin	Labtech	LM-A4118/100
Phenazine methosulfate	Sigma-Aldrich	P9625-500MG

(PMS)		
Proteinase K	Sigma-Aldrich	P2308-5MG
ProtoGel (30%)	National Diagnostics	EC-890
QIAquick PCR purification kit	QIAGEN	28104
QIAshredder	QIAGEN	79654
Ribonuclease A (RNase A)	Sigma-Aldrich	R5500-10MG
RNeasy Plus Mini Kit	QIAGEN	74134
Roswell Park Memorial Institute-1640 (RPMI-1640)	Scientific Laboratory Supplies	LZ12-167F24
SensiFAST™ SYBR® No-ROX Kit	Bioline	BIO-98005
SuperSignal West Femto Chemiluminescent Substrate	ThermoFisher Scientific	34095
SuperSignal West Pico Chemiluminescent Substrate	ThermoFisher Scientific	34080
Trypan Blue Solution	Sigma-Aldrich	T8154-20ML
Vybrant® FAM Caspase-8 Assay Kit, for flow cytometry	ThermoFisher Scientific	V35119

2.1.2   Table of Antibodies

Table 2.1.2 shows the antibodies used throughout the production of this thesis for both Western blotting and chromatin immunoprecipitation.

Table 2.1.2: Antibodies used throughout research.

Antibody	Supplier	Catalogue Number
Actin Antibody	Abcam	AB8227
Beclin-1 Antibody	Abcam	AB15417
Caspase-3 Antibody	New England Biolabs	9662S

Buffer			
GR (Phospho S211) Antibody	Abcam		ab55189
GR (Phospho S226) Antibody	Abcam		ab93104
GR monoclonal antibody (for chromatin immunoprecipitation)	Diagenode		C15200010 (MAb-010-050)
RIPK1 Antibody	Santa Cruz Biotechnology		SC-7881
Total GR Antibody (Westerns)	Santa Cruz Biotechnology		SC-8992

2.1.3 Table of Buffers

Buffers used throughout the research presented in this thesis, and their compositions, are shown in Table 2.1.3:

Table 2.1.3: List of buffers and their composition.

Buffer	Composition
0.1% PBS/Tween (PBST)	100ml 1xPBS, 900ml dH2O, 1ml Tween-20
10X SDS Running Buffer	247.7mM Tris, 1.9M Glycine, 35mM SDS
10X Western Transfer Buffer	272.4mM Tris, 1.5M Glycine
1XSDS Running Buffer	10% 10xSDS Running Buffer, 90% dH$_2$O
1XWestern Transfer Buffer	10% 10xWTB, 20% Methanol, 70% dH$_2$O
3XSDS Loading Buffer	187mM Tris, 30% Glycerol, 6% SDS,15% 2-mercaptoethanol, 0.01% bromophenol blue
ChIP Blocking	0.5% Bovine Serum Albumin w/v in PBS

Solution	
ChIP Buffer 1	10% Glycerol, 0.5% Igepal CA-630 0.25% Triton X-100, 50mM Hepes-KOH; pH 7.5, 1mM EDTA, 140mM NaCl
ChIP Buffer 2	10mM Tris-HCl; pH 8.0, 0.5mM EGTA, 1mM EDTA, 200mM NaCl
ChIP Buffer 3	0.5% N-lauroylsarcosine, 0.1% Sodium Deoxycholate, 0.5mM EGTA, 1mM EDTA, 100mM NaCl, 10mM Tris-HCl; pH 8.0
ChIP Elution Buffer	50mM Tris-HCl; pH 8, 100mM EDTA and 1% SDS w/v
Formaldehyde Solution	11% Formaldehyde, 50mM Hepes-KOH, 0.5mM EGTA, 1mM EDTA, 100mM NaCl
High Salt Lysis Buffer (HSLB)	45mM HEPES pH 7.5, 400mM NaCl, 1mM EDTA, 10% Glycerol, 0.5% NP-40 1mM DTT, 1mM PMSF, 1µg/ml protease inhibitors (leupeptin, pepstin, and aprotinin) 2mM NaOV, 20mM BGP, 5mM NaPPi
Phosphate Buffered Saline (PBS)	170mM NaCl, 3.3mM KCL, 1.8mM Na2HPO4, 10.6mM KH2PO4. Adjusted to pH 7.4 using concentrated HCL or NaOH.
Proteinase K Reconstitution Solution	50mM Tris-HCl pH 8.0 and 10mM CaCl2
RIPA Wash Buffer	1% Igepal CA-630, 0.7% Sodium Deoxycholate, 1mM EDTA, 500mM LiCl, 50mM Hepes-KOH; pH 7.5
TE Buffer	10mM Tris-HCl; pH 7.5, 1mM EDTA
Tris Buffered Saline (TBS)	150mM NaCl, 20mM Tris-HCl; pH 7.6
Western Blocking Solution	5% milk powder in PBS
Western Stripping Buffer	100mM 2-Mercaptoethanol, 2% SDS, 65.5mM Tris Hcl. pH 6.7

2.1.4   Cell Culture and Cell Lines

Two acute lymphoblastic leukaemia cell lines have been utilised throughout the wet laboratory half of this research, CEM-C1-15 (C1-15, resistant to glucocorticoid treatment) and CEM-C7-14 (C7-14, sensitive to glucocorticoid treatment). These cell lines are subclones of a parental ALL cell line CCRF-CEM, which was isolated from a female ALL patient aged four in 1964 (Foley et al., 1965).

From the original CCRF-CEM cell line, glucocorticoid-sensitive and glucocorticoid-resistant cell lines were isolated by Thompson's group through mutagenesis and incubation with dexamethasone (Norman and Thompson, 1977; Medh et al., 1998). (Harmon and Thompson, 1981). C7-14 and C1-15 are glucocorticoid-sensitive and glucocorticoid-resistant cell lines respectively that were isolated by Thompson's group (Medh et al., 2003).

Cells were grown in RPMI-1640 (Lonza) supplemented with 1% penicillin/streptomycin (Labtech), 1% l-glutamine (Labtech), and 10% foetal bovine serum (FBS, Labtech). Cells were kept in vented $25cm^3$ T25 flash (Fisher) and maintained in a humidified incubator at 5% CO_2 and 37°C, at a confluence suitable for CEM cells (less than $2x10^6$ cells/ml) (ATCC, 2016). Cells were subcultured every two to three days as and when required depending on cell confluence. Cell culture was at all times carried out in a Class II Biological Safety Cabinet for a sterile environment.

An important note to consider is that prior to any experiments, cell culture media was replaced with media that had been supplemented with dextran-coated charcoal treated FBS (DCC-FBS) instead of normal FBS and maintained in this media until the experiment's completion. The reason for this is that it has been shown that certain FBS constituents interfere with response to hormone treatment (such as a glucocorticoid), and that these causative constituents are absorbed by the charcoal (Chen, 1967). Furthermore, due to the fact that some treatments contain combination of hormone treatment with other treatments (such as combination dexamethasone and etoposide), all

cells for all treatments for all experiments were grown in media supplemented with DCC-FBS, to ensure experimental consistency.

2.1.5 Subculture of Leukaemia Cells

Cells were collected into a sterile 30ml universal tube and spun at 2000RPM for three minutes in a centrifuge to pellet living cells. After this the supernatant was aspirated and the pellet was resuspended in fresh media. The amount added to a pellet varied depending on how many cells were required for future experiments but for general subculture 5ml of fresh media was used to resuspend the pellet, after which 1ml was taken and transferred to a new flask containing 9ml of fresh media (therefore a 1:5 split from original confluence).

2.1.6 Freezing and Thawing of Leukaemia Cells

For freezing, cells were pelleted as per subculture, and 2ml of 10% DMSO (dimethyl sulphoxide)/FBS was used to resuspend the pellet following supernatant aspiration. The 2ml suspension was then split into two cryovials, which were stored first at -80°C, and subsequently transferred to liquid nitrogen for long-term storage.

For thawing, cryovials were rapidly thawed and immediately placed inside a T25 flask containing 13ml of fresh, pre-warmed media. The following day, the cells were collected, centrifuged as per subculture, and then the entirety of the pellet was transferred to a new flask containing 10ml fresh media. This was to remove the cytotoxic effect of DMSO on the cells.

2.1.7 Cell Counting

In order to seed specific numbers of cells for subsequent experiments, cell counting via haemocytometers (Labtech) was used to estimate the current number of cells and to calculate the dilution volume.
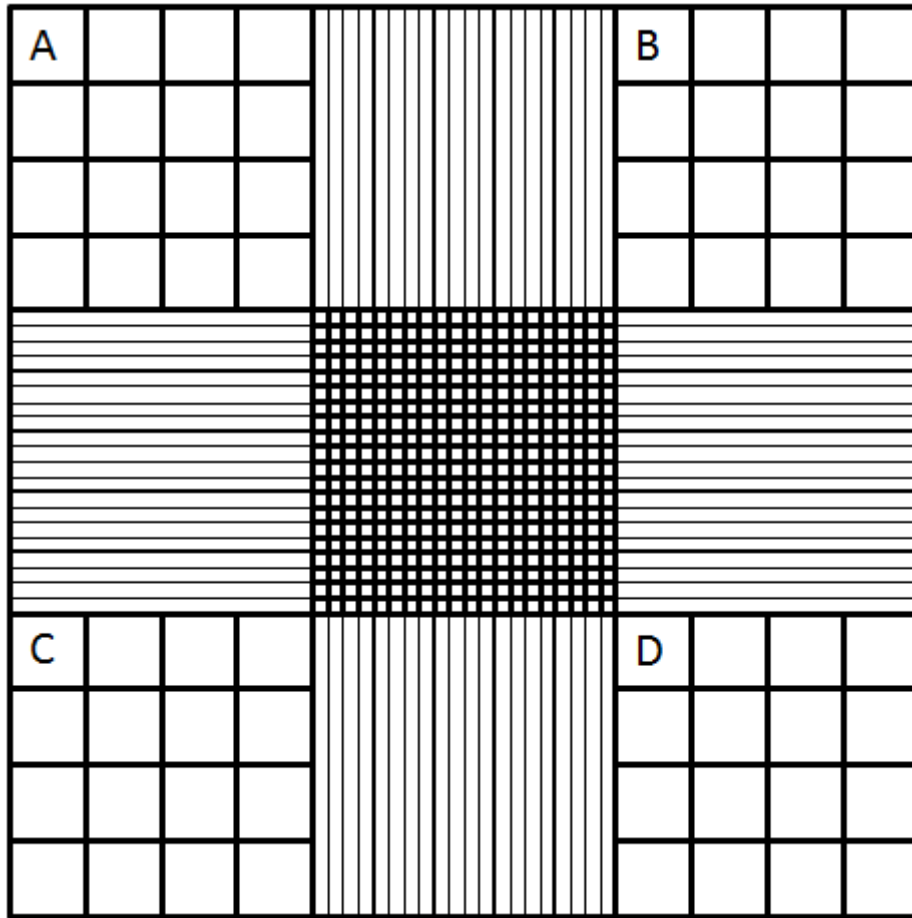
Figure 2.1.1: Typical layout of a haemocytometer.

Figure 2.1.1 above shows the typical layout of a haemocytometer when viewed under the microscope. 10µl of cells were taken from the flask and loaded onto the haemocytometer and cells were counted in the four corner squares A, B, C and D as shown above in Figure 2.1.1. An average of these four corner squares was then obtained and the current number of cells per ml was calculated by multiplying the average by 10^4.

After the approximate number of cells/ml was calculated, the equation $C_1V_1 = C_2V_2$ could be used to calculate how to obtain an appropriate number of cells/ml for specific subsequent experiments. Cell counting was often performed in tandem with the trypan blue exclusion assay (see Section 2.1.8) to count only living cells. This was particularly important for counting prior to cell viability assays.

2.1.8   Trypan Blue Exclusion Assay

Trypan blue may be used as an assay to assess viability of cells, and to give approximate ratios of alive/dead cells within a cell suspension. Thus, trypan blue allows for a base measurement of how healthy a cellular population is, and can be used prior to other assays (such as cytotoxic assays) to ensure that equal numbers of viable cells are seeded between different independent experimental replicates. To perform trypan blue, 10µl of cell suspension was mixed with 10µl of the trypan blue solution (Sigma-Aldrich) in an Eppendorf tube. 10µl of this mixture was then loaded onto the haemocytometer (depicted previously in Figure 2.1.1, Page 78). Living cells exclude the trypan blue dye (and thus appear colourless) whilst dead cells are stained blue.

2.1.9   MTS Assay

Cells were seeded at a concentration of approximately 40,000 cells per well (chosen based on previous experience and optimisation experiments), dosed with the relevant concentration of each drug or treatment, and incubated for the indicated length of time. MTS and PMS reagents were prepared according to the manufacturer's instructions (2mg/ml in sterile PBS for MTS and 0.92 mg/ml in sterile PBS for PMS), and following the end of incubation, the MTS working solution was prepared according to the manufacturer's instructions (100µl PMS per 2ml MTS). 20µl of the MTS working solution was then added to 100µl of the cell suspension. Each treatment was plated in triplicate onto a 96-well plate, providing three values for each treatment per experiment.

Following addition of MTS working solution, the plate was incubated for four hours in a humidified Galaxy CO_2 incubator at 5% CO_2 and 37°C. After this, the plate was read on a Thermo Labsystems Multiskan Ascent plate reader at both 490nm (suitable to detect the dye) and 690nm (as a reference wavelength to correct for background) (Promega, 2012). Following this, the 690nm reading was subtracted from the 490nm reading, and then all readings expressed relative to the Control/untreated cells to provide a percentage of cell growth.

2.1.10 Conditioned Media Generation

A bone marrow stromal cell line, HS5, was grown in RPMI-1640 media supplemented with 10% FBS, 1% l-glutamine and 1% penicillin/streptomycin. After growing cells to confluence, they were washed twice with PBS and incubated with 15ml of serum-free RPMI for 48 hours at 37°C and 5% CO_2. After 48 hours the cell-conditioned medium was collected, centrifuged at 1000g for 10 minutes to remove debris, and the supernatant was stored as conditioned media (CM) generated from bone marrow stromal fibroblasts.

2.1.11 Quantitative Reverse Transcriptase Polymerase Chain Reaction

For quantitative reverse transcriptase polymerase chain reaction (qRT-PCR) experiments, cells were seeded at a concentration of approximately $1x10^6$ cells per well, dosed with the appropriate concentration of treatments, and left to incubate at 37°C and 5% CO_2 for the duration of the treatment. After this, cells were collected, pelleted as per subculture, and the pellet was washed with cold PBS following aspiration of the supernatant. After this, the PBS was aspirated and the RNA was extracted from the cells using the RNeasy Plus Mini Kit (QIAGEN), in combination with QIAshredder (QIAGEN), following the manufacturer's instructions (QIAGEN, 2013). In brief, Buffer RLT was added to pellets after which samples were passed through QIAshredder columns to homogenise them. Following this lysates were passed through gDNA eliminator columns, mixed with equal volumes of 70% ethanol, loaded onto an RNeasy spin column and centrifuged, then washed with Buffer RW1 and centrifuged again. Buffer RPE was then used to wash cells twice with a centrifugation step following each wash. Columns were then dry spun and RNA eluted via centrifugation after the addition of RNase-free water.

Following extraction of RNA, its concentration was determined using NanoDrop 2000 Spectrophotometer and approximately 1μg was converted to cDNA using BioScript™ Reverse Transcriptase kit using an Oligo (dT)$_{18}$ primer, following the manufacturer's instructions (Bioline, 2016). In brief, Oligo (dT)$_{18}$, dNTPs, and DEPC-treated water

were mixed with the RNA sample on ice, after which samples were incubated at 70°C for five minutes and then chilled on ice for one minute. 5xRT Buffer, RNase Inhibitor, BioScript Reverse Transcriptase and DEPC-treated water were mixed together and added, after which samples were incubated at 42°C for thirty minutes, then reactions were terminated at 85°C for five minutes followed by chilling on ice.

After cDNA conversion, cDNA was diluted to a concentration of approximately 25ng/µl to allow for each PCR reaction to have 100ng per well (4µl DNA in a 20µl total reaction). DNA was then subjected to qPCR using the SensiMix™ SYBR® No-ROX Kit with the data analysis being performed in Opticon Monitor 3.1. After an initial denaturation step at 95°C, qPCR cycling conditions involved a ten-second incubation at 95°C (denaturation), followed by an incubation at a lower temperature that was dependent on primer melting temperature (typically two degrees lower) in a process known as annealing for ten seconds, whilst the third step of the cycle involved incubation at 72°C for ten seconds (extension). Approximately 45 cycles were used per qPCR experiment. After cycle completion the samples were held at 72°C for five minutes, and a melting curve analysis was then performed from 72-95°C, obtaining a reading at every degree. Data was analysed via the standard curve method. Primers utilised for qPCR are listed in Table 2.1.4:

Table 2.1.4: Primers for qRT-PCR.

Gene	Primer	Sequence
BECN1	Forward	TTG GCA CAA TCA ATA ACT TCA GGC
	Reverse	CCG TAA GGA ACA AGT CGG TAT CTC
BIRC3	Forward	ACT TGA ACA GCT GCT ATC CAC ATC
	Reverse	GTT GCT AGG ATT TTT CTC TGA ACT GTC
RIPK1	Forward	TGG AAA AGG CGT GAT ACA CA
	Reverse	GAC TTC TCT GTG GGC TTT GC
RPL19	Forward	ATG TAT CAC AGC CTG TAC CTG
	Reverse	TTC TTG GTC TCT TCC TCC TTG

To complement the primer sequences, amplicon regions for each gene are shown in the following figures:

```
ATGGAAGGGTCTAAGACGTCCAACAACAGCACCATGCAGGTGAGCTTCGTGTGCCAGCGCTGCAGCCAGCCC
CTGAAACTGGACACGAGTTTCAAGATCCTGGACCGTGTCACCATCCAGGAACTCACAGCTCCATTACTTACCAC
AGCCCAGGCGAAACCAGGAGAGACCCAGGAGGAAGAGACTAACTCAGGAGAGGAGCCATTTATTGAAACTC
CTCGCCAGGATGGTGTCTCTCGCAGATTCATCCCCCCAGCCAGGATGATGTCCACAGAAAGTGCCAACAGCTT
CACTCTGATTGGGGAGGCATCTGATGGCGGCACCATGGAGAACCTCAGCCGAAGACTGAAGGTCACTGGGG
ACCTTTTTGACATCATGTCGGGCCAGACAGATGTGGATCACCCACTCTGTGAGGAATGCACAGATACTCTTTTA
GACCAGCTGGACACTCAGCTCAACGTCACTGAAAATGAGTGTCAGAACTACAAACGCTGTTTGGAGATCTTAG
AGCAAATGAATGAGGATGACAGTGAACAGTTACAGATGGAGCTAAAGGAGCTGGCACTAGAGGAGGAGAG
GCTGATCCAGGAGCTGGAAGACGTGGAAAAGAACCGCAAGATAGTGGCAGAAAATCTCGAGAAGGTCCAGG
CTGAGGCTGAGAGACTGGATCAGGAGGAAGCTCAGTATCAGAGAGAATACAGTGAATTTAAACGACAGCAG
CTGGAGCTGGATGATGAGCTGAAGAGTGTTGAAAACCAGATGCGTTATGCCCAGACGCAGCTGGATAAGCTG
AAGAAAACCAACGTCTTTAATGCAACCTTCCACATCTGGCACAGTGGACAGT<span style="color:red">TTGGCACAATCAATAACTTCA</span>
<span style="color:red">GGC</span><span style="color:blue">TGGGTCGCCTGCCCAGTGTTCCCGTGGAATGGAATGAGATTAATGCTGCTTGGGGCCAGACTGTGTTGC</span>
<span style="color:blue">TGCTCCATGCTCTGGCCAATAAGATGGGTCTGAAATTTCA</span><span style="color:green">GAGATACCGACTTGTTCCTTACGG</span>AAACCATTCA
TATCTGGAGTCTCTGACAGACAAATCTAAGGAGCTGCCGTTATACTGTTCTGGGGGGTTGCGGTTTTTCTGGG
ACAACAAGTTTGACCATGCAATGGTGGCTTTCCTGGACTGTGTGCAGCAGTTCAAAGAAGAGGTTGAGAAAG
GCGAGACACGTTTTTGTCTTCCCTACAGGATGGATGTGGAGAAAGGCAAGATTGAAGACACAGGAGGCAGTG
GCGGCTCCTATTCCATCAAAACCCAGTTTAACTCTGAGGAGCAGTGGACAAAAGCTCTCAAGTTCATGCTGAC
GAATCTTAAGTGGGGTCTTGCTTGGGTGTCCTCACAATTTTATAACAAATGA
```

Figure 2.1.2: Amplicon region for *BECN1*.

The forward primer sequence is coloured in red, whilst the reverse complement of the reverse primer is coloured in green. Nucleotides between the two primer sequences are coloured in blue. The full sequence shown is of the nucleotide sequence for *BECN1*. Sequence obtained via CCDS from NCBI Gene.

ATGAACATAGTAGAAAACAGCATATTCTTATCAAATTTGATGAAAAGCGCCAACACGTTTGAACTGAAATACG
ACTTGTCATGTGAACTGTACCGAATGTCTACGTATTCCACTTTTCCTGCTGGGGTTCCTGTCTCAGAAAGGAGT
CTTGCTCGTGCTGGTTTCTATTACACTGGTGTGAATGACAAGGTCAAATGCTTCTGTTGTGGCCTGATGCTGGA
TAACTGGAAAAGAGGAGACAGTCCTACTGAAAAGCATAAAAAGTTGTATCCTAGCTGCAGATTCGTTCAGAG
TCTAAATTCCGTTAACAACTTGGAAGCTACCTCTCAGCCTACTTTTCCTTCTTCAGTAACAAATTCCACACACTCA
TTACTTCCGGGTACAGAAAACAGTGGATATTTCCGTGGCTCTTATTCAAACTCTCCATCAAATCCTGTAAACTCC
AGAGCAAATCAAGATTTTTCTGCCTTGATGAGAAGTTCCTACCACTGTGCAATGAATAACGAAAATGCCAGAT
TACTTACTTTTCAGACATGGCCATTGACTTTTCTGTCGCCAACAGATCTGGCAAAAGCAGGCTTTTACTACATA
GGACCTGGAGACAGAGTGGCTTGCTTTGCCTGTGGTGGAAAATTGAGCAATTGGGAACCGAAGGATAATGCT
ATGTCAGAACACCTGAGACATTTTCCCAAATGCCCATTTATAGAAAATCAGCTTCAAGACACTTCAAGATACAC
AGTTTCTAATCTGAGCATGCAGACACATGCAGCCCGCTTTAAAACATTCTTTAACTGGCCCTCTAGTGTTCTAGT
TAATCCTGAGCAGCTTGCAAGTGCGGGTTTTTATTATGTGGGTAACAGTGATGATGTCAAATGCTTTTGCTGTG
ATGGTGGACTCAGGTGTTGGGAATCTGGAGATGATCCATGGGTTCAACATGCCAAGTGGTTTCCAAGGTGTG
AGTACTTGATAAGAATTAAAGGACAGGAGTTCATCCGTCAAGTTCAAGCCAGTTACCCTCATCTACTTGAACA
GCTGCTATCCACATCAGACAGCCCAGGAGATGAAAATGCAGAGTCATCAATTATCCATTTTGAACCTGGAGAA
GACCATTCAGAAGATGCAATCATGATGAATACTCCTGTGATTAATGCTGCCGTGGAAATGGGCTTTAGTAGAA
GCCTGGTAAAACAGACAGTTCAGAGAAAAATCCTAGCAACTGGAGAGAATTATAGACTAGTCAATGATCTTGT
GTTAGACTTACTCAATGCAGAAGATGAAATAAGGGAAGAGGAGAGAGAAAGAGCAACTGAGGAAAAAGAAT
CAAATGATTTATTATTAATCCGGAAGAATAGAATGGCACTTTTTCAACATTTGACTTGTGTAATTCCAATCCTGG
ATAGTCTACTAACTGCCGGAATTATTAATGAACAAGAACATGATGTTATTAAACAGAAGACACAGACGTCTTT
ACAAGCAAGAGAACTGATTGATACGATTTTAGTAAAAGGAAATATTGCAGCCACTGTATTCAGAAACTCTCTG
CAAGAAGCTGAAGCTGTGTTATATGAGCATTTATTTGTGCAACAGGACATAAAATATATTCCCACAGAAGATG
TTTCAGATCTACCAGTGGAAGAACAATTGCGGAGACTACAAGAAGAAAGAACATGTAAAGTGTGTATGGACA
AAGAAGTGTCCATAGTGTTTATTCCTTGTGGTCATCTAGTAGTATGCAAAGATTGTGCTCCTTCTTTAAGAAAG
TGTCCTATTTGTAGGAGTACAATCAAGGGTACAGTTCGTACATTTCTTTCATGA

Figure 2.1.3: Amplicon region for *BIRC3*.

The forward primer sequence is coloured in red, whilst the reverse complement of the reverse primer is coloured in green. Nucleotides between the two primer sequences are coloured in blue. The full sequence shown is of the nucleotide sequence for *BIRC3*. Sequence obtained via CCDS from NCBI Gene.

ATGCAACCAGACATGTCCTTGAATGTCATTAAGATGAAATCCAGTGACTTCCTGGAGAGTGCAGAACTGGACA
GCGGAGGCTTTGGGAAGGTGTCTCTGTGTTTCCACAGAACCCAGGGACTCATGATCATGAAAACAGTGTACA
AGGGGCCCAACTGCATTGAGCACAACGAGGCCCTCTTGGAGGAGGCGAAGATGATGAACAGACTGAGACAC
AGCCGGGTGGTGAAGCTCCTGGGCGTCATCATAGAGGAAGGGAAGTACTCCCTGGTGATGGAGTACATGGA
GAAGGGCAACCTGATGCACGTGCTGAAAGCCGAGATGAGTACTCCGCTTTCTGTAAAAGGAAGGATAATTTT
GGAAATCATTGAAGGAATGTGCTACTTACATGGAAAAGGCGTGATACACAAGGACCTGAAGCCTGAAAATAT
CCTTGTTGATAATGACTTCCACATTAAGATCGCAGACCTCGGCCTTGCCTCCTTTAAGATGTGGAGCAAACTGA
ATAATGAAGAGCACAATGAGCTGAGGGAAGTGGACGGCACCGCTAAGAAGAATGGCGGCACCCTCTACTAC
ATGGCGCCCGAGCACCTGAATGACGTCAACGCAAAGCCCACAGAGAAGTCGGATGTGTACAGCTTTGCTGTA
GTACTCTGGGCGATATTTGCAAATAAGGAGCCATATGAAAATGCTATCTGTGAGCAGCAGTTGATAATGTGCA
TAAAATCTGGGAACAGGCCAGATGTGGATGACATCACTGAGTACTGCCCAAGAGAAATTATCAGTCTCATGA
AGCTCTGCTGGGAAGCGAATCCGGAAGCTCGGCCGACATTTCCTGGCATTGAAGAAAAATTTAGGCCTTTTTA
TTTAAGTCAATTAGAAGAAAGTGTAGAAGAGGACGTGAAGAGTTTAAAGAAAGAGTATTCAAACGAAAATGC
AGTTGTGAAGAGAATGCAGTCTCTTCAACTTGATTGTGTGGCAGTACCTTCAAGCCGGTCAAATTCAGCCACA
GAACAGCCTGGTTCACTGCACAGTTCCCAGGGACTTGGGATGGGTCCTGTGGAGGAGTCCTGGTTTGCTCCTT
CCCTGGAGCACCCACAAGAAGAGAATGAGCCCAGCCTGCAGAGTAAACTCCAAGACGAAGCCAACTACCATC
TTTATGGCAGCCGCATGGACAGGCAGACGAAACAGCAGCCCAGACAGAATGTGGCTTACAACAGAGAGGAG
GAAAGGAGACGCAGGGTCTCCCATGACCCTTTTGCACAGCAAAGACCTTACGAGAATTTTCAGAATACAGAG
GGAAAAGGCACTGCTTATTCCAGTGCAGCCAGTCATGGTAATGCAGTGCACCAGCCCTCAGGGCTCACCAGCC
AACCTCAAGTACTGTATCAGAACAATGGATTATATAGCTCACATGGCTTTGGAACAAGACCACTGGATCCAGG
AACAGCAGGTCCCAGAGTTTGGTACAGGCCAATTCCAAGTCATATGCCTAGTCTGCATAATATCCCAGTGCCT
GAGACCAACTATCTAGGAAATACACCCACCATGCCATTCAGCTCCTTGCCACCAACAGATGAATCTATAAAATA
TACCATATACAATAGTACTGGCATTCAGATTGGAGCCTACAATTATATGGAGATTGGTGGGACGAGTTCATCA
CTACTAGACAGCACAAATACGAACTTCAAAGAAGAGCCAGCTGCTAAGTACCAAGCTATCTTTGATAATACCA
CTAGTCTGACGGATAAACACCTGGACCCAATCAGGGAAAATCTGGGAAAGCACTGGAAAAACTGTGCCCGTA
AACTGGGCTTCACACAGTCTCAGATTGATGAAATTGACCATGACTATGAGCGAGATGGACTGAAAGAAAGG
TTTACCAGATGCTCCAAAAGTGGGTGATGAGGGAAGGCATAAAGGGAGCCACGGTGGGGAAGCTGGCCCAG
GCGCTCCACCAGTGTTCCAGGATCGACCTTCTGAGCAGCTTGATTTACGTCAGCCAGAACTAA

Figure 2.1.4: Amplicon region for *RIPK1*.

The forward primer sequence is coloured in red, whilst the reverse complement of the reverse primer is coloured in green. Nucleotides between the two primer sequences are coloured in blue. The full sequence shown is of the nucleotide sequence for *RIPK1*. Sequence obtained via CCDS from NCBI Gene.

ATGAGTATGCTCAGGCTTCAGAAGAGGCTCGCCTCTAGTGTCCTCCGCTGTGGCAAGAAGAAGGTCTGGTTA
GACCCCAATGAGACCAATGAAATCGCCAATGCCAACTCCCGTCAGCAGATCCGGAAGCTCATCAAAGATGGG
CTGATCATCCGCAAGCCTGTGACGGTCCATTCCCGGGCTCGATGCCGGAAAAACACCTTGGCCCGCCGGAAG
GGCAGGCACATGGGCATAGGTAAGCGGAAGGGTACAGCCAATGCCCGAATGCCAGAGAAGGTCACATGGAT
GAGGAGAATGAGGATTTTGCGCCGGCTGCTCAGAAGATACCGTGAATCTAAGAAGATCGATCGCCACATGTA
TCACAGCCTGTACCTGAAGGTGAAGGGGAATGTGTTCAAAAACAAGCGGATTCTCATGGAACACATCCACAA
GCTGAAGGCAGACAAGGCCCGCAAGAAGCTCCTGGCTGACCAGGCTGAGGCCCGCAGGTCTAAGACCAAGG
AAGCACGCAAGCGCCGTGAAGAGCGCCTCCAGGCCAAGAAGGAGGAGATCATCAAGACTTTATCCAAGGAG
GAAGAGACCAAGAAATAA

Figure 2.1.5: Amplicon region for *RPL19*.

The forward primer sequence is coloured in red, whilst the reverse complement of the reverse primer is coloured in green. Nucleotides between the two primer sequences are coloured in blue. The full sequence shown is of the nucleotide sequence for *RPL19*. Sequence obtained via CCDS from NCBI Gene.

2.1.12 Protein Extraction

Cells were counted by haemocytometer and seeded at a concentration of 1×10^6 cells per ml in a six-well plate and treated with indicated treatments for the specified times. To reduce loss of protein from the cells, protein extractions were carried out on ice. Following treatment, cells were pelleted as per subculture and the supernatant aspirated, after which the pellet was washed in ice-cold 1xPBS. After a second centrifugation step the supernatant was again aspirated and the pellet was resuspended in 130μl of high salt lysis buffer (HSLB) and transferred to an Eppendorf tube. Tubes were rotated for twenty minutes at 4°C, and then centrifuged at 12,000 RPM for fifteen minutes at 4°C. The supernatant after centrifugation was then kept as protein extract by transfer to a new Eppendorf without disturbing the pellet. After obtaining the protein extract, the Bradford Assay (see Section 2.1.13) was performed to quantify the levels of protein in the extract to ensure even amounts between different samples could be used for subsequent techniques.

2.1.13 Bradford Assay

The Bradford method is a well-established assay to determine protein concentration. 800μl of distilled water was used to dilute 200μl of the Bio-Rad reagent (Bio-Rad), creating the working solution. With each semi-micro cuvette containing 1ml working solution, either 2μl of the protein sample or 2μl HSLB (for calibration purposes) was added. Cuvettes were prepared in duplicates for each protein sample to obtain an average. Cuvettes were read at 595nm in a spectrophotometer, using the cuvette containing HSLB for calibration. 595nm is utilised as the dye-protein complex absorbs maximally at this wavelength (Lu et al., 2010).

Protein extraction was carried out prior to subsequent techniques such as Western blotting. To ensure equal amounts of protein were loaded between different samples for each experiment, calculations based on the values obtained at 595nm were performed. The sample with the lowest 595nm absorbance would have a value of 40μl (given the

maximal loading of the gels used for subsequent electrophoresis), whilst other samples would receive the appropriate relative amount using the formula (lowest absorbance*40)/595nm absorbance value of the current protein.

Based on these calculations, protein extracts could be frozen after the addition of 3xSDS sample buffer (with the amount of 3xSDS added being equal to half of the volume of the protein extract, hence diluting the loading buffer to 1xSDS).

2.1.14 <u>Sodium Dodecyl Sulfate Polyacrylamide Gel Electrophoresis</u>

Protein samples prepared as above were separated by size using sodium dodecyl sulfate polyacrylamide gel electrophoresis (SDS-PAGE) gels. Different percentage gels were used depending on the size of the proteins in question as well as the degree of separation required. For most experiments, 7.5% gels were used, however for finer separation (such as for separating the two cleaved caspase-3 bands at 17 and 19 kDa) 12% or 15% gels were used. Preparation for each is shown in Table 2.1.5:

Table 2.1.5: Preparation of gels for SDS-PAGE.

Constituent	7.5% Resolving	12% Resolving	15% Resolving	Stacking
Distilled Water	6.65ml	4.55ml	3.15ml	3.365ml
ProtoGel	3.5ml	5.6ml	7ml	835µl
1M Tris pH 6.95	N/A	N/A	N/A	625µl
1.5M Tris pH 8.95	3.5ml	3.5ml	3.5ml	N/A
0.2M EDTA	140µl	140µl	140µl	50µl
10% SDS	140µl	140µl	140µl	50µl
10% APS	78.5µl	78.5µl	78.5µl	78.5µl
TEMED	8.5µl	8.5µl	8.5µl	8.5µl

Following assembly of the Bio-Rad Mini PROTEAN 3 gel casting apparatus, the resolving gel was cast as shown in Table 2.1.5. Immediately after it was cast, 0.1% SDS was used to overlay the gel to remove air bubbles and generate a flat surface. After the resolving gel had set, the 0.1% SDS was removed and the stacking gel was added, at which point a 1.5mm comb was inserted to form the wells.

Once the stacking gel had polymerised, the gel was placed into the running chamber which was filled with 1xSDS running buffer. The 1.5mM comb was removed and samples were then boiled at 95°C for three minutes and briefly centrifuged. A Hamilton microlitre glass syringe was used to load all samples. In the first lane of every gel 5µl protein ladder (PageRuler 26616) was added to serve as a marker. Gels were run at 80V until the samples entered the resolving gel, at which point the voltage was increased to 110V until the samples had adequately resolved.

2.1.15 Western Blotting

Western blotting was employed to detect specific proteins from whole cell extracts. After SDS-PAGE, transfer cassettes were prepared as follows: sponge; filter paper; gel; polyvinylidene fluoride (PVDF) membrane (Millipore immobilon-p); filter paper; sponge. Prior to loading each cassette item they were all (except the gel and the membrane) soaked in 1xWestern transfer buffer. The PVDF membrane was first activated in methanol, and then washed in 1xWestern transfer buffer. Completed cassettes were loaded into the transfer chamber (Bio-Rad Mini Trans-Blot Electrophoretic Transfer Cell), which also had an ice-pack loaded and was filled with 1xWestern transfer buffer. A magnetic stirrer was also used to ensure even distribution of the Western transfer buffer constituents. Transfer was completed at 0.4 amperes for two hours, with the ice-pack being replaced halfway through to ensure a cool temperature.

Membranes were subsequently blocked with 5% milk/PBS for one hour at room temperature to prevent non-specific binding of the antibody to the membrane. After

blocking, membranes were incubated at 4°C overnight with the primary antibody (prepared in 2.5% milk/PBST with an appropriate dilution of antibody according to the manufacturer's instructions). Following overnight incubation with the primary antibody, membranes were washed three times at ten-minute intervals with PBST on a shaker and then incubated with the appropriate secondary antibody (prepared in 2.5% milk/PBST with an appropriate dilution of antibody according to the manufacturer's instructions) for one hour. After this hour, membranes were again washed three times in PBST at ten-minute intervals, after which the membrane was developed.

The working solution for Supersignal West Pico Chemiluminescent Substrate (Thermo Scientific) was prepared according to the manufacturer's instructions and developed on a Photon Ecomax Automatic X-Ray Film Processor using high-sensitivity blue-sensitive film. In cases where no band could be obtained with West Pico reagent even after extended exposure, SuperSignal West Femto Chemiluminescent Substrate (Thermo Scientific) was used due to its higher sensitivity.

After films were obtained, digital copies were created by scanning the film and saving them as high-quality PDF files. This digital copy was used both to create figures and also to analyse the bands obtained via densitometric software (see next subheading).

2.1.16 Densitometric Analysis of Western Blot Data

In order to carry out a more quantitative analysis of Western blot data, densitometry was employed through the use of ImageJ (https://imagej.nih.gov/ij/). Densitometry allows for a "semi-quantitative" analysis of blot data through measurement of optical density. An average of three readings was obtained for each band for the protein of interest, which was normalised to the average of three readings for the housekeeping/loading control protein (actin). Normalised band readings were then expressed as a percentage of the control (untreated cells) and bar charts were created using the average and SEM values from multiple percentages from independent experiments.

2.1.17 Stripping Western Membranes

After development of the first protein of interest, membranes could be stripped to allow for re-probing with another antibody. Stripping was only used when the two weights of the proteins were so close that their development would overlap; otherwise, if the weights were different enough that they would appear on different parts of the membrane, then stripping was not performed.

Stripping buffer was prepared as in Table 2.1.3 (Page 74) and placed into a closed container along with the membrane. This was then incubated at 55°C with occasional agitation for thirty minutes. After this, the stripping buffer was drained in the sink of a chemical hood and the membrane was immediately washed twice with PBST. Following the immediate wash, the membrane was washed twice with PBST at ten-minute intervals. Once complete, the membrane could be blocked with 5% milk/PBS and then incubated with the primary antibody.

2.1.18 Chromatin Immunoprecipitation (ChIP)

The chromatin immunoprecipitation procedure was adapted from Rajendran and colleagues (Rajendran et al., 2013). All buffers used in throughout ChIP are described in Table 2.1.3 (Page 74). Cells were left untreated or treated with dexamethasone for 24 hours. The day before cells were taken for processing, 100µl of magnetic beads per antibody per treatment were taken, and washed three times in 1ml ChIP blocking solution and then resuspended in 250µl ChIP blocking solution. 2µg of the antibody was then added. All experiments used total GR (Diagenode), S211-phosphorylated GR (Abcam) and S226-phosphorylated GR (Abcam) in addition to using a negative control IgG. After the addition of antibody, beads were rotated overnight at 4°C.

Following treatment, over 60×10^6 cells were collected per treatment. Proteins were crosslinked to DNA the addition of formaldehyde solution (11% formaldehyde in the formaldehyde solution itself, to a final concentration of 1% formaldehyde when added to the cells). Cells were incubated with formaldehyde on a rocker for ten minutes at

room temperature. After this, the effect of formaldehyde was quenched by rocking the cells for five minutes after the addition of glycine at a final concentration of 125mM. Cells were centrifuged to obtain a pellet, washed with cold 1xPBS, centrifuged again and then the pellet was resuspended in 2ml ice-cold ChIP Buffer 1 supplemented with 100μM PMSF and 1μg/ml protease inhibitors (leupeptin, pepstin, and aprotinin) (PI). After incubation and vortex with ChIP Buffer 1, cells were centrifuged at 4700 RPM for five minutes and the pellet was washed with 10ml ChIP Buffer 2 (again supplemented with 100μM PMSF and PI). After centrifugation at 4700 RPM for five minutes, the pellet was resuspended into 3ml ChIP Buffer 3 (again supplemented with 100μM PMSF and PI).

This 3ml cell suspension was then separated into six 500μl aliquots in 1.5 ml Bioruptor® Pico Microtubes and the chromatin was sheared using the Bioruptor Pico with 15 cycles and a pulse rate of 30 ON and 30 OFF (this setting was determined after performing a shearing efficiency experiment). After shearing, the lysate was cleared by centrifugation at 4°C at 11,400 RPM for ten minutes. During this waiting time the beads that were prepared on the previous day were washed three times in ChIP blocking solution and then resuspended in 100μl of ChIP blocking solution. After the centrifugation was complete, the supernatant was then transferred to fresh, sterile tubes. Some supernatant was stored at -20°C as input (to serve as a baseline for future analysis) whilst the remainder was split to incubate with each of the four antibodies/beads listed earlier. Beads were left to rotate overnight at 4°C.

After an overnight incubation, beads were collected and washed five times with 1ml RIPA Buffer, and then once with 1ml of Tris Buffered Saline (TBS). After the TBS wash the TBS is thoroughly removed (potentially by centrifugation or use of a magnetic stand) and the beads are resuspended in 200μl of ChIP Elution Buffer and incubated for 16 hours at 65°C.

Following the incubation in elution buffer, the supernatant was transferred to fresh tubes (as the DNA-Protein complex should have eluted from the beads at this point). The Input sample that was stored earlier was taken out of storage and to both Input and IP

samples an appropriate equal volume of TE Buffer was added. 8µl of 1mg/ml RNase A was added and then everything was incubated at 37°C for thirty minutes. 4µl of 20mg/ml Proteinase K was added and incubated at 55°C for two hours. After this the DNA was purified through QIAquick PCR purification kit, following the manufacturer's instructions. Quantitative PCR was then performed using primers designed around putative GREs, listed in Table 2.1.6:

Table 2.1.6: Primers used for ChIP Experiments.

Gene / GRE Number	Primer	Sequence
BECN1 GRE 1	Forward	ACT CCT GAC CTT GTG ATC CG
	Reverse	AGA ATC GCT TGA ACC TGG GA
BIRC3 GRE 3	Forward	AAG ATG TGT TAG CCA GTC CTG TT
	Reverse	CCC AAT TTT TCT CCA ATT AGT CA
BIRC3 GRE 5	Forward	TTA GTC GCC ACG CAG CAT
	Reverse	CCA CGT GAT AAA AAC CCA CA
RIPK1 GRE 1	Forward	CTC CGC AGC TCC CAG C
	Reverse	TGG GTA AGA GTG CTC GGA TT
RIPK1 GRE 2	Forward	AGT CTT GCT CTG TCA CCC A
	Reverse	GGT GAA GCC CTG TCT CTA CT

Data for each antibody from qPCR for ChIP was normalised first to its respective negative control IgG, and then values for each IgG-normalised antibody was further normalised to the value of the IgG-normalised antibody for untreated cells (thus allowing examination of the effect of dexamethasone on promoter occupancy as all antibodies for untreated cells become "1").

2.1.19 Cell Type Analysis and Caspase-8 Activation Assay

Cells were seeded at a concentration of $1x10^6$ cells/ml and treated with CM for 48 hours, dexamethasone for 36 hours, and etoposide for 24 hours. Following treatment cells were processed in accordance with the manufacturer's protocol (ChemoMetec, 2017). In brief, 5µl diluted FLICA (fluorochrome-labeled inhibitor of caspases assay)

reagent was added to 93µl of suspended cells, and 2µl 500 µg/ml Hoechst 33342 was added. After incubation at 37°C for one hour, cells were washed twice in 400µl 1x Apoptosis Wash Buffer, pelleted by centrifugation, and resuspended in 100µl of Apoptosis Wash Buffer supplemented with 10 µg/ml propidium iodide. 30µl of the sample was then immediately loaded onto an NC-Slide A2™, inserted into the NucleoCounter® NC-3000™ machine and ran under the "Caspase Assay" setting. Analysis of the data obtained utilised the gating approach in the ChemoMetec guide, which is also summarised in Figure 2.1.6.
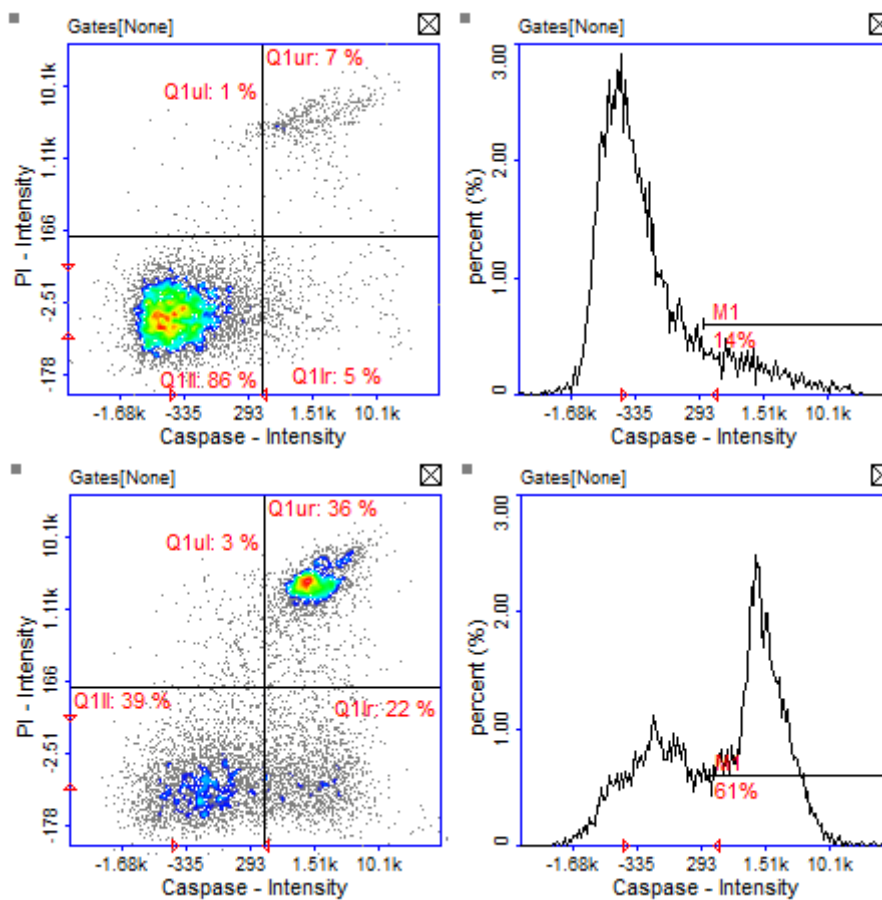
Figure 2.1.6: Gating strategy for cell types and caspase activation experiments.
Left panels gate for cell types (healthy in Q1ll, necrotic in Q1ul, late apoptotic in Q1ur and early apoptotic in Q1lr) based on dye intensity. Caspase activation is shown in the right panels. Untreated C7-14 cells are shown on the top whilst dexamethasone-treated C7-14 cells are shown on the bottom.

Following the gating of cells as shown above in Figure 2.1.6, the values obtained were expressed relative to untreated cells. For example for caspase activation in Figure 2.1.6,

for untreated cells it would be 100%, whilst for dexamethasone-treated cells it would be 435% (61/14*100).

2.1.20 Flow Cytometry

Cells were seeded at a concentration of approximately 1×10^6 cells and either left untreated or treated with CM for 48 hours, dexamethasone for 36 hours, or etoposide for 24 hours. After completion of treatments, cells were pelleted as per subculture and the pellet was washed in 1ml cold 1xPBS. After removal of the PBS cell pellets were resuspended in 1ml 50% ethanol/PBS which was added dropwise. Solutions were then stored at -20°C for thirty minutes and immediately analysed or stored at 4°C for up to one week before proceeding with analysis.

After this, cells were pelleted by centrifugation and the supernatant was aspirated, after which 200µl of 100µg/ml RNase A was added to the cells and then incubated at 37°C for fifteen minutes in the dark. Following a fifteen minute incubation period after the addition of 800µl 50µg/ml propidium iodide, the samples were loaded onto a BD FACSVerse™ flow cytometer and analysed using BD FACSuite™ software. Cells were captured on forward and side scatter and then gated for cell cycle phases based on propidium iodide intensity.

2.1.21 Concentrations of Treatments Used on Cells

Unless otherwise stated, the following concentrations and treatment lengths were used to treat cells:

Table 2.1.7: Concentration and duration of treatments.

Treatment	Concentration	Treatment Length
Dexamethasone	1µM	24 Hours
Etoposide	10µM	24 Hours
AT406 (BIRC3 Inhibitor)	10µM	48 Hours

Conditioned Media (CM)	1/6th Total Media (i.e. 500μl CM per 3ml total cell suspension)	48 hours

2.1.22 Identification of Transcription Factor Binding Sites

This approach was carried out following qRT-PCR and Western experiments which indicated possible regulation of genes by the GR. Thus, the QIAGEN Champion ChiP Transcription Factor Search Portal was used to search for putative GREs on BECN1 and RIPK1. By entering the NCBI Gene Official Symbol into Champion ChIP, potential regulators were listed. Following links within Champion ChIP would allow for the gene sequence to be seen, at which point the surrounding nucleotides around the putative GREs could be identified, allowing for the design of primers. Champion ChIP in addition to sequence analysis for GRE half-sites was used to identify putative GREs on *BECN1, BIRC3,* and *RIPK1*.

2.1.23 Statistical Analysis

Unless otherwise stated, data in figures represents the average of at least three independent experiments +/- SEM (standard error of the mean). Unless otherwise stated, asterisks (*) above bars indicate statistical significance at $p \leq 0.05$ when compared to the control, as assessed by a paired two-tail t-test.

2.2   Computational Approaches

2.2.1   Extraction from STRING and Manual Curation of Interactions

The STRING (Search Tool for the Retrieval of Interacting Genes/Proteins) database was chosen as the source of a starting point for predicted protein interactions, based on a previous extensive analysis of the available databases and which was most suitable (Tian, 2013). STRING was first introduced in the early 2000s (Snel et al., 2000), and is an excellent resource as it integrates information from various sources such as curated pathway databases, automatic text-mining, and high-throughput studies (Szklarczyk et al., 2011).

From the STRING website (http://string-db.org/, V9.1 at the time) the "protein.actions.v9.1.txt.gz" file was downloaded, decompressed, and opened in the UltraEdit text editor. This file was chosen as it is the part of the database that contains the predicted functional and physical links between proteins. The UltraEdit search function was used to extract all lines containing the STRING ID of the human glucocorticoid receptor (9606.ENSP00000231509). Only interactions with a high-confidence score (greater than or equal to 0.7) were retained after this initial extraction. Although given a low confidence score, EP300 and TSC22D3 (GILZ, glucocorticoid-induced leucine zipper) were also included due to similarity to CREBBP or for their known importance in GR signalling respectively.

Extensive literature searches were undertaken to manually curate each predicted interaction – this involved reading numerous papers for each interaction to ensure its validity. It should be noted that all curations for the interactions contained within this model were performed by the author of this thesis, but all curations were checked by the PhD Supervisor Professor Marija Krstic-Demonacos to ensure curations were correct and so that all interactions included in the model had been double-curated, thus increasing the reliability of the model. Often, STRING predicted a 'binding' reaction, which has no predicted activation or inhibition. However for these interactions literature searching often unveiled a functional activation/inhibition relationship that could be

included in the model. Completed curations of the interactions involving GR will from now be called the "primary layer" of the model.

Following construction of the primary layer, the "protein.actions.v9.1.txt.gz" file and UltraEdit were again used to extract interactions for the genes that interact with GR. These interactions were filtered both for high-confidence and interactions only between the genes in the primary layer. Manual curation through extensive literature searching was again carried out. Interactions between the genes in the primary layer will be referred to as the "second layer" of the model.

2.2.2 Connection to Model Outputs via the Gene Ontology Consortium

The Gene Ontology Consortium (GO Database, http://www.geneontology.org/) is a collaborative project which aims to provide vocabularies for gene annotations, gene products and sequences, with annotations being biological processes such as DNA binding (GO, 2008). The GO database was used to connect the model constituents to biological outputs. After curation of the second layer, direct annotations for each gene in the model were extracted and all annotations for all genes were compiled and ranked by the most common, and the most common annotations relating to cell death and inflammation (two of the important outputs for GR) were taken. Annotations such as "protein binding" were excluded as although this is a biological process, it is not a measurable or specific output compared to others such as apoptosis. Multiple annotations relating to the same overall process were pooled into one output, for example tissue-specific forms of apoptosis (such as GO:0043525, positive regulation of neuron apoptotic process) were all combined into one node of "CELL-DEATH". In all cases, all predicted annotations were confirmed by extensive literature searching to verify the effect of the gene on the biological process.

2.2.3 Cytoscape

Visualisation of networks was undertaken through the use of Cytoscape, an open-source software that may be used for network imaging (Cytoscape, 2016). Cytoscape is a

highly versatile program that can undertake model visualisation and analysis. Networks may either be manually created or automatically generated through Cytoscape accessing pathway databases (Cytoscape, 2016; Shannon et al., 2003). Manually curated interaction records were imported into the program and the network was visualised to the required standard by adjusting parameters such as node and edge colour. Node connectivity within the model was assessed via the NetworkAnalyzer plugin. Figure 2.2.1 shows an example network visualised through Cytoscape:
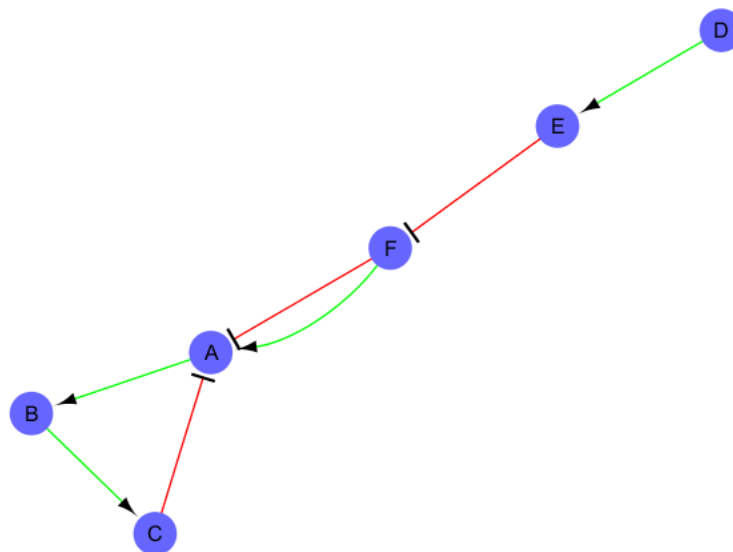
Figure 2.2.1: Example network visualised through Cytoscape.
Green directed arrows represent activation, whilst red blunted arrows represent inhibition.

2.2.4   Import to and Analysis in CellNetAnalyzer

After the model was fully constructed (i.e. primary layer, second layer, and outputs through GO are all complete), the final interaction list was imported into CellNetAnalyzer (CNA). CNA provides a powerful framework that allows for detailed model construction and analysis. CNA can handle two model types: mass-flow (i.e. metabolism models) and signal flow (i.e. gene regulatory models) (Klamt et al., 2007).

CNA is capable of performing multiple analyses, the first of which is the generation of an interaction matrix. The interaction matrix provides a visual representation of the role

of each node (gene/protein, input or output) in every interaction (edge). Three states are possible for every node in every interaction: -1 (green or red, denoting that the node plays a stimulatory or inhibitory role in the interaction respectively); 0 (black, node not involved) and 1 (blue, the node is regulated in this interaction). A "NOT" modifier ("!") may also be used to represent an inhibitory effect of the node with a -1 value (corresponding to negatively affecting the node with a value of 1). The interaction matrix thus provides a useful overview of the entire system. However, it is limited in that it only visualises what was input to CNA; there is no detailed analysis performed, as it more provides a visual reference of the basal model state. Figure 2.2.2 shows the interaction matrix for the network represented in Figure 2.2.1:
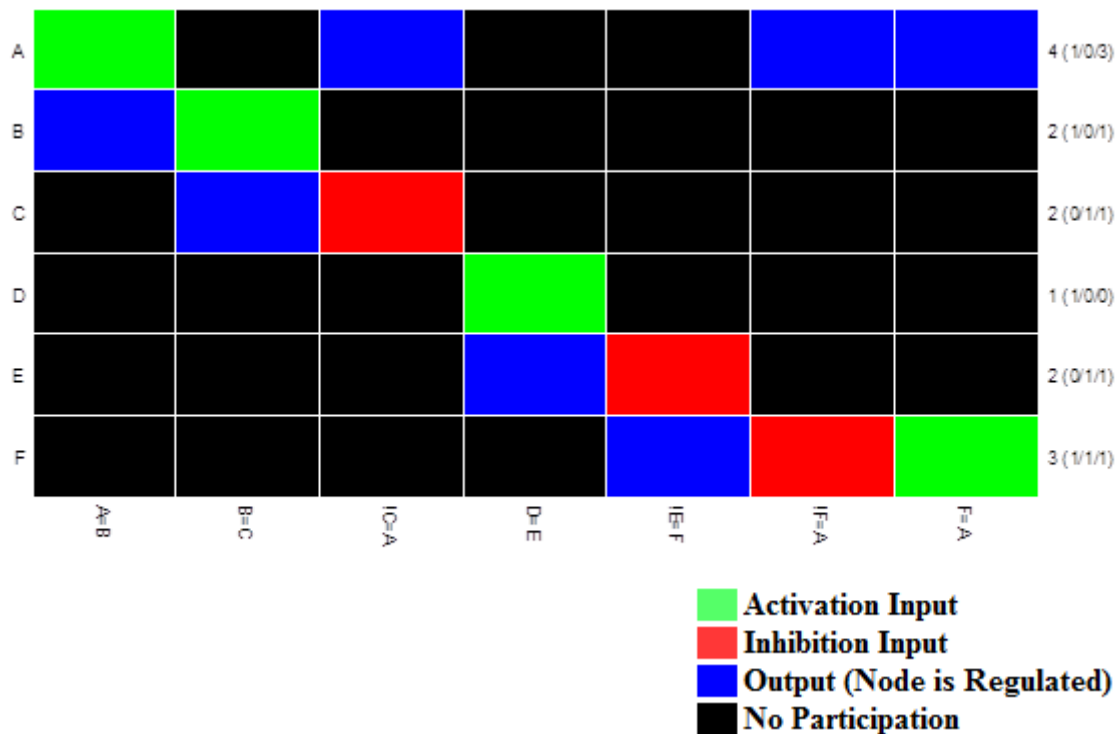
Figure 2.2.2: Interaction Matrix for the network shown in Figure 2.2.1.

Interactions are shown on the x-axis, whilst nodes are shown on the left-side y-axis. The right-hand y-axis details the number of reactions the node is involved in. Numbers in brackets represent the number of nodes it activates, the number of nodes it inhibits, and the number of nodes it is regulated by respectively.

Although an interaction matrix is useful for providing an overview of the network, for in-depth analysis other approaches such as logical steady state analysis (LSSA) and dependency matrix generation are utilised. Dependency matrices utilise graph theory to

calculate the overall effect of every node within the model upon every node within the model, by tracing paths based on the edges connecting nodes. Paths can be either positive (activation) or negative ("NOT" modifier/inhibition).

Thus, by taking into account all of the signalling present in the network, in addition to feedback loops, CNA can provide insight into relationships between individual nodes that may otherwise escape notice due to complicated signalling events. Furthermore, comparison of a wild-type dependency matrix to the dependency matrix of a KO model would allow for further elucidation as to how the system behaves following perturbation. Utilising a similar example to Klamt et al. (2007), the following details the six possible relationships possible in a dependency matrix:

1. A has no effect on B if there are no pathways (direct or indirect, positive or negative) between A and B.

2. A is a strong activator of B if there are positive paths between A and B, and no negative paths between A and B. A third node, C, may also exist. If A is connected to C, and C is connected to B (i.e. A influences C, C influences B), C must not be involved in a negative feedback loop to itself.

3. A is a weak activator of B if there are positive paths between A and B, and no negative paths between A and B. A third node, C, must also exist that affects A and is affected by B. Node C must also be involved in a negative feedback loop with itself.

4. A is a strong inhibitor of B if there are negative paths between A and B, and no positive paths between A and B. A third node, C, may also exist. If A has paths to C, and C has paths to B (i.e. A influences C, C influences B), C must not be involved in a negative feedback loop to itself.

5. A is a weak inhibitor of B if there are negative paths between A and B, and no positive paths between A and B. A third node, C, must also exist, that affects A and is affected by B. Node C must also be involved in a negative feedback loop with itself.

6. A is ambivalent to B if both positive and negative paths exist between A and B.

Figure 2.2.3 shows the dependency matrix for the example network shown in Figure 2.2.1:
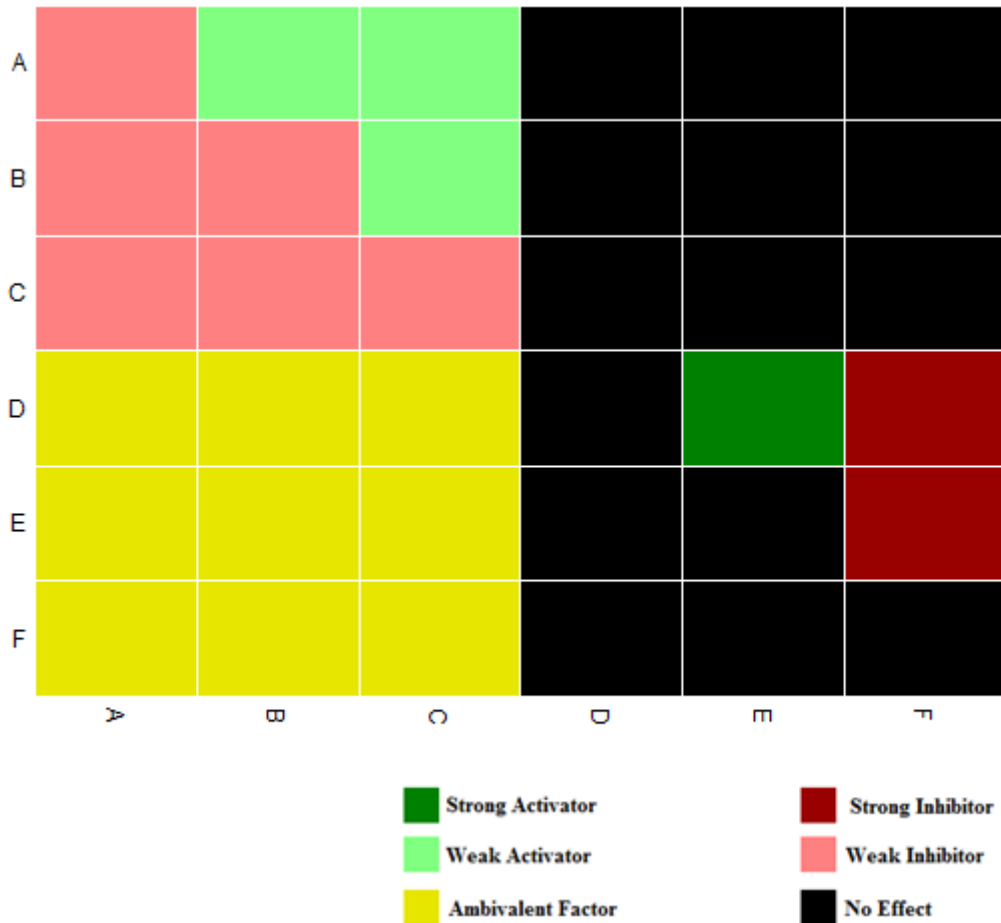
Figure 2.2.3: Dependency Matrix for example network shown in Figure 2.2.1.
Dependencies show the effect of the node on the y-axis on the node on the x-axis.

2.2.5   Application of LSSA and Comparison of LSSA Results

As mentioned earlier, logical steady state analysis (LSSA) is another analytical approach in CNA. LSSA calculates the steady state of every node in the model on the basis of a given set of input values and then proceeding with downstream reactions. By setting starting nodes to ON or OFF (such as the input of a glucocorticoid to ON for a GR model), CNA calculates node states downstream of the inputs based on the interactions in the model. Three states are possible: Activated (1), Inactivated (0) or, if

the node cannot be determined or may be active or inactive, undetermined (NaN) (Klamt et al., 2007).

In addition to the analyses described above, *in silico* knockouts were performed (i.e. removing a node in the model) and then analyses such as dependency matrix generation were repeated on the KO model. This allows simulation for a variety of *in vivo* mutation simulations such as GC-resistant cells (GR KO). LSSA and dependency matrix results were compared between the full model and various knockout models.

In addition to obtaining a logical steady state for each node under different conditions, comparisons between two sets of resultant node states were also performed as described previously (Tian et al., 2013). This approach allows the capturing of up and downregulation of nodes between the two LSSA result sets.

As stated earlier, LSSA assigns a state of either activated (1), undetermined (NaN) or inactivated (0) to nodes within the network. For LSSA Scenario 1, node i state was defined as $S(i)_1$ which takes the value of 1, 0 or NaN. Similarly for Scenario 2 (i.e. an LSSA where a node is OFF or deleted) node i state was defined as $S(i)_2$, which can take the same node state values. Lastly the value E_{mod} was used to calculate the predicted change in node state from Scenario 1 to Scenario 2, where 0 means the node state is unchanged, 1 means the node is upregulated and -1 means the node is downregulated:

$E_{mod} = 0$	if	$S(i)_1 = 1$	and	$S(i)_2 = 1$
$E_{mod} = 0$	if	$S(i)_1 = 0$	and	$S(i)_2 = 0$
$E_{mod} = 0$	if	$S(i)_1 = \text{NaN}$	and	$S(i)_2 = \text{NaN}$
$E_{mod} = 1$	if	$S(i)_1 = 0$	and	$S(i)_2 = 1$
$E_{mod} = 1$	if	$S(i)_1 = \text{NaN}$	and	$S(i)_2 = 1$
$E_{mod} = 1$	if	$S(i)_1 = 0$	and	$S(i)_2 = \text{NaN}$
$E_{mod} = -1$	if	$S(i)_1 = 1$	and	$S(i)_2 = 0$
$E_{mod} = -1$	if	$S(i)_1 = 1$	and	$S(i)_2 = \text{NaN}$

$E_{mod} = -1$ if $S(i)_1 = NaN$ and $S(i)_2 = 0$

E_{mod} was used to describe the overall predicted change from one state to another, but was also utilised to compare model predictions to experimental data, to allow for assessment of model accuracy.

2.2.6   Genome-Wide Model Validation

In order to assess model accuracy, model predictions based on E_{mod} were compared to experimentally-obtained microarray data (obtained from the Gene Expression Omnibus database). As E_{mod} was based on a comparison of two different LSSA states (for instance Scenario 1 could be the wild-type model, GC-sensitive, whilst Scenario 2 could be a GR KO model, GC-resistant) a value known as E_{exp} was generated via comparison between two different microarray experiments (for instance one from GC-sensitive, one from GC-resistant, thus matching the LSSA scenarios).

To generate E_{exp}, the method from Tian et al. (2013) and Hussain et al. (2015) was used. For each genome-wide validation a GC-resistant microarray was used as the target scenario whilst GC-sensitive arrays were used as the source scenario. Fold changes for all probe IDs between the target and source scenarios were calculated, in addition to Log_{10} values for the fold changes. Based on the average +/- standard deviation of all of the Log_{10} fold changes, a dynamic threshold was generated. The upper threshold was determined by the average + standard deviation, whilst the lower threshold was determined by the average – standard deviation.

To determine whether the genes present in the model were seen as upregulated, downregulated, or unchanged based on experimental data, the median value for all probe IDs for each gene in question was generated for both the target and source scenario, and the fold change of the median scores determined. In the case of model nodes such as NFKB which represented more than one gene, the median of all probe IDs for all constituent genes was used. The Log_{10} of the fold change was then compared to the dynamic threshold; if its value was higher than the upper threshold, then the gene

was determined as upregulated (1), whilst if its value was lower than the lower threshold, the gene was determined as downregulated (-1). Otherwise, if its score was between the lower and upper thresholds, the gene was determined as unchanged (0). This zero score indicates that that the gene was determined as unchanged as its value did not change significantly (as assessed by passing either threshold) between the two scenarios.

Model validation was carried out by calculating the absolute value of $E_{mod} - E_{exp}$. This could take three possible values: 0 (model prediction was correct), 1 (small scale error; model predicts for example that a gene is unchanged but it is increased, or for example that a gene is decreased but there is no change) and 2 (large scale error; model predicts opposite of what occurs, for example the model predicts a gene is downregulated when in fact it is upregulated). Scores of 0, 1 and 2 were tallied and percentages of correct predictions were created for each microarray validation.

2.2.7 Preliminary Clinical Validation of Model with Patient Data (LSSA)

Microarray data from thirteen leukaemia patients (taken after treatment with prednisolone) were obtained from the Gene Expression Omnibus database (detailed in Table 4.5.1, Page 170). For each patient individually, Log_{10} RMA values for all probe IDs were calculated. A dynamic threshold of upper and lower limits based on the average +/- standard deviation of the Log_{10} RMA values were calculated and genes were considered as upregulated, unchanged, or downregulated based on their relation to the threshold. If the Log10 of the median RMA values for the gene's probe IDs were higher than the upper threshold, genes were deemed upregulated (1); if lower than the lower threshold then genes were deemed downregulated (-1). Otherwise, if the values were between the lower and upper thresholds, genes were deemed unchanged (0). This value of up, down, or no change was then compared to LSSA results of a GC-sensitive simulation where (from the LSSA results) a value of 1 is equivalent to upregulation (1), 0 to downregulation (-1), and NaN to unchanged (0).

2.2.8   Signal Transduction Score Flow Algorithm (STSFA) Analysis

The STSFA is a Cytoscape plugin that allows for superimposition of microarray or ChIP-seq data onto a signalling model to allow for a more quantitative analysis to be performed (Isik et al., 2012). In this context, quantitative analysis indicates that rather than a Boolean fixed state of 1 or 0 to indicate ON or OFF, each node within the model could be assigned a "score" to allow for comparison of relative activation/inhibition. An overview of the principles of STSFA can be seen in Figure 2.2.4:
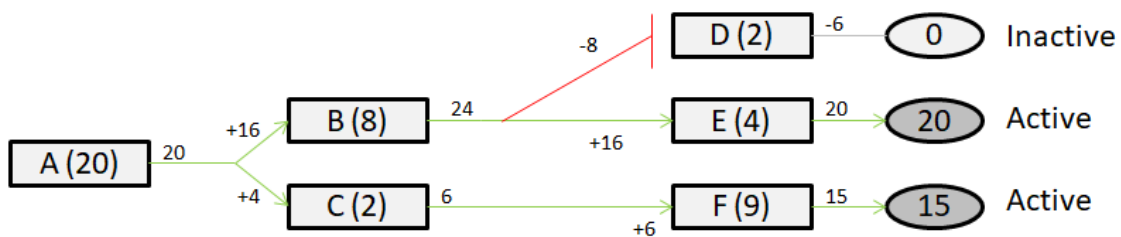
Figure 2.2.4: Principles of STSFA analysis.

STSFA assigns a starting score to every node based on its value from the ChIP-seq/microarray data. These scores then quantitatively traverse through the model depending on downstream signals to update node scores throughout the model, ending when outputs are reached. Figure adapted from Isik et al. (2012).

Under STSFA analysis each node within the model is given a starting score based on (for example) the microarray data. Downstream reactions are then processed based on the node score; for instance Node A in Figure 2.2.4 has a starting score of 20. It has two downstream nodes (Node B, with a starting score of 8, and Node C with a starting score of 2). The total of eight and two is ten, so Node B receives 80% (8/10) of Node A's score, whilst node C receives 20% (2/10) of Node A's score. This corresponds to 16 and 4 respectively. Node C only has one downstream node (Node F) so it receives 100% of Node C's score (6). Combined with its starting score of 9, Node F now has a score of 15 which it uses to activate its biological output (which serves as a "stop" signal of sorts for STSFA analysis) (Isik et al., 2012).

Comparatively, Node B has two downstream nodes (Node D and Node E). Notably, Node D is negatively regulated by Node B, whilst Node E is positively regulated. Node

D has a starting score of 2, whilst Node E has a starting score of 4. Thus, Node D receives 33.33% (2/6) of Node B's score, whilst Node E receives 66.66% (4/6). However, Node B regulates Node D in a negative manner, so a weight of -8 (one-third of 24) is added to the edge. Since Node D's starting score was 2, its score now drops to zero and its output is inactive. Node E, however, receives a score of 16 (two-thirds of 24) which, combined with its starting score of 4, gives it a new value of 20 which activates its output (Isik et al., 2012).

To perform STSFA analysis, as with previous studies Log_2 microarray values were scaled up by a factor of 100 and superimposed onto the model using the STSFA plugin (Pathway Scoring plugin) (Hussain et al., 2014). One limitation of STSFA is that due to the method it uses to assess effects on downstream nodes, directly ambivalent relationships cannot be considered. For instance, if Node A directly activates and inhibits Node B, then STSFA cannot compute this effectively. To correct for this, all direct ambivalent interactions were removed from the model before STSFA analysis. From a mathematical perspective this is reasonable as even if the direct ambivalent interactions were taken into account, the net effect would be zero as it would theoretically be positively and negatively regulated by the same amount.

STSFA results based on GC-sensitive and GC-resistant microarray data were used to generate an E_{mod} value, which could then be compared to the E_{exp} value obtained by direct comparison of microarray data (E_{exp} was generated as detailed previously in Section 2.2.6, Page 102). To generate E_{mod} for STSFA output data, fold changes between resistant and sensitive node scores were calculated, followed by Log_{10} of each fold change. Based on the Log_{10} fold change for each node a dynamic threshold was generated based on the average +/- standard deviation of the fold changes. Nodes were determined as upregulated if they exceeded the upper threshold, downregulated if they were less than the lower threshold, and unchanged if their values lay between the lower and upper thresholds. These E_{mod} values were compared to the E_{exp} values to assess STSFA predictive power. This again allowed for assessment of model accuracy, in addition to assessing the accuracy of STSFA analysis compared to LSSA.

2.2.9   <u>Preliminary Clinical Validation of Model with Patient Data (STSFA)</u>

The capacity of the GEB052 model as a predictive clinical tool was assessed using patient microarray data extracted from a previous study (Schmidt et al., 2006). Microarray data from thirteen paediatric acute lymphoblastic leukaemia patients were taken from the Gene Expression Omnibus database (detailed in Table 4.6.2, Page 174) and each in turn was processed as described above to be used with STSFA for the model. The microarray data files used were taken prior to patients being treated.

STSFA generates scores for each node of the model, including and stopping at biological outputs such as cell death, which is one output of the model described in this thesis. Model edges are also assigned weights based on the interactions within the model (Isik et al., 2012). All incoming edge weights to the node CELL-DEATH were totalled for each patient. Patients were divided into two groups (alive at risk assessment or dead at risk assessment) and the average total edge weight for each group was calculated, thus correlating model predictions with clinical outcomes.

Chapter 3   Wet Laboratory Results

3.1   Introduction to Wet Laboratory Research

As described in the Introduction, the bone marrow microenvironment (which may be mimicked *in vitro* through the use of bone cell-conditioned media) represents a source of chemoresistance in leukaemia. The research in this chapter presents molecular and functional analysis of the effects of CM and the chemotherapeutic drugs dexamethasone and etoposide in varying combinations on glucocorticoid-sensitive (C7-14) and glucocorticoid-resistant (C1-15) cell lines. In particular, the effect of these treatments on proteins relating to cell death and survival has been investigated, in addition to their effects on GR phosphorylation, and GR occupancy on potential glucocorticoid-regulated genes has also been assessed.

3.2   CM and Chemotherapy Alter Leukaemic Cell Fate

Before carrying out molecular analysis, MTS assays were performed to determine the appropriate concentration of CM and to assess the effects of CM and chemotherapy on C1-15 and C7-14 cells. Concentrations and treatment lengths for dexamethasone (1μM, 36 hours) and etoposide (10μM, 24 hours) were chosen based on optimisation experiments previously conducted within the laboratory (Qattan, 2014), whilst CM concentration was chosen as one-sixth CM/total media based on MTS optimisation experiments (see Appendices). Based on these concentrations, an MTS assay was performed with all three treatments in various combinations:
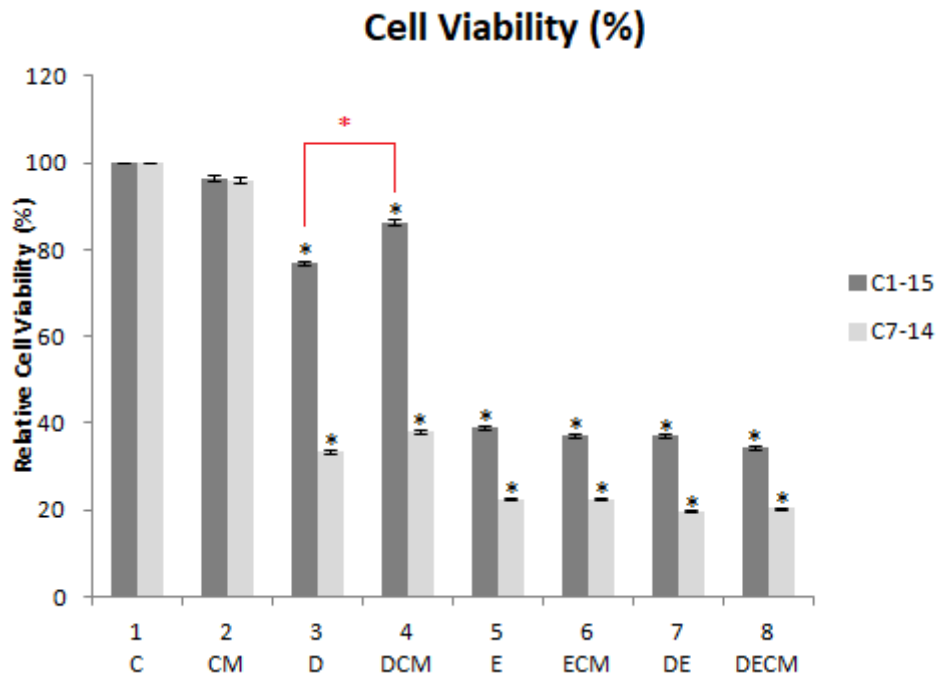
Figure 3.2.1: Cell viability under CM and chemotherapy.

Cell viability was assessed by MTS assays. C1-15 and C7-14 cells were treated with CM for 48 hours, 1μM dexamethasone (D) for 36 hours and 10μM etoposide (E) for 24 hours individually or in combination. Data represents the average of at least three independent experiments +/- SEM. P-value ≤0.05 is indicated by * (black asterisk for comparison of treatment to control). Red asterisks indicate statistical significance at p≤0.05 between other groups.

As shown above, CM did not exert any significant effects on cell death for either cell line (compare lane 2 to lane 1). Dexamethasone exerted a highly significant cytotoxic effect in C7-14 cells, whilst it also inhibited the growth of C1-15 cells, though to a much lower degree (compare dark and light bars of lane 3 to lane 1). Addition of CM, in both cell lines, resulted in a slight increase in viability (with the difference being statistically significant in C1-15 cells), which may suggest a trend for CM to increase survival (compare lane 4 to lane 3). In both cell lines, etoposide demonstrated a significant cytotoxic effect. C7-14 cells were more sensitive to the drug and showed consistently higher cytotoxicity rates compared to C1-15 for all treatments containing etoposide (compare light to dark bars of lanes 5-8).

3.3   Conditioned Media Influences The Glucocorticoid Receptor

As established in Section 1.10 (Page 39) the phosphorylation status of the GR is a crucial determinant of its activity. It is known that ligand-binding ultimately leads to altered phosphorylation status, and that GC-sensitive and GC-resistant cells exhibit different patterns of phosphorylation.

Due to the widespread effects of the microenvironment and the key role of the GR in numerous physiological pathways, it was hypothesised that the microenvironment (and CM) could alter GR levels or post-translational status, which in turn could affect response of leukaemia cells to dexamethasone or other chemotherapeutic agents.

To investigate this, Western blot analysis (complemented by densitometry) was employed on C1-15 and C7-14 cells under CM, dexamethasone and etoposide treatment in varying combinations. The proteins analysed were Total GR (H300), S211-phosphorylated GR, S226-phosphorylated GR, with Actin being used as a loading control:
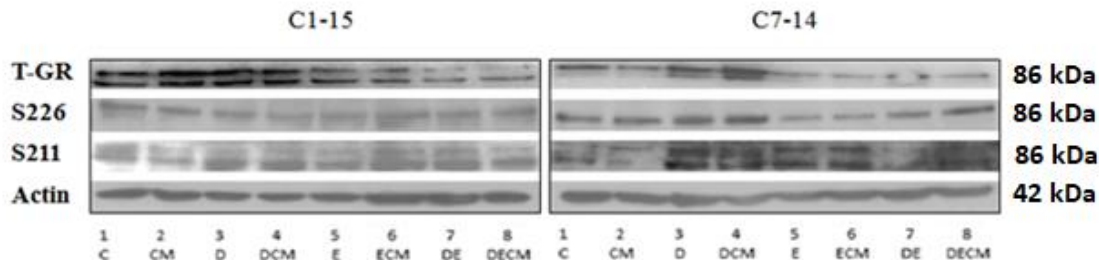
Figure 3.3.1: Western blot analysis of the GR and its phosphoisoforms.
C1-15 and C7-14 cells were treated with CM for 48 hours, 1μM dexamethasone (D) for 24 hours or 10μM etoposide (E) for 24 hours individually or in combination. Cells were lysed and the GR and two phosphoisoforms were detected by Western blot analysis. Actin was used as a loading control. Data is representative of at least three independent experiments.

Although the Westerns above provide a visual analysis, densitometry allows for a semi-quantitative approach to the Western data. Each antibody above will be analysed in the following sections.

3.3.1 Analysis of Total GR

Figure 3.3.2: Densitometric analysis of GR protein levels.

C1-15 and C7-14 cells were treated with CM for 48 hours, 1μM dexamethasone (D) for 24 hours or 10μM etoposide (E) for 24 hours individually or in combination. Blots were analysed with ImageJ. GR band readings were normalised to the corresponding actin band reading and then expressed relative to untreated cells. This Figure contains quantification of blot data generated by both the author of this thesis and an additional researcher. Data is representative of at least three independent experiments +/- SEM. P-value ≤ 0.05 is indicated by *.

In Figure 3.3.2 above, CM trends towards reducing the GR in C1-15 cells, but increasing the GR in C7-14 cells (lane 2, compare dark bars to light bars). The difference in cellular response to hormone can be observed under dexamethasone treatment, with C7-14 cells showing tendency towards increased GR levels under hormone treatment (lane 3, compare dark to light bars). Etoposide trended towards reducing GR levels, whilst dexamethasone and etoposide combination led to a statistically significant reduction in GR levels (compare light bars of lanes 1 and 7). This is consistent with established knowledge, as it has been shown previously that GR and TP53 (activated by etoposide) may exhibit negative crosstalk (Sengupta et al., 2000).

3.3.2 Analysis of S226-Phosphorylated GR

S226 Protein Levels
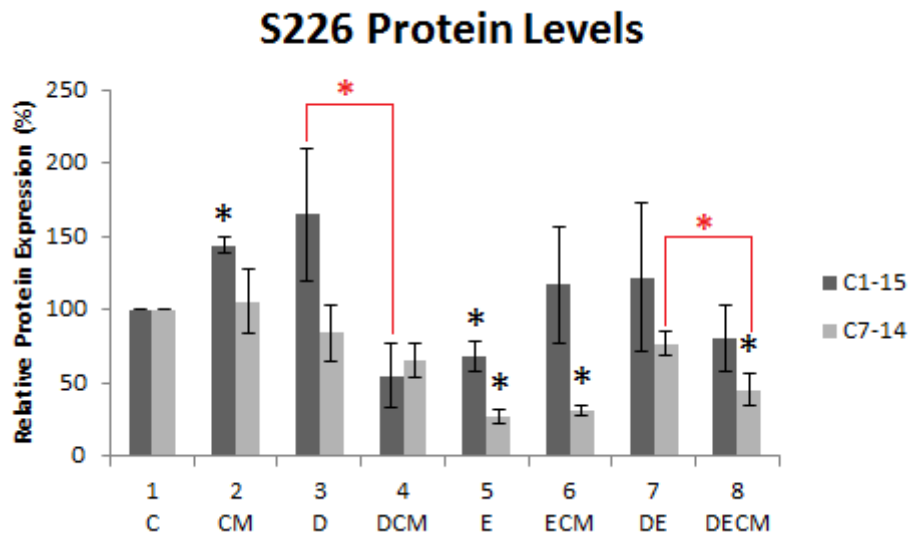
Figure 3.3.3: Densitometric analysis of S226-phosphorlated GR.

C1-15 and C7-14 cells were treated with CM for 48 hours, 1µM dexamethasone (D) for 24 hours or 10µM etoposide (E) for 24 hours individually or in combination. Blots were analysed with ImageJ and S226 values were normalised to the corresponding actin-normalised total GR values. Values were then expressed relative to untreated cells. This Figure contains quantification of blot data generated by both the author of this thesis and an additional researcher. Data is representative of at least three independent experiments +/- SEM. P-value ≤ 0.05 is indicated by * (black asterisk for comparison of treatment to control). Red asterisks indicate statistical significance at $p \leq 0.05$ between other groups.

As shown in Figure 3.3.3, differential effects of CM between C1-15 and C7-14 cells are still observed. In C1-15 cells, CM induces a statistically significant increase in S226-phosphorylated GR, whilst this effect is not seen in C7-14 cells (lane 2, compare dark to light bars). This correlates with the trend towards reduction of T-GR by CM in Figure 3.3.2, given that phosphorylation at S226 is associated with nuclear export and reduced GR activity (Galliher-Beckley and Cidlowski, 2009).

Opposing effects of dexamethasone on phosphorylation at S226 were observed between C1-15 and C7-14 cells, with C1-15 trending towards an increase whilst C7-14 cells trended towards a decrease (lane 3, compare dark to light bars of Figure 3.3.3). However, addition of CM to this led to a decrease in S226-phosphorylated GR levels (compare dark bar of lane 4 to dark bar of lanes 3 and 1 of Figure 3.3.3). In C1-15 cells, etoposide induced a statistically significant downregulation of S226-phosphorylated

GR, which was inhibited by the addition of CM (compare dark bars of lane 5 to lane 6 of Figure 3.3.3).

A similar effect was observed with dexamethasone and etoposide combination treatment; although etoposide lead to a statistically significant decrease in S226-phosphorylated GR, this was lost following the addition of dexamethasone (compare dark bars of lane 5 to lane 7 of Figure 3.3.3). This provides further evidence for the role of dexamethasone in increasing S226 phosphorylation in C1-15 cells. However, addition of CM to dexamethasone and etoposide combination reduced levels of S226-phosphorylated GR, though there was no change in statistical significance. Thus, it appears CM exerts different effects depending on the treatment combinations; most effects in C1-15 cells appear to be increasing S226-phosphorylated GR, with the exception of when dexamethasone is present, at which point CM appears to exert a negative effect, potentially interfering with the hormone response.

Although etoposide lead to a statistically significant reduction of S226-phosphorylated GR in C7-14 cells, this effect was not inhibited by CM, indicating a cell-specific difference in response to CM (compare light bars of lanes 5 and 6 of Figure 3.3.3). Although dexamethasone and etoposide lead to a slight loss of the inhibition of S226-phosphorylated GR (compare light bars of lanes 5 and 7 of Figure 3.3.3). Lastly, addition of CM to dexamethasone and etoposide treatment led to a statistically significant reduction in S226 levels relative to dexamethasone and etoposide alone in C7-14 cells (compare light bars of lanes 7 and 8 of Figure 3.3.3). Thus, CM appears to have a generally negative effect on S226 expression in C7-14 cells, while its effects in C1-15 cells may be slightly more complex.

3.3.3   Analysis of S211-Phosphorylated GR

S211 Protein Levels
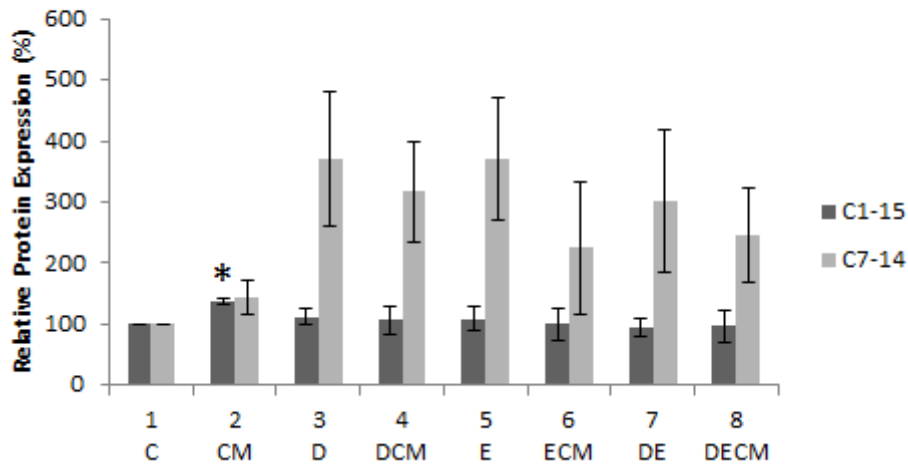
Figure 3.3.4: Densitometric analysis of S211-phosphorylated GR.

C1-15 and C7-14 cells were treated with CM for 48 hours, 1µM dexamethasone (D) for 24 hours or 10µM etoposide (E) for 24 hours individually or in combination. Blots were analysed with ImageJ and S211 values were normalised to the corresponding actin-normalised total GR values. Values were then expressed relative to untreated cells. This Figure contains quantification of blot data generated by both the author of this thesis and an additional researcher. Data is representative of at least three independent experiments +/- SEM. P-value ≤ 0.05 is indicated by *.

Analysis of phosphorylation at S211 indicates a trend for CM to increase its expression in both C1-15 and C7-14 cells. Other than CM treatment, levels of S211-phosphorylated GR were largely unchanged for C1-15 cells, whilst C7-14 showed increase in S211-phosphorylated GR across all treatments.

3.4   Modulation of cell death and survival markers by CM and chemotherapy

Results described in Section 3.3 above suggest that the microenvironment modulates glucocorticoid receptor levels and phosphorylation status, which in turn may impact its effects on downstream cellular processes such as apoptosis, autophagy and necroptosis. Importantly, a microarray carried out by a colleague prior to this study indicated that CM modulated the expression of numerous genes, including a repression of RIPK1, further highlighting it as an interesting target and providing a basis for its study via qRT-PCR validation and immunoblotting (Qattan, 2014). Thus, CM alone may affect

apoptotic, necroptotic or autophagic pathways either independently of the GR or through altering cellular processes downstream of the GR.

In order to investigate this hypothesis, qRT-PCR and Western blot analysis was performed BECN1 (marker for autophagy), RIPK1 (marker for necroptosis) and caspase-3 (marker for apoptosis). For caspase-3, only protein levels were followed as the important event demonstrating apoptosis is cleavage of the full-length caspase to two smaller subunits.

3.4.1 Effects on *BECN1* and *RIPK1* mRNA
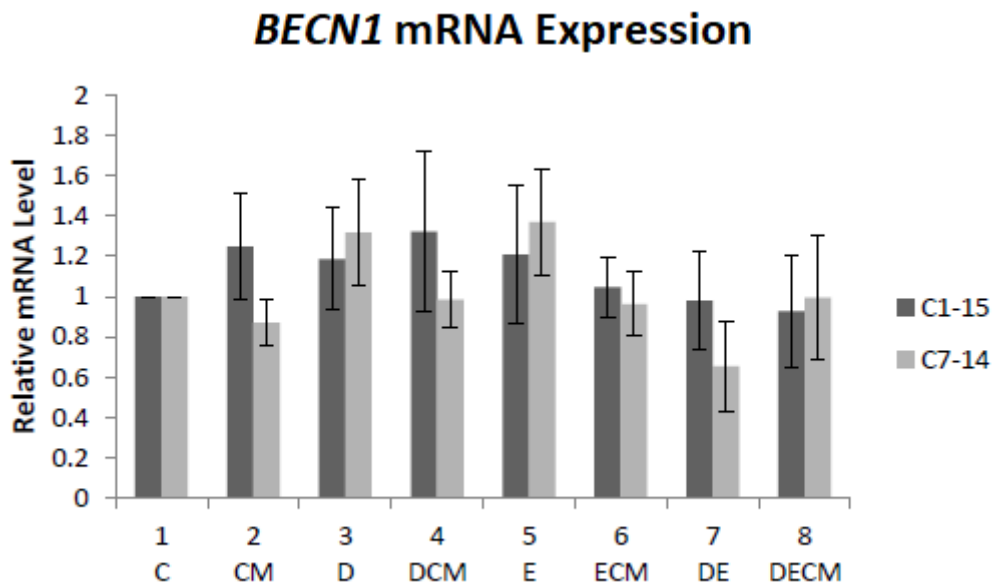
Figure 3.4.1: *BECN1* mRNA Expression.
C1-15 and C7-14 cells were treated with CM for 48 hours, 1μM dexamethasone (D) for 24 hours or 10μM etoposide (E) for 24 hours individually or in combination. RNA extracts from the cells were processed to cDNA and subjected to qPCR. Data represents at least three independent experiments +/- SEM.

Despite trends appearing in *BECN1* mRNA levels under various treatments (Figure 3.4.1 above), no statistically significant differences were observed. The previous finding of CM exerting opposing cell-specific differences was again observed, as CM treatment for C1-15 trended towards increasing *BECN1* mRNA, whilst the trend for C7-14 was a

114

marginal decrease (lane 2, compare dark to light bars). Increasing *BECN1*, which is linked to the potentially pro-survival process of autophagy, may increase cell viability and be a route by which CM exerts a cytoprotective effect. Although dexamethasone trended towards increasing *BECN1* mRNA, these levels were again statistically insignificant. Treatments in general did not exert significant effects for *BECN1*, at least at the mRNA level.

RIPK1 mRNA Expression
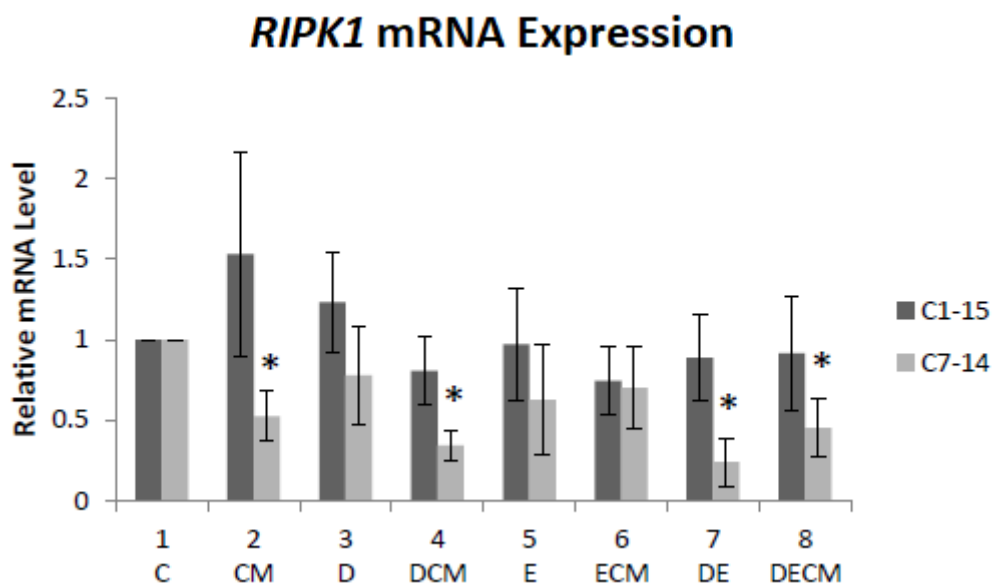
Figure 3.4.2: *RIPK1* mRNA Expression.

C1-15 and C7-14 cells were treated with CM for 48 hours, 1µM dexamethasone (D) for 24 hours or 10µM etoposide (E) for 24 hours individually or in combination. RNA extracts from the cells were processed to cDNA and subjected to qPCR. Data represents at least three independent experiments +/- SEM. P-value ≤ 0.05 is indicated by *.

CM appears to exert opposite effects between C7-14 and C1-15 cells, with C1-15 trending towards increase of *RIPK1* mRNA whilst C7-14 cells under CM treatment exhibit a statistically significant loss of *RIPK1* mRNA (compare dark and light bars of lane 2 to lane 1 of Figure 3.4.2). Importantly, this demonstrates a validation of the microarray described previously, providing further evidence for the role of CM in repressing *RIPK1* in C7-14 cells. Dexamethasone in C7-14 cells trended towards decreasing *RIPK1* levels; however this was not seen in C1-15 cells (lane 3, compare dark to light bars of Figure 3.4.2). Combination of CM with dexamethasone further

repressed *RIPK1* in C7-14, restoring the statistical significance (compare light bars of lanes 1 and 4 of Figure 3.4.2). Again, this was not seen for C1-15 cells.

Dexamethasone treatment in C7-14 cells did not result in a statistically significant decrease of *RIPK1* levels. However, a trend towards reduction was observed and further evidence for *RIPK1* repression in GC-sensitive cells can be seen by the fact that etoposide alone did not have a significant effect on *RIPK1* (though a trend for reduction was seen), whilst dexamethasone and etoposide combination lead to a statistically significant loss of *RIPK1* levels (compare light bars of lanes 5 and 7 of Figure 3.4.2). This loss was maintained following the addition of CM (compare light bars of lanes 7 and 8 of Figure 3.4.2). The same treatments in C1-15 cells did not exhibit any significant changes or notable trends.

3.4.2   Effects on BECN1, Caspase-3 and RIPK1 Protein Levels
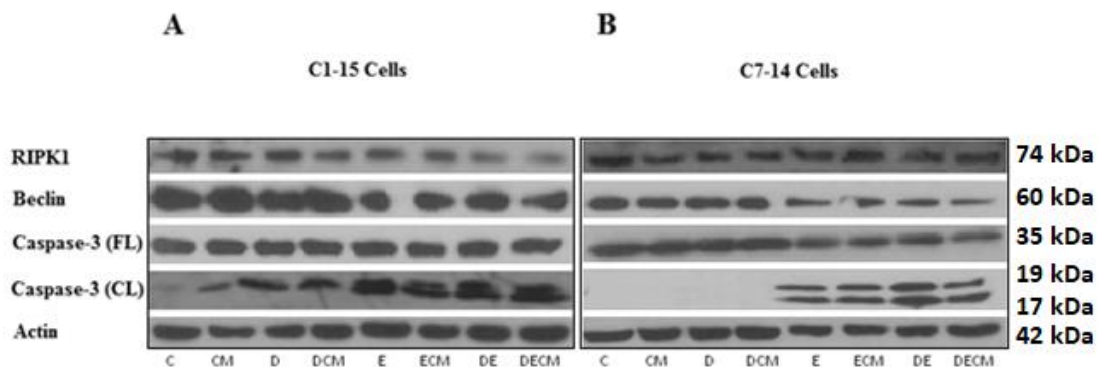
Figure 3.4.3: CM and chemotherapy modulate BECN1, caspase-3 and RIPK1.

C1-15 and C7-14 cells were treated with CM for 48 hours, 1μM dexamethasone (D) for 24 hours or 10μM etoposide (E) for 24 hours individually or in combination. Cells were lysed and Western blot analysis was used to detect RIPK1, BECN1, caspase-3 (FL, full-length) and caspase-3 (CL, cleaved). Actin was used as a loading control. Data is representative of at least three independent experiments.

Although the raw immunoblot data presented above is useful for visual analysis, densitometry has also been applied to analyse this data and additional western blot replicates (data not shown) in a more quantitative manner:

116
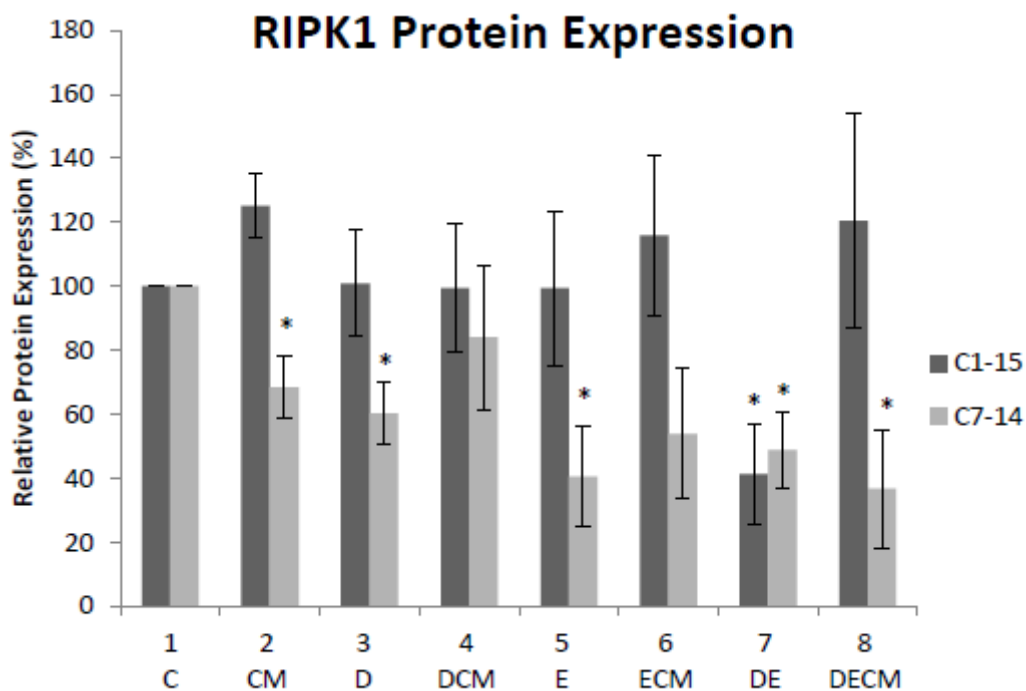
Figure 3.4.4: Densitometric analysis of RIPK1 protein levels.

C1-15 and C7-14 cells were treated with CM for 48 hours, 1μM dexamethasone (D) for 24 hours or 10μM etoposide (E) for 24 hours individually or in combination. Blots were analysed with ImageJ. RIPK1 band readings were normalised to the corresponding actin band reading and then expressed relative to untreated cells. Data is representative of at least three independent experiments +/- SEM. P-value ≤ 0.05 is indicated by *.

Densitometric analysis of RIPK1 protein levels reveals a good degree of consistency between this and the previous experiments on mRNA levels (Figure 3.4.2, Page 115). Opposing effects of CM are seen and show the same pattern as for mRNA levels, with C1-15 trending towards increased RIPK1 and C7-14 exhibiting statistically significantly lower RIPK1 protein levels (compare dark and light bars of lane 2 to lane 1). In C7-14 cells dexamethasone leads to a statistically significant reduction of RIPK1 protein levels, whilst this is not seen for C1-15 cells (compare dark and light bars of lane 3 to lane 1). This again correlates with the trend towards lower *RIPK1* mRNA identified in C7-14 cells in Figure 3.4.2 (Page 115). Notably, although CM and dexamethasone individually each repress RIPK1 protein to a significant degree in C7-14 cells, combined CM/dexamethasone treatment abolishes this downregulation.

In general, RIPK1 expression is lowered in C7-14 cells across the majority of the treatments, whilst for C1-15 it is largely unchanged, save for a trend for increase under CM treatment and a statistically significant reduction following combination treatment with dexamethasone and etoposide (compare dark bars of lanes 2 and 7 to lane 1).
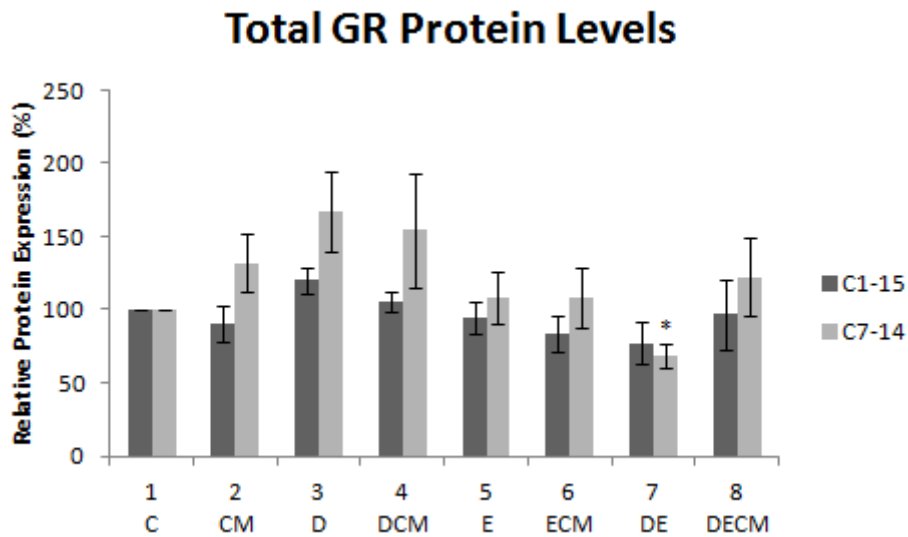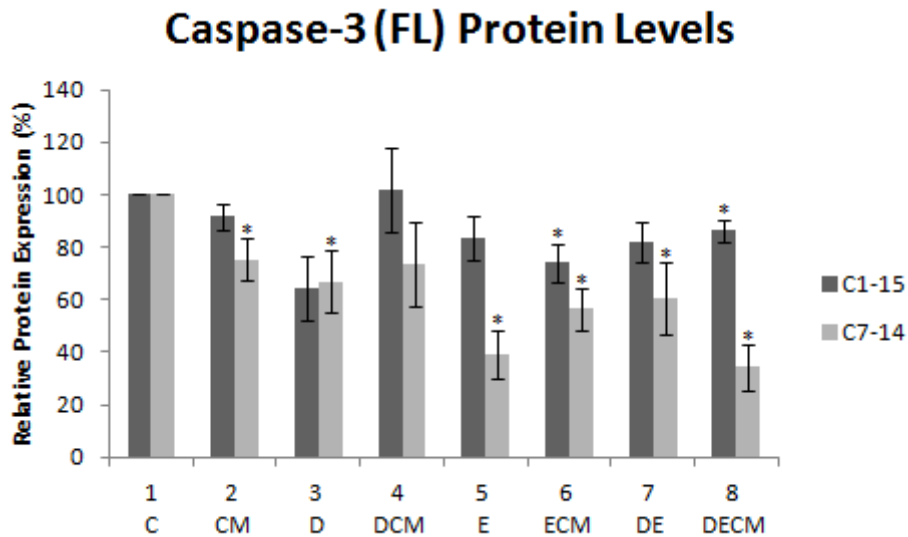

Figure 3.4.5: Densitometric analysis of caspase-3 (FL) protein levels.

C1-15 and C7-14 cells were treated with CM for 48 hours, 1μM dexamethasone (D) for 24 hours or 10μM etoposide (E) for 24 hours individually or in combination. Blots were analysed with ImageJ. Caspase-3 (FL) band readings were normalised to the corresponding actin band reading and then expressed relative to untreated cells. This Figure contains quantification of blot data generated by both the author of this thesis and an additional researcher. Data is representative of at least three independent experiments +/- SEM. P-value ≤ 0.05 is indicated by *.

Caspase-3 (FL) analysis revealed a significant degree of modulation across numerous treatments in both cell lines. For both cell lines, CM reduced the expression of Caspase-3 (FL), though the reduction is only statistically significant for C7-14, and a similar pattern is seen for dexamethasone (compare lanes 2 and 3 to lane 1). However, dexamethasone and CM combination treatment removed this loss, or at least its statistical significance in C7-14 cells (compare lane 4 to lane 3). A difference can be seen in etoposide treatment between the cells; for C7-14, etoposide induces a statistically significant loss of the full-length caspase, whilst although a loss was also seen in C1-15 cells, the reduction was not statistically significant (compare dark and

light bars of lane 5). Etoposide and CM combination in both cell lines statistically significantly reduces Caspase-3 (FL), though a higher loss is seen in C7-14 cells, and this trend is observed across all treatments containing etoposide (compare lanes 5-8 to lane 1).
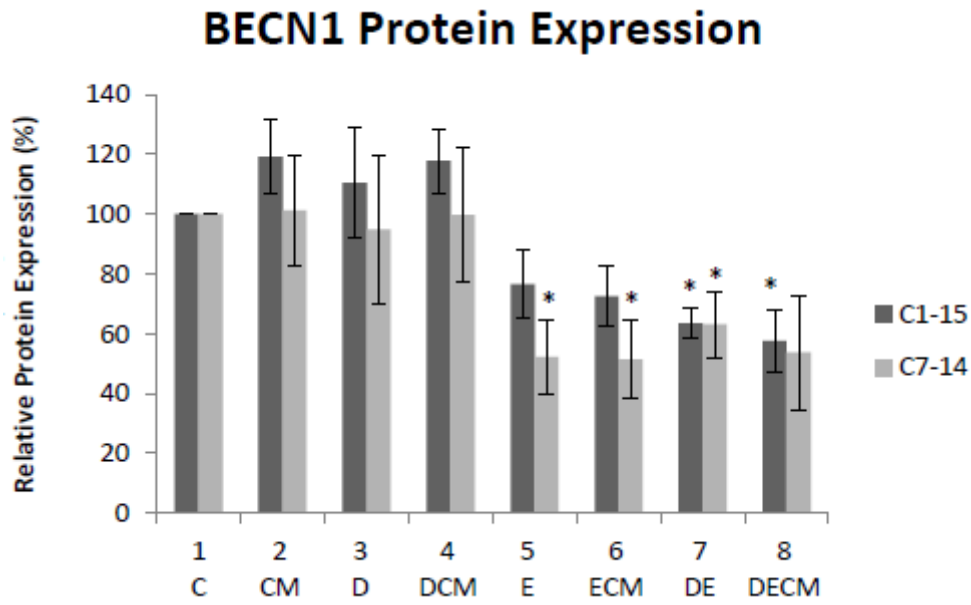
Figure 3.4.6: Densitometric analysis of BECN1 protein levels.

C1-15 and C7-14 cells were treated with CM for 48 hours, 1µM dexamethasone (D) for 24 hours or 10µM etoposide (E) for 24 hours individually or in combination. Blots were analysed with ImageJ. BECN1 band readings were normalised to the corresponding actin band reading and then expressed relative to untreated cells. This Figure contains quantification of blot data generated by both the author of this thesis and an additional researcher. Data is representative of at least three independent experiments +/- SEM. P-value ≤ 0.05 is indicated by *.

Similar to the mRNA analysis for *BECN1* (Figure 3.4.1, Page 114), CM trends towards increasing BECN1 protein levels in C1-15 cells, though again similar to mRNA analysis this change was not statistically significant (compare dark bars of lane 2 to 1). Overall, dexamethasone had no significant effect in either cell line.

Generally, higher levels of BECN1 protein were detected in C1-15 than C7-14 cells across all treatments (compare dark to light bars in lanes 2-8). Etoposide reduces BECN1 protein levels in both cell lines, though a larger (and statistically significant) loss is observed in C7-14 cells (compare lane 5 to lane 1). Dexamethasone and

etoposide combination treatment for both C1-15 and C7-14 induced a statistically significant loss of BECN1 protein, and yet addition of CM to this resulted in a loss of statistical significance in the decrease for C7-14 cells. Taken together, the protein data for BECN1 indicates that CM may modulate its expression in a positive manner, reducing the chemotherapy-induced downregulation of BECN1 to promote survival.

3.5   GR Occupancy on the *BECN1* and *RIPK1* Promoters

Section 3.4 above identified that dexamethasone exerts a negative effect on RIPK1 expression in glucocorticoid-sensitive cells. BECN1 and RIPK1 are both interesting targets not only for their involvement in cell death and survival pathways, but also for their known interaction with factors such as NF-κB, which is known to have high levels of crosstalk with GCs and GR signalling.

3.5.1   GRE Identification for *BECN1* and *RIPK1*

In order to investigate if the GR occupies the *BECN1* and *RIPK1* upstream genetic regions (and thus identify whether *BECN1* and *RIPK1* may be under GR control) bioinformatics approaches were first used to identify putative GREs within the two regions. Using the QIAGEN Champion ChiP Transcription Factor Search Portal and sequence analysis to identify GRE half-sites, numerous GREs were identified on the *BECN1* genetic region, with several identified by QIAGEN Champion ChiP Transcription Factor Search Portal:
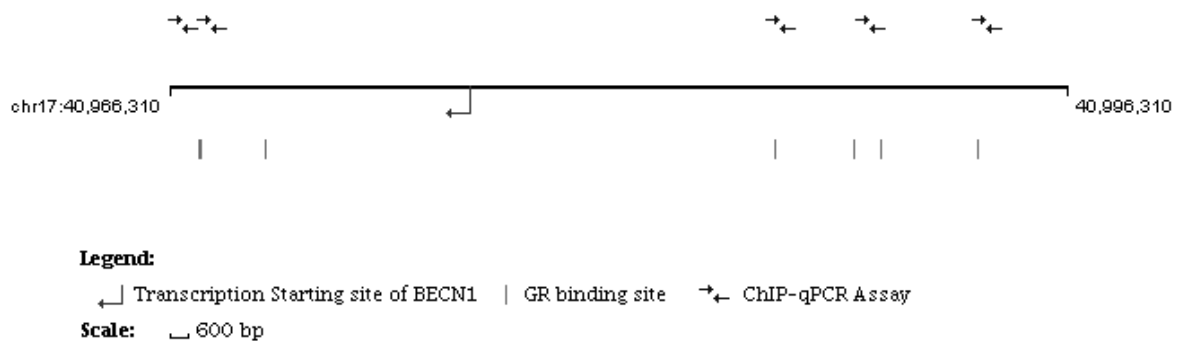
Figure 3.5.1: Identification of putative GREs on the *BECN1* upstream region.

Figure adapted from the QIAGEN Champion ChiP Transcription Factor Search Portal.

Such a high number of putative GR binding sites half-sites strongly suggests the possibility that *BECN1* is a target for GR, albeit under possibly a very complex control. Furthermore, some GREs were adjacent to NF-κB binding sites, indicating the possibility of crosstalk, which may further complicate the potential regulation of BECN1 by the GR.

The QIAGEN Champion ChiP Transcription Factor Search Portal was also used to identify putative GREs on the *RIPK1* upstream region:
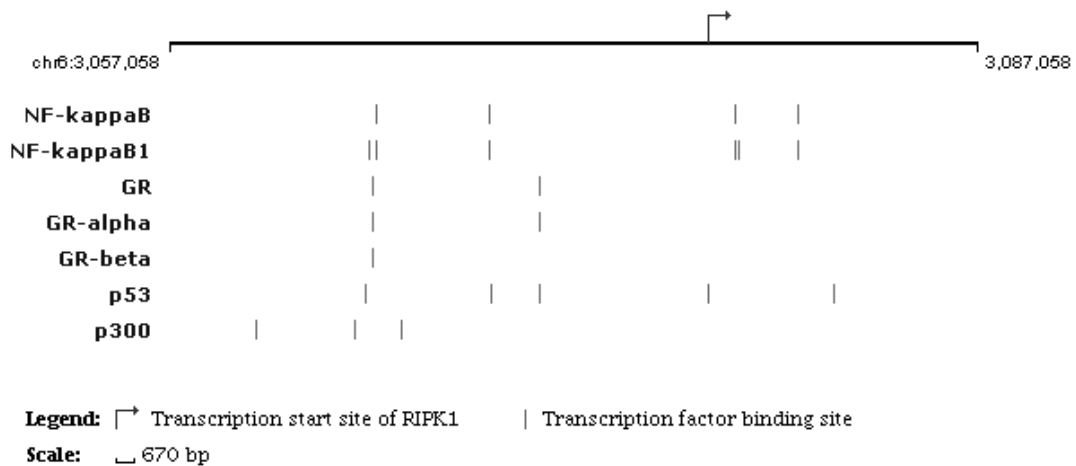
Figure 3.5.2: Identification of putative GREs on the *RIPK1* upstream region.
Figure adapted from the QIAGEN Champion ChiP Transcription Factor Search Portal.

Two putative GREs were identified by the QIAGEN Champion ChiP Transcription Factor Search Portal on the *RIPK1* upstream region. Similar to *BECN1*, these GREs were located close to NF-κB binding sites.

The Champion ChiP Transcription Factor Search Portal uses SABiosciences' Text Mining Application and the University of California Santa Cruz (UCSC) Genome Browser as a data source (SABiosciences, 2012). To verify that the genetic region shown in Figure 3.5.1 and Figure 3.5.2 is active the UCSC Genome Browser was used for K562 cells:
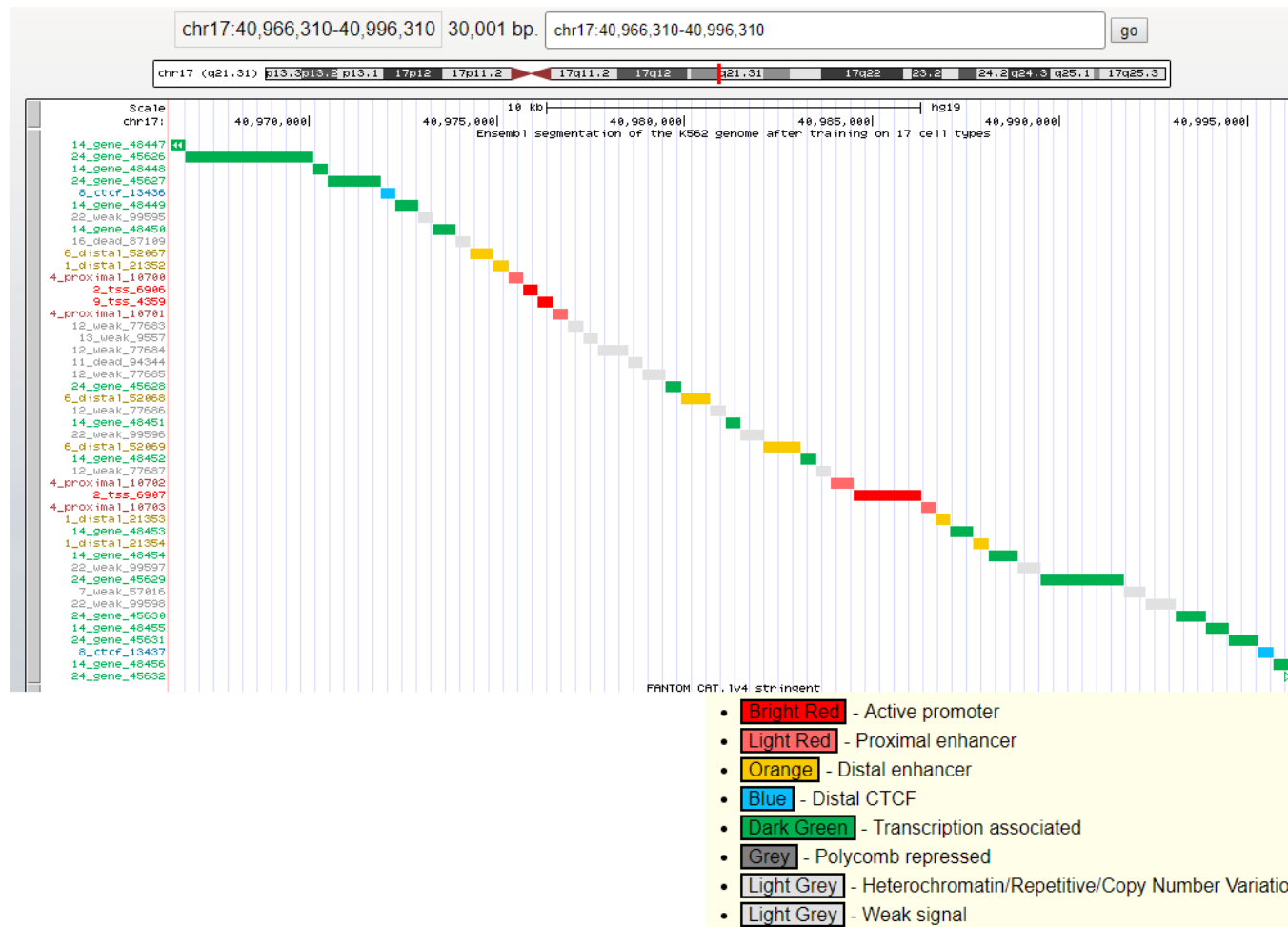
Figure 3.5.3: UCSC Genome Browser output for the *BECN1* region shown in Figure 3.5.1.

Figure adapted from the UCSC Genome Browser.
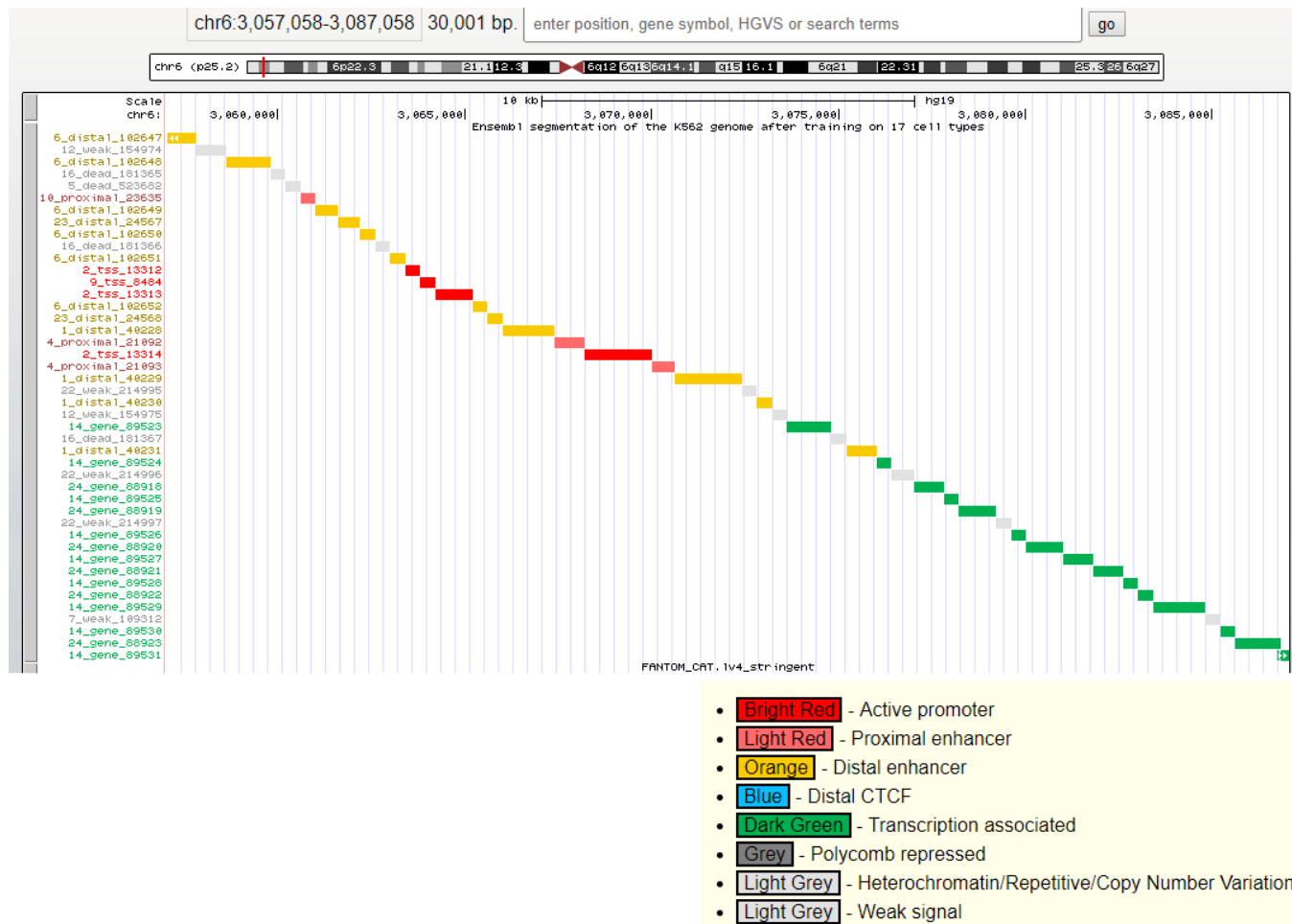
Figure 3.5.4: UCSC Genome Browser output for the *RIPK1* region shown in Figure 3.5.2.

Figure adapted from the UCSC Genome Browser.

3.5.2   Occupancy of the GR on the *BECN1* and *RIPK1* Upstream Region

Following identification of the putative GREs described above ChIP experiments were performed against one putative GRE for *BECN1* and both putative GREs for *RIPK1*, using antibodies against total GR, S211-phosphorylated GR and S226-phosphorylated GR.
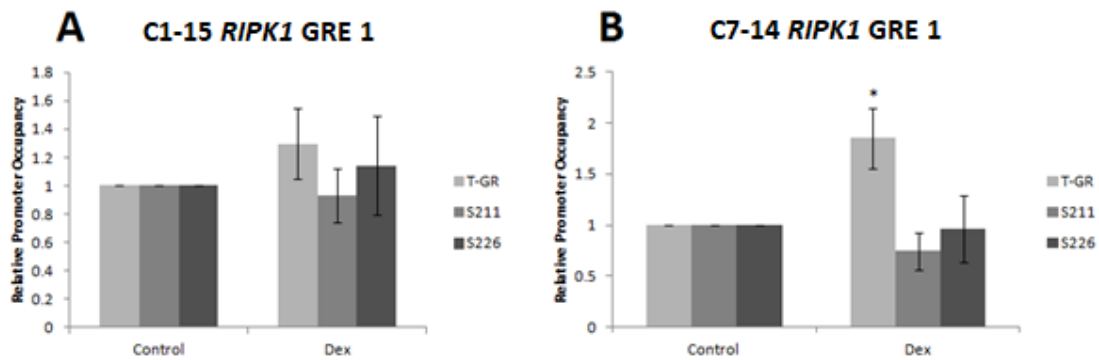
Figure 3.5.5: Relative promoter occupancy at *RIPK1* GRE 1.

C1-15 and C7-14 cells were treated with dexamethasone (1µM) for 24 hours and subjected to chromatin immunoprecipitation analysis. Data for each antibody was normalised first to the respective negative control IgG, and then to the IgG-normalised value for the antibody for untreated cells.

Data represents the average of at least three independent experiments +/- SEM. P-value ≤ 0.05 is indicated by *.

No significant difference in promoter occupancy was identified in C1-15 cells following dexamethasone treatment, regardless of the GR antibody used Figure 3.5.5A). Contrary to this, as shown in Figure 3.5.5B, dexamethasone induced a statistically significant increase in the relative promoter occupancy of T-GR in C7-14 cells, indicating presence of the GR at this GRE. However, there was no overall change (and in fact a trend towards reduced levels) of S211/S226-phosphorylated GR.
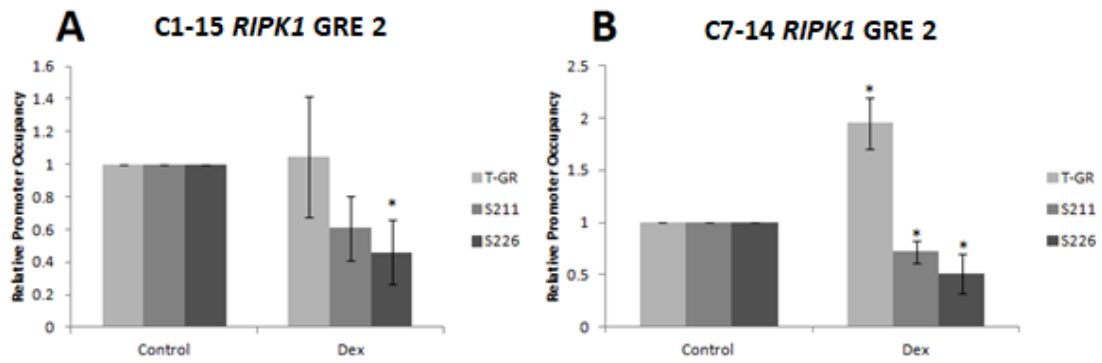
Figure 3.5.6: Relative promoter occupancy at *RIPK1* GRE 2.

C1-15 and C7-14 cells were treated with dexamethasone (1μM) for 24 hours and subjected to chromatin immunoprecipitation analysis. Data for each antibody was normalised first to the respective negative control IgG, and then to the IgG-normalised value for the antibody for untreated cells.

Data represents the average of at least three independent experiments +/- SEM. P-value ≤0.05 is indicated by *.

As before with *RIPK1* GRE 1, there was no significant difference in recruitment for T-GR for C1-15 cells following dexamethasone treatment (Figure 3.5.6A). Curiously, there was a noted decrease in the phosphorylated forms of the GR following hormone treatment. The same was shown – and statistically significant – for the phosphorylated forms of the GR in C7-14 cells Figure 3.5.6B). However, as with *RIPK1* GRE 1 (Figure 3.5.5B), treatment with dexamethasone lead to a statistically significant increase in the relative promoter occupancy of T-GR in C7-14 cells (Figure 3.5.6B). Thus, a difference between GC-resistant and GC-sensitive cells has been highlighted, as has the identification of *RIPK1* as a target for control by GR through promoter binding.

In addition to the two putative GREs within the *RIPK1* promoter, one putative GRE within the *BECN1* promoter was assessed by ChIP experiments:
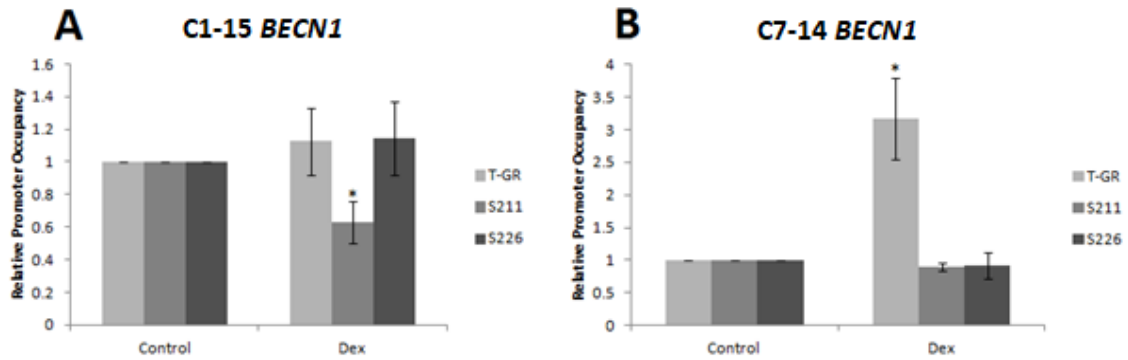
Figure 3.5.7: Relative promoter occupancy at a putative GRE at *BECN1*.

C1-15 and C7-14 cells were treated with dexamethasone (1µM) for 24 hours and subjected to chromatin immunoprecipitation analysis. Data for each antibody was normalised first to the respective negative control IgG, and then to the IgG-normalised value for the antibody for untreated cells.

Data represents the average of at least three independent experiments +/- SEM. P-value ≤ 0.05 is indicated by *.

For C1-15 cells, there was no significant change in recruitment of either T-GR or S226-phosphorylated GR, whilst there was a statistically significant reduction in S211-phosphorylated GR promoter occupancy following hormone treatment (Figure 3.5.7A). The same was not seen in C7-14 cells; there was no change, positive or negative for either phosphorylated form of the GR following hormone treatment, whilst there was a statistically significant increase in the relative promoter occupancy of T-GR Figure 3.5.7B).

3.6   Modulation of BIRC3 and Caspase-8 by CM and chemotherapy

BIRC3 (Baculoviral IAP Repeat-Containing Protein 3, also known as cIAP2) is a protein that, as a member of the Inhibitor of Apoptosis (IAP) family, has an established anti-apoptotic function. IAP family members are aberrantly expressed amongst a variety of cancer types (Fulda, 2008) and their expression has thus been implicated in the development of chemoresistance. BIRC3 is particularly relevant to this study due to the fact it is involved in the ubiquitination of RIPK1 which, depending on its ubiquitination status, may alter cell fate to either pro-survival signalling through NF-κB activation (Wu et al., 2012), promotion of apoptosis when deubiquitinated (Schenk and Fulda, 2015), or promotion of necroptotic signalling when caspase-8 activity (and subsequent

caspase-8-mediated RIPK1 cleavage) is blocked (Schenk and Fulda, 2015). This thus highlights BIRC3 and caspase-8 as important targets to follow due to their role in determining cell fate.

3.6.1 Analysis of BIRC3 mRNA Levels

As clarified above, the interplay between caspase-8, RIPK1, and BIRC3 can be a key determinant of cell fate. Due to this, mRNA levels of *BIRC3* were followed under CM and chemotherapy treatment under the hypothesis that its expression would be modulated, thus providing insight into therapeutic shortcomings.
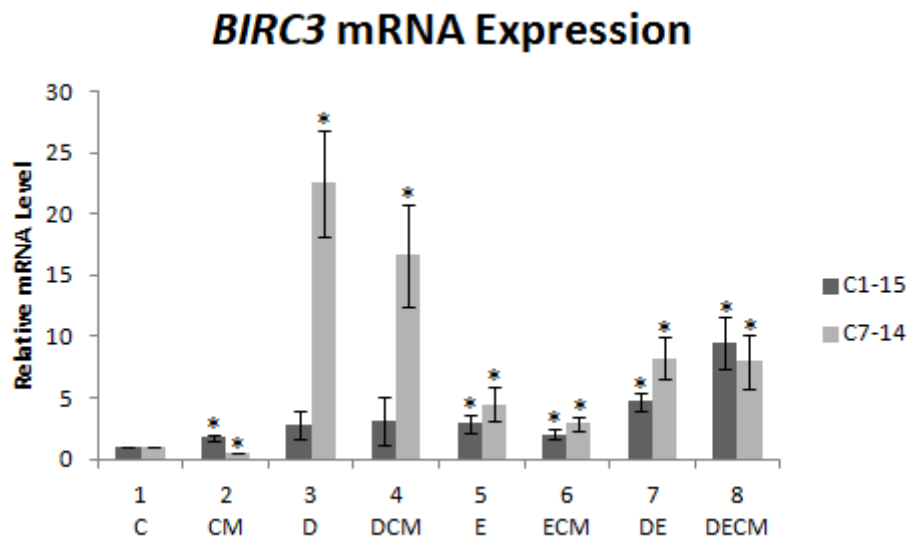
Figure 3.6.1: *BIRC3* mRNA Expression.

C1-15 and C7-14 cells were treated with CM for 48 hours, 1μM dexamethasone (D) for 24 hours or 10μM etoposide (E) for 24 hours individually or in combination. RNA extracts from the cells were processed to cDNA and subjected to qPCR. Data represents at least three independent experiments +/- SEM. P-value ≤ 0.05 is indicated by *.

In C1-15, a statistically significant upregulation of *BIRC3* was observed when cells were treated with CM (compare dark bars of lanes 1 and 2 of Figure 3.6.1), indicating a potential route through which CM exerts its cytoprotective effects. All treatments containing etoposide lead to significant increase in *BIRC3*, with the most prominent being dexamethasone, etoposide and CM combination (compare dark bars of lane 1 to

127

lanes 5-8 of Figure 3.6.1). The same effects of etoposide were recapitulated in C7-14 cells, with all treatments containing etoposide demonstrating a statistically significant increase of *BIRC3* expression (compare light bars of lane 1 to lanes 5-8 of Figure 3.6.1). However, CM resulted in a statistically significant reduction in *BIRC3* levels in C7-14 cells (compare light bars of lanes 1 and 2 of Figure 3.6.1). This is curious, given the established pro-survival influence of CM and the fact that this anti-apoptotic protein is significantly repressed. Dexamethasone, and to a slightly lesser extent dexamethasone and CM combination, both induced a dramatic, statistically significant increase in *BIRC3* expression (compare lanes 3 and 4 of Figure 3.6.1). Crucially, dexamethasone and etoposide combination lead to a sharp decrease in *BIRC3* levels relative to dexamethasone alone (compare lanes 3 and 5 of Figure 3.6.1), which may indicate the molecular basis for the beneficial effects observed with this combination therapy in the clinic.

3.6.2   Occupancy of the GR on the *BIRC3* Promoter

Due to the highly significant increase in *BIRC3* expression following dexamethasone treatment identified in the previous section, ChIP experiments were employed to investigate the occupancy of the GR on the *BIRC3* promoter in C1-15 and C7-14 cells. Five putative GREs within the *BIRC3* sequence were identified; three in the promoter region and two in the coding region. To address the occupancy of GR, two putative GREs were investigated: one in the coding region (GRE 5) and one in the promoter region (GRE 3).
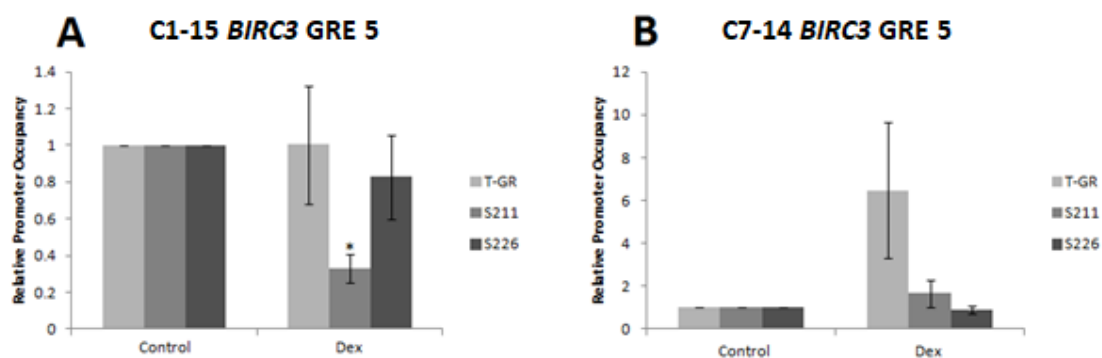
Figure 3.6.2: Relative promoter occupancy at putative GRE 5 on *BIRC3*.

C1-15 and C7-14 cells were treated with dexamethasone (1μM) for 24 hours and subjected to chromatin immunoprecipitation analysis. Data for each antibody was normalised first to the respective negative control IgG, and then to the IgG-normalised value for the antibody for untreated cells.

Data represents the average of at least three independent experiments +/- SEM. P-value ≤ 0.05 is indicated by *. Due to the fact that experimental differences here result in lack of statistical significance, the individual replicates used to generate this figure are shown in Appendix Figure 6 - Appendix Figure 8 (Page 211).

No significant differences in recruitment for T-GR or S226-phosphorylated GR following dexamethasone treatment was observed in C1-15 cells at putative GRE 5. However, a significant loss of S211-phosphorylated GR was observed following hormone treatment, which may indicate the possibility of some regulation at that GRE by the GR (Figure 3.6.2A). For C7-14 cells, no change in either phosphorylated form was observed, whilst an increase of the recruitment of T-GR was seen following hormone treatment (Figure 3.6.2B). However, this recruitment increase was not statistically significant.
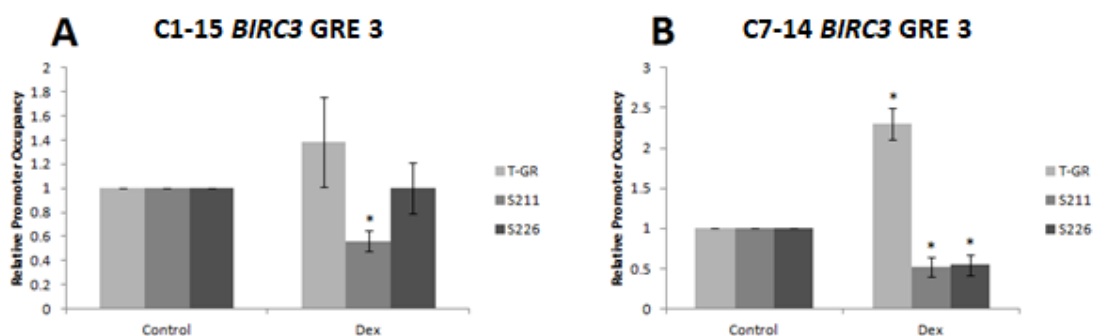
Figure 3.6.3: Relative promoter occupancy at putative GRE 3 on *BIRC3*.

C1-15 and C7-14 cells were treated with dexamethasone (1μM) for 24 hours and subjected to chromatin immunoprecipitation analysis. Data for each antibody was normalised first to the respective negative control IgG, and then to the IgG-normalised value for the antibody for untreated cells.

Data represents the average of at least three independent experiments +/- SEM. P-value ≤ 0.05 is indicated by *.

As with putative GRE 5 in Figure 3.6.2, there was no significant change in recruitment for T-GR and S226-phosphorylated GR at putative GRE 3 following hormone treatment in C1-15 cells, whilst a significant loss of S211-phosphorylated GR was seen (Figure 3.6.3A). C7-14 cells showed a statistically significant loss of occupancy for S211/S226-

phosphorylated GR following hormone treatment, whilst there was a statistically significant increase in the occupancy of T-GR.

3.6.3   Analysis of Caspase-8 Activation
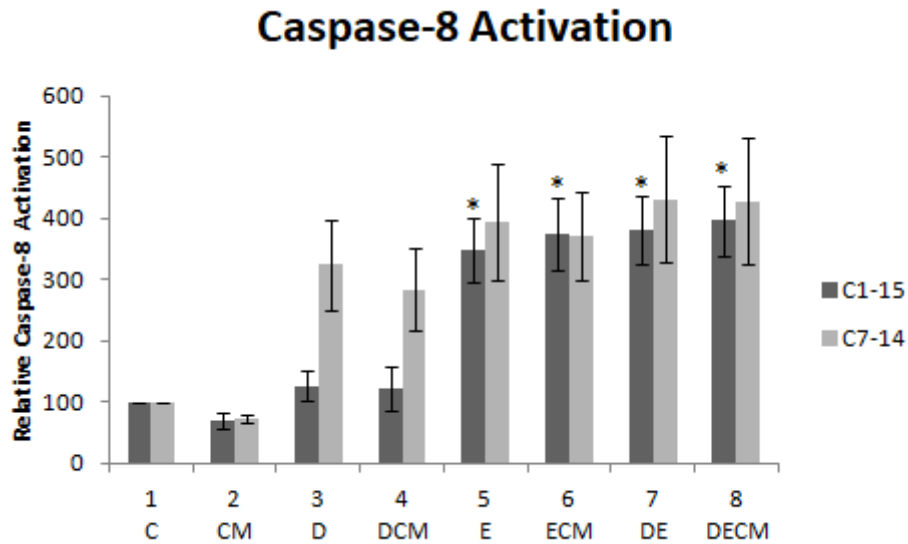
Figure 3.6.4: Caspase-8 activation under CM and chemotherapy treatments.

Cells were treated with CM for 48 hours, 1μM dexamethasone (D) for 36 hours and 10μM etoposide (E) for 24 hours individually or in combination. Cells were processed and loaded onto the NucleoCounter machine and ran under the "Caspase Assay" setting. Data is representative of the average of three independent experiments +/- SEM. P-value ≤ 0.05 is indicated by *.

Although not statistically significant, CM in both cell lines resulted in a trend for reduction of caspase-8 activation, representing another mechanism by which the microenvironment may promote cell survival (Figure 3.6.4, compare lane 2 to lane 1). The differential cellular response to hormone can be seen, with C7-14 cells exhibiting a trend of higher levels of caspase activation, whereas C1-15 cells did not achieve higher levels of caspase activation under the same treatment (Figure 3.6.4, compare dark and light bars of lane 3). Addition of CM did not alter activation levels for C1-15, but a slight reduction in activation for C7-14 (Figure 3.6.4, compare lanes 3 and 4) was seen. Etoposide, in both cell lines, trended towards or statistically significantly increased caspase-8 activation, with C7-14 generally displaying a higher trend of activation than C1-15 (Figure 3.6.4, compare dark to light bars of lanes 5-8). This higher activation, in

combination with other findings detailed previously, may partially explain the higher sensitivity of C7-14 to etoposide.

3.7   Functional analysis of CM and chemotherapy effects

In order to validate and expand upon the molecular findings described above, functional assays were undertaken to verify the observed effects at a whole-cell level. Two approaches were employed: cell type analysis (sorting cells into healthy cells and apoptotic cells) and fluorescence activated cell sorting (FACS) cell cycle analysis, with a focus on dead cells in Sub-G1. As detailed Section 2.1.19 (Page 91), this cell type analysis was captured in parallel with the caspase-8 activation shown previously.

3.7.1   Cell Type Analysis
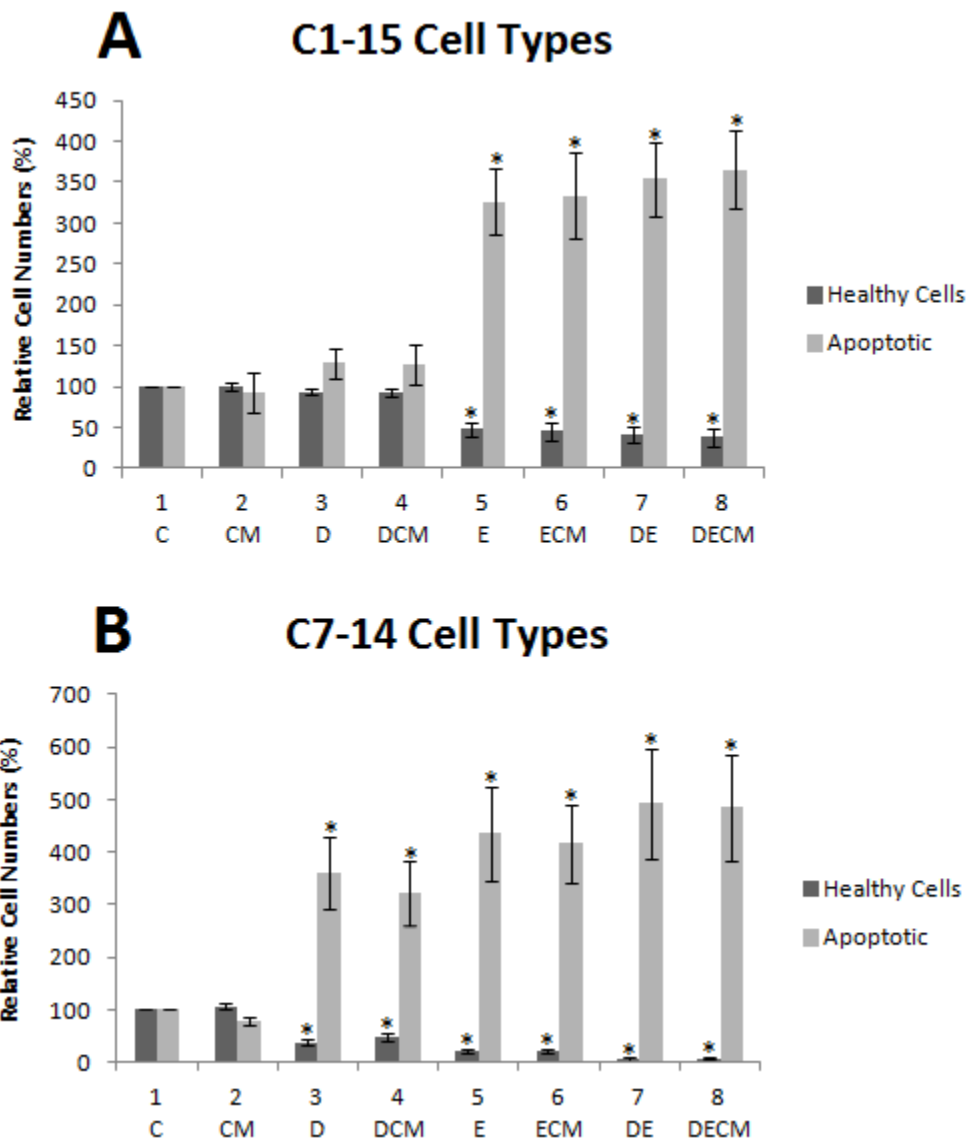
Figure 3.7.1: Cell type analysis under CM and chemotherapy treatments.

Cells were treated with CM for 48 hours, 1µM dexamethasone (D) for 36 hours and 10µM etoposide (E) for 24 hours individually or in combination. Cells were processed and loaded onto the NucleoCounter machine and ran under the "Caspase Assay" setting (results in this Figure were captured concurrently with capturing of caspase-8 activation results (Figure 3.6.4)). Four cell types are recognised by the machine: healthy; early apoptotic; late apoptotic and necrotic (Figure 2.1.6, Page 92). In this figure early and late apoptotic are combined. Necrotic cells are shown in Appendix Figure 9 (Page 212). Data is representative of the average of three independent experiments +/- SEM. P-value ≤ 0.05 is indicated by *.

Cell type analysis unveiled a trend for CM towards decreasing the number of apoptotic cells in C7-14 cells, whilst this effect was not seen in C1-15 cells (compare light bars of lane 2 to lane 1 in Figure 3.7.1A and Figure 3.7.1B). This is somewhat consistent with

the caspase-8 activation levels shown previously, where CM trended towards decreasing caspase-8 activation (Figure 3.6.4). Similar to this, C1-15 cells did not show significant changes in healthy or apoptotic cells following hormone treatment, or indeed under dexamethasone and CM combination treatment (compare lanes three and four to lane 1 of Figure 3.7.1A). However, this was not the case for C7-14 cells, where dexamethasone and dexamethasone/CM combination treatment both lead to a statistically significant decrease in healthy cells (compare dark bars of lanes 3 and 4 to lane 1 of Figure 3.7.1B) and a statistically significant increase in apoptotic cells (compare light bars of lanes 3 and 4 to lane 1 of Figure 3.7.1B). In both cell lines, all treatments containing etoposide lead to a statistically significant reduction in healthy cells (compare dark bars of lanes 5-8 to lane 1 of Figure 3.7.1) as well as a statistically significant increase in apoptotic cells (compare light bars of lanes 5-8 to lane 1 of Figure 3.7.1).

3.7.2 Sub-G1 FACS Analysis of CM and Chemotherapy Effects

Analysis of cell types by the NucleoCounter provided insight into distribution of cell types present within an aliquot of cells. However, the identification of healthy and apoptotic cells is dependent upon gating intensities of caspase-8 activity and PI intensity (see gating strategy in Figure 2.1.6, Page 92). Thus, this approach does not analyse cells individually, but rather based on the staining intensities of a whole population. To complement this approach, FACS analysis was employed due to it analysing data on a cell-by-cell basis. Cell cycle analysis was performed, and the Sub-G1 phase (representative of dead cells) was examined:
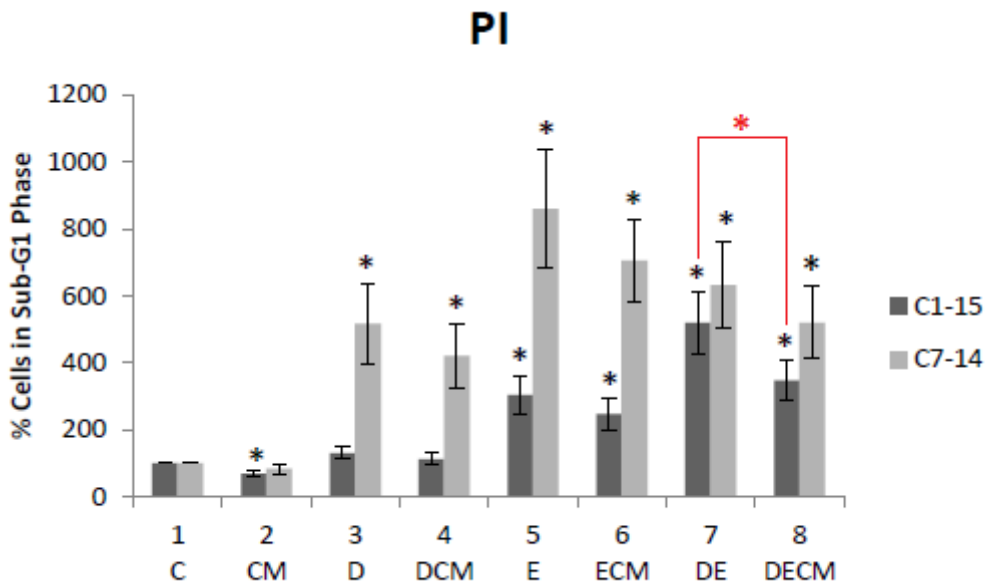
Figure 3.7.2: FACS analysis of CM and chemotherapy effects.

C1-15 and C7-14 cells were treated with CM for 48 hours, 1μM dexamethasone (D) for 36 hours and 10μM etoposide (E) for 24 hours individually or in combination. Cell cycle phases were gated and values for Sub-G1 across different treatments were expressed as a percentage of the value for untreated cells. Data in this Figure combines results from both the author of this thesis and an additional researcher. Data represents at least three independent experiments +/- SEM. P-value ≤ 0.05 is indicated by * (black asterisk for comparison of treatment to control). Red asterisks indicate statistical significance at $p \leq 0.05$ between other groups.

The FACS data presented in Figure 3.7.2 above shows that CM reduces the number of cells accumulating in the Sub-G1 phase in both cell lines, though the effect was only statistically significant for C1-15 cells (compare lane 2 to lane 1). A similar effect was observed for C1-15 cells under dexamethasone, etoposide and CM treatment compared to dexamethasone and etoposide treatment alone (compare dark bars of lane 7 and 8). As expected, and consistent with the caspase-8 activation experiment (Figure 3.6.4, Page 130) and cell types analysis (Figure 3.7.1 Page 132), C1-15 cells were insensitive to dexamethasone as well as dexamethasone/CM combination, with both treatments showing no significant change in the number of cells in Sub-G1 (compare dark bars of lanes 3 and 4 to lane 1 of Figure 3.7.2). Conversely, and again consistent with previous experiments, dexamethasone induced a statistically significant increase in the number of cells accumulating in the Sub-G1 phase (compare light bars of lane 3 to lane 1 of Figure 3.7.2). Addition of CM resulted in a reduction in the number of cells accumulating in

Sub-G1 phase, though its increase compared to untreated cells was still statistically significant (compare light bars of lanes 4 and 3 of Figure 3.7.2). In both cell lines, all treatments containing etoposide increased the number of cells accumulating in Sub-G1 phase, with higher Sub-G1 accumulation in C7-14 cells (compare lanes 5-8 to lane 1 of Figure 3.7.2).

3.8   Analysis of Putative Ubiquitinated RIPK1 and BIRC3 Inhibition

Previous sections have identified repression of RIPK1 by CM; regulation at the mRNA level may be through factors such as microRNAs or influence of upstream regulators, whilst regulation at the protein level can be due to previous downregulation at the mRNA level or protein-specific regulation such as targeting to degradation pathways through post-translational modifications. RIPK1 ubiquitination status plays a role in the determination of cell fate, whilst BIRC3 is known to be involved in the ubiquitination of RIPK1. The molecular weight of RIPK1 is approximately 74kDa, and during the Western experiments against RIPK1 (Figure 3.4.3 and Figure 3.4.4) a consistent band pattern under CM treatment at approximately 130kDa across several experiments was detected. The consistency of the band pattern suggested that these were not non-specific bands, but rather that they may potentially represent a modified RIPK1, such as a sumoylated or ubiquitinated form of the protein. This was investigated through Western blot analysis via treatment with AT406, a BIRC3 inhibitor. If these high molecular weight proteins are altered by AT406 treatment, it provides an indication that they may indeed represent ubiquitinated RIPK1, given that BIRC3 is known to ubiquitinate RIPK1.
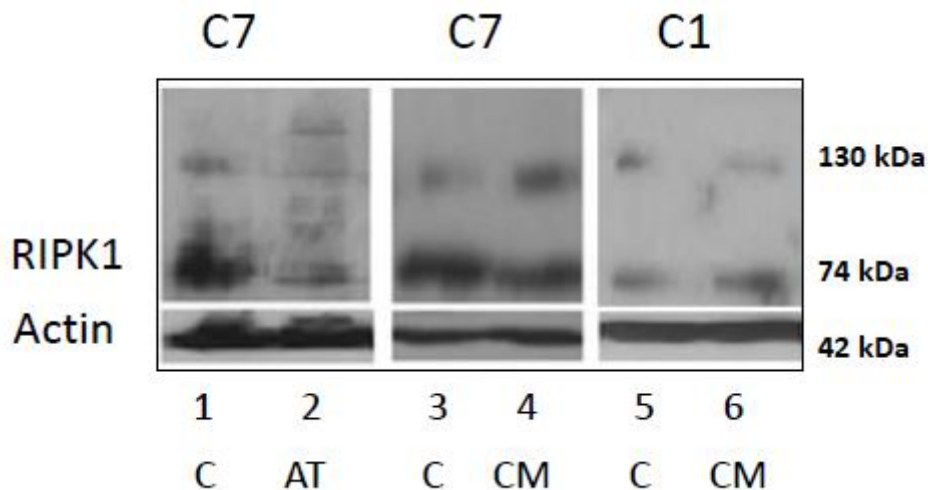
Figure 3.8.1: Preliminary analysis of putative ubiquitinated RIPK1.

C1-15 and C7-14 cells were treated either with 10μM AT406 (AT) or CM for 48 hours. Actin was used as a loading control. The bottom of the RIPK1 panel represents the native RIPK1 at approximately 74kDa whilst higher bands are at approximately 130kDa.

As shown above, treatment with CM decreased the band intensity of the approximately 74kDa RIPK1 in C7-14 cells (compare lower part of RIPK1 panel in lanes 3 and 4), whilst this effect was not seen in C1-15 cells (compare lower part of RIPK1 panel in compare lanes 5 and 6). Treatment with AT406 led to a significant reduction in the approximately 74kDa RIPK1 (compare lower part of RIPK1 panel in lanes 1 and 2). By contrast, the approximately 130kDa RIPK1 (high molecular weight bands interacting with the RIPK1 antibody) were significantly reduced by AT406 treatment (compare higher part of RIPK1 panel in lanes 1 and 2) in C7-14 cells, whilst the same bands were increased by CM (compare higher part of RIPK1 panel in lanes 3 and 4) in C7-14 cells, whilst there was no effect in C1-15 cells (compare higher part of RIPK1 panel in lanes 5 and 6). Though preliminary, the reduction of these bands by AT406 indicates that they may represent ubiquitinated RIPK1, given the role of BIRC3 in ubiquitinating RIPK1. Furthermore, this putative ubiquitination of RIPK1 is likely to be polyubiquitination given the increase in molecular weight and it is unlikely to be dimerisation of proteins due to the denaturing nature of the SDS gel.

Chapter 4   Computational Results

4.1   Introduction to Computational Research

As established in the Introduction, computational systems biology offers the possibility of generating models that can be used to provide insight into how a system behaves following network perturbation. This approach has been successfully applied to cancer research previously, such as the generation of TP53 models (Tian et al., 2013; Hussain et al., 2015). Here, a computational model of the GR signalling network has been established, with the model predictions being validated at both a laboratory and clinical level. The model (GEB052) demonstrated good predictive ratios and indicates key points for future expansion.

4.2   GEB052: A Systems Approach to Uncover GR Signalling Dynamics

As a complement to the detailed molecular approaches described in the previous chapter, computational systems biology has also been applied to develop an *in silico* model of the glucocorticoid receptor protein signalling network. An overview of the workflow is shown in Figure 4.2.1:
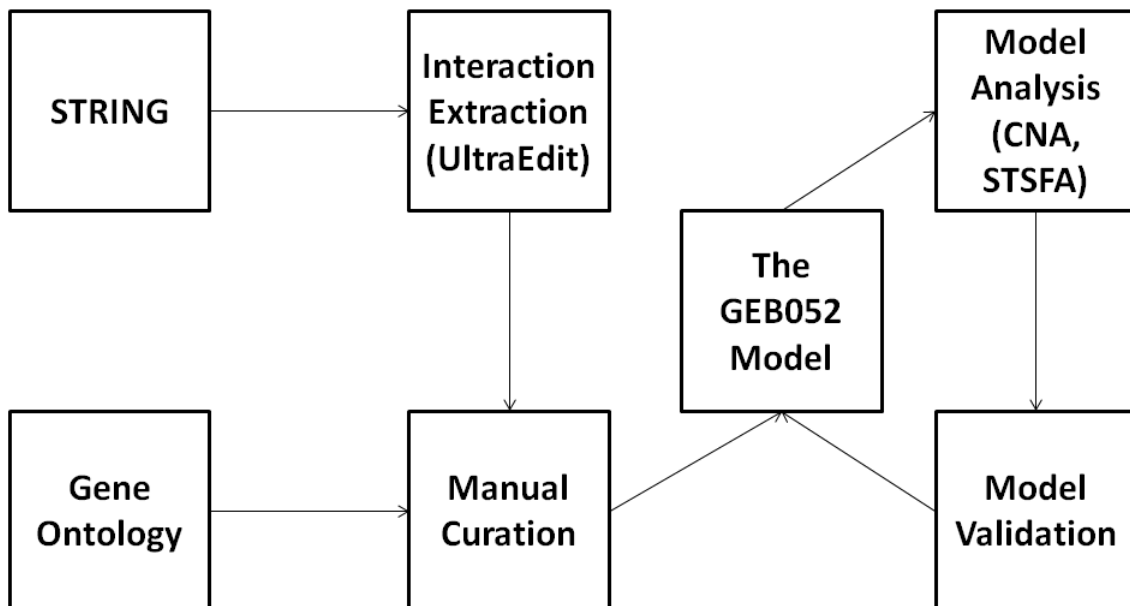
Figure 4.2.1: Overview of GEB052 model generation and analysis.

The modelling process begins with extraction of predicted protein interactions from STRING using UltraEdit. These interactions are then manually curated, and form the GEB052 model. Model outputs are added via the manual curation of gene ontology annotations. Following completion of the model, analysis is undertaken through CellNetAnalyzer and STSFA, with model validation assessing model accuracy. Model validation may be by literature searching, wet laboratory verification, or genome-wide validation by comparison to microarray data. Model validation can then be used to feed back to the model, identifying its shortcomings and indicating components for improvements.

During the modelling process, several rules regarding the interactions to be included were put into place to ensure model consistency. For the primary layer, proteins interacting directly with GR would be included within the model. Regarding cofactors for the GR (such as NCOA1, NCOR2, and others), a general rule was established that corepressors repress the GR, whilst coactivators would activate the GR. The extensive literature curation to verify each predicted interaction would provide at least one PubMed ID for a paper to provide evidence for the interaction. In the case of cofactors, this evidence would either be of the activation/inhibition of the GR or of the fact that it was a coactivator/corepressor.

The second layer, consisting of interactions between the proteins that interact with GR, established the "intermediary rule" in cases where it was discovered (following literature curation of a predicted direct relationship between Protein 1 and Protein 2) that Protein 1 modulates Protein 2 indirectly via modulation of a third protein between the two (i.e. Protein 1 → Intermediary Protein → Protein 2). If the intermediary protein was within the primary layer (i.e. it already existed within the model) then the reactions would be included in the model as Protein 1 → Intermediary Protein → Protein 2, even if STRING predicted a direct relationship (provided no additional evidence of a direct relationship was found). If the intermediary protein was not in the primary layer (i.e. it

138

is not already present in the model) then the reaction would be put as directly occurring from Protein 1 → Protein 2.

In several cases, multiple individual proteins were combined into one node within the model, often in cases where both proteins were subunits of a heterodimer or proteins from the same family were grouped into one node. Within the model, these nodes are AP-1 (consisting of FOS and JUN), NFKB (consisting of RELA and NFKB1) and 14-3-3 (consisting of various 14-3-3 proteins such as SFN/YWHAS, YWHAB, YWHAE, YWHAH, YWHAG, YWHAQ, and YWHAZ). Similarly, CREBBP and EP300 are combined as one CREBBP/EP300 node, and SUMO consists of interactions for SUMO1, SUMO2, SUMO3 and SUMO4. It is also worth noting that the node named PKA actually contains only the interactions for PRKACG, the gamma catalytic subunit of PKA (as this was the only PKA constituent to have a predicted high-confidence interaction with GR). However it is named PKA so that it may serve as an intermediary in the interactions between ABCA1/IL-10 and CRH/AP-1 (in both cases, STRING predicted a direct reaction but literature verification unveiled PKA as an intermediary). Lastly, the node named HSP90 contains only interactions for HSP90AA1 (HSP90 alpha).

The model was connected to the outputs of cell death and inflammation, as these are the two of the most important outputs for the GR. As detailed in Section 2.2.2 (Page 96) model outputs were based on GO direct annotations for all nodes in the model, ranked by the most common, and the most common annotations relating to cell death and inflammation were taken.

Presented in this and subsequent sections is the GEB052 (Glucocorticoid Receptor model by Emyr Bakker, consisting of 52 nodes) model, consisting of 52 nodes (proteins, inputs or outputs) connected by 241 logical interactions, in addition to detailed analysis and model validation. Sections 4.2.1 - 4.2.3 detail all of the interactions present within the model, as well as providing PubMed ID evidence for each interaction as the result of extensive literature verification of STRING predictions.

4.2.1   List of Primary Layer Interactions in the GEB052 Model

Table 4.2.1: List of primary layer interactions in the GEB052 model.

Node 1	Activates (1) or Inhibits (0)	Node 2	PubMed ID Evidence
14-3-3	0	GR	12730237
14-3-3	1	GR	9079630, 11266503, 16338219
AP-1	0	GR	8388998
AP-1	1	GR	8388998
ARHGAP35	0	GR	10385430, 20427664 , 1894621
BAG1	0	GR	11101523, 9603979, 19595997.
CREB1	0	GR	1387550
CREBBP/EP 300	0	GR	8616895, 10528999
CREBBP/EP 300	1	GR	17884810, 9792627, 10528999
DAP3	1	GR	10903152, 12099703
DAXX	0	GR	12595526, 17081986
GC	1	GR	No PMID - Logical Input For Model
GR	0	ABCA1	16254209
GR	1	ABCA1	17241464
GR	1	AFP	11549270
GR	0	AP-1	2169352, 2169353, 9731701
GR	1	AP-1	7583019
GR	1	ARHGAP35	1894621
GR	0	CD2	9144521
GR	1	CD2	9172010
GR	1	CD40LG	11160161
GR	0	CREB1	21804312
GR	1	CREB1	21804312, 14668092
GR	1	CREBBP/EP 300	23125313
GR	0	CRH	22232675, 19177170

GR	0	FSCN1	10026156
GR	1	GLUL	10453053, 14962810
GR	0	HDAC1	16762839, 12727880
GR	0	HDAC6	20538901
GR	1	IL10	10940925, 16341266
GR	0	IL6	22042221, 12114264, 11007957
GR	0	LIF	10080876, 8432990, 7579343, 9099902
GR	1	MED1	17827210
GR	0	NCOA1	11196413, 12039076
GR	0	NFKB	7823959, 8290595
GR	1	NFKB	9885901, 23693080
GR	1	NR1I3	11093784, 12511605, 15557560
GR	1	NR2F2	14739255
GR	1	PKA	16319314
GR	1	POU2F1	9584182
GR	0	POU2F2	1714379
GR	1	POU2F2	9584182
GR	1	SCAP	15133039
GR	1	SGK1	22590650, 17595317
GR	0	SMAD3	10518526
GR	0	STAT3	20881248
GR	1	STAT3	14522952
GR	1	STAT5B	9973262, 15037546
GR	0	TP53	11562347, 11080152
GR	1	TSC22D3	9430225, 16239257
GR	1	UBC	17875808, 11872750, 10913373,
HDAC1	0	GR	15826950
HDAC1	1	GR	15826950, 16762839
HDAC6	0	GR	20018896
HSP90	0	GR	2005120, 16087666
HSP90	1	GR	2005120, 16087666
IL10	1	GR	16341266
LIF	0	GR	15985451

MED1	1	GR	17827210, 10508170, 16239257, 19630272
NCOA1	1	GR	12569182, 16339206
NCOA2	1	GR	19805480
NCOA3	1	GR	11094166, 16179382
NCOA6	1	GR	10567404
NCOR1	0	GR	12011091, 12569182, 23428870
NCOR2	0	GR	10598585
NFKB	0	GR	7823959, 8290595
NR2F2	0	GR	14739255
NRIP1	0	GR	10364267, 12773562
POU2F1	1	GR	9584182
PRKDC	0	GR	9038175
PTGES3	0	GR	17261597
PTGES3	1	GR	17438133
SGK1	1	GR	23650397
SMAD3	1	GR	12753290
SMARCA4	0	GR	17043312
STAT3	1	GR	9388192, 12904256,20204302
STAT5B	0	GR	8878484
SUMO	0	GR	12193561
SUMO	1	GR	12193561
TP53	0	GR	9215863
TSG101	0	GR	10508170, 15033475
TSG101	1	GR	15657031

4.2.2 List of Second Layer Interactions in the GEB052 Model

Table 4.2.2: List of second layer interactions in the GEB052 model.

Node 1	Activates (1) or Inhibits (0)	Node 2	PubMed ID Evidence

14-3-3	0	TP53	18339856
14-3-3	1	TP53	9620776, 14517281
ABCA1	0	IL6	19783654, 17079792
ABCA1	1	PKA	23055522
AP-1	1	CREB1	11976688, 1827203
AP-1	1	IL10	16569682, 22634314, 15067049
AP-1	1	IL6	8453101, 15158360, 20833374
AP-1	0	NFKB	12181357
AP-1	1	NFKB	9468519, 8404856
AP-1	0	SMAD3	10903323, 10871633, 17660955
AP-1	1	SMAD3	16730810, 11134003
AP-1	1	STAT3	11356008
AP-1	0	TP53	10072388, 11136975
BAG1	1	AP-1	11329370, 20516211
CREB1	0	AP-1	1840296, 2140898
CREB1	1	AP-1	12432566, 9770464, 16151051, 2140898
CREB1	1	IL10	19564345, 16920714, 18263767
CREBBP/EP300	0	AP-1	11689449
CREBBP/EP300	1	AP-1	7588605, 21937452, 9388250, 10327051, 8545107
CREBBP/EP300	1	CREB1	13678586

CREB BP/EP 300	0	HDAC 1	16762839
CREB BP/EP 300	1	NCOA 1	15688032
CREB BP/EP 300	1	NCOA 2	20448036, 9430642, 10899170
CREB BP/EP 300	0	NFKB	12419806
CREB BP/EP 300	1	NFKB	9890939, 9096323, 11739381
CREB BP/EP 300	1	SMAD 3	9679056
CREB BP/EP 300	1	STAT3	15649887, 15653507
CREB BP/EP 300	0	TP53	19805293
CREB BP/EP 300	1	TP53	18485870, 9288775
CRH	0	IL6	10922080, 11602623, 1731761
CRH	1	IL6	1623564, 8246669
CRH	1	PKA	1663213 17895291, 11960782, 7783858, 8793851, 11325519 (N.B. Full pathway is CRH --> PKA --> AP-1)
DAXX	0	CREB 1	22185778
DAXX	1	SUMO	17081986

DAXX	0	TP53	15570294, 15364927
DAXX	1	TP53	14557665
HDAC 1	0	CREB 1	12567184
HDAC 1	0	CREB BP/EP 300	14968110
HDAC 1	0	NFKB	11931769
HDAC 1	0	SMAD 3	16876108
HDAC 1	0	STAT3	15653507, 18611949
HDAC 1	1	SUMO	18025037
HDAC 1	0	TP53	12426395, 10777477
HDAC 1	0	UBC	19304753
HDAC 6	1	HSP90	15916966, 19158084, 18591380
HSP90	1	HDAC 6	21109931
HSP90	1	PRKD C	22753480, 16263121
HSP90	1	PTGES 3	15040786
HSP90	1	STAT3	12559950, 18339423, 12235142
IL10	1	ABCA 1	16336952, 20354139
IL10	0	AP-1	9864163, 8709636, 20045008
IL10	0	IL6	12017175
IL10	1	IL6	8703029
IL10	1	STAT3	8830676

IL6	1	ABCA1	21757719
IL6	1	AP-1	10465257, 9240403, 17018293, 8398910
IL6	1	CRH	1846105, 2845968, 10465257
IL6	1	IL10	23349310
IL6	1	LIF	12151548
IL6	1	NCOA2	19240160
IL6	1	STAT3	17065510, 18160665
IL6	0	TP53	15930285, 1852210
LIF	1	AP-1	9711940, 9545305, 8621626, 1628710, 8917449, 2144331
LIF	1	IL6	11160255
LIF	1	STAT3	9813052
NCOA1	1	AP-1	9642216, 10847592, 18511550, 16860316
NCOA1	1	CREBBP/EP300	15688032
NCOA1	1	NCOA3	20685850
NCOA1	1	NFKB	9556555
NCOA1	1	STAT3	11773079
NCOA2	1	AP-1	18511550
NCOA2	1	CREBBP/EP300	15731352, 20448036
NCOA3	1	CREBBP/EP300	10866661
NCOA3	1	NCOA1	20685850

NCOA 6	1	PRKD C	12519782
NCOR 1	1	NCOA 3	12089344
NCOR 2	1	NCOA 3	20392877
NCOR 2	0	NFKB	10777532
NCOR 2	0	POU2F 1	11134019
NFKB	1	AP-1	8404856
NRIP1	0	AP-1	12554755, 10379892
PKA	1	AP-1	1663213 17895291, 11960782, 7783858, 8793851, 11325519 (N.B. Full pathway is CRH --> PKA --> AP-1)
PKA	1	CREB 1	15337521
PKA	1	IL10	23055522
PKA	0	NFKB	15642694
PRKD C	1	HSP90	22270370, 19021771
PRKD C	1	NCOA 6	12519782
PRKD C	0	POU2F 1	14612514
PRKD C	1	POU2F 1	17213819
PRKD C	1	TP53	9363941
PTGES 3	0	HSP90	11812147
PTGES 3	1	HSP90	9148915, 11060043
SGK1	1	CREB 1	15733869

SGK1	0	TP53	19756449
SMAD 3	0	AP-1	14752027
SMAD 3	1	AP-1	21829441, 9125213
SMAR CA4	0	AP-1	12372840, 10082538
SMAR CA4	1	AP-1	11053448
SMAR CA4	1	SMAD 3	21900401, 18003620
SMAR CA4	1	STAT3	21785422
SMAR CA4	0	TP53	19448667, 18822392
STAT3	1	AP-1	16205632, 9271408, 11319221, 7568080, 10490649, 20463008, 12600988, 19404962 (mutual activation due to widespread synergy)
STAT3	1	FSCN1	21937440
STAT3	1	HSP90	9461509, 23228483
STAT3	1	IL10	19234181
STAT3	1	IL6	19751774, 19284588, 18160665, 21122157
STAT3	0	TP53	16107692, 22303479
SUMO	0	AP-1	16055710, 10788439, 23396363
SUMO	1	DAXX	17081986
SUMO	0	HDAC 1	11960997
SUMO	1	HDAC 1	24068740
SUMO	0	TP53	21900752
SUMO	1	TP53	17012228
TP53	1	14-3-3	14517281, 17546054
TP53	1	CREB BP/EP	9194564

		300	
TP53	0	IL6	21092249, 11830554
TP53	1	SGK1	19756449, 8647846
TSC22 D3	0	AP-1	11397794, 12391160
TSC22 D3	1	SGK1	20947508

4.2.3   List of GEB052 Output Interactions (Cell Death and Inflammation)

Table 4.2.3: GEB052 model links to cell death.

Node 1	Activates (1) or Inhibits (0)	Node 2	PubMed ID Evidence
14-3-3	0	CELL-DEATH	12426317, 11222372, 24626062, 22562251
AP-1	1	CELL-DEATH	10080190
AP-1	0	CELL-DEATH	9141200
BAG1	0	CELL-DEATH	11257006
CD2	1	CELL-DEATH	9270771
CD40LG	0	CELL-DEATH	12697681
CD40LG	1	CELL-DEATH	12885753
CRH	0	CELL-DEATH	23380766
CRH	1	CELL-DEATH	23686762, 22494987, 11790788, 22763913.
DAP3	1	CELL-DEATH	20563667, 17135360

DAXX	1	CELL-DEATH	1598338
GR	1	CELL-DEATH	15940303, 21530661, 12039857
IL10	0	CELL-DEATH	8312229
IL10	1	CELL-DEATH	9184696
IL6	0	CELL-DEATH	7595060, 11751424
IL6	1	CELL-DEATH	9949178
NFKB	0	CELL-DEATH	10747850, 10849002
NFKB	1	CELL-DEATH	10747850
SGK1	0	CELL-DEATH	17571248
SMAD3	0	CELL-DEATH	14517210
SMAD3	1	CELL-DEATH	15107418, 11839804
STAT3	0	CELL-DEATH	23807222
STAT3	1	CELL-DEATH	21336304
STAT5B	0	CELL-DEATH	21826656
TP53	1	CELL-DEATH	19879762
TSC22D3	0	CELL-DEATH	9430225
UBC	0	CELL-DEATH	17491588

		CELL-DEATH	15033975, 15620210
UBC	1		

Table 4.2.4: List of GEB052 model links to inflammation.

Node 1	Activates (1) or Inhibits (0)	Node 2	PMID
AP-1	1	INFLAMMATION	23163821
CD40LG	1	INFLAMMATION	9468137
CRH	0	INFLAMMATION	17117478
CRH	1	INFLAMMATION	17117478
IL10	0	INFLAMMATION	10443688, 12452830, 14971032
IL6	1	INFLAMMATION	2199284, 10443688, 25031389
NFKB	0	INFLAMMATION	18270204, 20457564
NFKB	1	INFLAMMATION	18029230, 23776175, 20457564
SMAD3	0	INFLAMMATION	14752027
SMAD3	1	INFLAMMATION	20231525, 15253712
STAT5B	0	INFLAMMATION	24412367
STAT5B	1	INFLAMMATION	17148664

4.2.4 GEB052 Network Structure

Figure 4.2.2: The GEB052 Model.

Nodes are shown in small blue circles, whilst the Input Node (GC) is shown as a larger green circle. The central node (GR) is shown as a larger red circle. Model outputs (cell death and inflammation) are shown in blue squares. Activation reactions are represented by directed green arrows, whilst inhibition reactions are shown as directed blunted red arrows.

The GEB052 model, visualised above in Figure 4.2.2, consists of 52 nodes connected by 241 logical interactions. Although the visualisation is useful for providing a detailed overview of the network (thus quickly identifying features such as whether there are more activation or inhibition reactions or identifying the most highly connected nodes), following individual interactions can be difficult. To complement the full model

152

visualisation shown above, an interaction matrix (generated in CNA) of the model is shown in Figure 4.2.3:
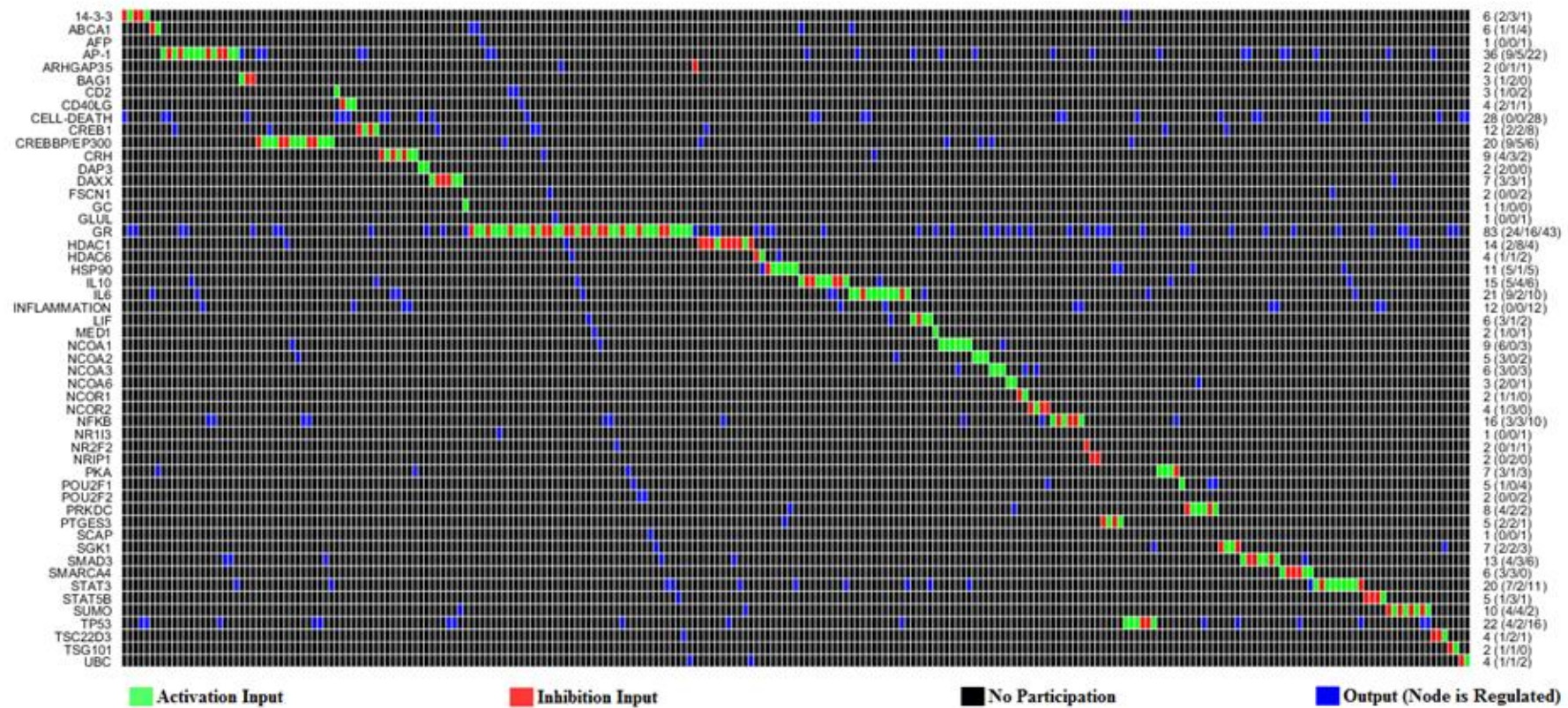
Figure 4.2.3: Interaction Matrix for GEB052 model.

Figure adapted from the interaction matrix generated in CNA. Nodes are shown on the left-side y-axis. The right-side y-axis details the number of reactions the node is involved in. Numbers in brackets represent the number of nodes it activates, the number of nodes it inhibits, and the number of nodes it is regulated by respectively. Every node for every reaction in the interaction matrix is assigned a value. Black means no participation within the reaction, whilst blue means the node is regulated (i.e. affected) by the interaction. Green means the node has an activation input whilst red means the node has an inhibition input.

154

As has been previously shown, feedback loops within a biological network are often crucial towards maintenance of network integrity and resistance to perturbation (Tian et al., 2013). Feedback loops within the model can be excessively long and consider numerous reactions; therefore, to further facilitate analysis, only two-step feedback loops are to be considered, consistent with previous research into interactome modelling (Tian et al., 2013). When limited to two-step feedback loops, 64 loops were identified, 26 of which (40.6%) involve the GR. An example of a two-step feedback loop is the classical regulation of TP53 by MDM2; TP53 activates MDM2 whilst MDM2 inhibits TP53 (Tian et al., 2013).

To further assess connectivity within the model, the NetworkAnalyzer plugin in Cytoscape was used to analyse the network topology to uncover node connectivity:
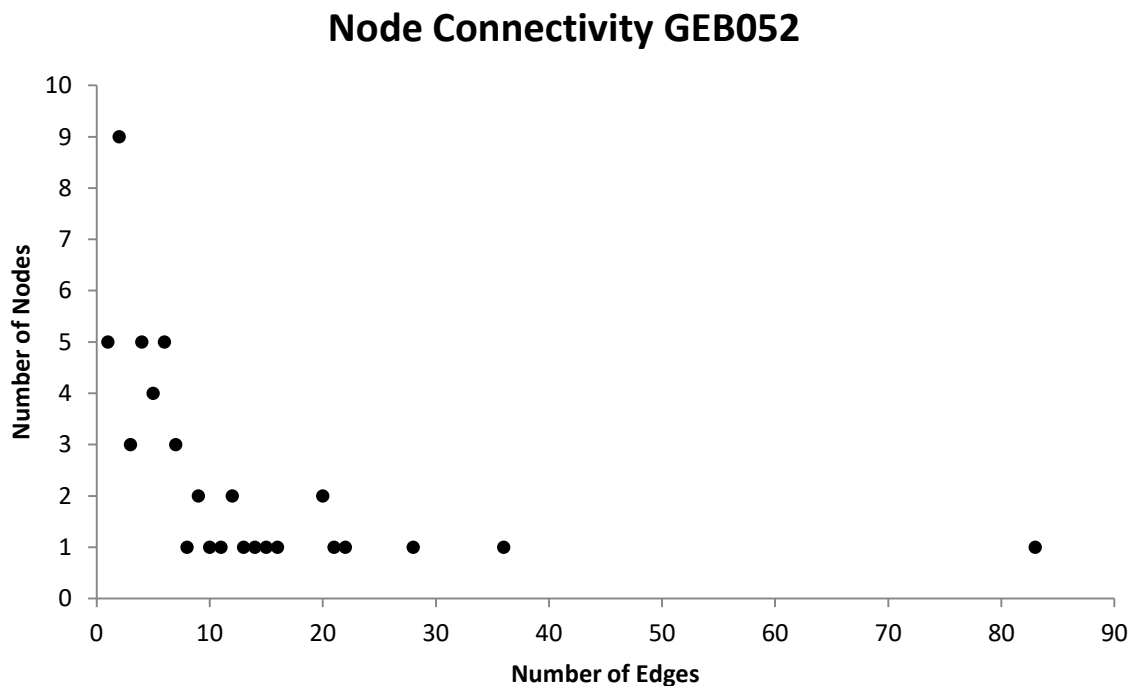
Figure 4.2.4: Node connectivity of GEB052 model.

Values were generated in the NetworkAnalyzer plugin for Cytoscape and imported into Excel.

The node connectivity of the GEB052 model shown above in Figure 4.2.4 demonstrates the high node connectivity within the model. Excluding model Outputs, six nodes exhibited a very high degree of connectivity (20 or more interactions). On the far right

of Figure 4.2.4 is the GR, with 83 interactions. Other nodes exhibiting a very high degree of connectivity include AP-1 (36 interactions), TP53 (22 interactions), IL6 (21 interactions), CREBBP/EP300 (20 interactions) and STAT3 (20 interactions). Highly connected nodes (exhibiting ten or more interactions but excluding Outputs) include NFKB (16 interactions), IL10 (15 interactions), HDAC1 (14 interactions), SMAD3 (13 interactions), CREB1 (12 interactions), HSP90 (11 interactions) and SUMO (10 interactions). Other than these, other nodes (n=37) exhibited a lower degree of connectivity, possessing less than ten interactions. The following summarises the node connectivity within the model:

Table 4.2.5: Node connectivity of GEB052 model.

Node Connectivity Range	Number of Nodes	Percentage of Total Nodes
Connectivity>80	1	1.9%
10≤Connectivity≤80	14	26.9%
0<Connectivity<10	37	71.2%

Understanding node connectivity is crucial for further downstream analysis, as *in silico* knockouts are performed on highly connected nodes (due to their high connectivity, their removal will have the biggest impact on signalling within the network). Subsequent sections detailing *in silico* knockout analysis results involved the knockout of the highly connected nodes (each having ten or more interactions) identified in this section.

4.3   Dependency and *in silico* knockout analysis of the GEB052 model

As detailed in Figure 2.2.3 (Page 100, Section 2.2.4), within CNA it is possible to undertake an in-depth analysis of the effects of every model constituent on every model constituent. This is performed through the generation of a dependency matrix, which takes into account all possible signalling and feedback loops within the model to

determine the overall effect of every node on every node. Figure 4.3.1 shows the dependency matrix for the GEB052 model:
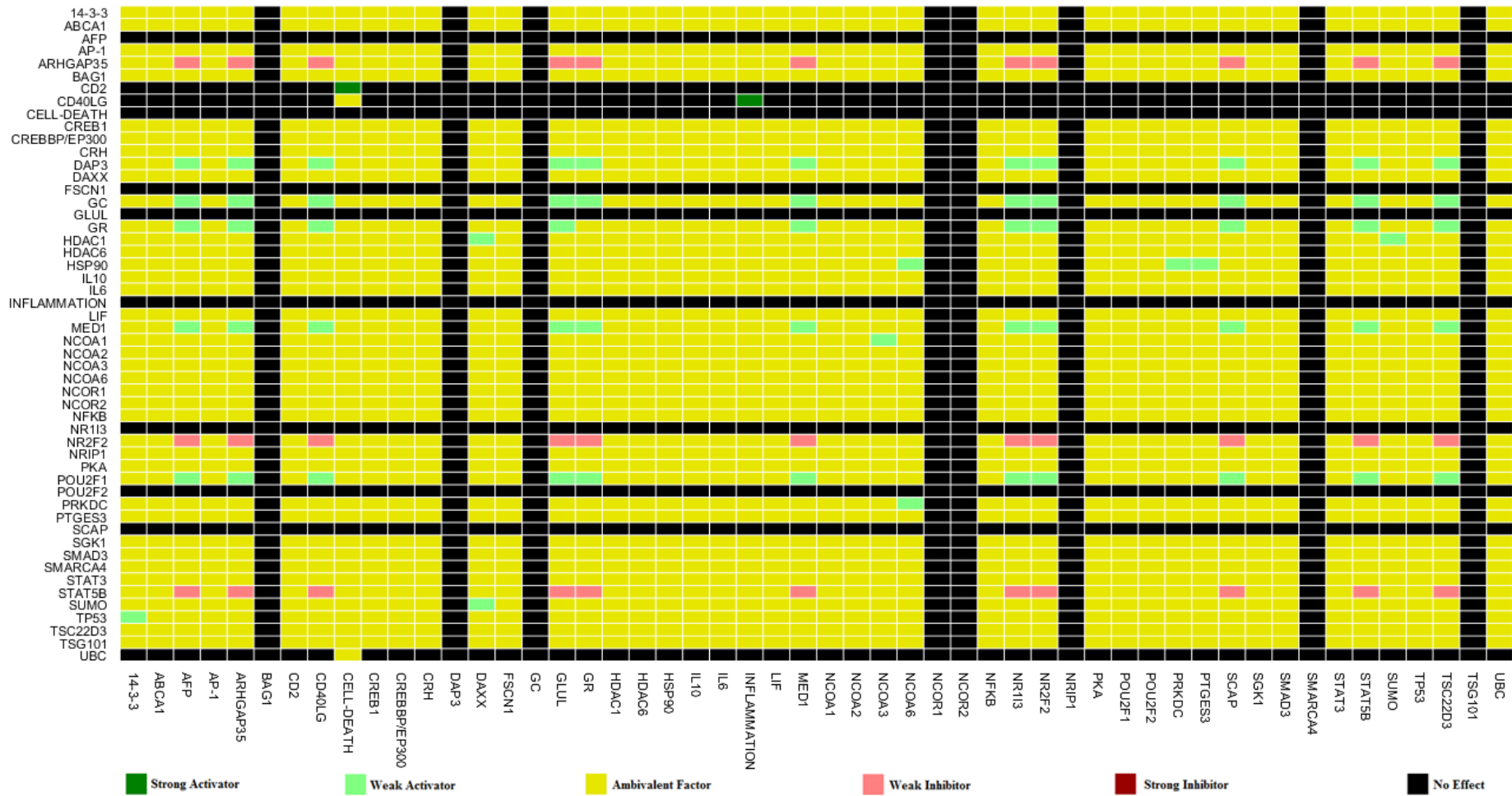
Figure 4.3.1: Dependency Matrix for GEB052 Model.

Dependencies show the effect of the node on the y-axis on the node on the x-axis.

Dependency analysis of the full model, visualised above in Figure 4.3.1, shows that the overwhelming majority of dependencies within the model are ambivalent (meaning the source node exerts both a positive and negative influence on the target node). This correlates with the large number of feedback loops present within the model, as the feedback loops can lead to negative autoregulation and thus a negative as well as a positive influence. The high number of ambivalent dependencies further demonstrates the interconnectivity of the model, and provides an excellent starting point for *in silico* knockout analysis as ambivalent dependencies are the ones most likely to change following network perturbation (Tian et al., 2013). In total, 2704 (52*52) dependencies were identified in the full GEB052 model. Of these, 896 were of no effect, 1710 were ambivalent, 33 were weak inhibitors, 63 were weak activators, 2 were strong activators and there were no strong inhibitors. The strong activators in the wild-type model were CD2 as a strong activator of cell death and CD40LG as a strong activator of inflammation.

As described in the Introduction, one of the benefits of computational biology is the ability to conduct numerous different analyses to unveil how models may change following a loss of network elements. It has been demonstrated across several studies that *in silico* knockout analysis can provide good insight into *in vivo* behaviour, for example by mimicking mutation effects through node deletion or activating hormone-dependent GR activation through turning node ON or OFF, provided the model is well-constructed.

To analyse the potential effects of the loss of network elements, *in silico* knockouts were performed against the highly connected (≥10 interactions) nodes identified previously in Section 4.2.4 (Page 151), with the exception of model outputs (as they have no outgoing reactions, their removal would have no effect on other nodes within the model). The following summarises the effects of the knockouts on network relationships:

Table 4.3.1: Dependency matrix alterations following *in silico* knockouts.

Scenario	Number of Each Dependency						
	No Effect	Ambivalent	Weak Inhibitor	Weak Activator	Strong Inhibitor	Strong Activator	Total
Full Model	896	1710	33	63	0	2	2704
AP-1 KO	877	1581	66	75	0	2	2601
CREB1 KO	877	1626	33	63	0	2	2601
CREBBP/ EP300 KO	877	1576	61	85	0	2	2601
GR KO	1602	955	5	35	1	3	2601
HDAC1 KO	953	1541	36	65	0	6	2601
HSP90 KO	993	1481	53	68	0	6	2601
IL6 KO	877	1607	43	72	0	2	2601
IL10 KO	877	1626	33	63	0	2	2601
NFKB KO	877	1626	33	63	0	2	2601
SMAD3 KO	877	1626	33	63	0	2	2601
STAT3 KO	877	1574	63	85	0	2	2601
SUMO KO	917	1589	33	60	0	2	2601
TP53 KO	917	1579	36	67	0	2	2601

All KO scenarios above have only 2601 (51*51) total reactions (as opposed to 2704) due to the removal of the node (in turn removing all of its dependencies). As expected based on the number of interactions it participates in and its centrality to the network, the removal of the GR had the largest effect on the dependencies within the network:
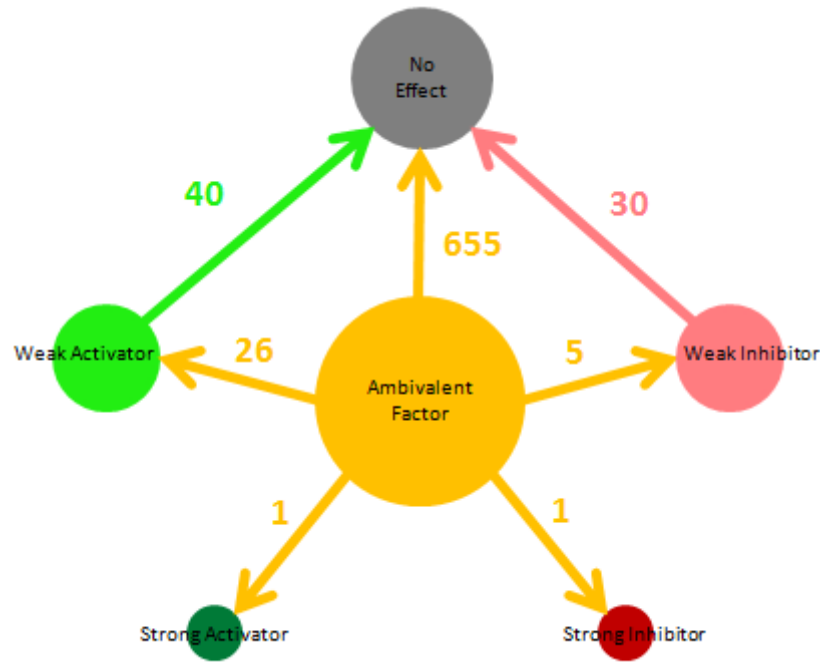
Figure 4.3.2: Distribution of dependency alterations following GR KO.

The majority of dependency changes were from ambivalent factors to no effect, which is logically consistent when it is considered that many nodes will signal through the GR to affect others. Thus, removal of this central node removes many of the effects between other node pairs. However, there were also numerous changes from ambivalent factors to weak activators or weak inhibitors, as well as strong activators and strong inhibitors. Previous research (Hussain et al., 2015; Tian et al., 2013) has focussed primarily on the change to strong activators or strong inhibitors (as defined in Section 2.2.4, Page 97), as these are the changes most likely to show effects at the biological level. In addition to this, only strong activators and inhibitors are considered due to the sheer number of predictions generated. Across all knockout scenarios for the GEB052 model, 1249 predictions as to how model relationships change following a knockout was obtained. Even if changes from ambivalent factors to no effect are discarded (as there is no net change in activation or inhibition) then across all the knockout scenarios GEB052 produced 323 predictions in dependency changes. Analysis of this high number would be cumbersome, so there is a necessary focus on strong activators and strong inhibitors.

Following removal of the GR, one ambivalent dependency was changed to a strong activator, and another ambivalent dependency was changed to a strong inhibitor. Both

of these dependencies related to the output of cell death; in the full model, STAT5B is ambivalent to cell death, whereas following removal of the GR it becomes a strong inhibitor of cell death. Conversely, DAP3 is ambivalent to cell death in the full model, whereas following removal of the GR it becomes a strong activator of cell death. Identifying aberrant signalling following loss of functional GR is a key factor in improving therapies. It is known that STAT5 has an anti-apoptotic role in haematopoietic cells (Debierre-Grockiego, 2004), however it is interesting that the model indicates its pro-survival effect is stronger in glucocorticoid-resistant (which GR KO simulates) cells, which may point towards the potential of combining glucocorticoid treatment with anti-STAT5B treatments.

Other than the GR KO scenario, only two of the knockout scenarios detailed in Table 4.3.1 (Page 159) demonstrated changes to strong activators or inhibitors: HDAC1 KO and HSP90 KO. Their changes are tracked in Figure 4.3.3:
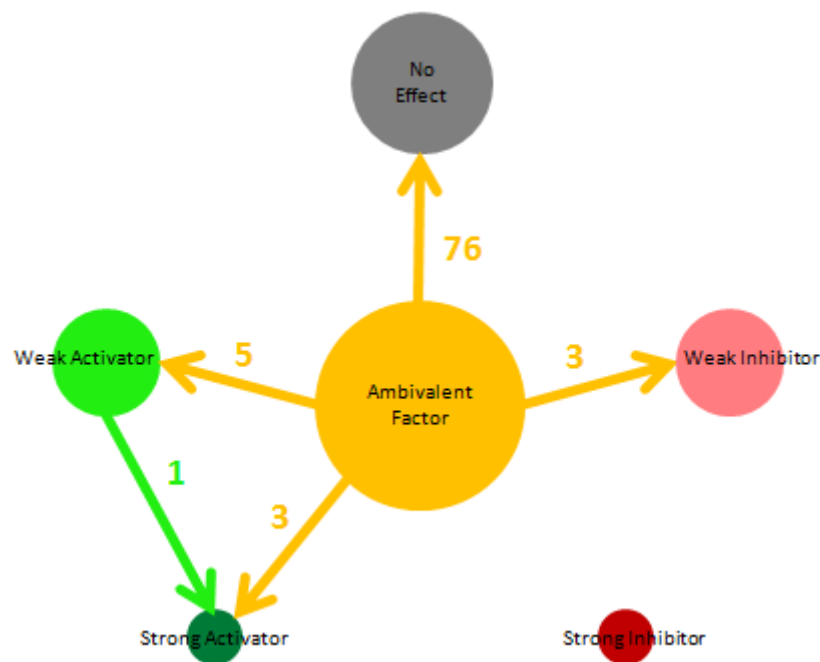
Figure 4.3.3: Distribution of dependency alterations following HDAC1 KO.

Loss of HDAC1 promoted four new strong activation dependencies. Dependency analysis takes into account all of the signalling within the model and thus even the effect of nodes on themselves can be seen. In the full model, DAXX was ambivalent to

itself and to SUMO, whilst SUMO was also ambivalent to itself. Loss of HDAC1, however, promoted a change in these dependencies; DAXX became a strong activator of itself, as did SUMO, whilst DAXX also became a strong activator of SUMO. In the full model, SUMO was a weak activator of DAXX, whereas following the loss of HDAC1 it became a strong activator of DAXX.
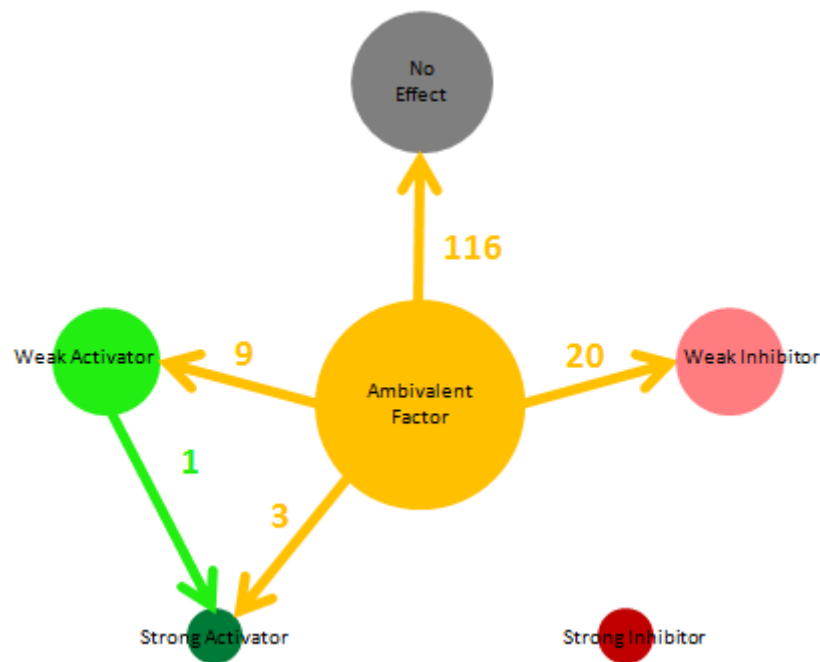
Figure 4.3.4: Distribution of dependency alterations following HSP90 KO.

Loss of HSP90 promoted four new strong activator dependencies to emerge. In the full model, NCOA6 was ambivalent to itself and PRKDC, whilst PRKDC was ambivalent to itself. Loss of HSP90, however, changed all of these dependencies to strong activation. In the full model, PRKDC was a weak activator of NCOA6, whilst in the HSP90 KO model it became a strong activator of NCOA6.

4.4   Genome-Wide Model Analysis

Although the dependency analysis detailed in the previous section provided some useful insight into a small subset of genes within the whole model, one of the larger aims of systems biology is to simulate and assess entire systems. This section aimed to assess the state of every network element in a simulation of glucocorticoid-responsive cells

and glucocorticoid-resistant cells, and to compare the model predictions to microarray data (thus verifying nodes/genes within the model based on genome-wide data).

4.4.1   Logical Steady State Analysis of GEB052 Model

As described in Section 2.2.4 (Page 97) CellNetAnalyzer has two main analytical functions: dependency matrix generation and logical steady state analysis (LSSA). LSSA allows for the capture of the overall activation state of a node (ON, OFF or undetermined) following upstream inputs. At the beginning of an LSSA, every node (other than selected inputs which are manually modified) is given a value of NaN (undetermined). After setting any input nodes to the desired value, LSSA is then ran which processes all reactions downstream of the input, and iterates until each node reaches a "steady state" (ON, OFF or undetermined). To simulate glucocorticoid-sensitive cells, all nodes were left as NaN, GC turned to 1, and then the simulation was ran. To simulate GC-resistant cells, all nodes were left as NaN, excepting GR which was set to 0 (OFF), and GC turned to 1. E_{mod} was calculated as described in the Materials and Methods (Section 2.2.6, Page 102) whereby -1 is equivalent to downregulation in the GC-resistant scenario relative to the GC-sensitive, 0 is equivalent to no change, and 1 is equivalent to upregulation.

Table 4.4.1: LSSA Results for GEB052 Model.

Node	GC-Sensitive (GC=1) Simulation	GC-Resistant (GC=1, GR=0) Simulation	E_{mod}
14-3-3	1	1	0
ABCA1	1	1	0
AFP	1	0	-1
AP-1	1	1	0
ARHGAP35	1	0	-1
BAG1	NaN	NaN	0
CD2	1	1	0
CD40LG	1	0	-1

CELL-DEATH	1	1	0
CREB1	1	1	0
CREBBP/EP300	1	1	0
CRH	1	1	0
DAP3	NaN	NaN	0
DAXX	NaN	1	1
FSCN1	1	1	0
GC	1	1	0
GLUL	1	0	-1
GR	1	0	-1
HDAC1	NaN	1	1
HDAC6	1	1	0
HSP90	1	1	0
IL10	1	1	0
IL6	1	1	0
INFLAMMATION	1	1	0
LIF	1	1	0
MED1	1	0	-1
NCOA1	1	1	0
NCOA2	1	1	0
NCOA3	1	1	0
NCOA6	1	1	0
NCOR1	NaN	NaN	0
NCOR2	NaN	NaN	0
NFKB	1	1	0
NR1I3	1	0	-1
NR2F2	1	0	-1
NRIP1	NaN	NaN	0
PKA	1	1	0
POU2F1	1	1	0

POU2F2	1	1	0
PRKDC	1	1	0
PTGES3	1	1	0
SCAP	1	0	-1
SGK1	1	1	0
SMAD3	1	1	0
SMARCA4	NaN	NaN	0
STAT3	1	1	0
STAT5B	1	0	-1
SUMO	NaN	1	1
TP53	1	1	0
TSC22D3	1	0	-1
TSG101	NaN	NaN	0
UBC	1	0	-1
% ON	80.8	63.5	
% OFF	0	23.1	
% Determined	80.8	86.6	
% Undetermined	19.2	13.4	

Although more determined nodes (ON or OFF) were seen in the GC-resistant scenario (86.6% against 80.8% in the sensitive simulation), an overall loss in functionality of the network was also observed through the sharp increase in nodes that were OFF (23.1% against 0% in the sensitive simulation). The E_{mod} value shows the change from sensitive to resistant (-1 equalling downregulation, 0 equalling no change, and 1 equalling upregulation). The following summarises the E_{mod} values for each node:

Table 4.4.2: Node state comparison from GC-sensitive to GC-resistant scenarios.
Upregulated means the node is more activated in the GC-resistant scenario than the GC-sensitive scenario, whilst downregulated means the node is less activated in the GC-resistant scenario than the GC-sensitive scenario.

Upregulated (3)	Unchanged (37)	Downregulated (12)
DAXX, HDAC1, SUMO	14-3-3, ABCA1, AP-1, BAG1, CREBBP/EP300, CD2, CELL-DEATH, CREB1, CRH, DAP3, FSCN1, GC, HDAC6, HSP90, IL10, IL6, INFLAMMATION, LIF, NCOA1, NCOA2, NCOA3, NCOA6, NCOR1, NCOR2, NFKB, NRIP1, PTGES3, TP53, PKA, POU2F1, POU2F2, PRKDC, SGK1, SMAD3, SMARCA4, STAT3, TSG101	AFP, NR1I3, CD40LG, GLUL, GR, ARHGAP35, MED1, NR2F2, SCAP, STAT5B, TSC22D3, UBC

The model predictions in terms of the overall activation/state of a node can be verified either by literature searching or experimental approaches. For example, the model predicted that GLUL would be downregulated in the GC-resistant simulation, which is consistent with a previous report showing GLUL to be downregulated in GC-resistant cells (Beesley et al., 2009). However, validation of all model predictions in this way would be cumbersome and provide less information than high-throughput methodologies; therefore, model predictions have been validated via comparison to cell-based microarray data, detailed in the following section.

4.4.2   High-throughput Model Validation

In order to assess model accuracy on a larger scale, the E_{mod} values obtained in the previous section have been compared to microarray data. In total twelve sets of microarray data have been utilised, resulting in six comparisons that have been used to validate model predictions. For each Comparison, an E_{exp} value for each node was obtained as detailed in Section 2.2.6 (Page 102). Details for each Comparison (including treatment conditions and the GEO ID for the microarray dataset) are shown in Table 4.4.3. For all microarray validations, all genes within the model were identified within the microarray data files.

Table 4.4.3: Microarray data comparisons used to validate model predictions.

Comparison	GC-Sensitive Array	GC-Resistant Array
Comparison 1	T-ALL (C7H2 Cells), 24 Hours Dexamethasone Treatment (GEO ID GSM60544)	T-ALL (C1 Cells), 24 Hours Dexamethasone Treatment (GEO ID GSM60562)
Comparison 2	T-ALL (C7H2 Cells), 6 Hours Dexamethasone Treatment (GEO ID GSM60543)	T-ALL (C1 Cells), 6 Hours Dexamethasone Treatment (GEO ID GSM60561)
Comparison 3	T-ALL (C7H2 Cells), 6 Hours 0.1% Ethanol Treatment (GEO ID GSM60542)	T-ALL (C1 Cells), 6 Hours 0.1% Ethanol Treatment (GEO ID GSM60560)
Comparison 4	B-ALL (PreB 697 Cells), 24 Hours Dexamethasone Treatment (GEO ID GSM60547)	B-ALL (PreB 697 R4G4 Cells), 24 Hours Dexamethasone Treatment (GEO ID GSM60586)
Comparison 5	B-ALL (PreB 697 Cells), 6 Hours Dexamethasone Treatment (GEO ID GSM60546)	B-ALL (PreB 697 R4G4 Cells), 6 Hours Dexamethasone Treatment (GEO ID GSM60583)
Comparison 6	B-ALL (PreB 697 Cells), 6	B-ALL (PreB 697 R4G4

	Hours 0.1% Ethanol Treatment (GEO ID GSM60545)	Cells), 6 Hours 0.1% Ethanol Treatment (GEO ID GSM60581)

For each comparison shown above, the E_{exp} values obtained were compared to the model predictions (E_{mod}). Tables for each comparison are shown in Appendix Table 1 - Appendix Table 6 (Page 212-221) whilst a summary is shown in Table 4.4.4. Note that for all comparisons, model inputs and outputs (GC, CELL-DEATH, INFLAMMATION) were all excluded from validation as these are impossible to assess through microarray data. Similarly, the GR was excluded from analysis as during the LSSA for GC-resistant cells it was manually set to zero (rather than its inactive state being a model prediction). Thus, comparison exists solely on the 48 remaining nodes.

A summary of the correct/small error/large error percentages for each comparison is provided in Table 4.4.4.

Table 4.4.4: Summary of prediction rates from all LSSA comparison scenarios.

Comparison	Correct (%)	Small Error (%)	Large Error (%)
1	58.3	41.7	0.0
2	54.2	43.8	2.1
3	60.4	37.5	2.1
4	58.3	39.6	2.1
5	54.2	41.7	4.2
6	54.2	45.8	0.0
AVERAGE	56.6	41.7	1.8

As summarised above, the GEB052 model displayed consistently accurate prediction rates. The correct prediction range for GEB052 (54.17% to 60.42%, with an average of 56.60%) represents a good level of correct prediction. Given that there are three possible outcomes (correct, small error and large error) a fully random model would demonstrate a correct prediction rate of 33.33%. 56.60% is significantly higher than 33.33%, and furthermore if the six correct percentage values are compared to six

33.33% via statistical analysis, the p-value is less than 0.01, providing further evidence for the strength of the GEB052 model and its potential value.

4.5   Preliminary Clinical Validation of GEB052 Model (LSSA)

Following analysis of the model and validation through comparison to cell-based microarray data, model validation using patient data has also been performed to assess model accuracy at a whole-organism and disease-specific level. Microarray data from thirteen leukaemia patients were utilised, with the microarray data being taken after treatment with prednisolone.

Table 4.5.1: Patient microarray data used for validation of LSSA results.
Patient data obtained from Schmidt et al. (2006). Microarray data obtained from the GEO database after its deposit from the original study (Schmidt et al., 2006).

Patient Number	Gender	Age (Years)	Clustering	Status at Risk Assessment?	GEO ID
2	M	8.5	T-ALL	Alive	GSM51710
13	M	5.9	Not assigned	Alive	GSM51677
17	F	14.7	Hyperploidy	Deceased	GSM51680
20	M	5	T-ALL	Alive	GSM51704
24	M	2.6	Not assigned	Alive	GSM51674
25	F	10.3	T-ALL	Alive	GSM51707
31	F	17.2	Hyperploidy	Alive	GSM51683
32	F	3.7	TEL-AML	Alive	GSM51686
33	M	2.5	Hyperploidy	Alive	GSM51689
37	F	15.1	Not assigned	Alive	GSM51692
38	M	3.2	TEL-AML	Alive	GSM51695

40	M	17.3	Not assigned	Alive	GSM51698
43	F	1.6	TEL-AML	Alive	GSM51701

Each microarray data set shown above was assessed and compared to LSSA results. As previously, predictions were marked as correct, small error, or large error:
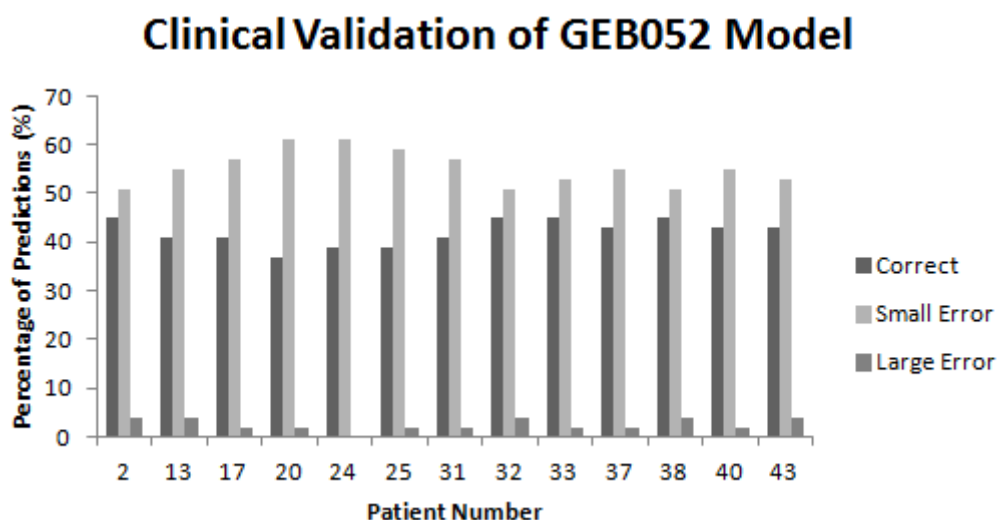
Figure 4.5.1: Clinical validation of GEB052 model against LSSA results.
The "patient number" shown on the x-axis refers to the number of the individual patient from the original study that these thirteen patients were taken from (Schmidt et al., 2006).

As shown in Figure 4.5.1 above, the model performs less well with clinical data from patients than cell-based microarrays. Using patient data, an average of 42% correct predictions was obtained, with an average of 55% small error and 3% large error. Thus, although there are a high number of small error predictions, the fact that there is less than 5% large error is promising. Furthermore, although 42% correct is less than what was obtained for cell-based data, if the correct prediction score for each of these thirteen patients is compared to what a random model would obtain (33.3% due to three possible outcomes) then the p-value is <0.0001, indicating the higher correct predictions and improvement over a random model. In addition to this, although 42% is relatively low, such a score could arguably make sense given the tissue-specific differential effects

glucocorticoid hormones have, when the fact that the model is not yet tissue-specific is taken into consideration, as well as the relatively small size of the model.

4.6   Quantitative Model Analysis

As established in the Introduction, different modelling types are available depending on the end goal. For large networks, Boolean models are usually employed, as the simplified logic allows for a lower computational demand, whilst mathematically precise models are typically used for smaller-scale networks. One persistent limitation of Boolean models is that the discrete states (1, 0, NaN) allow for only a limited capturing of the overall state of a node. There is a continuing drive to develop algorithms that allow for a more quantitative analysis to be performed on Boolean models. One such algorithm is the STSFA, which superimposes ChIP-seq and/or microarray data onto a model to analyse it quantitatively (Isik et al., 2012).

4.6.1   Model Validation by STSFA Analysis

The same twelve microarray datasets described in Table 4.4.3 (Page 168) were used to analyse the model via the STSFA and the same six comparisons were used to evaluate the prediction accuracy of STSFA. Individual comparison results are shown in Appendix Table 7 - Appendix Table 12 (Page 223-238).

A summary of the correct/small error/large error percentages for each comparison is provided in Table 4.6.1. Comparisons 1-6 are the same comparisons performed previously (Table 4.4.3, Page 168)

Table 4.6.1: Summary of prediction rates from all STSFA comparison scenarios.

Comparison	Correct (%)	Small Error (%)	Large Error (%)
1	82.6	17.4	0.0
2	83.0	17.0	0.0
3	87.2	12.8	0.0
4	72.3	25.5	2.1

5	74.5	23.4	2.1
6	80.9	17.0	2.1
AVERAGE	80.1	18.9	1.0

Examination of Table 4.6.1 shows high correct prediction rates obtained via STSFA analysis. With a correct prediction range from approximately 72% to 87% and large errors occurring at 2.1% in three simulations (0% in the other three), the increased accuracy provided by the semi-quantitative approach of the STSFA provides a more robust analysis.

4.6.2   Comparison of LSSA and STSFA

It is expected that quantitative (even semi-quantitative) analysis would yield better prediction outcomes than static Boolean analysis, and indeed this has been shown previously (Hussain et al., 2014). The correct prediction rates of LSSA and STSFA with cell-based microarray data (Table 4.4.4, Page 169 for LSSA and Table 4.6.1, Page 172 for STSFA) were compared as shown in Figure 4.6.1:
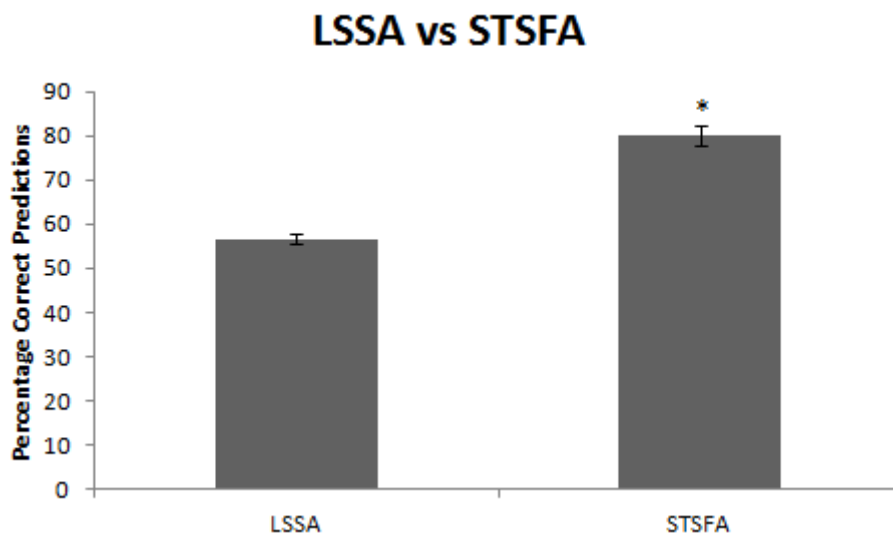
Figure 4.6.1: LSSA vs STSFA.

Data represents the average correct predictions across the six comparisons detailed in Table 4.4.3 (Page 168) +/- SEM. P-value ≤ 0.05 is indicated by * as assessed by an unpaired two-tail t-test.

As shown above, the use of the STSFA lead to a significantly higher level of correct predictions obtained when compared to LSSA. Although both were improved over a random model, STSFA still remains higher than LSSA likely due to its semi-quantitative nature.

4.6.3 Preliminary Clinical Validation of GEB052 Model (STSFA)

To assess the predictive power of the model under STSFA analysis at the clinical level, microarray data from thirteen leukaemia patients (taken before patients were treated) were used.

Table 4.6.2: Patient microarray data used for STSFA analysis.

Patient data obtained from Schmidt et al. (2006). Microarray data obtained from the GEO database after its deposit from the original study (Schmidt et al., 2006).

Patient Number	Gender	Age (Years)	Clustering	Status at Risk Assessment?	GEO ID
2	M	8.5	T-ALL	Alive	GSM51712
13	M	5.9	Not assigned	Alive	GSM51679
17	F	14.7	Hyperploidy	Deceased	GSM51682
20	M	5	T-ALL	Alive	GSM51706
24	M	2.6	Not assigned	Alive	GSM51676
25	F	10.3	T-ALL	Alive	GSM51709
31	F	17.2	Hyperploidy	Alive	GSM51685
32	F	3.7	TEL-AML	Alive	GSM51688
33	M	2.5	Hyperploidy	Alive	GSM51691
37	F	15.1	Not assigned	Alive	GSM51694
38	M	3.2	TEL-AML	Alive	GSM51697
40	M	17.3	Not	Alive	GSM51700

			assigned		
43	F	1.6	TEL-AML	Alive	GSM51703

The microarray data shown above were each in turn superimposed onto the model and analysed via the STSFA. The edge weights for all edges to cell death were totalled (for each patient individually) and patients were grouped as shown in Figure 4.6.2:
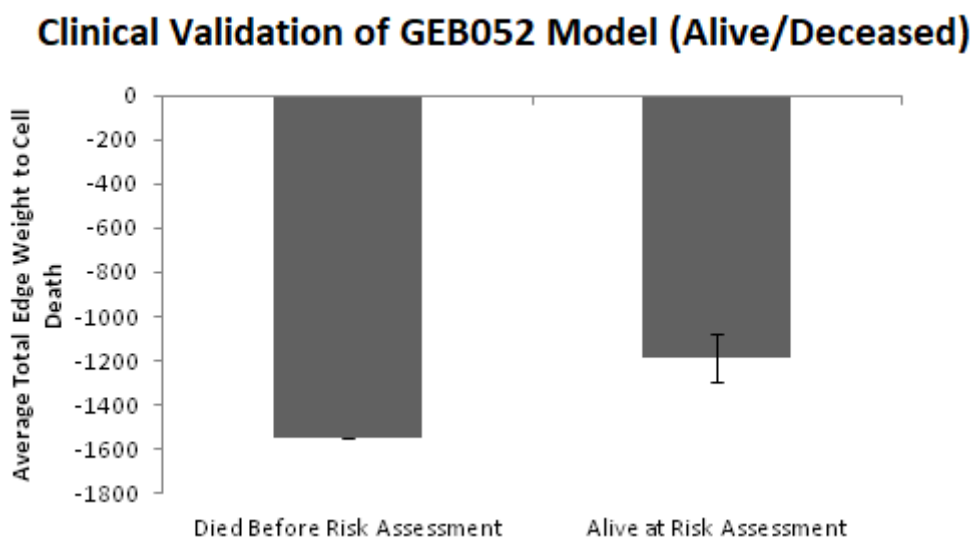
Figure 4.6.2: Preliminary clinical validation of GEB052 model (STSFA, alive/deceased status).
Patient groups (Died Before Risk Assessment, n=1, Alive at Risk Assessment, n=12) are shown on the x-axis, whilst the y-axis shows the average for each group of the total edge weights targeting cell death +/- SEM.

As shown above, the model under STSFA analysis predicted that the patient who died before risk assessment would have a lower (more negative) total edge weight for edges that affect cell death than those who were alive at risk assessment. What this translates to is that cell death is "more inhibited" in that patient than those who were alive at risk assessment, at least according to the model predictions. Given that cell death in this context equates to the death of the cancer cells, the fact that this patient died before risk assessment (i.e. before other patients) is consistent with the model prediction. However, the sample size and unequal groupings make the above data insufficient to draw full conclusions, though it is a promising and interesting indication nonetheless.

To complement the above analysis, patients were also grouped by age:
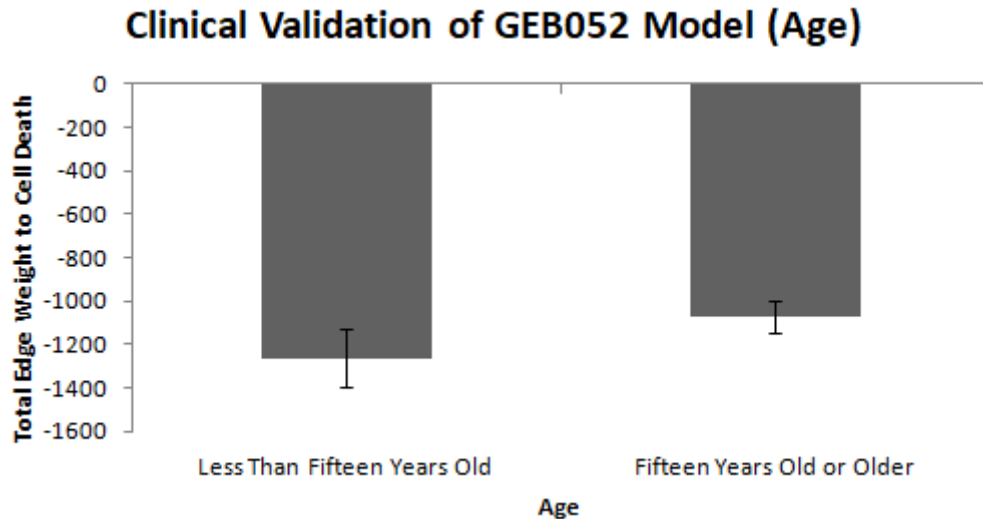
Figure 4.6.3: Preliminary clinical validation of GEB052 model (STSFA, age groupings). Patient groups (<15 years old, n=10, ≥15 years old, n=3) are shown on the x-axis whilst the y-axis shows the average for each group of the total edge weights targeting cell death +/- SEM.

According to Cancer Research UK, ALL patients aged fourteen or younger have a five-year survival rate of approximately 90%, whilst patients aged between fifteen and twenty-four have a five-year survival rate of approximately 70% (CRUK, 2015c). Therefore, if this difference in survival rate was seen through the GEB052 model predictions as shown in Figure 4.6.3, then the first group (less than fifteen years old) would have a higher (less negative) total edge weight to cell death. However, this is not the case. Although the difference between the two groups was statistically insignificant (p>0.05), the trend shown in Figure 4.6.3 is that patients who were less than fifteen years old have cell death as more negatively regulated (in turn, meaning less death of the cancer cells and arguably reduced survival). Thus, although the alive/deceased status shown in Figure 4.6.2 appears to correlate with clinical outcomes, this does not appear to be the case for Figure 4.6.3, which indicates some shortcomings of the model and required improvements.

Chapter 5   Discussion

5.1   Detailed discussion of wet-laboratory results

5.1.1   Alteration of cell fate by CM

It is established that the bone marrow microenvironment, known to be important for the maintenance of HSCs, plays a role in chemoresistance in leukaemia via two-way communication with cancer cells through mechanisms including cell-cell contact (such as Kurtova and colleagues who found a contact-dependent protective effect of stromal cells on chronic lymphocytic leukaemia (CLL) cells (Kurtova et al., 2009)) and secreted factors (such as Nefedova and colleagues who found that soluble factors produced following bone marrow stromal cell-myeloma cell interaction protected myeloma cells from mitoxantrone (Nefedova et al., 2003)) (Bakker et al., 2016). Two-way exchange of signalling between leukaemic cells and the constituents of the microenvironment may occur through a variety of mechanisms such as through cell contact between osteoblasts and leukaemic cells or through secreted factors.

Simulation of the microenvironment may be carried out in multiple ways, though the most common is direct co-culture of stromal cells and leukaemia cells and use of bone cell-conditioned media which is fed to the leukaemia cells. One study by Konopleva and colleagues demonstrated that co-culture of two leukaemic cell lines (HL-60 and NB-4) with MS-5 stromal cells led to reduced level of apoptosis through the upregulation of anti-apoptotic proteins. Importantly, these effects were reproduced with the use of MS-5 conditioned media instead of co-culture (Konopleva et al., 2002).

Konopleva and colleagues utilised conditioned media at a concentration of 30% and saw a reduction in apoptotic cells (Konopleva et al., 2002). This is consistent with the data in this thesis, where one-third CM/total media led to an increased number of viable C7-14 cells (as assessed by MTS assays - Appendix Figure 2, Page 208), compare light bars). However, a negative effect of one-third CM/total media was seen with C1-15 cells (compare dark bars of Appendix Figure 2, Page 208). However, MTS assays are a

limited approach in that the approach shows only whole cell populations, and that it is dependent on mitochondrial activity. Thus, any treatments that affect mitochondria will have an impact on the outcomes of an MTS assay. CM was ultimately used at a final concentration of $1/6^{th}$ CM/total media, and future functional assays were designed either to analyse whole cells individually (Sub-G1 FACS analysis) or populations based on fluorescence intensity of dyes to classify cells as healthy or apoptotic (which due to quantitative measurement is more reliable than mitochondrial activity). Thus MTS assays were used as an initial starting point but further analyses relied on a more functional approach.

5.1.2 GR phosphorylation is modulated by CM and chemotherapy

Numerous factors control the level of a cell's response to glucocorticoid treatment, including the expression levels of the GR, the relative activity of the GR, and the phosphorylation status of the GR (Bakker et al., 2016). Thus understanding these key determinants can improve therapeutic opportunities and aid in elucidating the link between treatment and response. In particular, an effect of the microenvironment on the GR would provide a direct link to a key determinant of the chemotherapeutic response, potentially providing a route to targeted therapy.

The phosphorylation status of the GR is important determinant of its activity, as detailed in Section 1.10 (Page 39). GR may be phosphorylated in the absence and presence of a ligand (Galliher-Beckley et al., 2011). Phosphorylation at S134 occurs in the absence of ligand and appears to be controlled via p38 MAPK (Galliher-Beckley et al., 2011). There are numerous characterised phosphorylation sites for the GR such as S203, which is thought to be an inactive form of the GR due to its localisation to the cytoplasm (Galliher-Beckley and Cidlowski, 2009). Among the most well-characterised and important for GR function are S211 and S226. Phosphorylation at S211 is mediated by kinases such as p38 MAPK and is one of the key determinants of GR activity; in most cell types the GR is hyperphosphorylated at S211 following hormone binding, which leads to increased promoter occupancy and glucocorticoid-induced apoptosis (Galliher-Beckley and Cidlowski, 2009). Contrasted with S211 is S226, which is primarily

associated with reduced GR activity through enhanced nuclear export of the GR (Itoh et al., 2002). Due to their opposed effects the ratio between S211/S226 has been considered an indicator for GR activity (Simic et al., 2013). Interestingly, alteration of one phosphoisoform can lead to altered levels of another; for instance, it has been shown that inhibition of JNK, which phosphorylates GR at S226, can ultimately lead to restored GR activity and phosphorylation at S211 (Miller et al., 2007; Galliher-Beckley and Cidlowski, 2009). Thus, the phosphorylation status of the GR is important in determining its activity; it was for this reason that the phosphorylation status of the GR was followed under CM and chemotherapy (Section 3.3, Page 108).

In agreement with previously published research, C7-14 cells exhibited a consistent trend for higher levels of GR protein than C1-15 cells, particularly following hormone treatment (compare light to dark bars of Figure 3.3.2, Page 110) (Lynch et al., 2010). Interestingly, CM trended towards a decrease in total GR in C1-15 cells, which correlates with the statistically significant increase in S226-phosphorylated GR following CM treatment (compare dark bars of lane 2 to lane 1 of Figure 3.3.2, Page 110 and Figure 3.3.3, Page 111). S226 is classically associated with reduced GR activity, excepting the emergence of target gene-specific phosphorylation (Lynch et al., 2010). Thus this negative effect of CM on the GR, key receptor for ALL chemotherapy, in C1-15 cells could represent a mechanism by which the microenvironment may exert its effects. However analysis is complex in that CM, under MTS assays, did not improve survival of C1-15 cells (though for FACS analysis, arguably a more reliable technique, an improved survival was seen and similar to this an improved survival for C1-15 cells was seen when comparing dexamethasone to dexamethasone and CM treatment under MTS assays (Figure 3.2.1)). A further complication is that in C1-15 cells dexamethasone and CM combination treatment had a statistically significantly lower level of S226-phoshorylated GR than dexamethasone treated cells (Figure 3.3.3, Page 111).

Dexamethasone lead to an increase in S226-phosphorylated GR in C1-15 cells, whilst this effect was not seen in C7-14 cells (compare dark to light bars of lane 3 of Figure 3.3.3, Page 111). S226 phosphorylation was generally predominant in C1-15 cells; in

particular, the increase in S226 phosphorylation could partially explain the resistance of these cells to dexamethasone.

Converse to S226 levels and consistent with established literature, S211 phosphorylation was higher in C7-14 cells than C1-15 cells (compare light to dark bars of Figure 3.3.4, Page 113). The positive effects of S211 phosphorylation on GR, correlated with the relative expression levels of it between the two cell lines, could again partially explain the difference in GC-sensitivity that is seen between C1-15 and C7-14 cells.

The respective roles of different kinases under treatments can be elucidated through the use of specific inhibitors. For instance, SB203580 is a p38 MAPK inhibitor whilst SP600125 is a JNK inhibitor. Use of these inhibitors would lead to altered GR phosphorylation, and there is some preliminarily evidence supporting this (Qattan, 2014; Lynch et al., 2010).

Based on the data presented in this thesis, there was no significant increase in S226 phosphorylation in C7-14 cells following treatment with CM (Figure 3.3.3, Page 111). It is possible that inhibition of one kinase (and in turn reduction of the phosphorylated form it modulates) would lead to altered predominance of phosphoisoforms. CM may positively modulate p38 MAPK, in turn affecting GR, due to the trend for CM to increase phosphorylation at S211 (compare light bars of lane 2 to lane 1 of Figure 3.3.4, Page 113). Inhibition of p38 MAPK would therefore blunt this potential stimulatory effect of CM, and thus alter the phosphorylation status of GR.

Data presented in this thesis have indicated that the microenvironment can influence the post-translational state of the GR, which given the importance of GR phosphorylation in determining its activity, provides a link from the microenvironment to drug response and resistance. Comparison of the results obtained to unpublished data generated by a former colleague has indicated that the effects of the microenvironment on the GR may be mediated through kinases such as p38 MAPK.

5.1.3 CM and chemotherapy affect BECN1, RIPK1, Caspase-3 and BIRC3

The choice for a cell to undergo apoptosis, necroptosis or autophagy is determined by complex crosstalk involving numerous proteins. To provide preliminary insight as to the effect of CM and chemotherapy on these pathways, a key marker for each (BECN1 for autophagy, RIPK1 for necroptosis and caspase-3 for apoptosis) was analysed by both qRT-PCR and Western blotting.

Analysis of *BECN1* mRNA did not reveal any significant changes, though there were trends identified such as increasing *BECN1* expression in C1-15 cells (Figure 3.4.1, Page 114). Conversely, at the protein level, a statistically significant loss of BECN1 was seen in C7-14 cells following etoposide, etoposide/CM combination, and dexamethasone and etoposide combination. However, dexamethasone, etoposide and CM combination did not show a statistically significant loss of BECN1 (see light bars of lanes 5-7 of Figure 3.4.6, Page 119), which may indicate pro-survival effects of CM through modifying cellular response to combination chemotherapy. C1-15 cells exhibited a consistently higher level of BECN1 protein expression across all treatments, particularly for treatments containing etoposide. Given that BECN1 is linked to the generally pro-survival process of autophagy, this higher expression could represent an explanation for why C1-15 cells exhibit less sensitivity to etoposide treatment (see MTS experiment, Figure 3.2.1, Page 108).

BECN1 represents an interesting target not only for its link to autophagy, but also for the fact that there are previously reported studies linking the glucocorticoid receptor and BECN1. For instance, it has been shown by Laane et al (2009) that BECN1 may be required for dexamethasone-induced cell death in lymphoid leukaemia (Laane et al., 2009). Further evidence for the fact that BECN1 may be influenced by glucocorticoids is the fact that numerous putative GR binding sites were identified by QIAGEN Champion ChIP (Figure 3.5.1, Page 120), which was verified by chromatin immunoprecipitation experiments, where C7-14 cells exhibited a statistically significant increase in promoter occupancy following hormone treatment (Figure 3.5.7, Page 126). Thus, the GR has been identified as occupant on the *BECN1* promoter; combined with

previous literature detailing BECN1 to be important for dexamethasone-induced apoptosis (Laane et al., 2009), it is likely that some level of crosstalk exists between these two proteins. However, no significant changes under dexamethasone treatment were observed for either cell line at the mRNA or protein level (Figure 3.4.1 and Figure 3.4.6, Pages 114 and 119 respectively), which indicates a need for further research to fully elucidate the relationship between the GR and BECN1. It is possible that the regulation of *BECN1* by the GR is complicated due to the high number of putative GR binding sites, in addition to the fact that *BECN1* is known to be regulated by the NF-κB subunit RELA (Copetti et al., 2009).

As summarised in Figure 1.14.3 (Page 52) autophagy is a multistep process involving numerous genes. Autophagy is a particularly interesting process due to the fact that although it is generally pro-survival, there have been reports of autophagy-dependent cell death, potentially due to overactivation of the "self-eating" process (Laane et al., 2009; Gump and Thorburn, 2011). As previously described, autophagy involves several steps such as autophagosome formation and maturation (Mizushima, 2007). Autophagic vesicle formation is dependent upon proteins such as BECN1 and class III phosphatidylinositol 3-kinase (PI3KIII), whilst class I PI3K/Akt signalling is an upstream inhibitor of autophagy (Laane et al., 2009).

Promyelocytic leukemia protein (PML) has been shown to be a negative regulator of PI3K/Akt signalling by blocking Akt through recruitment of the Akt phosphatase PP2a and nuclear Akt into PML bodies (Trotman et al., 2006). In PML KO cells there is a nuclear clearing deficiency of phosphorylated Akt (Trotman et al., 2006). Thus, PML serves as a negative regulator of Akt signalling. Akt itself is an upstream activator of MTOR (mechanistic target of rapamycin), which serves as a negative regulator of autophagy (Grander et al., 2009).

Laane et al. (2009) identified that dexamethasone appears to induce PML in glucocorticoid-sensitive but not glucocorticoid-resistant cells, and that PML was essential for dexamethasone-induced cell death. Thus, they concluded that dexamethasone induces cell death through PML/Akt-dependent induction of autophagy

(Laane et al., 2009). Thus, it is clear that there is some crosstalk between glucocorticoid treatment and autophagy, however the downstream pathways are complex as dexamethasone is known to regulate members of the BCL-2 superfamily, which are highly important for apoptosis (Lynch et al., 2010).

Caspase-3 experiments result in two sets of bands – the full-length (uncleaved) caspase (Caspase-3 (FL)), and the cleaved bands (Caspase-3 (CL)), which are produced following apoptotic signalling. Analysis of Caspase-3 (FL) a reduction in these bands by CM in both cell lines, though the effect was statistically significant only for C7-14 cells (compare lane to lane 1 of Figure 3.4.5, Page 118). Loss of Caspase-3 (FL) was also seen in dexamethasone-treated C7-14 cells, as well as some treatments containing etoposide for both C1-15 and C7-14 cells (Figure 3.4.5, Page 118).

Loss of full-length caspase-3 may either be due to cleavage of the protein during apoptotic processes, or general loss of the protein as a whole due to reduced stimulation of its mRNA. If a loss of Caspase-3 (FL) is observed and yet there is a corresponding increase in Caspase-3 (CL), it is possible that the loss of full-length is due to its processing to the cleaved form. By the same logic, if a loss of Caspase-3 (FL) is observed but there is no corresponding increase in Caspase-3 (CL), it is again not unreasonable to assume that this loss is due to less caspase-3 being present within the cell. Thus, the reduction of Caspase-3 (FL) by CM, due to the fact that there is generally no corresponding increase in cleaved bands, indicates a potential route by which CM is suppressing apoptotic pathways.

Further evidence for the above is that, based on the microarray, phosphatidylinositol-4-phosphate 3-kinase catalytic subunit type 2 beta (PIK3C2B) was upregulated by CM, and phosphatidylinositol-4-phosphate 3-kinase is known to block caspase-3 (Qattan, 2014). Opposite to this is the fact that etoposide induces a significant loss of Caspase-3 (FL), and yet there is a significant increase in the abundance of Caspase-3 (CL). This is best seen by examining Figure 3.4.3 (Page 116) and comparing bands for Caspase-3 (FL) to Caspase-3 (CL). The fact that C1-15 cells exhibit less loss of Caspase-3 (FL) compared to C7-14 cells may be due to less caspase-3 cleavage, in turn explaining the

183

relative resistance of the cells to etoposide treatment (Figure 3.2.1, Page 108, Figure 3.7.1, Page 132 and Figure 3.7.2, Page 134).

It was observed that dexamethasone treatment did not result in the formation of Caspase-3 (CL) bands (Figure 3.4.3, Page 116). It has been previously shown that dexamethasone induces cleavage of caspse-3 (Grander et al., 2009) and perhaps this is due to a cell type-specific phenomenon. However, dexamethasone-induced apoptosis in eosinophils did not appear to activate caspase-3 or caspase-8 (Zhang et al., 2000). Similarly, analysis in 697 B-ALL cells demonstrated that dexamethasone-induced apoptosis was dependent upon cleavage of caspase-6, not caspase-3 (Miyashita et al., 1998). Thus, the results of dexamethasone not inducing caspase-3 cleavage are reasonable and consistent with previously published data on lymphoid malignancies. Interestingly, dexamethasone demonstrated a clear trend for high activation levels of caspase-8 (Figure 3.6.4, Page 130) indicating some evidence of apoptotic signalling.

RIPK1 represents an interesting target for numerous reasons, including its role as a mediator of necroptosis (Berghe et al., 2010) and its role as a determinant of a cell's choice to undergo apoptosis, necroptosis, or pro-survival signalling through NF-κB activation (Wu et al., 2012). The initial microarray analysis which provided the basis for much of this study indicated that *RIPK1* was repressed by CM in C7-14 cells (Qattan, 2014). This was validated by qRT-PCR, where additional experiments also indicated a trend for dexamethasone to repress *RIPK1* in C7-14 cells (Figure 3.4.2, Page 115). At the protein level, RIPK1 was again suppressed by CM in C7-14 cells, whilst dexamethasone also led to a statistically significant reduction in RIPK1 levels (Figure 3.4.4, Page 117). Most treatments containing etoposide (other than etoposide/CM combination) in C7-14 cells exhibited a statistically significant reduction in RIPK1 levels, whilst for C1-15 cells the only statistically significant change was dexamethasone/etoposide combination, whilst also exhibiting a trend for CM to increase it (Figure 3.4.4, Page 117).

To further verify the regulation of *RIPK1* by the GR, GREs were identified by QIAGEN Champion ChIP (Figure 3.5.2, Page 121) and chromatin immunoprecipitation

performed against the two putative GREs (Figure 3.5.5 and Figure 3.5.6, Page 124 and Page 125). No increase in recruitment in C1-15 cells was seen following hormone stimulation at both GREs, whereas C7-14 cells exhibited a statistically significant increase in GR recruitment following dexamethasone treatment at both GREs. Thus, the GR has been identified as occupant on the *RIPK1* promoter, and it exerts a negative effect on *RIPK1* protein levels (a repressive trend was seen at mRNA level, though not statistically significant). Curiously, S211- and S226-phosphorylated GR were both recruited less in both cell lines following hormone stimulation. This is surprising given the propensity for S211-phosphorylated GR to be active at GREs. Previous research has assessed promoter occupancy of S211- and S226-phosphorylated GR demonstrating recruitment at genes such as *GILZ* (Blind and Garabedian, 2008). If phosphoisoforms are recruited less in the presence of hormone but the total GR is recruited more (as was seen for the *RIPK1* ChIP experiments) this could be due to either quality of antibodies, selective recruitment of different GR posttranslationally modified forms or other unknown factors. Given that numerous phosphorylation sites exist on GR it is possible they play a role in this promoter. In any case, the occupancy of the GR on the *RIPK1* promoter, combined with glucocorticoid effects on its protein and mRNA levels, suggests that *RIPK1* may be a target for GR control.

The link of RIPK1 being involved in the activation of NF-κB (Oberst, 2016) is a particularly interesting one, given that the crosstalk between the GR and NF-κB is very well-established and GR-mediated suppression of NF-κB signalling is a common explanation for the anti-inflammatory effects of glucocorticoid treatment (Barnes, 1998). Thus, the identification of the repression of RIPK1 by dexamethasone may represent a potentially novel explanation for the anti-inflammatory effects of glucocorticoid steroids. RIPK1, and necroptosis, are also interesting to study as it has been shown that glucocorticoid resistance may be overcome through autophagy-dependent necroptosis (Bonapace et al., 2010).

In particular, Bonapace et al. (2010) demonstrated that the use of obatoclax (a putative antagonist against BCL-2 family members) reverted glucocorticoid resistance, which was associated with release of BECN1 from a complex with myeloid cell leukemia

sequence 1 (MCL-1) and a reduction in MTOR activity (Bonapace et al., 2010). Combination dexamethasone/obatoclax lead to MTOR inhibition, and ultimately autophagy-dependent necroptosis, which is interesting as this agrees with the findings by Laane et al. (2009) detailed previously regarding dexamethasone promoting autophagy via the upregulation of PML (and subsequent downstream inhibition of Akt and MTOR). Bonapace et al. (2009) indicated RIPK1 as key for the execution of cell death, is interesting given that the results presented in this thesis demonstrate downregulation of RIPK1 in glucocorticoid-sensitive cells that die from dexamethasone exposure. It is possible that this can be explained by the multiple pathways RIPK1 is involved in, including NF-κB signalling that can promote inflammation and survival as well as in determination of whether cell will undergo necrosis, necroptosis of apoptosis depending on the above described molecular complexes and signals.

BIRC3 is known to ubiquitinate RIPK1, whose ubiquitination status plays a role in determining (along with other factors such as caspase-8 activity) cell fate between apoptosis, necroptosis and pro-survival signalling (Wu et al., 2012; Schenk and Fulda, 2015). BIRC3 is already known as a target gene of the GR (Webster et al., 2002), though the results presented in this thesis verify that in leukaemic cells (at least glucocorticoid-sensitive C7-14 cells) *BIRC3* is significantly stimulated by dexamethasone treatment (Figure 3.6.1, 127) and that the GR is occupant on its promoter following hormone stimulation, though curiously the same phenomenon of phosphoisoforms being less recruited following hormone stimulation was apparent (Figure 3.6.3, Page 129).

CM altered the expression of *BIRC3* in opposing ways between C1-15 and C7-14 cells, increasing its expression in C1-15 and decreasing in C7-14 (Figure 3.6.1, Page 127). The anti-apoptotic role of BIRC3 would explain its stimulation in C1-15 cells (pro-survival influence of the microenvironment), though its decrease by CM in C7-14 cells is puzzling. C7-14 cells exhibited a dramatic increase in *BIRC3* mRNA following dexamethasone treatment (approximately 22-23 fold), which was significantly blunted following co-treatment with etoposide (compare lane 7 to lane 3 of Figure 3.6.1, Page 127), which may indicate the molecular basis of the benefits of co-therapy in the clinic.

186

Alternatively, given that *BIRC3* has established anti-apoptotic function, this upregulation by a chemotherapy drug is highly interesting, as it points to either aberrant BIRC3 activity or highlights BIRC3 as a prospective target for drug development.

5.1.4 Effects of CM and chemotherapy on cell fate

As stated in the previous section, caspase-8 activation is a determinant of cell fate. Caspase-8 activation was tracked in C1-15 and C7-14 cells to assess its relative activation across different treatments. In both cell lines, CM decreased caspase-8 activation (Figure 3.6.4, Page 130), which provides further evidence for CM suppressing apoptotic pathways. Caspase-8 activity was increased in C7-14 for dexamethasone treatments, whilst this was less so for C1-15. Treatments containing etoposide showed maximal caspase-8 activation (Figure 3.6.4, Page 130). Cell type analysis demonstrated a reduction in apoptotic cells for C7-14 cells, whilst drug treatments (excepting dexamethasone or dexamethasone/CM combination for C1-15 cells) in both cell lines caused a significant reduction in healthy cells and a significant increase in apoptotic cells (Figure 3.7.1, Page 132). This generally correlates with both cell viability assessment via MTS assays (Figure 3.2.1, Page 108) and the Sub-G1 FACS analysis (Figure 3.7.2, Page 134).

Although the MTS assays (Figure 3.2.1, Page 108) did not show significant or negative differences with CM treatment, this was not the case for the Sub-G1 FACS analysis, as in both cell lines a reduction in the number of cells accumulating in Sub-G1 was observed following CM treatment, with the effect in C1-15 cells being statistically significant (Figure 3.7.2, Page 134). Though this is slightly inconsistent, it is arguably not unreasonable and the difference may be explained through the difference in how each technique generates the data. MTS assays are dependent on mitochondrial activity and simply rely on the entire cell population converting a dye to the product. By contrast, Sub-G1 FACS analysis scans cells individually one-by-one and tracks the cell's fluorescence intensity. Thus, Sub-G1 FACS analysis is arguably more reliable than MTS assays, potentially explaining the difference in results observed.

Ultimately, the functional analysis discussed here represents the end outcome of the molecular approaches detailed previously. The microenvironment modulates numerous pathways and genes, including the GR, caspase-3/8 and RIPK1, with the overall modulation appearing to be a promotion of cell-survival based on the outcome of treatments.

5.1.5 Putative ubiquitinated RIPK1 and BIRC3 inhibition

During experiments on RIPK1 protein levels, consistent high molecular weight band patterns were observed, with CM generally increasing a band seen at 130kDa. The consistency of this band appearance and its effect being seen primarily in C7-14 cells led to the hypothesis that these high molecular weight bands represented some modified form of RIPK1, potentially ubiquitinated RIPK1. AT406, a BIRC3 inhibitor, was used to determine if this band formed in its presence and indeed the high molecular weight bands were reduced following AT406 treatment (Figure 3.8.1, Page 136). Thus, although this is preliminary as further evidence is required before confirming these bands are modified forms of RIPK1, there is some evidence here to suggest that part of the microenvironment's effect is achieved through alteration of post-translational status. Particularly for RIPK1, due to its ubiquitination status being a determinant of cell fate, this provides novel insight that may be of therapeutic benefit.

5.2   Detailed discussion of computational results

5.2.1   Application of modelling to GR research

One of the most significant challenges facing scientific research at present is the integration and analysis of high-throughput data. Particularly for fields such as cancer research, where the molecular details of drug signalling pathways is increasingly complex, modelling may provide additional insight that traditional laboratory-based research cannot uncover. Ultimately, models aim to be a predictive tool.

As described in the Introduction (Section 1.22, Page 68), modelling techniques have previously been applied to glucocorticoid/nuclear receptor research. These include approaches such as a top-down approach which utilised microarray data to build mechanistic models of corticosteroid effects (Jin et al., 2003), development of ODE models of glucocorticoid direct and indirect gene induction based on detailed mRNA and protein levels (Chen et al., 2010) or virtual screening for potential nuclear receptor ligands (Ai et al., 2009).

Given the good prediction ratios obtained by the original TP53 interactome (Tian et al., 2013), the STSFA analysis of the original TP53 interactome (Hussain et al., 2014) and the expanded TP53 interactome (Hussain et al., 2015), a similar approach was utilised here to undertake the novel application of this modelling approach to GR research. The GEB052 model is distinguished from other published models in that it aims to integrate hundreds of interactions at once as a Boolean model, incorporating not only GR signalling but interactions between GR interaction partners as well as linking the model to the measurable biological outputs of cell death and inflammation. This discussion compares the GEB052 model to the TP53 interactomes generated previously, as these models were built using the same approaches herein and thus they represent a good comparison point for relative model analysis.

5.2.2   GEB052 Network Structure

Following extensive literature curation, the GEB052 model was developed, consisting of 52 nodes and 241 logical interactions, one input of a glucocorticoid activating the GR, and two outputs of cell death and inflammation. The model consists of 64 two-step feedback loops, signifying the interconnectivity of the model. Interestingly, the TP53 model described previously (consisting of 206 nodes and 738 interactions) contained only 30 two-step feedback loops (Tian et al., 2013), whilst the expanded TP53 interactome published at a later date (consisting of 260 nodes with 980 interactions) contained only 34 feedback loops (Hussain et al., 2015). Despite the much smaller size of the GEB052 model (only 52 nodes compared to 206 or 280), there is a much higher number of feedback loops within it, potentially signifying a greater degree of interconnectivity between model constituents.

The node connectivity assessment indicated that 15 out of 52 nodes (29%) exhibited high connectivity ($\geq$10 interactions), with each of these nodes, excepting outputs, being taken forward for *in silico* knockout analysis. The original TP53 model had 31 nodes with a connectivity of equal to or more than ten (Tian et al., 2013), which corresponds to 15% of the nodes. This provides further evidence of the interconnectivity of the GEB052 model compared to the TP53 model.

This enhanced connectivity could have arose either due to higher inherent connectivity for GR signalling *in vivo*, updates to the STRING database, or differences in the filtering process following automatic extraction. During the curation of the interaction records for the GEB052 model, all possible interactions were considered, even those where a predicted interaction of activation or inhibition was not present (i.e. "binding" reactions). Though these interactions did not have a predicted activation or inhibition based on STRING data, literature curation would often unveil a stimulatory or inhibitory relationship between the two proteins. Thus, a significant number of the activation/inhibition interactions in GEB052 model were based off "binding" predictions. The thesis describing the construction of the TP53 model indicates that only posttranslational modification, activation, and inhibition interactions from STRING were considered (Tian, 2013). Thus, the expanded scope of starting interactions in the

GEB052 model can partially explain its more significant degree of interconnectivity, despite the smaller size of the network.

5.2.3   Dependency Analysis of GEB052 model

Dependency analysis of the GEB052 model unveiled that the most significant dependency matrix alterations occurred for those nodes exhibiting the highest connectivity. Removal of the GR, which is the most connected node in the model, lead to the most significant alterations in the dependency matrix. Surprisingly, despite performing thirteen KO scenarios (for nodes, other than outputs, whose connectivity was $\geq$10), only three KO scenarios (GR KO, HSP90 KO, and HDAC1 KO) demonstrated changes to strong activators or strong inhibitors. As stated previously, it is typical that changes to strong activators or strong inhibitors are focussed on, as these are the changes most likely to exhibit an effect *in vivo* due to their relative rarity and lack of feedback loops making their effects stronger.

The TP53 interactome model, across its numerous KO scenarios, demonstrated a significant number (63) of alterations to strong activators/inhibitors (Tian et al., 2013). Comparatively, of all the KO scenarios performed on the GEB052 model, only ten alterations to strong activators/inhibitors were seen. Changes to or from weak activators and inhibitors may well exert an effect on the cell, however analysis of these dependencies would be cumbersome due to the high number. As previously stated, across all KO scenarios in the GEB052 model a total of 1249 dependency alterations were observed; when ambivalent to no effect changes were removed, this dropped to 323 dependency alterations. Although more manageable, 323 is still a significant amount of changes to follow individually and thus initial analysis has focussed only on changes to or from strong activators/inhibitors.

Although less significant (changes to or from strong activators or inhibitors) alterations were seen, it is important to note that only three of the thirteen (23%) KO scenarios yielded changes. Comparatively, for the TP53 model, 11 out of 31 KO scenarios (35%) yielded significant changes (Tian et al., 2013). Thus, the TP53 model in general was

more prone to disruption. This is potentially justified given the enhanced connectivity of the GEB052 model relative to the TP53 model, as described earlier. With a significantly higher number of two-step feedback loops (especially relative to model size), and more interconnectivity between the nodes, the model relationships and dependencies would be less prone to disruption, which may explain why fewer significant changes to the dependencies were observed.

Despite changes to or from strong activators or inhibitors being most likely changes to exert an effect *in vivo*, it is possible that changes to or from weak activators or weak inhibitors would also demonstrate an effect *in vivo*, particularly if all of the dependencies for which a node is the target are altered. Furthermore, as indicated in Table 4.3.1 (Page 159) and figures such as Figure 4.3.2 (Page 161), numerous alterations to or from weak activators or inhibitors were seen. Thus, analysis of these changes across the KO scenarios represents a point for future work.

5.2.4   LSSA Interpretation and Validation

The use of LSSA allows for the capturing of the overall state of a network element following completion of its input signals. To assess model predictive power, LSSA was performed to simulate both GC-sensitive cells and GC-resistant cells (Table 4.4.1, Page 164), and model predictions of node state changes were compared to microarray data from glucocorticoid-resistant and glucocorticoid-sensitive cells (Table 4.4.4, Page 169). The average correct prediction rate across the six validations was 56.60%, whilst small errors accounted for 41.67%, and large errors accounted for 1.74%.

The TP53 model developed using a similar methodology to GEB052 displayed correct prediction rates ranging from 52% to 71% (Tian et al., 2013). Although the range of correct predictions for GEB052 is smaller (54.17% to 60.42%), less large error predictions were seen in the GEB052 model. Every validation of the TP53 model had at least two large errors (large error prediction ranged from 2% to 6%). However, the presence of large errors was significantly less in the GEB052 model, with two out of six simulations showing no large errors, and the other four showing a large error range from

2.08% to 4.17%. Interestingly, the expanded TP53 interactome later published showed less large errors than the original TP53 inteactome, though all validations included at least one large error (Hussain et al., 2015). Thus, model expansion may represent a way to improve model accuracy, which in turn indicates a future direction for the GEB052 model.

In addition to the validation based on microarray data obtained from cells, the model LSSA results have also been compared to microarray data from thirteen patients following treatment with glucocorticoids (Figure 4.5.1, Page 171). Correct predictions here dropped to an average of 42%, with 55% small error and 3% large error. Although the level of correct predictions is lower than that for cell-based microarray data (42% against 56.6%), this is potentially justified given that the model is currently of a small size, in addition to the fact that the evidence used for the interactions are primarily from cell-based studies. Furthermore, the GEB052 model encapsulates only a small part of the signalling that occurs following hormone treatment, and model expansion may improve predictive power. Lastly, effects of glucocorticoids are very cell-type specific, and yet the model does not account for cell type at present. This thus represents a source of future work for the model.

Furthermore, the validation methodology was different between the two approaches, as the cell-based microarray data had obvious groups that could be compared (i.e. sensitive to resistant microarray, compared to sensitive to resistant LSSA). However, this was not possible for the patient data utilised and thus this represents a further reason for why the correct prediction rate at the patient level is lower than for cell-based microarray data. However, this falls largely as a limit for LSSA, as other approaches allow for a more quantitative analysis to be performed, even for individual patients (see STSFA discussion in the subsequent section).

Comparison of the LSSA results for the glucocorticoid-sensitive and glucocorticoid resistant scenarios unveiled that the majority of the nodes (37 out of 52) were unchanged between the two scenarios, whilst three were upregulated in GC-resistant cells and twelve were downregulated in GC-resistant cells (Table 4.4.2, Page 167).

It is interesting that DAXX, a pro-apoptotic node, was upregulated in the GC-resistant simulation. However, other genes affecting cell death were downregulated in the GC-resistant simulation (relative to GC-sensitive). CD40LG and UBC are each directly ambivalent to cell death (and as such, they cannot be classified alone as pro- or anti-apoptotic within the model). TSC22D3 and STAT5B, the former of which is better known as the anti-inflammatory protein GILZ (glucocorticoid-induced leucine zipper) (Hahn et al., 2014) and the latter of which is a transcription factor implicated in pancreatic chemoresistance that is activated by the GR and negatively feeds back to the GR (Stocklin et al., 1996; Sumiyoshi et al., 2016; Wyszomierski et al., 1999) are both anti-apoptotic nodes within the model, and each were downregulated in the GC-resistant scenario. Importantly, most nodes under LSSA were unchanged, with only three exhibiting upregulation in the GC-resistant scenario and eleven (excluding the GR) exhibiting downregulation; the remainder were unchanged, and this includes several nodes linked to cell death (n=13). This again highlights a limit of LSSA; fixed states limit the analysis. If a more quantitative analysis was employed (as performed later via STSFA) it is likely these unchanged nodes would show differences and provide further insight. Although it is surprising that a pro-apoptotic node was upregulated in resistant simulation, and these two anti-apoptotic nodes were downregulated in the resistant simulation, it may be worth noting that the cytotoxic effects of GCs are limited to very few cell types, whereas they exert pro-survival effects in other tissues (Bailly-Maitre et al., 2001). The model is not yet tissue-specific, and so predictive power could be further improved by building cell type-specific versions of the GEB052 model.

For the nodes relating to inflammation, only CD40LG and STAT5B were shown to have altered expression between the sensitive and resistant simulations (the remainder were unchanged), and both were downregulated in the resistant simulation. STAT5B has been previously discussed. CD40LG is stimulated by glucocorticoids and plays a role in isotype switching, a process that allows for B-cells to change the type of antibodies they produce (Jabara et al., 2001) STAT5B is directly ambivalent to inflammation, meaning that similar to before it alone cannot be classified as pro- or anti-inflammatory within the model's framework. However, CD40LG, a pro-

inflammatory node, was downregulated in the resistant simulation relative to the sensitive simulation. Again, this is quite surprising, as glucocorticoids should reduce inflammation, in theory through the modulation of inflammatory-related genes. If a pro-inflammatory gene is less active in resistant cells, then that means there is less inflammation in resistant cells, which is contrary to the logic that the resistant cells are unresponsive to glucocorticoid treatment.

Potential explanations for this finding include the fact that the model is small, consisting of 52 highly connected nodes. Furthermore, only eight nodes had a direct reaction with the inflammation node. It is needless to say that the inflammatory process *in vivo* is affected by far more than eight genes, and thus CD40LG is only one gene out of many. In addition to this, this observation highlights a shortcoming in the LSSA approach, in that values are fixed and show 1, 0 or NaN. Thus, if a node receives even one stimulatory signal, it achieves a state of 1. In addition to the nodes themselves, all edges (interaction) in the model under LSSA are represented with a steady state, which does not allow for quantitative analysis. It is for this reason that following analysis of the LSSA results, a more quantitative approach by STSFA was used.

5.2.5   Quantitative Model Analysis

The use of STSFA (Isik et al., 2012) has previously been shown to have enhanced predictive power over LSSA (Hussain et al., 2014). The nature of STSFA is that it allows for semi-quantitative analysis of Boolean models by superimposing numerical data (based on microarray or ChIP-Seq data) onto nodes and assigning weights to each edge. Thus, rather than having states of ON, OFF, or undetermined, node and edges are assigned a numerical value following the completion of signalling paths within the network.

Application of STSFA to the GEB052 model led to significantly more accurate predictions being generated. Six comparisons were used to validate STSFA results. Curiously, large errors appeared only in simulations for B-ALL, and not for T-ALL

(Table 4.6.1, Page 172). This may be an indication that the model predicts T-ALL better than B-ALL, though this remains to be seen.

Compared to LSSA, STSFA demonstrated a statistically significantly higher level of correct predictions, to a degree of 56.6% for LSSA and 80.1% correct for STSFA (Figure 4.6.1, Page 173). This is consistent with previous application of the STSFA to the TP53 model, where it was again shown that the STSFA resulted in more accurate predictions (Hussain et al., 2014), though the application of the STSFA to the TP53 model lead to a correct prediction rate of approximately 77%, indicating that application of the STSFA to the GR model results in slightly more accurate predictions than those obtained for the TP53 model (80.1% against 77%). LSSA and STSFA both have their respective advantages and disadvantages. STSFA, though more quantitatively precise and appearing to demonstrate improved predictive power, requires expression data prior to use and cannot handle directly ambivalent relationships. LSSA, though more qualitative in its analysis, does not require expression data and can still provide insight into the function of the network. However, LSSA's use of fixed states presents a limitation on its accuracy as eventually quantitative analysis is required to provide deeper insights.

Due to the enhanced predictive power of the STSFA, the algorithm was also used to superimpose patient microarray data (taken before treatment) to analyse the model (Figure 4.6.2, Page 175). Thirteen leukaemia patients were divided into two groups: Dead at Risk Assessment (one patient) and Alive at Risk Assessment (twelve patients) and the edge weights relating to cell death were totalled for each patient, and an average was made for each group. Though preliminary due to the small patient number, and the uneven group number, it is nonetheless highly interesting that GEB052 under the STSFA predicted a "more negative" total for the patient who died before risk assessment than for those who were alive at risk assessment. This translates to more negative signals towards apoptosis, which results in more tumour growth, in turn posing a bigger risk to the patient. What is particularly interesting is that the microarray data used for this was taken before the patients were treated. Thus, what is seen here is a true prediction, as it is not following treatment with prednisolone or dexamethasone. In

theory, if several different models are built of different chemotherapy drug receptors, then the same microarray data taken before treatment could be applied to each of these models, which would provide an indication of which drugs may work best on an individual level. It is still too preliminary for this, as the model requires tissue specificity and expansion, but this clinical assessment of GEB052 is highly promising indication nonetheless. Furthermore, an additional issue is that the age group cell death edge weight analysis (Figure 4.6.3) did not appear to correlate with clinical outcomes, indicating a need for model refinement.

5.3   Conclusions and Summary of Key Findings

The data presented in this thesis suggests that the bone marrow microenvironment facilitates leukaemic cell survival through alteration of multiple pathways within the cell. Cell viability assay suggested that CM alters leukaemic cell fate, which is corroborated by the fact that. CM was identified as exerting effects on GR phosphorylation (Section 3.3, Page 108), which suggests modified GR function by the microenvironment and provides a link from the microenvironment to drug response. Markers relating to cell death and survival were also modulated by CM and chemotherapy (Section 3.4, Page 113), with some evidence that CM modulates BECN1, in turn indicating a potential regulation of autophagy. CM reduced RIPK1 mRNA and protein, indicating a potential suppression of necroptosis, though analysis of RIPK1 is complicated given its link to NF-κB. Dexamethasone trended towards reducing *RIPK1*, though effects were only statistically significant at the protein level. Again, given the link of RIPK1 to NF-κB, a primary driver of inflammation, this repression could represent a novel route through which glucocorticoids exert their anti-inflammatory effect. Lastly, CM reduced caspase-3 protein levels and caspase-8 activation, which indicates a potential suppression of apoptotic signalling. Thus, CM appears to exert an effect on numerous pathways that are important in determining cell fate.

GR occupancy on the *BECN1*, *RIPK1* and *BIRC3* upstream regions is an interesting outcome, particularly the high number of putative GREs on *BECN1*. GR presence on the *BECN1* and *RIPK1* promoters may indicate the discovery of novel glucocorticoid-regulated genes, though this has not been fully shown within this thesis. Although dexamethasone lead to some modulation of RIPK1 (trending towards reduction at mRNA, and a statistically significant reduction at the protein level), no clear effects were observed for BECN1. If the GR is indeed occupant on the *BECN1* promoter, its effects could be complicated via crosstalk with other transcription factors and the fact that there are numerous putative GR binding sites. Although BIRC3 is a known target of the GR (Webster et al., 2002), it is surprising that this anti-apoptotic protein is strongly stimulated by dexamethasone in lymphoblast cells, given that glucocorticoids induce leukaemic cell death and indicates a potential co-therapy of BIRC3 inhibition and

cheomotherapy. Use of the BIRC3 inhibitor AT406 indicated that CM effects may be partially mediated by alteration of protein post-translational status (Section 3.8, Page 135).

The GEB052 model represents the novel application of this modelling approach to GR research (Section Chapter 4, Page 137) and demonstrates good predictive rates across numerous different analyses such as LSSA, dependency matrices, *in silico* KOs and STSFA. Model validation by cell-based microarray data led to a correct prediction rate of 54-60%, whilst large errors constituted only a minor of prediction outcomes (average <2%) (Section 4.4, Page 163). When validated with clinical data from thirteen individual patients, the ratio of correct predictions dropped to an average of approximately 42%, indicating some potential shortcomings of the model (Section 4.5, Page 170). However, large errors were again seen to only a minor degree (less than 5% across all simulations), which suggests that the model, though not yet ready for clinical applications under basic LSSA approaches, has the potential to improve.

Model validation by STSFA analysis showed a significantly higher level of correct predictions, with an average of 80% across the six simulations (Section 4.6, Page 172). Large error predictions accounted only for an average of 1% across the six simulations. When LSSA and STSFA analyses were compared, STSFA demonstrated a statistically significantly higher level of correct predictions, proving the improved power of quantitative or semi-quantitative analysis over classical Boolean. The improved power of STSFA was again demonstrated when microarray data from thirteen leukaemia patients was used to analyse the model, with the analytical output showing good correlation with clinical data. Thus, the semi-quantitative analysis by STSFA demonstrates significantly more accurate predictions than fixed LSSA states. Though preliminary, the validation using STSFA and patient microarray data shows good correlation with clinical outcomes and is a promising indicator of the strength of the GEB052 model.

5.4   Study Limitations

5.4.1   Limitations of Wet Laboratory Research

One limitation of the present study is that the work has been conducted on only two leukaemia cell lines, both of which originate from the same parental line. Although some preliminary validation has been performed in another leukaemia cell line (MOLT-4; Appendix Figure 4 and Appendix Figure 5, Page 209 and Page 210 respectively) more experiments are required to ensure that the effects observed in this study are not isolated to only one glucocorticoid-sensitive and one glucocorticoid-resistant cell line.

There are some limitations of the laboratory techniques used that have to be considered. For qRT-PCR, SYBR Green was used instead of TaqMan and it is known that this approach may generate false positive results. Although this is mitigated through assessment of primer efficiency, melting curve analysis and careful primer design, it is nonetheless a point to consider. Western analysis is semi-quantitative at best; therefore, although another approach such as the enzyme-linked immunosorbent assay has a higher false positive rate and lower specificity, it is more quantitatively precise. The chromatin immunoprecipitation assays, though yielding positive results, are also limited as there is a lack of suitable antibodies to assess occupancy of specific phosphoisoforms of the GR; the S211 and S226 antibodies used were the same as for western blotting, whilst the total GR was a specific ChIP-grade antibody.

A recurrent problem with *in vitro* studies is *in vitro-in vivo* extrapolation; how well the findings here translate to both animal and clinical models remains to be seen. This is particularly relevant when considering the fact that molecular biology necessitates focussing on only a small part of the whole molecular signalling network.

5.4.2   Limitations of Computational Research

A persistent limitation of Boolean modelling is that the qualitative nature of the approach limits the information that can be garnered from the study. Although this can

be mitigated through approaches that aim to allow for a more quantitative analysis (such as the STSFA), these models remain mechanistically imprecise. Despite the mechanistic imprecision, the GEB052 model demonstrated good predictive ratios across all scenarios. However, the model has currently only been validated using data from either B-ALL or T-ALL cell-based microarrays or clinical data from leukaemia patients. Therefore, one limitation to the current study is that the model's predictive capacity for other cell types (such as lung, which would be important for the use of glucocorticoids in diseases such as chronic obstructive pulmonary disease) has not been assessed. Similarly, the model is currently at a very small size (only 52 nodes connected by 241 edges) and thus it cannot fully simulate glucocorticoid-regulated pathways. These points therefore represent a source for future work.

5.5   Future Directions

5.5.1   Future Directions for Wet Laboratory Research

The microenvironment may communicate with cells in a variety of ways such as cell-cell contact mediated by factors such as integrins or secreted factors such as microvesicles (exosomes), which may contain contents such as proteins, microRNAs or nucleic acids (Bakker et al., 2016). Previous fractionation of CM unveiled that one chemoprotective fraction (<3kDa) was Proteinase K, RNase and heat resistant, and that this fraction contained exosomes (Liu et al., 2012). If the constituents of CM are identified, then targeted co-therapy combining chemotherapy and specific antagonists of CM constituents could be used to improve clinical outcomes. In addition to this, if microRNAs are hypothesised to be contained within CM exosomes, then bioinformatics approaches could be used to identify potential microRNAs that modulate the expression of the genes identified in this thesis as modulated by CM (i.e. RIPK1).

The occupancy of the GR on the BECN1 and RIPK1 promoters was a particularly interesting find, as it indicates that their expression may in some way be under glucocorticoid control. However, the results presented within this thesis do not show this completely, as although dexamethasone led to a statistically significant decrease in

RIPK1 protein levels, its effects at mRNA were less clear and analysis of BECN1 was inconclusive. In particular, the adjacency of the putative GREs to putative NF-κB binding sites should be investigated, as well as the potential anti-inflammatory route of GR to NF-κB through RIPK1 modulation. Although no clear effects of GR were observed on BECN1, it is possible that different concentrations, time of treatment or ligands could unveil this.

Although the use of IAP inhibitors is currently highly investigated due to their aberrant expression in multiple cancer types, this thesis has identified that they are particularly relevant for leukaemia where glucocorticoids are used in treatment, due to the stimulatory effect of glucocorticoids on this anti-apoptotic protein. Combination therapy of prednisolone/dexamethasone with anti-IAP treatments may yield improved therapeutic outcomes. AT406 in this thesis was used only to assess putative ubiquitination, though its effects on apoptosis, autophagy and necroptosis in leukaemia cells should be investigated.

5.5.2 Future Directions for Computational Research

The GEB052 model at present consists of 52 nodes, which despite being highly interconnected is a relatively small model. Therefore, model expansion and reevaluation is the first source for future research. This can be carried out in numerous ways; re-extraction following updates to the STRING database; consideration of all predicted interactions regardless of confidence or addition of a "third layer" to the model.

Two other useful future research approaches would be to make the model tissue-specific and to validate the model using microarray data from cell types other than leukaemia. Tissue specificity was applied to a preliminary version of the model (Bakker et al., 2014) which indicated differential predictions based on the tissue-type simulated. Since glucocorticoids are used to treat a variety of diseases and have varying effects depending on the cell type, models catering to different cell types such as leukaemic and lung would be highly useful. Furthermore, the current GEB052 model could undergo genome-wide validation using microarrays from other tissue types (such as lung, which

may be useful for diseases such as chronic obstructive pulmonary disease). This was not performed in this thesis due to the thesis' focus on leukaemia. In addition, wet laboratory verification of the predictions generated by dependency matrix comparisons would be useful. Lastly, further clinical assessment of the model with a larger patient cohort would strengthen the STSFA clinical validation findings presented in this thesis.

Chapter 6   Appendices

6.1   Publications and Conference Proceedings Resulting From Research

Throughout the course of research during the PhD, results (preliminary or otherwise) have been presented at both national and international conferences. Thus part of the work within this thesis has been published as part as conference proceedings. Following from this are the generation of original research articles, which are either published at or submitted to peer-reviewed journals. The author of this thesis has also published a review article on the field in Biochimica et Biophysica Acta (BBA) - Molecular Cell Research. All publications and conference proceedings relevant to this thesis are listed as follows:

6.1.1   Conference Proceedings

BAKKER, E., TIAN, K., ANDREWS, J., DEMONACOS, C., SCHWARTZ, J.-M. & KRSTIC-DEMONACOS, M. 2014. Glucocorticoid receptor interactome. Society for Endocrinology BES 2014. Liverpool, UK: Endocrine Abstracts.

QATTAN, M., CHEN, D. W. C., SAHA, V., LIU, J. Z., ZEEF, L., SCHWARTZ, J. M., **BAKKER, E.**, DEMONACOS, C. & KRSTIC-DEMONACOS, M. 2014. Determinants of drug and microenvironment response in acute lymphoblastic leukaemia. *International Journal of Molecular Medicine,* 34**,** S112-S112. 19th World Congress on Advances in Oncology and 17th International Symposium on Molecular Medicine Athens, Greece.

QATTAN, M., **BAKKER, E**., CHEN, DW-C., SAHA, V., LIU, JZ., ZEEF, L., SCHWARTZ, J-M., DEMONACOS, C. & KRSTIC-DEMONACOS, M. 2015. Implications of the bone marrow microenvironment in drug response and resistance in acute lymphoblastic leukaemia (ALL). Genes & Cancer Annual Meeting 2015. Cambridge, UK.

QATTAN, M., **BAKKER, E**., SAHA, V., LIU, JZ., ZEEF, L., SCHWARTZ, J-M., DEMONACOS, C. & KRSTIC-DEMONACOS, M. 2015. The effect of bone marrow-derived factors on cell death and survival signalling and resistance to chemotherapy. Nuclear receptors: From molecules to humans. Ajaccio, France.

QATTAN, M., **BAKKER, E.**, RAJENDRAN, R., CHEN, D. W. C., SAHA, V., LIU, J. Z., ZEEF, L., SCHWARTZ, J. M., MUTTI, L., DEMONACOS, C. & KRSTIC-DEMONACOS, M. 2016. The role of the microenvironment in acute lymphoblastic leukaemia drug response. *International Journal of Molecular Medicine,* 38**,** S46-S46. 21st World Congress on Advances in Oncology and 19th International Symposium on Molecular Medicine. Athens, Greece.

6.1.2   Articles

Articles relating to the thesis:

BAKKER, E., QATTAN, M., MUTTI, L., DEMONACOS, C. & KRSTIC-DEMONACOS, M. 2016. The role of microenvironment and immunity in drug response in leukemia. *Biochim Biophys Acta,* 1863**,** 414-26.

QATTAN, M. Y.*, **BAKKER, E. Y.***, RAJENDRAN, R., CHEN, D. W., SAHA, V., LIU, J., ZEEF, L., SCHWARTZ, J. M., MUTTI, L., DEMONACOS, C.# & KRSTIC-DEMONACOS, M.# 2017. Differential regulation of cell death pathways by the microenvironment correlates with chemoresistance and survival in leukaemia. *PLoS One,* 12**,** e0178606.
*#Authors contributed equally

BAKKER, E., TIAN, K., DEMONACOS, C., SCHWARTZ, J.M.* & KRSTIC-DEMONACOS, M.*. 2017. Insight into glucocorticoid receptor signalling through interactome model analysis. [*manuscript invited for resubmission at PLOS Computational Biology*]
*Authors contributed equally

In addition to the above, the author of this thesis has also contributed towards review articles relating to mesothelioma:

GUAZZELLI, A., **BAKKER, E.**, KRSTIC-DEMONACOS, M., LISANTI, M. P., SOTGIA, F. & MUTTI, L. 2017a. Anti-CTLA-4 therapy for malignant mesothelioma. *Immunotherapy,* 9**,** 273-280.

BAKKER, E., GUAZZELLI, A., KRSTIC-DEMONACOS, M., LISANTI, M., SOTGIA, F. & MUTTI, L. 2017b. Current and prospective pharmacotherapies for the treatment of pleural mesothelioma. *Expert Opinion on Orphan Drugs,* 5**,** 455-465.

GUAZZELLI, A., **BAKKER, E.**, TIAN, K., DEMONACOS, C., KRSTIC-DEMONACOS, M. & MUTTI, L. 2017. Promising investigational drug candidates in phase I and phase II clinical trials for mesothelioma. *Expert Opinion on Investigational Drugs,* 26**,** 933-944.

BAKKER, E., GUAZZELLI, A., ASHTIANI, F., DEMONACOS, C., KRSTIC-DEMONACOS, M. & MUTTI, L. 2017a. Immunotherapy advances for mesothelioma treatment. *Expert Review of Anticancer Therapy,* 17**,** 799-814.

6.2   Supplementary Data

This section includes several results that are related to the thesis, but were not included in the primary results section.

6.2.1   CM Concentration Optimisation
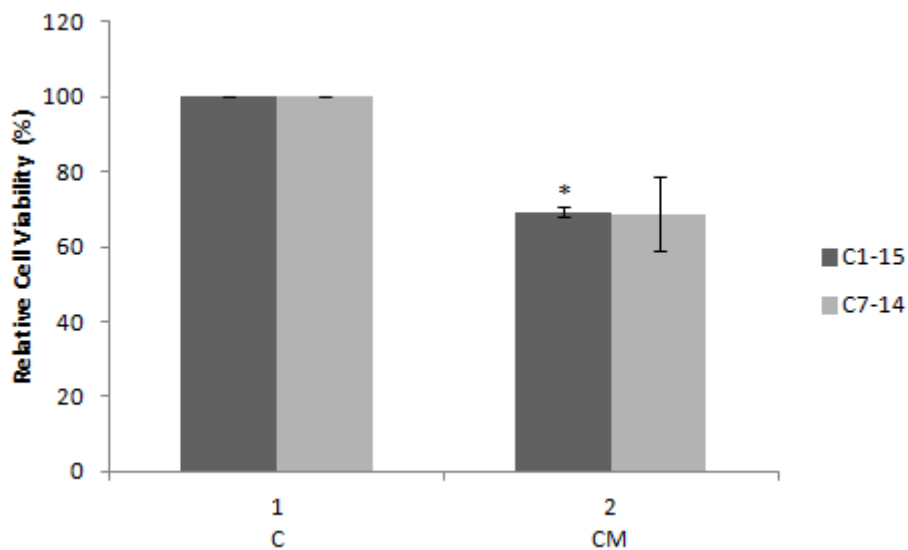
Appendix Figure 1: Viability of leukaemia cells grown in 100% CM for 48 hours.
Cell viability was assessed by MTS assays. Data is representative of three experiments +/- SEM. An asterisk (*) indicates $p \leq 0.05$.

As shown above, there was a negative effect on the growth of both C1-15 and C7-14 leukaemic cells grown in 100% CM. This is contrary to established literature and also what was hypothesised at the beginning of the study.

However, after reflection it was thought that this negative effect could be due to the method used to generate CM as well as the incubation conditions the experiment was carried out in. Routine cell culture requires specific growth media for the cells, such as RPMI-1640 supplemented with l-glutamine and FBS. To generate CM, HS5 cells were incubated with serum-free RPMI for 48 hours. Not only would this deplete nutrients within the RPMI before it is even fed to the leukaemia cells, but cells grown in 100% CM would be serum-free. This quite clearly would lead to a negative effect on the

growth of cells. To further assess the role of CM, another concentration (1/3rd CM) was used:
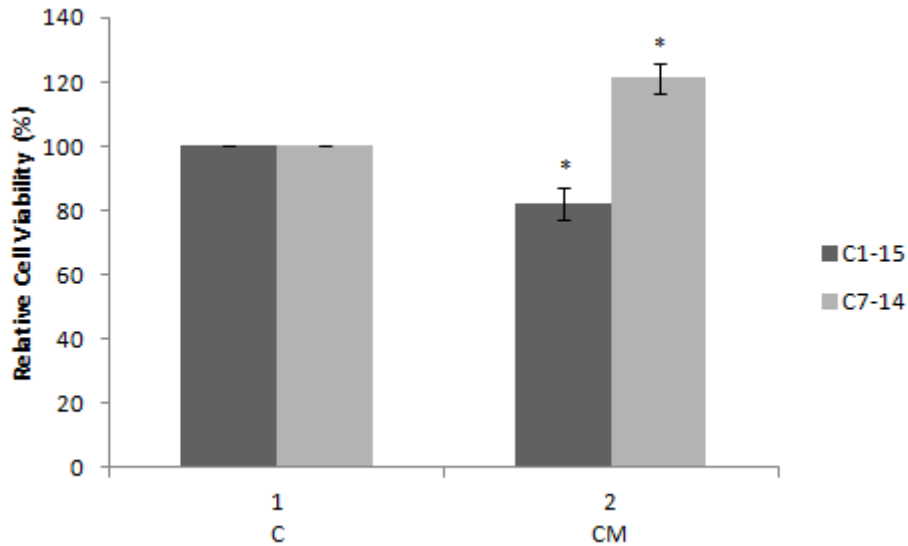
Appendix Figure 2: Viability of leukaemia cells grown in 1/3rd CM for 48 hours.
Cell viability was assessed by MTS assays. Data is representative of two independent experiments, each performed in triplicate +/- SEM. An asterisk (*) indicates p≤0.05.

The use of 1/3rd CM was motivated in part by a previous study which utilised 30% CM from and for different cells and saw chemoprotective effect (Konopleva et al., 2002). This is partially consistent with what is shown in Appendix Figure 2, with C7-14 cells showing a statistically significant increase in viability. However, C1-15 cells exhibited a negative response to 1/3rd CM. 1/6th CM was then examined:
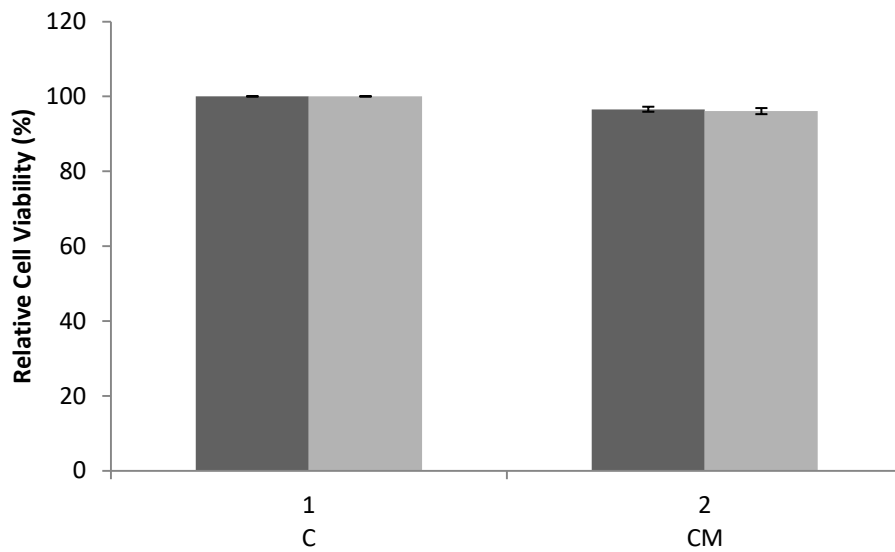
Appendix Figure 3: Viability of leukaemia cells grown in $1/6^{th}$ CM for 48 hours.

Cell viability was assessed by MTS assays Data represents at least three independent experiments +/- SEM.

Appendix Figure 3 above demonstrates the effects of $1/6^{th}$ CM on leukaemic cell fate. Importantly, 1/6th CM did not exert a significant change (positive or negative) on either cell line, and therefore represents a good balance for further study. MTS assays are useful only as an indication, due to their dependence on mitochondrial activity. Metabolic rates between C1-15 and C7-14 cells could differ and may be affected by CM, and thus additional assays were employed to investigate CM effects.

6.2.2   Validation of CM Effects in Another Cell Line (MOLT-4)
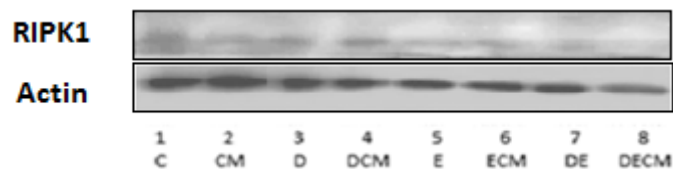
Appendix Figure 4: RIPK1 protein expression in MOLT-4 cells.

Experiment carried out two times.

Appendix Figure 4 shows RIPK1 analysis in MOLT-4 cells, another ALL cell line. Experiments were performed in MOLT-4 cells to provide an additional validation that

effects seen by treatments (particularly CM) were not isolated to one cell line. Appendix Figure 5 shows the quantification of two experiments:
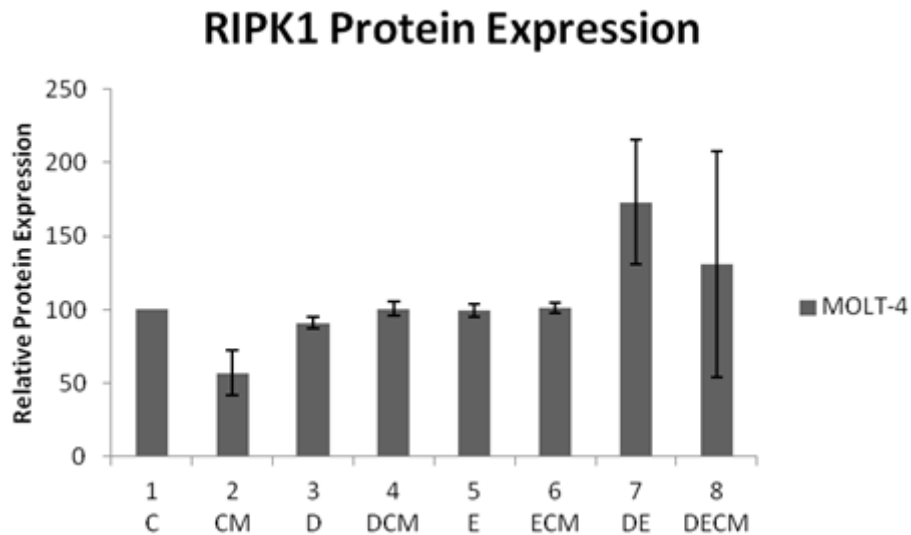
Appendix Figure 5: Quantification of MOLT-4 RIPK1 blot data.

RIPK1 band readings were normalised to the corresponding actin and these actin-normalised values were then expressed as a percentage of untreated cells. Data is the average of two experiments +/- SEM.

Appendix Figure 5 above shows that the effects of CM repressing RIPK1 are also shown as a trend in MOLT-4 cells. Thus, although primary analysis is performed in C1-15 and C7-14 cells, this provides some initial evidence that CM affects multiple ALL cell lines, and not simply CCRF-CEM cells or those subcloned from them.

6.2.3   BIRC3 GRE 5 Separate Experiments

The following figures show the individual experiments used to create Figure 3.6.2 (Page 128):
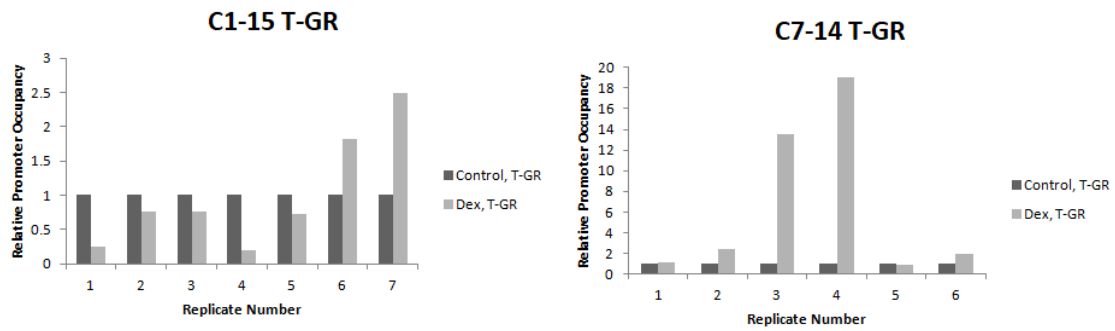
Appendix Figure 6: Individual experiments used for T-GR for Figure 3.6.2 (Page 128).
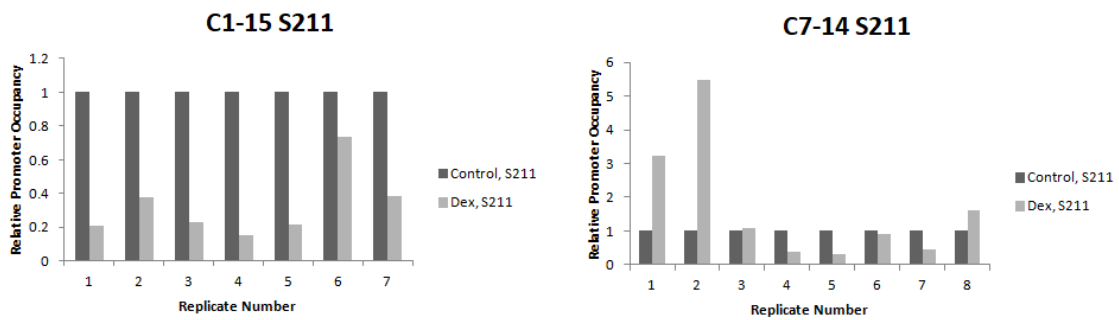
Appendix Figure 7: Individual experiments used for S211 for Figure 3.6.2 (Page 128).
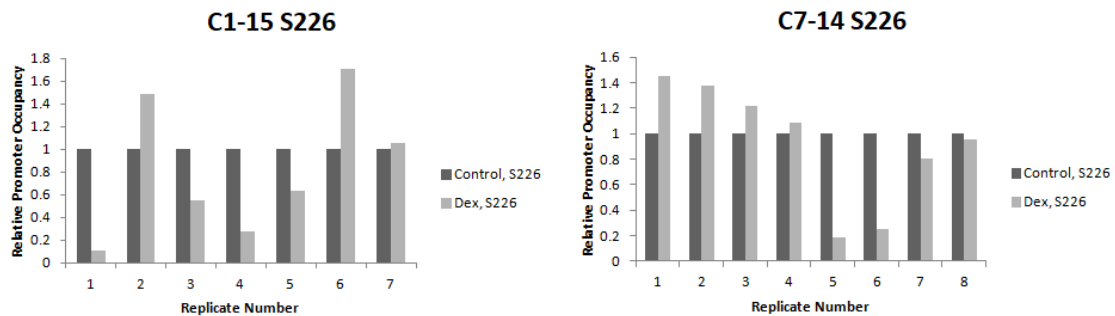
Appendix Figure 8: Individual experiments used for S226 for Figure 3.6.2 (Page 128).

6.2.4   Cell Type Analysis – Necrotic Cells

In addition to the healthy and apoptotic cells captured in Figure 3.7.1 (Page 132), necrotic cells were also captured:
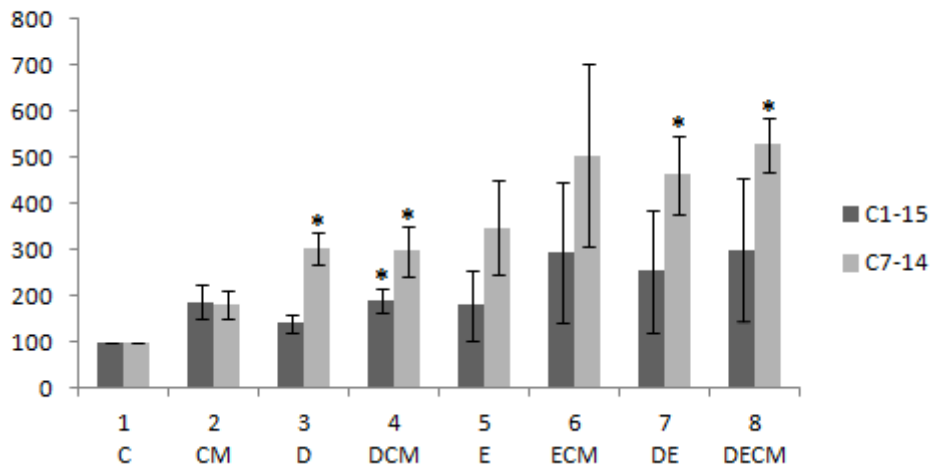
Appendix Figure 9: Necrotic cell type analysis.

Data represents the average of four independent experiments +/-SEM. An asterisk (*) indicates $p \leq 0.05$.

6.2.5 GEB052 Model Validation by Microarray Data

The following tables show the individual results for each comparison shown in Table 4.4.4 (Page 169).

Appendix Table 1: GEB052 model validation by microarray data (Comparison 1).

Comparison 1	E_{mod}	E_{exp}	ABS (E_{mod}-E_{exp})
14-3-3.	0	0	0
ABCA1	0	0	0
AFP	-1	0	1
AP-1	0	-1	1
ARHGAP35	-1	0	1
BAG1	0	0	0
CD2	0	0	0
CD40LG	-1	0	1
CREB1	0	0	0
CREBBP/EP300	0	0	0
CRH	0	0	0
DAP3	0	0	0
DAXX	1	0	1
FSCN1	0	1	1
GLUL	-1	-1	0

	E_{mod}	E_{exp}	ABS (E_{mod}-E_{exp})
HDAC1	1	0	1
HDAC6	0	0	0
HSP90	0	0	0
IL10	0	-1	1
IL6	0	0	0
LIF	0	0	0
MED1	-1	0	1
NCOA1	0	-1	1
NCOA2	0	0	0
NCOA3	0	0	0
NCOA6	0	0	0
NCOR1	0	0	0
NCOR2	0	0	0
NFKB	0	-1	1
NR1I3	-1	0	1
NR2F2	-1	0	1
NRIP1	0	0	0
PKA	0	0	0
POU2F1	0	0	0
POU2F2	0	0	0
PRKDC	0	0	0
PTGES3	0	0	0
SCAP	-1	0	1
SGK1	0	-1	1
SMAD3	0	-1	1
SMARCA4	0	1	1
STAT3	0	0	0
STAT5B	-1	0	1
SUMO	1	0	1
TP53	0	0	0
TSC22D3	-1	-1	0
TSG101	0	0	0
UBC	-1	0	1
Correct	28	58.3%	
Small Error	20	41.7%	
Large Error	0	0.0%	

Appendix Table 2: GEB052 model validation by microarray data (Comparison 2).

Comparison 2	E_{mod}	E_{exp}	ABS (E_{mod}-E_{exp})

14-3-3.	0	0	0
ABCA1	0	-1	1
AFP	-1	0	1
AP-1	0	-1	1
ARHGAP35	-1	0	1
BAG1	0	0	0
CD2	0	0	0
CD40LG	-1	0	1
CREB1	0	1	1
CREBBP/EP 300	0	0	0
CRH	0	0	0
DAP3	0	0	0
DAXX	1	0	1
FSCN1	0	1	1
GLUL	-1	-1	0
HDAC1	1	0	1
HDAC6	0	0	0
HSP90	0	0	0
IL10	0	-1	1
IL6	0	0	0
LIF	0	0	0
MED1	-1	0	1
NCOA1	0	0	0
NCOA2	0	0	0
NCOA3	0	1	1
NCOA6	0	0	0
NCOR1	0	0	0
NCOR2	0	0	0
NFKB	0	0	0
NR1I3	-1	0	1

NR2F2	-1	0	1
NRIP1	0	1	1
PKA	0	0	0
POU2F1	0	0	0
POU2F2	0	1	1
PRKDC	0	0	0
PTGES3	0	0	0
SCAP	-1	0	1
SGK1	0	0	0
SMAD3	0	-1	1
SMARCA4	0	0	0
STAT3	0	0	0
STAT5B	-1	0	1
SUMO	1	-1	2
TP53	0	0	0
TSC22D3	-1	0	1
TSG101	0	0	0
UBC	-1	0	1
Correct	26	54.2%	
Small Error	21	43.8%	
Large Error	1	2.1%	

Appendix Table 3: GEB052 model validation by microarray data (Comparison 3).

Comparison 3	E_{mod}	E_{exp}	**ABS (E_{mod}-E_{exp})**
14-3-3.	0	0	0
ABCA1	0	0	0
AFP	-1	0	1
AP-1	0	-1	1
ARHGAP35	-1	0	1
BAG1	0	0	0

CD2	0	0	0
CD40LG	-1	0	1
CREB1	0	0	0
CREBBP/EP 300	0	0	0
CRH	0	0	0
DAP3	0	0	0
DAXX	1	0	1
FSCN1	0	1	1
GLUL	-1	-1	0
HDAC1	1	0	1
HDAC6	0	0	0
HSP90	0	0	0
IL10	0	0	0
IL6	0	0	0
LIF	0	0	0
MED1	-1	0	1
NCOA1	0	0	0
NCOA2	0	0	0
NCOA3	0	1	1
NCOA6	0	0	0
NCOR1	0	0	0
NCOR2	0	0	0
NFKB	0	0	0
NR1I3	-1	0	1
NR2F2	-1	0	1
NRIP1	0	1	1
PKA	0	0	0
POU2F1	0	0	0
POU2F2	0	0	0
PRKDC	0	0	0

	E_{mod}	E_{exp}	ABS (E_{mod}-E_{exp})
PTGES3	0	0	0
SCAP	-1	0	1
SGK1	0	0	0
SMAD3	0	-1	1
SMARCA4	0	1	1
STAT3	0	0	0
STAT5B	-1	0	1
SUMO	1	-1	2
TP53	0	0	0
TSC22D3	-1	0	1
TSG101	0	0	0
UBC	-1	0	1
Correct	29	60.4%	
Small Error	18	37.5%	
Large Error	1	2.1%	

Appendix Table 4: GEB052 model validation by microarray data (Comparison 4).

Comparison 4	E_{mod}	E_{exp}	ABS (E_{mod}-E_{exp})
14-3-3.	0	0	0
ABCA1	0	1	1
AFP	-1	-1	0
AP-1	0	0	0
ARHGAP35	-1	0	1
BAG1	0	0	0
CD2	0	0	0
CD40LG	-1	0	1
CREB1	0	0	0
CREBBP/EP 300	0	0	0
CRH	0	0	0

DAP3	0	1	1
DAXX	1	0	1
FSCN1	0	-1	1
GLUL	-1	-1	0
HDAC1	1	0	1
HDAC6	0	0	0
HSP90	0	0	0
IL10	0	0	0
IL6	0	0	0
LIF	0	-1	1
MED1	-1	1	2
NCOA1	0	-1	1
NCOA2	0	0	0
NCOA3	0	0	0
NCOA6	0	0	0
NCOR1	0	0	0
NCOR2	0	0	0
NFKB	0	-1	1
NR1I3	-1	0	1
NR2F2	-1	0	1
NRIP1	0	0	0
PKA	0	0	0
POU2F1	0	0	0
POU2F2	0	-1	1
PRKDC	0	0	0
PTGES3	0	0	0
SCAP	-1	-1	0
SGK1	0	1	1
SMAD3	0	0	0
SMARCA4	0	0	0
STAT3	0	-1	1

STAT5B	-1	0	1
SUMO	1	0	1
TP53	0	-1	1
TSC22D3	-1	-1	0
TSG101	0	0	0
UBC	-1	0	1
Correct	28	58.3%	
Small Error	19	39.6%	
Large Error	1	2.1%	

Appendix Table 5: GEB052 model validation by microarray data (Comparison 5).

Comparison 5	E_{mod}	E_{exp}	**ABS (E_{mod}-E_{exp})**
14-3-3.	0	0	0
ABCA1	0	1	1
AFP	-1	1	2
AP-1	0	0	0
ARHGAP35	-1	0	1
BAG1	0	0	0
CD2	0	0	0
CD40LG	-1	0	1
CREB1	0	0	0
CREBBP/EP 300	0	0	0
CRH	0	0	0
DAP3	0	1	1
DAXX	1	-1	2
FSCN1	0	-1	1
GLUL	-1	-1	0
HDAC1	1	0	1
HDAC6	0	0	0

HSP90	0	0	0
IL10	0	0	0
IL6	0	0	0
LIF	0	0	0
MED1	-1	0	1
NCOA1	0	0	0
NCOA2	0	0	0
NCOA3	0	0	0
NCOA6	0	0	0
NCOR1	0	-1	1
NCOR2	0	-1	1
NFKB	0	-1	1
NR1I3	-1	0	1
NR2F2	-1	0	1
NRIP1	0	-1	1
PKA	0	0	0
POU2F1	0	0	0
POU2F2	0	0	0
PRKDC	0	-1	1
PTGES3	0	0	0
SCAP	-1	-1	0
SGK1	0	0	0
SMAD3	0	0	0
SMARCA4	0	-1	1
STAT3	0	0	0
STAT5B	-1	0	1
SUMO	1	0	1
TP53	0	-1	1
TSC22D3	-1	0	1
TSG101	0	0	0
UBC	-1	0	1

Correct	26	54.2%	
Small Error	20	41.7%	
Large Error	2	4.2%	

Appendix Table 6: GEB052 model validation by microarray data (Comparison 6).

Comparison 6	E_{mod}	E_{exp}	ABS (E_{mod}-E_{exp})
14-3-3.	0	0	0
ABCA1	0	1	1
AFP	-1	0	1
AP-1	0	0	0
ARHGAP35	-1	0	1
BAG1	0	0	0
CD2	0	0	0
CD40LG	-1	0	1
CREB1	0	0	0
CREBBP/EP 300	0	0	0
CRH	0	0	0
DAP3	0	1	1
DAXX	1	0	1
FSCN1	0	-1	1
GLUL	-1	0	1
HDAC1	1	0	1
HDAC6	0	0	0
HSP90	0	0	0
IL10	0	1	1
IL6	0	0	0
LIF	0	0	0
MED1	-1	0	1
NCOA1	0	0	0

NCOA2	0	0	0
NCOA3	0	0	0
NCOA6	0	0	0
NCOR1	0	-1	1
NCOR2	0	0	0
NFKB	0	0	0
NR1I3	-1	0	1
NR2F2	-1	0	1
NRIP1	0	-1	1
PKA	0	0	0
POU2F1	0	0	0
POU2F2	0	0	0
PRKDC	0	-1	1
PTGES3	0	0	0
SCAP	-1	-1	0
SGK1	0	0	0
SMAD3	0	0	0
SMARCA4	0	-1	1
STAT3	0	0	0
STAT5B	-1	-1	0
SUMO	1	0	1
TP53	0	-1	1
TSC22D3	-1	0	1
TSG101	0	1	1
UBC	-1	0	1
Correct	26	54.2%	
Small Error	22	45.8%	
Large Error	0	0.0%	

6.2.6   <u>GEB052 Quantitative Model Analysis</u>

The following tables show the individual results for each comparison shown in Table 4.6.1 (Page 172).

Appendix Table 7: Model validation by STSFA analysis (Comparison 1).

Note that TP53 is excluded from this analysis as the final node score for TP53 for the sensitive array was zero; as such, calculating fold-change was not possible.

Node	Resistant Score	Sensitive Score	Fold Change (FC)	Log10 FC	E_{mod}	E_{exp}	ABS (E_{mod}-E_{exp})
14-3-3	1111	1062	1.04613936	0.019589542	0	0	0
ABCA1	374	463	0.807775378	-0.092709389	0	0	0
AFP	330	347	0.951008646	-0.021815535	0	0	0
AP-1	20	529	0.037807183	-1.422425676	-1	-1	0
ARHGAP35	496	557	0.89048474	-0.050373519	0	0	0
BAG1	801	787	1.017789072	0.007657784	0	0	0
CD2	295	292	1.010273973	0.004439165	0	0	0
CD40LG	361	380	0.95	-0.022276395	0	0	0
CREB1	983	1225	0.80244898	-0.095582571	0	0	0
CREBBP/EP300	1355	1191	1.137699412	0.056027534	0	0	0
CRH	389	396	0.982323232	-0.007745585	0	0	0
DAP3	908	858	1.058275058	0.024598561	0	0	0
DAXX	2138	1647	1.29811779	0.113314102	0	0	0
FSCN1	1154	887	1.301014656	0.114282189	0	1	1
GLUL	290	1119	0.259159964	-0.586432089	-1	-1	0
GR	243	881	0.275822928	-0.559369635	-1	-1	0
HDAC1	692	710	0.974647887	-0.011152254	0	0	0
HDAC6	1117	1110	1.006306306	0.002730194	0	0	0

HSP90	3483	3173	1.097699338	0.040483402	0	0	0
IL10	618	1029	0.60058309	-0.2214269	0	-1	1
IL6	367	364	1.008241758	0.003564681	0	0	0
LIF	462	460	1.004347826	0.001884144	0	0	0
MED1	758	763	0.99344692	-0.002855332	0	0	0
NCOA1	1179	1194	0.987437186	-0.005490522	0	-1	1
NCOA2	743	643	1.155520995	0.062777841	0	0	0
NCOA3	1180	1127	1.047027507	0.019958091	0	0	0
NCOA6	1486	1413	1.051663128	0.021876648	0	0	0
NCOR1	644	645	0.998449612	-0.000673847	0	0	0
NCOR2	484	476	1.016806723	0.007238409	0	0	0
NFKB	338	442	0.764705882	-0.116505569	0	-1	1
NR1I3	290	299	0.969899666	-0.01327319	0	0	0
NR2F2	243	261	0.931034483	-0.031034234	0	0	0
NRIP1	838	847	0.989374262	-0.004639392	0	0	0
PKA	1005	1138	0.883128295	-0.0539762	0	0	0
POU2F1	510	528	0.965909091	-0.015063746	0	0	0
PRKDC	2523	2316	1.089378238	0.037178695	0	0	0
PTGES3	2456	2280	1.077192982	0.032293515	0	0	0
SCAP	833	830	1.003614458	0.001566909	0	0	0
SGK1	986	1126	0.875666075	-0.057661476	0	-1	1
SMAD3	608	808	0.752475248	-0.123507782	0	-1	1
SMARCA4	891	818	1.089242054	0.0371244	0	1	1
STAT3	2712	2740	0.989781022	-0.004460878	0	0	0
STAT5B	665	711	0.935302391	-0.029047955	0	0	0
SUMO	1920	1728	1.111111111	0.045757491	0	0	0
TP53	105	0	N/A	N/A	N/A	N/A	N/A

TSC22D3	895	1112	0.804856115	-0.094281752	0	-1	1
UBC	1143	1191	0.959697733	-0.017865531	0	0	0
			AVG	-0.065376166		**Correct**	82.6%
			STDEV	0.242351648		**Small Error**	17.4%
			Upper	0.176975481		**Large Error**	0.0%
			Lower	-0.307727814			

Appendix Table 8: Model validation by STSFA analysis (Comparison 2).

Node	**Resistant Score**	**Sensitive Score**	**Fold Change (FC)**	**Log10 FC**	E_{mod}	E_{exp}	**ABS (E_{mod}-E_{exp})**
14-3-3	1096	1089	1.006427916	0.002782674	0	0	0
ABCA1	366	470	0.778723404	-0.108616773	0	-1	1
AFP	373	364	1.024725275	0.010607448	0	0	0
AP-1	3	330	0.009090909	-2.041392685	-1	-1	0
ARHGAP35	533	535	0.996261682	-0.001626573	0	0	0
BAG1	760	775	0.980645161	-0.00848811	0	0	0
CD2	359	351	1.022792023	0.009787332	0	0	0
CD40LG	360	338	1.065088757	0.0273858	0	0	0
CREB1	971	959	1.01251303	0.00540062	0	1	1

225

			4	3			
CREBBP/EP300	1300	1072	1.212686567	0.083748567	0	0	0
CRH	433	425	1.018823529	0.008098966	0	0	0
DAP3	896	894	1.002237136	0.000970491	0	0	0
DAXX	2115	1791	1.180904523	0.072214786	0	0	0
FSCN1	1156	961	1.202913632	0.080234446	0	1	1
GLUL	316	1049	0.301239276	-0.521088406	-1	-1	0
GR	65	506	0.128458498	-0.89123716	-1	-1	0
HDAC1	694	728	0.953296703	-0.020771909	0	0	0
HDAC6	1259	1132	1.112190813	0.046179303	0	0	0
HSP90	3479	3202	1.086508432	0.036033101	0	0	0
IL10	655	779	0.840821566	-0.075296158	0	-1	1
IL6	374	335	1.11641791	0.047826795	0	0	0
LIF	488	439	1.111617312	0.045955302	0	0	0
MED1	754	747	1.009370817	0.004050744	0	0	0
NCOA1	1094	1058	1.034026465	0.014531654	0	0	0
NCOA2	652	591	1.10321489	0.042660115	0	0	0
NCOA3	1101	934	1.178800857	0.071440443	0	1	1

NCOA6	1488	1393	1.068198134	0.028651815	0	0	0
NCOR1	638	674	0.946587537	-0.023839218	0	0	0
NCOR2	496	490	1.012244898	0.005285596	0	0	0
NFKB	306	344	0.889534884	-0.050837016	0	0	0
NR1I3	267	303	0.881188119	-0.054931367	0	0	0
NR2F2	250	250	1	0	0	0	0
NRIP1	832	751	1.107856192	0.044483389	0	1	1
PKA	1036	1110	0.933333333	-0.029963223	0	0	0
POU2F1	491	533	0.92120075	-0.035645717	0	0	0
PRKDC	2521	2362	1.067315834	0.028292952	0	0	0
PTGES3	2425	2359	1.027977957	0.011983802	0	0	0
SCAP	806	831	0.969915764	-0.013265982	0	0	0
SGK1	980	894	1.096196868	0.039888557	0	0	0
SMAD3	608	685	0.887591241	-0.051786992	0	-1	1
SMARCA4	867	846	1.024822695	0.010648734	0	0	0
STAT3	2564	2386	1.074601844	0.031247582	0	0	0

				-			
STAT5B	662	690	0.95942029	0.01799110 1	0	0	0
SUMO	1915	1877	1.02024507 2	0.00870450 6	0	-1	1
TP53	141	138	1.02173913	0.00934002 6	0	0	0
TSC22D3	886	959	0.92387904 1	- 0.03438488 5	0	0	0
UBC	1146	1131	1.01326259 9	0.00572201 3	0	0	0
			AVG	- 0.06695756 8		**Correc t**	83.0%
			STDEV	0.33278922 3		**Small Error**	17.0%
			Upper	0.26583165 5		**Large Error**	0.0%
			Lower	- 0.39974679 1			

Appendix Table 9: Model validation by STSFA analysis (Comparison 3).

Node	**Resistant Score**	**Sensitive Score**	**Fold Change (FC)**	**Log10 FC**	E_{mod}	E_{exp}	**ABS (E_{mod}- E_{exp})**
14-3-3	1091	1104	0.98822463 8	- 0.00514432 3	0	0	0
ABCA1	382	379	1.00791556 7	0.00342415 3	0	0	0
AFP	358	349	1.02578796 6	0.0110576	0	0	0
AP-1	181	368	0.49184782 6	- 0.30816924 4	-1	-1	0

ARHGAP35	546	553	0.987341772	-0.005532489	0	0	0
BAG1	806	776	1.038659794	0.016473321	0	0	0
CD2	318	355	0.895774648	-0.047801233	0	0	0
CD40LG	372	401	0.927680798	-0.032601433	0	0	0
CREB1	899	868	1.035714286	0.015239967	0	0	0
CREBBP/EP300	1352	1169	1.156544055	0.06316218	0	0	0
CRH	437	417	1.047961631	0.020345382	0	0	0
DAP3	894	905	0.987845304	-0.00531106	0	0	0
DAXX	2169	2052	1.057017544	0.024082196	0	0	0
FSCN1	1250	1062	1.177024482	0.070785496	0	1	1
GLUL	302	942	0.32059448	-0.49404396	-1	-1	0
GR	65	171	0.380116959	-0.420082754	-1	-1	0
HDAC1	684	739	0.925575101	-0.033588337	0	0	0
HDAC6	1215	1249	0.972778223	-0.01198616	0	0	0
HSP90	3614	3520	1.026704545	0.011445485	0	0	0
IL10	750	706	1.062322946	0.026256562	0	0	0
IL6	412	429	0.96037296	-0.01756007	0	0	0

				6			
LIF	481	483	0.995859213	-0.001802054	0	0	0
MED1	749	726	1.031680441	0.013545197	0	0	0
NCOA1	1204	1115	1.079820628	0.03335162	0	0	0
NCOA2	657	595	1.104201681	0.043048404	0	0	0
NCOA3	1129	991	1.13925328	0.056620287	0	1	1
NCOA6	1534	1433	1.070481507	0.029579169	0	0	0
NCOR1	663	660	1.004545455	0.001969593	0	0	0
NCOR2	513	486	1.055555556	0.023481096	0	0	0
NFKB	321	343	0.935860058	-0.028789088	0	0	0
NR1I3	272	289	0.941176471	-0.026328939	0	0	0
NR2F2	226	256	0.8828125	-0.054131526	0	0	0
NRIP1	862	765	1.126797386	0.051845831	0	1	1
PKA	1083	1091	0.992667278	-0.003192944	0	0	0
POU2F1	502	504	0.996031746	-0.001726819	0	0	0
PRKDC	2654	2504	1.059904153	0.025266594	0	0	0
PTGES3	2498	2474	1.00970088	0.00419273	0	0	0

			9	9			
SCAP	842	825	1.020606061	0.008858143	0	0	0
SGK1	766	700	1.094285714	0.03913073	0	0	0
SMAD3	639	694	0.92074928	-0.035858612	0	-1	1
SMARCA4	938	855	1.097076023	0.040236724	0	1	1
STAT3	2762	2617	1.055406955	0.023419952	0	0	0
STAT5B	644	679	0.948453608	-0.022983907	0	0	0
SUMO	1949	1996	0.976452906	-0.010348698	0	-1	1
TP53	130	143	0.909090909	-0.041392685	0	0	0
TSC22D3	506	535	0.945794393	-0.024203265	0	0	0
UBC	1139	1125	1.012444444	0.005371202	0	0	0
			AVG	-0.020646667		**Correct**	87.2%
			STDEV	0.107902042		**Small Error**	12.8%
			Upper	0.087255375		**Large Error**	0.0%
			Lower	-0.128548708			

Appendix Table 10: Model validation by STSFA analysis (Comparison 4).

Node	Resistant Score	Sensitive Score	Fold Change (FC)	Log10 FC	E_{mod}	E_{exp}	ABS (E_{mod}- E_{exp})
14-3-3	1054	1099	0.959053685	-0.018157082	0	0	0
ABCA1	692	472	1.466101695	0.166164096	1	1	0
AFP	346	395	0.875949367	-0.057520997	0	-1	1
AP-1	151	111	1.36036036	0.133653969	1	0	1
ARHGAP35	520	528	0.984848485	-0.006630579	0	0	0
BAG1	828	805	1.028571429	0.012234456	0	0	0
CD2	343	304	1.128289474	0.052420536	0	0	0
CD40LG	375	401	0.935162095	-0.029113105	0	0	0
CREB1	1330	1215	1.094650206	0.039275363	0	0	0
CREBBP/EP300	1456	1386	1.050505051	0.021398145	0	0	0
CRH	395	422	0.936018957	-0.028715355	0	0	0
DAP3	914	853	1.071512309	0.029997165	0	1	1
DAXX	1898	1920	0.988541667	-0.005005021	0	0	0
FSCN1	664	1017	0.652900688	-0.18515287	-1	-1	0

			4			
GLUL	952	1014	0.93885601 6	- 0.02740100 7	0	-1	1
GR	379	153	2.47712418 3	0.39394777 9	1	-1	2
HDAC1	643	695	0.92517985 6	- 0.03377383 2	0	0	0
HDAC6	1178	1167	1.00942587 8	0.00407443 4	0	0	0
HSP90	3462	3258	1.06261510 1	0.02637598 4	0	0	0
IL10	805	724	1.11187845 3	0.04605731 4	0	0	0
IL6	273	340	0.80294117 6	-0.09531627	-1	0	1
LIF	429	516	0.83139534 9	- 0.08019240 9	0	-1	1
MED1	815	715	1.13986014	0.05685156 7	0	1	1
NCOA1	1225	1307	0.93726090 3	- 0.02813949 9	0	-1	1
NCOA2	860	810	1.06172839 5	0.02601343 2	0	0	0
NCOA3	1185	1168	1.01455479 5	0.00627550 8	0	0	0
NCOA6	1308	1268	1.03154574 1	0.01348849	0	0	0
NCOR1	613	643	0.95334370 1	- 0.02075049 8	0	0	0
NCOR2	431	479	0.89979123 2	- 0.04585824 3	0	0	0
NFKB	336	408	0.82352941	-	-1	-1	0

			2	0.08432088 6			
NR1I3	269	294	0.91496598 6	-0.03859505	0	0	0
NR2F2	278	250	1.112	0.04610478 7	0	0	0
NRIP1	1097	1121	0.97859054 4	- 0.00939898 5	0	0	0
PKA	1201	1158	1.03713298 8	0.01583444 8	0	0	0
POU2F1	502	523	0.95984703 6	- 0.01779797 2	0	0	0
PRKDC	2473	2356	1.04966044 1	0.02104883	0	0	0
PTGES3	2436	2304	1.05729166 7	0.02419480 9	0	0	0
SCAP	719	775	0.92774193 5	- 0.03257281 2	0	-1	1
SGK1	1110	1097	1.01185050 1	0.00511635 1	0	1	1
SMAD3	1040	969	1.07327141 4	0.03070956 2	0	0	0
SMARCA4	878	929	0.94510226	- 0.02452119 8	0	0	0
STAT3	2437	2626	0.92802741 8	- 0.03243919 3	0	-1	1
STAT5B	649	647	1.00309119	0.00134041 6	0	0	0
SUMO	1760	1705	1.03225806 5	0.01378828 4	0	0	0
TP53	74	100	0.74	-0.13076828	-1	-1	0
TSC22D3	718	839	0.85578069 1	- 0.06763751	0	-1	1

			7			
UBC	1110	1097	1.01185050 1	0.00511635 1	0	0	0

			AVG	0.00195113 7		**Correct**	72.3%
			STDEV	0.08230800 7		**Small Error**	25.5%
			Upper	0.08425914 4		**Large Error**	2.1%
			Lower	- 0.08035687 1		

Appendix Table 11: Model validation by STSFA analysis (Comparison 5).

Node	Resistant Score	Sensitive Score	Fold Change (FC)	Log10 FC	E_{mod}	E_{exp}	ABS (E_{mod}-E_{exp})
14-3-3	1055	1102	0.95735027 2	- 0.01892913 5	0	0	0
ABCA1	649	437	1.48512585 8	0.17176326	1	1	0
AFP	410	325	1.26153846 2	0.10090049 6	1	1	0
AP-1	123	110	1.11818181 8	0.04851242 6	0	0	0
ARHGAP35	500	504	0.99206349 2	- 0.00346053 2	0	0	0
BAG1	804	801	1.00374531 8	0.00162353 3	0	0	0
CD2	294	280	1.05	0.02118929 9	0	0	0
CD40LG	371	358	1.03631284 9	0.01549088 3	0	0	0
CREB1	1353	1203	1.12468827 9	0.05103216 9	0	0	0

CREBBP/EP300	1465	1429	1.025192442	0.010805396	0	0	0
CRH	397	395	1.005063291	0.002193411	0	0	0
DAP3	924	887	1.041713641	0.017748351	0	1	1
DAXX	1917	1990	0.963316583	-0.016230964	0	-1	1
FSCN1	701	938	0.747334755	-0.12648482	-1	-1	0
GLUL	972	1016	0.956692913	-0.019227443	0	-1	1
GR	429	171	2.50877193	0.399461182	1	-1	2
HDAC1	646	680	0.95	-0.022276395	0	0	0
HDAC6	1102	1142	0.96497373	-0.015484509	0	0	0
HSP90	3472	3323	1.044839001	0.019049375	0	0	0
IL10	734	670	1.095522388	0.039621257	0	0	0
IL6	266	342	0.777777778	-0.109144469	-1	0	1
LIF	416	471	0.883227176	-0.053927577	0	0	0
MED1	815	769	1.059817945	0.025231269	0	0	0
NCOA1	1217	1191	1.021830395	0.009378817	0	0	0
NCOA2	863	854	1.010538642	0.004552925	0	0	0

NCOA3	1182	1161	1.01808785 5	0.00778525 7	0	0	0
NCOA6	1277	1287	0.99222999 2	- 0.00338765	0	0	0
NCOR1	578	641	0.90171606 9	- 0.04493019 1	0	-1	1
NCOR2	437	490	0.89183673 5	- 0.04971464 3	0	-1	1
NFKB	313	377	0.83023872 7	- 0.08079701 3	0	-1	1
NR1I3	293	282	1.03900709 2	0.01661851 2	0	0	0
NR2F2	231	244	0.94672131 1	- 0.02377784 6	0	0	0
NRIP1	1062	1119	0.94906166 2	- 0.02270557	0	-1	1
PKA	1216	1076	1.13011152 4	0.05312130 4	0	0	0
POU2F1	499	492	1.01422764 2	0.00613544 3	0	0	0
PRKDC	2464	2495	0.98757515	- 0.00542984 6	0	-1	1
PTGES3	2465	2372	1.03920742	0.01670223 9	0	0	0
SCAP	724	757	0.95640686 9	- 0.01935731 3	0	-1	1
SGK1	1194	1176	1.01530612 2	0.00659700 5	0	0	0
SMAD3	941	972	0.96810699 6	- 0.01407664 1	0	0	0
SMARCA4	854	916	0.93231441	-	0	-1	1

Node	Resistant Score	Sensitive Score	Fold Change (FC)	Log10 FC	E_{mod}	E_{exp}	ABS (E_{mod}-E_{exp})
				0.030437603			
STAT3	2439	2397	1.017521902	0.007543766	0	0	0
STAT5B	630	650	0.969230769	-0.013572807	0	0	0
SUMO	1790	1792	0.998883929	-0.000484974	0	0	0
TP53	41	117	0.35042735	-0.455402005	-1	-1	0
TSC22D3	779	784	0.993622449	-0.002778605	0	0	0
UBC	1108	1101	1.006357856	0.002752441	0	0	0
			AVG	-0.00204699		Correct	74.5%
			STDEV	0.100561938		Small Error	23.4%
			Upper	0.098514947		Large Error	2.1%
			Lower	-0.102608928			

Appendix Table 12: Model validation by STSFA analysis (Comparison 6).

Node	Resistant Score	Sensitive Score	Fold Change (FC)	Log10 FC	E_{mod}	E_{exp}	ABS (E_{mod}-E_{exp})
14-3-3	1063	1082	0.982439926	-0.007693996	0	0	0
ABCA1	722	457	1.579868709	0.198620997	1	1	0

AFP	337	344	0.979651163	-0.008928542	0	0	0
AP-1	199	218	0.912844037	-0.039603417	0	0	0
ARHGAP35	526	515	1.021359223	0.009178515	0	0	0
BAG1	801	812	0.986453202	-0.005923513	0	0	0
CD2	312	311	1.003215434	0.001394205	0	0	0
CD40LG	389	370	1.051351351	0.021747877	0	0	0
CREB1	1298	1234	1.051863857	0.021959533	0	0	0
CREBBP/EP300	1509	1481	1.018906144	0.008134181	0	0	0
CRH	389	409	0.951100244	-0.021773707	0	0	0
DAP3	926	887	1.043968433	0.018687367	0	1	1
DAXX	1956	2009	0.973618716	-0.011611086	0	0	0
FSCN1	672	1010	0.665346535	-0.176952101	-1	-1	0
GLUL	956	951	1.005257624	0.002277375	0	0	0
GR	560	196	2.857142857	0.455931956	1	-1	2
HDAC1	629	668	0.941616766	-0.026125817	0	0	0
HDAC6	1138	1121	1.01516503	0.00653664	0	0	0

			1	9			
HSP90	3570	3442	1.037187682	0.01585735	0	0	0
IL10	976	752	1.29787234	0.113231977	1	1	0
IL6	234	351	0.666666667	-0.176091259	-1	0	1
LIF	401	453	0.885209713	-0.052953829	0	0	0
MED1	848	817	1.037943696	0.016173796	0	0	0
NCOA1	1242	1213	1.023907667	0.010260795	0	0	0
NCOA2	876	896	0.977678571	-0.009803903	0	0	0
NCOA3	1223	1207	1.013256007	0.005719187	0	0	0
NCOA6	1360	1361	0.999265246	-0.000319217	0	0	0
NCOR1	590	652	0.904907975	-0.043395584	0	-1	1
NCOR2	467	454	1.028634361	0.012261028	0	0	0
NFKB	329	384	0.856770833	-0.067135326	0	0	0
NR1I3	266	283	0.939929329	-0.026904799	0	0	0
NR2F2	245	235	1.042553191	0.018098222	0	0	0
NRIP1	1087	1142	0.951838879	-0.02143656	0	-1	1

PKA	1256	1112	1.129496403	0.052884852	0	0	0
POU2F1	512	511	1.001956947	0.000849061	0	0	0
PRKDC	2559	2591	0.987649556	-0.005397127	0	-1	1
PTGES3	2512	2446	1.026982829	0.011563182	0	0	0
SCAP	735	786	0.935114504	-0.029135207	0	-1	1
SGK1	1061	1094	0.969835466	-0.013301938	0	0	0
SMAD3	960	934	1.027837259	0.011924357	0	0	0
SMARCA4	865	928	0.932112069	-0.030531869	0	-1	1
STAT3	2517	2492	1.010032103	0.004335178	0	0	0
STAT5B	644	678	0.949852507	-0.022343827	0	-1	1
SUMO	1819	1817	1.001100715	0.000477772	0	0	0
TP53	61	91	0.67032967	-0.173711557	-1	-1	0
TSC22D3	489	511	0.956947162	-0.019112041	0	0	0
UBC	1126	1107	1.017163505	0.00739077	0	0	0
			AVG	0.000751276		**Correct**	80.9%

		STDEV	0.09025993 2		Small Error	17.0%
		Upper	0.09101120 8		Large Error	2.1%
		Lower	- 0.08950865 7			

References

AboutKidsHealth. 2010. Acute Lymphoblastic Leukemia: Chemotherapy Phases [Online]. Available: http://www.aboutkidshealth.ca/en/resourcecentres/leukemia/treatingleukemia/treatingacutelymphoblasticleukemia/pages/chemotherapyphasesforall.aspx [Accessed 15 January 2017].

ACS. 2010. THE GLOBAL ECONOMIC COST OF CANCER [Online]. Available: http://www.cancer.org/acs/groups/content/@internationalaffairs/documents/document/acspc-026203.pdf [Accessed 05 January 2017].

Adcock, I. M. 2001. Glucocorticoid-regulated transcription factors. *Pulm Pharmacol Ther,* 14**,** 211-9.

Ai, N., Krasowski, M. D., Welsh, W. J. & Ekins, S. 2009. Understanding Nuclear Receptors Using Computational Methods. *Drug Discov Today,* 14**,** 486-94.

Akman, O. E., Watterson, S., Parton, A., Binns, N., Millar, A. J. & Ghazal, P. 2012. Digital clocks: simple Boolean models can quantitatively describe circadian systems. *J R Soc Interface,* 9**,** 2365-82.

Albert, R. & Othmer, H. G. 2003. The topology of the regulatory interactions predicts the expression pattern of the segment polarity genes in Drosophila melanogaster. *J Theor Biol,* 223**,** 1-18.

Amat, R., Solanes, G., Giralt, M. & Villarroya, F. 2007. SIRT1 is involved in glucocorticoid-mediated control of uncoupling protein-3 gene transcription. *J Biol Chem,* 282**,** 34066-76.

ASH. 2008. Leukemia [Online]. Available: http://www.hematology.org/Patients/Cancers/Leukemia.aspx [Accessed 07 January 2017].

ATCC. 2016. CCRF-CEM [CCRF CEM] (ATCC® CCL-119™) [Online]. Available: https://www.lgcstandards-atcc.org/products/all/CCL-119.aspx?geo_country=gb#culturemethod [Accessed 27 January 2017].

Bailly-Maitre, B., de Sousa, G., Boulukos, K., Gugenheim, J. & Rahmani, R. 2001. Dexamethasone inhibits spontaneous apoptosis in primary cultures of human and rat hepatocytes via Bcl-2 and Bcl-xL induction. *Cell Death Differ,* 8**,** 279-88.

Baker, S. M., Poskar, C. H., Schreiber, F. & Junker, B. H. 2013. An improved constraint filtering technique for inferring hidden states and parameters of a biological model. *Bioinformatics,* 29**,** 1052-9.

Bakker, E., Qattan, M., Mutti, L., Demonacos, C. & Krstic-Demonacos, M. 2016. The role of microenvironment and immunity in drug response in leukemia. *Biochim Biophys Acta,* 1863**,** 414-26.

Bakker, E., Tian, K., Andrews, J., Demonacos, C., Schwartz, J.-M. & Krstic-Demonacos, M. 2014. Glucocorticoid receptor interactome. *Society for Endocrinology BES 2014.* Liverpool, UK: Endocrine Abstracts.

Barnes, P. J. 1998. Anti-inflammatory actions of glucocorticoids: molecular mechanisms. *Clin Sci (Lond),* 94**,** 557-72.

Bashyam, M. D. 2002. Understanding cancer metastasis. *Cancer,* 94**,** 1821-1829.

Beesley, A. H., Firth, M. J., Ford, J., Weller, R. E., Freitas, J. R., Perera, K. U. & Kees, U. R. 2009. Glucocorticoid resistance in T-lineage acute lymphoblastic leukaemia is associated with a proliferative metabolism. *Br J Cancer,* 100**,** 1926-36.

Belz, K. S. H. W. S. W. A. B. H. K. T. F. I. F. S. 2014. Smac mimetic and glucocorticoids synergize to induce apoptosis in childhood ALL by promoting ripoptosome assembly. *Blood,* 124**,** 240-250.

Berghe, T. V., Vanlangenakker, N., Parthoens, E., Deckers, W., Devos, M., Festjens, N., Guerin, C. J., Brunk, U. T., Declercq, W. & Vandenabeele, P. 2010. Necroptosis,

necrosis and secondary necrosis converge on similar cellular disintegration features. *Cell Death Differ,* 17**,** 922-30.

Bettenbrock, K., Fischer, S., Kremling, A., Jahreis, K., Sauter, T. & Gilles, E. D. 2006. A quantitative approach to catabolite repression in Escherichia coli. *J Biol Chem,* 281**,** 2578-84.

Bioline. 2016. BioScript™ Reverse Transcriptase [Online]. Available: http://www.bioline.com/uk/downloads/dl/file/id/2707/bioscript_product_manual.pdf [Accessed 07 February 2017].

Blind, R. & Garabedian, M. J. 2008. Differential recruitment of glucocorticoid receptor phospho-isoforms to glucocorticoid-induced genes. *The Journal of steroid biochemistry and molecular biology,* 109**,** 150-157.

Bonapace, L., Bornhauser, B. C., Schmitz, M., Cario, G., Ziegler, U., Niggli, F. K., Schafer, B. W., Schrappe, M., Stanulla, M. & Bourquin, J. P. 2010. Induction of autophagy-dependent necroptosis is required for childhood acute lymphoblastic leukemia cells to overcome glucocorticoid resistance. *J Clin Invest,* 120**,** 1310-23.

Bray, K., Mathew, R., Lau, A., Kamphorst, J. J., Fan, J., Chen, J., Chen, H. Y., Ghavami, A., Stein, M., DiPaola, R. S., Zhang, D., Rabinowitz, J. D. & White, E. 2012. Autophagy suppresses RIP kinase-dependent necrosis enabling survival to mTOR inhibition. *PLoS One,* 7**,** e41831.

Bruggeman, F. J. & Westerhoff, H. V. 2007. The nature of systems biology. *Trends Microbiol,* 15**,** 45-50.

Cardoso, B. A., Girio, A., Henriques, C., Martins, L. R., Santos, C., Silva, A. & Barata, J. T. 2008. Aberrant signaling in T-cell acute lymphoblastic leukemia: biological and therapeutic implications. *Braz J Med Biol Res,* 41**,** 344-50.

Carrigan, A., Walther, R. F., Salem, H. A., Wu, D., Atlas, E., Lefebvre, Y. A. & Hache, R. J. 2007. An active nuclear retention signal in the glucocorticoid receptor functions as a strong inducer of transcriptional activation. *J Biol Chem,* 282**,** 10963-71.

Chang, J. S., Zhou, M., Buffler, P. A., Chokkalingam, A. P., Metayer, C. & Wiemels, J. L. 2011. Profound deficit of IL10 at birth in children who develop childhood acute lymphoblastic leukemia. *Cancer Epidemiol Biomarkers Prev,* 20**,** 1736-40.

Chaouiya, C. 2007. Petri net modelling of biological networks. *Brief Bioinform,* 8**,** 210-9.

Charmandari, E., Chrousos, G. P., Ichijo, T., Bhattacharyya, N., Vottero, A., Souvatzoglou, E. & Kino, T. 2005. The human glucocorticoid receptor (hGR) beta isoform suppresses the transcriptional activity of hGRalpha by interfering with formation of active coactivator complexes. *Mol Endocrinol,* 19**,** 52-64.

ChemoMetec. 2017. Application note No. 3021. Rev. 1.3 NucleoCounter® NC-3000™ Caspase assay using the Fluorochrome-labeled inhibitor of caspases assay (FLICA) FAM-DEVD-FMK (caspase 3/7), FAM-LETD-FMK (caspase 8) or FAM- LEHD-FMK (caspase 9) [Online]. Available: https://marketing.chemometec.com/acton/attachment/21287/f-00f0/1/-/-/-/-/994-3021-FLICA-Caspase-Assay.pdf [Accessed 08 February 2017].

Chen, D., Krstic-Demonacos, M. & Schwartz, J.-M. 2012. Modelling the mechanism of GR/c-Jun/Erg crosstalk in apoptosis of acute lymphoblastic leukaemia. *Frontiers in Physiology,* 3.

Chen, D. W.-C., Lynch, J. T., Demonacos, C., Krstic-Demonacos, M. & Schwartz, J.-M. 2010. Quantitative analysis and modeling of glucocorticoid-controlled gene expression. *Pharmacogenomics,* 11**,** 1545-1560.

Chen, L., Qi-Wei, G., Nakata, M., Matsuno, H. & Miyano, S. 2007. Modelling and simulation of signal transductions in an apoptosis pathway by using timed Petri nets. *Journal of Biosciences,* 32**,** 113-127.

Chen, R. F. 1967. Removal of Fatty Acids from Serum Albumin by Charcoal Treatment. *Journal of Biological Chemistry,* 242**,** 173-181.

Chipuk, J. E. & Green, D. R. 2006. Dissecting p53-dependent apoptosis. *Cell Death Differ,* 13**,** 994-1002.

Conaway, R. C. & Conaway, J. W. 2004. *Proteins in Eukaryotic Transcription*, Elsevier Science.

Cooper, G. M. 2000. *The Cell: A Molecular Approach*, ASM Press.

Cooper, S. L. & Brown, P. A. 2015. Treatment of Pediatric Acute Lymphoblastic Leukemia. *Pediatric clinics of North America,* 62**,** 61-73.

Copetti, T., Bertoli, C., Dalla, E., Demarchi, F. & Schneider, C. 2009. p65/RelA modulates BECN1 transcription and autophagy. *Mol Cell Biol,* 29**,** 2594-608.

CRUK. 2014a. Cancer survival for common cancers [Online]. Available: http://www.cancerresearchuk.org/health-professional/cancer-statistics/survival/common-cancers-compared#heading-Zero [Accessed 07 January 2017].

CRUK. 2014b. Types of cancer [Online]. Available: http://www.cancerresearchuk.org/about-cancer/what-is-cancer/how-cancer-starts/types-of-cancer#main [Accessed 07 January 2017].

CRUK. 2015a. About the blood and chronic lymphocytic leukaemia (CLL) [Online]. Available: http://www.cancerresearchuk.org/about-cancer/type/cll/about/about-the-blood-and-chronic-lymphocytic-leukaemia [Accessed 07 January 2017].

CRUK. 2015b. Cancer Statistics for the UK [Online]. Cancer Research UK. Available: http://www.cancerresearchuk.org/health-professional/cancer-statistics [Accessed 05 January 2017].

CRUK. 2015c. Survival [Online]. Available: http://www.cancerresearchuk.org/about-cancer/acute-lymphoblastic-leukaemia-all/survival [Accessed 27 August 2017].

CRUK. 2015d. What is cancer? [Online]. Available: http://www.cancerresearchuk.org/about-cancer/what-is-cancer [Accessed 07 January 2017].

CRUK. 2016. Cancer incidence for common cancers [Online]. Available: http://www.cancerresearchuk.org/health-professional/cancer-statistics/incidence/common-cancers-compared#heading-Zero [Accessed 07 January 2017].

Cytoscape. 2016. Cytoscape Network Data Integration, Analysis, and Visualization in a Box [Online]. Available: http://www.cytoscape.org/ [Accessed 12 February 2017].

Davies, L., Karthikeyan, N., Lynch, J. T., Sial, E. A., Gkourtsa, A., Demonacos, C. & Krstic-Demonacos, M. 2008. Cross talk of signaling pathways in the regulation of the glucocorticoid receptor function. *Mol Endocrinol,* 22**,** 1331-44.

de Almagro, M. C., Goncharov, T., Izrael-Tomasevic, A., Duttler, S., Kist, M., Varfolomeev, E., Wu, X., Lee, W. P., Murray, J., Webster, J. D., Yu, K., Kirkpatrick, D. S., Newton, K. & Vucic, D. 2017. Coordinated ubiquitination and phosphorylation of RIP1 regulates necroptotic cell death. *Cell Death Differ,* 24**,** 26-37.

de Jong, H. 2002. Modeling and simulation of genetic regulatory systems: a literature review. *J Comput Biol,* 9**,** 67-103.

Debierre-Grockiego, F. 2004. Anti-apoptotic role of STAT5 in haematopoietic cells and in the pathogenesis of malignancies. *Apoptosis,* 9**,** 717-28.

Del Monaco, M., Covello, S. P., Kennedy, S. H., Gilinger, G., Litwack, G. & Uitto, J. 1997. Identification of novel glucocorticoid-response elements in human elastin promoter and demonstration of nucleotide sequence specificity of the receptor binding. *J Invest Dermatol,* 108**,** 938-42.

Deshmukh, C. T. 2007. Minimizing side effects of systemic corticosteroids in children. *Indian J Dermatol Venereol Leprol,* 73**,** 218-21.

Donley, N. & Thayer, M. J. 2013. DNA Replication Timing, Genome Stability and Cancer. *Semin Cancer Biol,* 23**,** 80-9.

Druker, J., Liberman, A. C., Antunica-Noguerol, M., Gerez, J., Paez-Pereda, M., Rein, T., Iñiguez-Lluhí, J. A., Holsboer, F. & Arzt, E. 2013. RSUME Enhances

Glucocorticoid Receptor SUMOylation and Transcriptional Activity. *Molecular and Cellular Biology,* 33**,** 2116-2127.

Duma, D., Jewell, C. M. & Cidlowski, J. A. 2006. Multiple glucocorticoid receptor isoforms and mechanisms of post-translational modification. *J Steroid Biochem Mol Biol,* 102**,** 11-21.

Echeverría, P. C., Mazaira, G., Erlejman, A., Gomez-Sanchez, C., Pilipuk, G. P. & Galigniana, M. D. 2009. Nuclear Import of the Glucocorticoid Receptor-hsp90 Complex through the Nuclear Pore Complex Is Mediated by Its Interaction with Nup62 and Importin β. *Molecular and Cellular Biology,* 29**,** 4788-4797.

Edinger, A. L. & Thompson, C. B. 2004. Death by design: apoptosis, necrosis and autophagy. *Curr Opin Cell Biol,* 16**,** 663-9.

Edwards, L. M. & Thiele, I. 2013. Applying systems biology methods to the study of human physiology in extreme environments. *Extrem Physiol Med,* 2**,** 8.

Elmore, S. 2007. Apoptosis: A Review of Programmed Cell Death. *Toxicologic pathology,* 35**,** 495-516.

Endler, A., Chen, L. & Shibasaki, F. 2014. Coactivator recruitment of AhR/ARNT1. *Int J Mol Sci,* 15**,** 11100-10.

Esterhay, R. J., Jr., Wiernik, P. H., Grove, W. R., Markus, S. D. & Wesley, M. N. 1982. Moderate dose methotrexate, vincristine, asparaginase, and dexamethasone for treatment of adult acute lymphocytic leukemia. *Blood,* 59**,** 334-45.

Faus, H. & Haendler, B. 2006. Post-translational modifications of steroid receptors. *Biomed Pharmacother,* 60**,** 520-8.

Feist, A. M., Henry, C. S., Reed, J. L., Krummenacker, M., Joyce, A. R., Karp, P. D., Broadbelt, L. J., Hatzimanikatis, V. & Palsson, B. O. 2007. A genome-scale metabolic reconstruction for Escherichia coli K-12 MG1655 that accounts for 1260 ORFs and thermodynamic information. *Mol Syst Biol,* 3**,** 121.

Foley, G. E., Lazarus, H., Farber, S., Uzman, B. G., Boone, B. A. & McCarthy, R. E. 1965. Continuous culture of human lymphoblasts from peripheral blood of a child with acute leukemia. *Cancer,* 18**,** 522-529.

Freedman, D. M., Stewart, P., Kleinerman, R. A., Wacholder, S., Hatch, E. E., Tarone, R. E., Robison, L. L. & Linet, M. S. 2001. Household solvent exposures and childhood acute lymphoblastic leukemia. *Am J Public Health,* 91**,** 564-7.

Fryer, C. J. & Archer, T. K. 1998. Chromatin remodelling by the glucocorticoid receptor requires the BRG1 complex. *Nature,* 393**,** 88-91.

Fulda, S. 2008. Targeting inhibitor of apoptosis proteins (IAPs) for cancer therapy. *Anticancer Agents Med Chem,* 8**,** 533-9.

Fulda, S. & Debatin, K. M. 2006. Extrinsic versus intrinsic apoptosis pathways in anticancer chemotherapy. *Oncogene,* 25**,** 4798-811.

Galigniana, M. D., Scruggs, J. L., Herrington, J., Welsh, M. J., Carter-Su, C., Housley, P. R. & Pratt, W. B. 1998. Heat shock protein 90-dependent (geldanamycin-inhibited) movement of the glucocorticoid receptor through the cytoplasm to the nucleus requires intact cytoskeleton. *Mol Endocrinol,* 12**,** 1903-13.

Galliher-Beckley, A. J. & Cidlowski, J. A. 2009. Emerging roles of glucocorticoid receptor phosphorylation in modulating glucocorticoid hormone action in health and disease. *IUBMB Life,* 61**,** 979-86.

Galliher-Beckley, A. J., Williams, J. G. & Cidlowski, J. A. 2011. Ligand-Independent Phosphorylation of the Glucocorticoid Receptor Integrates Cellular Stress Pathways with Nuclear Receptor Signaling. *Molecular and Cellular Biology,* 31**,** 4663-4675.

Gehring, U., Segnitz, B., Foellmer, B. & Francke, U. 1985. Assignment of the human gene for the glucocorticoid receptor to chromosome 5. *Proc Natl Acad Sci U S A,* 82**,** 3751-5.

Gelmetti, V., Zhang, J., Fanelli, M., Minucci, S., Pelicci, P. G. & Lazar, M. A. 1998. Aberrant recruitment of the nuclear receptor corepressor-histone deacetylase complex by the acute myeloid leukemia fusion partner ETO. *Mol Cell Biol,* 18**,** 7185-91.

GO 2008. The Gene Ontology project in 2008. *Nucleic Acids Research,* 36**,** D440-D444.

Gordon, P. M., Dias, S. & Williams, D. A. 2014. Cytokines secreted by bone marrow stromal cells protect c-KIT mutant AML cells from c-KIT inhibitor-induced apoptosis. *Leukemia,* 28**,** 2257-60.

Govindan, M. V. 2010. Recruitment of cAMP-response element-binding protein and histone deacetylase has opposite effects on glucocorticoid receptor gene transcription. *J Biol Chem,* 285**,** 4489-510.

Grander, D., Kharaziha, P., Laane, E., Pokrovskaja, K. & Panaretakis, T. 2009. Autophagy as the main means of cytotoxicity by glucocorticoids in hematological malignancies. *Autophagy,* 5**,** 1198-200.

Grzechnik, P., Tan-Wong, S. M. & Proudfoot, N. J. 2014. Terminate and make a loop: regulation of transcriptional directionality. *Trends in Biochemical Sciences,* 39**,** 319-327.

Gump, J. M. & Thorburn, A. 2011. Autophagy and apoptosis: what is the connection? *Trends Cell Biol,* 21**,** 387-92.

Hahn, R. T., Hoppstadter, J., Hirschfelder, K., Hachenthal, N., Diesel, B., Kessler, S. M., Huwer, H. & Kiemer, A. K. 2014. Downregulation of the glucocorticoid-induced leucine zipper (GILZ) promotes vascular inflammation. *Atherosclerosis,* 234**,** 391-400.

Hanahan, D. & Weinberg, R. A. 2000. The hallmarks of cancer. *Cell,* 100**,** 57-70.

Hanahan, D. & Weinberg, R. A. 2011. Hallmarks of cancer: the next generation. *Cell,* 144**,** 646-74.

Harmon, J. M. & Thompson, E. B. 1981. Isolation and characterization of dexamethasone-resistant mutants from human lymphoid cell line CEM-C7. *Molecular and Cellular Biology,* 1**,** 512-521.

Hoffbrand, A. V. & Moss, P. A. 2011. *Essential haematology*, John Wiley & Sons.

Huang, C., Luo, Y., Zhao, J., Yang, F., Zhao, H., Fan, W. & Ge, P. 2013. Shikonin kills glioma cells through necroptosis mediated by RIP-1. *PLoS One,* 8**,** e66326.

Hussain, M., Stutchbury, B., Tian, K., Atalay, R., Schwartz, J. & Krstic-Demonacos, M. 2014. Applications of p53 interactome analysis to personalised drug discovery. *Conference: International Work-Conference on Bioinformatics and Biomedical Engineering (IWBBIO 2014).* Universidad de Granada, Granada, Spain.

Hussain, M., Tian, K., Mutti, L., Krstic-Demonacos, M. & Schwartz, J.-M. 2015. The Expanded p53 Interactome as a Predictive Model for Cancer Therapy. *2015,* 1.

Imbalzano, A. N., Zaret, K. S. & Kingston, R. E. 1994. Transcription factor (TF) IIB and TFIIA can independently increase the affinity of the TATA-binding protein for DNA. *J Biol Chem,* 269**,** 8280-6.

Inaba, H. & Pui, C. H. 2010. Glucocorticoid use in acute lymphoblastic leukemia: comparison of prednisone and dexamethasone. *Lancet Oncol,* 11**,** 1096-106.

Isik, Z., Ersahin, T., Atalay, V., Aykanat, C. & Cetin-Atalay, R. 2012. A signal transduction score flow algorithm for cyclic cellular pathway analysis, which combines transcriptome and ChIP-seq data. *Mol Biosyst,* 8**,** 3224-31.

Itoh, M., Adachi, M., Yasui, H., Takekawa, M., Tanaka, H. & Imai, K. 2002. Nuclear export of glucocorticoid receptor is enhanced by c-Jun N-terminal kinase-mediated phosphorylation. *Mol Endocrinol,* 16**,** 2382-92.

Jabara, H. H., Brodeur, S. R. & Geha, R. S. 2001. Glucocorticoids upregulate CD40 ligand expression and induce CD40L-dependent immunoglobulin isotype switching. *J Clin Invest,* 107**,** 371-8.

Japiassu, A. M., Salluh, J. I., Bozza, P. T., Bozza, F. A. & Castro-Faria-Neto, H. C. 2009. Revisiting steroid treatment for septic shock: molecular actions and clinical effects--a review. *Mem Inst Oswaldo Cruz,* 104**,** 531-48.

Jee, Y. K., Gilmour, J., Kelly, A., Bowen, H., Richards, D., Soh, C., Smith, P., Hawrylowicz, C., Cousins, D., Lee, T. & Lavender, P. 2005. Repression of interleukin-5 transcription by the glucocorticoid receptor targets GATA3 signaling and involves histone deacetylase recruitment. *J Biol Chem,* 280**,** 23243-50.

Jeong, H., Mason, S. P., Barabasi, A. L. & Oltvai, Z. N. 2001. Lethality and centrality in protein networks. *Nature,* 411**,** 41-2.

Jin, J. Y., Almon, R. R., DuBois, D. C. & Jusko, W. J. 2003. Modeling of corticosteroid pharmacogenomics in rat liver using gene microarrays. *J Pharmacol Exp Ther,* 307**,** 93-109.

Kadmiel, M. & Cidlowski, J. A. 2013. Glucocorticoid receptor signaling in health and disease. *Trends Pharmacol Sci,* 34**,** 518-30.

Kang, R., Zeh, H. J., Lotze, M. T. & Tang, D. 2011. The Beclin 1 network regulates autophagy and apoptosis. *Cell Death and Differentiation,* 18**,** 571-580.

Kerr, J. F. 1965. A histochemical study of hypertrophy and ischaemic injury of rat liver with special reference to changes in lysosomes. *J Pathol Bacteriol,* 90**,** 419-35.

Kerr, J. F., Wyllie, A. H. & Currie, A. R. 1972. Apoptosis: a basic biological phenomenon with wide-ranging implications in tissue kinetics. *Br J Cancer,* 26**,** 239-57.

Khan, F. M., Schmitz, U., Nikolov, S., Engelmann, D., Putzer, B. M., Wolkenhauer, O. & Vera, J. 2014. Hybrid modeling of the crosstalk between signaling and transcriptional networks using ordinary differential equations and multi-valued logic. *Biochim Biophys Acta,* 1844**,** 289-98.

Khan, S. H., Ling, J. & Kumar, R. 2011. TBP Binding-Induced Folding of the Glucocorticoid Receptor AF1 Domain Facilitates Its Interaction with Steroid Receptor Coactivator-1. *PLOS ONE,* 6**,** e21939.

Klamt, S., Saez-Rodriguez, J. & Gilles, E. 2007. Structural and functional analysis of cellular networks with CellNetAnalyzer. *BMC Systems Biology,* 1**,** 2.

Klamt, S., Saez-Rodriguez, J., Lindquist, J. A., Simeoni, L. & Gilles, E. D. 2006. A methodology for the structural and functional analysis of signaling and regulatory networks. *BMC Bioinformatics,* 7**,** 56.

Klipp, E., Liebermeister, W., Wierling, C., Kowald, A., Lehrach, H. & Herwig, R. 2009. *Systems Biology: A Textbook*, John Wiley & Sons.

Konopleva, M., Konoplev, S., Hu, W., Zaritskey, A. Y., Afanasiev, B. V. & Andreeff, M. 2002. Stromal cells prevent apoptosis of AML cells by up-regulation of anti-apoptotic proteins. *Leukemia,* 16**,** 1713-24.

Konopleva, M., Tabe, Y., Zeng, Z. & Andreeff, M. 2009. Therapeutic targeting of microenvironmental interactions in leukemia: mechanisms and approaches. *Drug Resist Updat,* 12**,** 103-13.

Krepska, E., Bonzanni, N., Feenstra, A., Fokkink, W., Kielmann, T., Bal, H. & Heringa, J. 2008. Design Issues for Qualitative Modelling of Biological Cells with Petri Nets. *In:* Fisher, J. (ed.) *Formal Methods in Systems Biology: First International Workshop, FMSB 2008, Cambridge, UK, June 4-5, 2008. Proceedings.* Berlin, Heidelberg: Springer Berlin Heidelberg.

Krstic, M. D., Rogatsky, I., Yamamoto, K. R. & Garabedian, M. J. 1997. Mitogen-activated and cyclin-dependent protein kinases selectively and differentially modulate transcriptional enhancement by the glucocorticoid receptor. *Mol Cell Biol,* 17**,** 3947-54.

Kumar, R. & Thompson, E. B. 2005. Gene regulation by the glucocorticoid receptor: structure:function relationship. *J Steroid Biochem Mol Biol,* 94**,** 383-94.

Kurtova, A. V., Balakrishnan, K., Chen, R., Ding, W., Schnabl, S., Quiroga, M. P., Sivina, M., Wierda, W. G., Estrov, Z., Keating, M. J., Shehata, M., Jäger, U., Gandhi, V., Kay, N. E., Plunkett, W. & Burger, J. A. 2009. Diverse marrow stromal cells protect CLL cells from spontaneous and drug-induced apoptosis: development of a reliable and

reproducible system to assess stromal cell adhesion-mediated drug resistance. *Blood,* 114**,** 4441-50.

Laane, E., Tamm, K. P., Buentke, E., Ito, K., Kharaziha, P., Oscarsson, J., Corcoran, M., Bjorklund, A. C., Hultenby, K., Lundin, J., Heyman, M., Soderhall, S., Mazur, J., Porwit, A., Pandolfi, P. P., Zhivotovsky, B., Panaretakis, T. & Grander, D. 2009. Cell death induced by dexamethasone in lymphoid leukemia is mediated through initiation of autophagy. *Cell Death Differ,* 16**,** 1018-29.

Lawen, A. 2003. Apoptosis-an introduction. *Bioessays,* 25**,** 888-96.

Le, P. P., Friedman, J. R., Schug, J., Brestelli, J. E., Parker, J. B., Bochkis, I. M. & Kaestner, K. H. 2005. Glucocorticoid receptor-dependent gene regulatory networks. *PLoS Genet,* 1**,** e16.

Liberman, A. C., Antunica-Noguerol, M., Ferraz-de-Paula, V., Palermo-Neto, J., Castro, C. N., Druker, J., Holsboer, F., Perone, M. J., Gerlo, S., De Bosscher, K., Haegeman, G. & Arzt, E. 2012. Compound A, a dissociated glucocorticoid receptor modulator, inhibits T-bet (Th1) and induces GATA-3 (Th2) activity in immune cells. *PLoS One,* 7**,** e35155.

Lillacci, G. & Khammash, M. 2010. Parameter Estimation and Model Selection in Computational Biology. *PLoS Comput Biol,* 6.

Liu, J., Masurekar, A., Holland, M., Johnson, S., Krishnan, S., Alexander, S., Parker, C., Dempsey, C. & Saha, V. 2012. Abstract 1506: Bone marrow microenvironment mediated redox adaptation confers drug resistance in acute lymphoblastic leukemia. *Cancer Research,* 72**,** 1506-1506.

Liu, J., Masurekar, A., Johnson, S., Chakraborty, S., Griffiths, J., Smith, D., Alexander, S., Dempsey, C., Parker, C., Harrison, S., Li, Y., Miller, C., Di, Y., Ghosh, Z., Krishnan, S. & Saha, V. 2015. Stromal cell-mediated mitochondrial redox adaptation regulates drug resistance in childhood acute lymphoblastic leukemia. *Oncotarget,* 6**,** 43048-64.

Liu, Y., Gu, Q., Hou, J. P., Han, J. & Ma, J. 2014. A network-assisted co-clustering algorithm to discover cancer subtypes based on gene expression. *BMC Bioinformatics,* 15**,** 37.

Loder, S., Fakler, M., Schoeneberger, H., Cristofanon, S., Leibacher, J., Vanlangenakker, N., Bertrand, M. J., Vandenabeele, P., Jeremias, I., Debatin, K. M. & Fulda, S. 2012. RIP1 is required for IAP inhibitor-mediated sensitization of childhood acute leukemia cells to chemotherapy-induced apoptosis. *Leukemia,* 26**,** 1020-9.

Lu, N. Z. & Cidlowski, J. A. 2005. Translational regulatory mechanisms generate N-terminal glucocorticoid receptor isoforms with unique transcriptional target genes. *Mol Cell,* 18**,** 331-42.

Lu, T.-S., Yiao, S.-Y., Lim, K., Jensen, R. V. & Hsiao, L.-L. 2010. Interpretation of biological and mechanical variations between the Lowry versus Bradford method for protein quantification. *North American Journal of Medical Sciences,* 2**,** 325-328.

Lukic, I., Mitic, M., Soldatovic, I., Jovicic, M., Maric, N., Radulovic, J. & Adzic, M. 2015. Accumulation of Cytoplasmic Glucocorticoid Receptor Is Related to Elevation of FKBP5 in Lymphocytes of Depressed Patients. *Journal of molecular neuroscience : MN,* 55**,** 951-958.

Lynch, J. T., Rajendran, R., Xenaki, G., Berrou, I., Demonacos, C. & Krstic-Demonacos, M. 2010. The role of glucocorticoid receptor phosphorylation in Mcl-1 and NOXA gene expression. *Mol Cancer,* 9**,** 38.

Macmillan. 2016. Acute lymphoblastic leukaemia (ALL) in children [Online]. Available: http://www.macmillan.org.uk/cancerinformation/cancertypes/childrenscancers/typesofchildrenscancers/acutelymphoblasticleukaemia.aspx [Accessed 14 January 2017].

Mangelsdorf, D. J., Thummel, C., Beato, M., Herrlich, P., Schutz, G., Umesono, K., Blumberg, B., Kastner, P., Mark, M., Chambon, P. & Evans, R. M. 1995. The nuclear receptor superfamily: the second decade. *Cell,* 83**,** 835-9.

Margileth, D. A., Poplack, D. G., Pizzo, P. A. & Leventhal, B. G. 1977. Blindness during remission in two patients with acute lymphoblastic leukemia: a possible complication of multimodality therapy. *Cancer, 39***,** 58-61.

Medh, R. D., Saeed, M. F., Johnson, B. H. & Thompson, E. B. 1998. Resistance of Human Leukemic CEM-C1 Cells Is Overcome by Synergism between Glucocorticoid and Protein Kinase A Pathways: Correlation with c-Myc Suppression. *Cancer Research, 58***,** 3684-3693.

Medh, R. D., Webb, M. S., Miller, A. L., Johnson, B. H., Fofanov, Y., Li, T., Wood, T. G., Luxon, B. A. & Thompson, E. B. 2003. Gene expression profile of human lymphoid CEM cells sensitive and resistant to glucocorticoid-evoked apoptosis. *Genomics, 81***,** 543-555.

Miller, A., Garza, A., Johnson, B. & Thompson, E. B. 2007. Pathway interactions between MAPKs, mTOR, PKA, and the glucocorticoid receptor in lymphoid cells. *Cancer Cell International, 7***,** 3.

Miyashita, T., Nagao, K., Krajewski, S., Salvesen, G. S., Reed, J. C., Inoue, T. & Yamada, M. 1998. Investigation of glucocorticoid-induced apoptotic pathway: processing of caspase-6 but not caspase-3. *Cell Death Differ, 5***,** 1034-41.

Mizushima, N. 2007. Autophagy: process and function. *Genes Dev, 21***,** 2861-73.

Moalli, P. A., Pillay, S., Krett, N. L. & Rosen, S. T. 1993. Alternatively spliced glucocorticoid receptor messenger RNAs in glucocorticoid-resistant human multiple myeloma cells. *Cancer Res, 53***,** 3877-9.

Mokra, D. & Mokry, J. 2011. Glucocorticoids in the treatment of neonatal meconium aspiration syndrome. *Eur J Pediatr, 170***,** 1495-505.

Morrison, S. J. & Spradling, A. C. 2008. Stem cells and niches: mechanisms that promote stem cell maintenance throughout life. *Cell, 132***,** 598-611.

NCI. 2016a. Childhood Acute Lymphoblastic Leukemia Treatment (PDQ®)–Health Professional Version [Online]. Available:

https://www.cancer.gov/types/leukemia/hp/child-all-treatment-pdq#section/all
[Accessed 14 January 2017].

NCI. 2016b. Childhood Acute Lymphoblastic Leukemia Treatment (PDQ®)–Patient Version [Online]. Available: https://www.cancer.gov/types/leukemia/patient/child-all-treatment-pdq#section/all [Accessed 14 January 2017].

Nefedova, Y., Landowski, T. H. & Dalton, W. S. 2003. Bone marrow stromal-derived soluble factors and direct cell contact contribute to de novo drug resistance of myeloma cells by distinct mechanisms. *Leukemia,* 17**,** 1175-82.

NHS. 2016. Acute lymphoblastic leukaemia [Online]. Available: http://www.nhs.uk/Conditions/Leukaemia-acute-lymphoblastic/Pages/Introduction.aspx#symptoms [Accessed 04 April 2017].

Nicolaides, N. C., Galata, Z., Kino, T., Chrousos, G. P. & Charmandari, E. 2010. The human glucocorticoid receptor: molecular basis of biologic function. *Steroids,* 75**,** 1-12.

NIH. 2010. NIH WORKING DEFINITION OF BIOINFORMATICS AND COMPUTATIONAL BIOLOGY [Online]. Available: http://www.bisti.nih.gov/docs/compubiodef.pdf [Accessed 29 April 2014].

Norman, M. R. & Thompson, E. B. 1977. Characterization of a Glucocorticoid-sensitive Human Lymphoid Cell Line. *Cancer Research,* 37**,** 3785-3791.

O'Connor, T. M., O'Halloran, D. J. & Shanahan, F. 2000. The stress response and the hypothalamic-pituitary-adrenal axis: from molecule to melancholia. *Qjm,* 93**,** 323-33.

Oakley, R. H. & Cidlowski, J. A. 2011. Cellular processing of the glucocorticoid receptor gene and protein: new mechanisms for generating tissue-specific actions of glucocorticoids. *J Biol Chem,* 286**,** 3177-84.

Oakley, R. H., Jewell, C. M., Yudt, M. R., Bofetiado, D. M. & Cidlowski, J. A. 1999. The dominant negative activity of the human glucocorticoid receptor beta isoform. Specificity and mechanisms of action. *J Biol Chem,* 274**,** 27857-66.

Oberst, A. 2016. Death in the fast lane: What's next for necroptosis? *The FEBS journal,* 283**,** 2616-2625.

Pinkerton, C. R., Bowman, A., Holtzel, H. & Chessells, J. M. 1987. Intensive consolidation chemotherapy for acute lymphoblastic leukaemia (UKALL X pilot study). *Arch Dis Child,* 62**,** 12-8.

Piovan, E., Yu, J., Tosello, V., Herranz, D., Ambesi-Impiombato, A., Da Silva, A. C., Sanchez-Martin, M., Perez-Garcia, A., Rigo, I., Castillo, M., Indraccolo, S., Cross, J. R., de Stanchina, E., Paietta, E., Racevskis, J., Rowe, J. M., Tallman, M. S., Basso, G., Meijerink, J. P., Cordon-Cardo, C., Califano, A. & Ferrando, A. A. 2013. Direct reversal of glucocorticoid resistance by AKT inhibition in acute lymphoblastic leukemia. *Cancer Cell,* 24**,** 766-76.

Ploner, C., Rainer, J., Niederegger, H., Eduardoff, M., Villunger, A., Geley, S. & Kofler, R. 2008. The BCL2 rheostat in glucocorticoid-induced apoptosis of acute lymphoblastic leukemia. *Leukemia,* 22**,** 370-377.

Presman, D. M., Ogara, M. F., Stortz, M., Alvarez, L. D., Pooley, J. R., Schiltz, R. L., Grontved, L., Johnson, T. A., Mittelstadt, P. R., Ashwell, J. D., Ganesan, S., Burton, G., Levi, V., Hager, G. L. & Pecci, A. 2014. Live cell imaging unveils multiple domain requirements for in vivo dimerization of the glucocorticoid receptor. *PLoS Biol,* 12**,** e1001813.

Promega. 2012. TECHNICAL BULLETIN CellTiter 96® AQueous One Solution Cell Proliferation Assay Instructions for Use of Products G3580, G3581 and G3582 [Online]. Available: http://www.promega.co.uk/~/media/Files/Resources/Protocols/Technical%20Bulletins/0/CellTiter%2096%20AQueous%20One%20Solution%20Cell%20Proliferation%20Assay%20System%20Protocol.pdf [Accessed 06 February 2017].

Pui, C. H., Behm, F. G., Singh, B., Schell, M. J., Williams, D. L., Rivera, G. K., Kalwinsky, D. K., Sandlund, J. T., Crist, W. M. & Raimondi, S. C. 1990. Heterogeneity of presenting features and their relation to treatment outcome in 120 children with T-cell acute lymphoblastic leukemia. *Blood,* 75**,** 174-9.

Qattan, M. 2014. *The role of inducible transcription factors and microenvironment in leukemia.* PhD, The University of Manchester.

Qattan, M. Y., Bakker, E. Y., Rajendran, R., Chen, D. W., Saha, V., Liu, J., Zeef, L., Schwartz, J. M., Mutti, L., Demonacos, C. & Krstic-Demonacos, M. 2017. Differential regulation of cell death pathways by the microenvironment correlates with chemoresistance and survival in leukaemia. *PLoS One,* 12**,** e0178606.

QIAGEN. 2013. RNeasy Plus Mini Handbook [Online]. Available: https://www.qiagen.com/gb/resources/resourcedetail?id=c8cdc6bf-5bbf-4e3b-a0f4-476da9215012&lang=en [Accessed 07 February 2017].

Quax, R. A., Manenschijn, L., Koper, J. W., Hazes, J. M., Lamberts, S. W. J., van Rossum, E. F. C. & Feelders, R. A. 2013. Glucocorticoid sensitivity in health and disease. *Nat Rev Endocrinol,* 9**,** 670-686.

Rajendran, R., Garva, R., Ashour, H., Leung, T., Stratford, I., Krstic-Demonacos, M. & Demonacos, C. 2013. Acetylation mediated by the p300/CBP-associated factor determines cellular energy metabolic pathways in cancer. *Int J Oncol,* 42**,** 1961-72.

Ramamoorthy, S. & Cidlowski, J. A. 2013. Ligand-induced repression of the glucocorticoid receptor gene is mediated by an NCoR1 repression complex formed by long-range chromatin interactions with intragenic glucocorticoid response elements. *Mol Cell Biol,* 33**,** 1711-22.

Rathmell, J. C., Lindsten, T., Zong, W. X., Cinalli, R. M. & Thompson, C. B. 2002. Deficiency in Bak and Bax perturbs thymic selection and lymphoid homeostasis. *Nat Immunol,* 3**,** 932-9.

Rochette-Egly, C. 2003. Nuclear receptors: integration of multiple signalling pathways through phosphorylation. *Cell Signal,* 15**,** 355-66.

Ross, K. E., Arighi, C. N., Ren, J., Huang, H. & Wu, C. H. 2013. Construction of protein phosphorylation networks by data mining, text mining and ontology integration: analysis of the spindle checkpoint. *Database (Oxford),* 2013**,** bat038.

Saadatpour, A. & Albert, R. 2012. Discrete dynamic modeling of signal transduction networks. *Methods Mol Biol,* 880**,** 255-72.

SABiosciences. 2012. EpiTect ChIP qPCR Primers [Online]. Available: http://www.sabiosciences.com/chipqpcrsearch.php?gene=RIPK1&factor=Over+200+TF&species_id=0&ninfo=n&ngene=n&nfactor=y [Accessed 26 August 2017].

Savory, J. G., Prefontaine, G. G., Lamprecht, C., Liao, M., Walther, R. F., Lefebvre, Y. A. & Hache, R. J. 2001. Glucocorticoid receptor homodimers and glucocorticoid-mineralocorticoid receptor heterodimers form in the cytoplasm through alternative dimerization interfaces. *Mol Cell Biol,* 21**,** 781-93.

Schaaf, M. J. & Cidlowski, J. A. 2002. Molecular mechanisms of glucocorticoid action and resistance. *J Steroid Biochem Mol Biol,* 83**,** 37-48.

Schenk, B. & Fulda, S. 2015. Reactive oxygen species regulate Smac mimetic/TNFalpha-induced necroptotic signaling and cell death. *Oncogene,* 34**,** 5796-806.

Schlossmacher, G., Stevens, A. & White, A. 2011. Glucocorticoid receptor-mediated apoptosis: mechanisms of resistance in cancer cells. *J Endocrinol,* 211**,** 17-25.

Schmidt, S., Rainer, J., Ploner, C., Presul, E., Riml, S. & Kofler, R. 2004. Glucocorticoid-induced apoptosis and glucocorticoid resistance: molecular mechanisms and clinical relevance. *Cell Death Differ,* 11 Suppl 1**,** S45-55.

Schmidt, S., Rainer, J., Riml, S., Ploner, C., Jesacher, S., Achmüller, C., Presul, E., Skvortsov, S., Crazzolara, R., Fiegl, M., Raivio, T., Jänne, O. A., Geley, S., Meister, B. & Kofler, R. 2006. Identification of glucocorticoid-response genes in children with acute lymphoblastic leukemia. *Blood,* 107**,** 2061.

Schoneveld, O. J., Gaemers, I. C. & Lamers, W. H. 2004. Mechanisms of glucocorticoid signalling. *Biochim Biophys Acta,* 1680**,** 114-28.

Scott, D. K., Stromstedt, P. E., Wang, J. C. & Granner, D. K. 1998. Further characterization of the glucocorticoid response unit in the phosphoenolpyruvate

carboxykinase gene. The role of the glucocorticoid receptor-binding sites. *Mol Endocrinol,* 12**,** 482-91.

Sedwick, C. 2014. Wanted: A New Model for Glucocorticoid Receptor Transactivation and Transrepression. *PLoS Biol,* 12.

Segard-Maurel, I., Rajkowski, K., Jibard, N., Schweizer-Groyer, G., Baulieu, E.-E. & Cadepond, F. 1996. Glucocorticosteroid Receptor Dimerization Investigated by Analysis of Receptor Binding to Glucocorticosteroid Responsive Elements Using a Monomer−Dimer Equilibrium Model. *Biochemistry,* 35**,** 1634-1642.

Sengupta, S., Vonesch, J. L., Waltzinger, C., Zheng, H. & Wasylyk, B. 2000. Negative cross-talk between p53 and the glucocorticoid receptor and its role in neuroblastoma cells. *Embo j,* 19**,** 6051-64.

Sever, R. & Glass, C. K. 2013. Signaling by Nuclear Receptors. *Cold Spring Harbor Perspectives in Biology,* 5**,** a016709.

Shandilya, J. & Roberts, S. G. 2012. The transcription cycle in eukaryotes: from productive initiation to RNA polymerase II recycling. *Biochim Biophys Acta,* 1819**,** 391-400.

Shannon, P., Markiel, A., Ozier, O., Baliga, N. S., Wang, J. T., Ramage, D., Amin, N., Schwikowski, B. & Ideker, T. 2003. Cytoscape: a software environment for integrated models of biomolecular interaction networks. *Genome Res,* 13**,** 2498-504.

Simic, I., Maric, N. P., Mitic, M., Soldatovic, I., Pavlovic, Z., Mihaljevic, M., Andric, S., Radojcic, M. B. & Adzic, M. 2013. Phosphorylation of leukocyte glucocorticoid receptor in patients with current episode of major depressive disorder. *Prog Neuropsychopharmacol Biol Psychiatry,* 40**,** 281-5.

Sison, E. A., Rau, R. E., McIntyre, E., Li, L., Small, D. & Brown, P. 2013. MLL-rearranged acute lymphoblastic leukaemia stem cell interactions with bone marrow stroma promote survival and therapeutic resistance that can be overcome with CXCR4 antagonism. *Br J Haematol,* 160**,** 785-97.

Snel, B., Lehmann, G., Bork, P. & Huynen, M. A. 2000. STRING: a web-server to retrieve and display the repeatedly occurring neighbourhood of a gene. *Nucleic Acids Research,* 28**,** 3442-3444.

Spierings, D., McStay, G., Saleh, M., Bender, C., Chipuk, J., Maurer, U. & Green, D. R. 2005. Connected to death: the (unexpurgated) mitochondrial pathway of apoptosis. *Science,* 310**,** 66-7.

Stanbury, R. & Graham, E. 1998. Systemic corticosteroid therapy—side effects and their management. *Br J Ophthalmol,* 82**,** 704-8.

Stocklin, E., Wissler, M., Gouilleux, F. & Groner, B. 1996. Functional interactions between Stat5 and the glucocorticoid receptor. *Nature,* 383**,** 726-8.

Sumiyoshi, H., Matsushita, A., Nakamura, Y., Matsuda, Y., Ishiwata, T., Naito, Z. & Uchida, E. 2016. Suppression of STAT5b in pancreatic cancer cells leads to attenuated gemcitabine chemoresistance, adhesion and invasion. *Oncol Rep,* 35**,** 3216-26.

Swensen, A. R., Ross, J. A., Severson, R. K., Pollock, B. H. & Robison, L. L. 1997. The age peak in childhood acute lymphoblastic leukemia: exploring the potential relationship with socioeconomic status. *Cancer,* 79**,** 2045-51.

Szapary, D., Huang, Y. & Simons, S. S., Jr. 1999. Opposing effects of corepressor and coactivators in determining the dose-response curve of agonists, and residual agonist activity of antagonists, for glucocorticoid receptor-regulated gene expression. *Mol Endocrinol,* 13**,** 2108-21.

Szklarczyk, D., Franceschini, A., Kuhn, M., Simonovic, M., Roth, A., Minguez, P., Doerks, T., Stark, M., Muller, J., Bork, P., Jensen, L. J. & Mering, C. v. 2011. The STRING database in 2011: functional interaction networks of proteins, globally integrated and scored. *Nucleic Acids Research,* 39**,** D561-D568.

Teurich, S. & Angel, P. 1995. The glucocorticoid receptor synergizes with Jun homodimers to activate AP-1-regulated promoters lacking GR binding sites. *Chem Senses,* 20**,** 251-5.

Teusink, B., Passarge, J., Reijenga, C. A., Esgalhado, E., van der Weijden, C. C., Schepper, M., Walsh, M. C., Bakker, B. M., van Dam, K., Westerhoff, H. V. & Snoep, J. L. 2000. Can yeast glycolysis be understood in terms of in vitro kinetics of the constituent enzymes? Testing biochemistry. *Eur J Biochem,* 267**,** 5313-29.

Tian, K. 2013. *Logical models of DNA damage induced pathways to cancer.* PhD Traditional, The University of Manchester.

Tian, K., Rajendran, R., Doddananjaiah, M., Krstic-Demonacos, M. & Schwartz, J.-M. 2013. Dynamics of DNA Damage Induced Pathways to Cancer. *PLoS ONE,* 8**,** e72303.

Tindall, M. 2012. Teaching Modelling Using Simulation Tools: Examples using Copasi and Matlab [Online]. Available: https://biomathed.files.wordpress.com/2012/07/biomaths-2012-tindall.pdf [Accessed 21 January 2017].

Tomlinson, J. W. & Stewart, P. M. 2001. Cortisol metabolism and the role of 11beta-hydroxysteroid dehydrogenase. *Best Pract Res Clin Endocrinol Metab,* 15**,** 61-78.

Trotman, L. C., Alimonti, A., Scaglioni, P. P., Koutcher, J. A., Cordon-Cardo, C. & Pandolfi, P. P. 2006. Identification of a tumour suppressor network opposing nuclear Akt function. *Nature,* 441**,** 523-7.

Vandevyver, S., Dejager, L. & Libert, C. 2012. On the trail of the glucocorticoid receptor: into the nucleus and back. *Traffic,* 13**,** 364-74.

Velders, M. P., ter Horst, S. A. & Kast, W. M. 2001. Prospect for immunotherapy of acute lymphoblastic leukemia. *Leukemia,* 15**,** 701-6.

Wang, E. 2010. A Roadmap of Cancer Systems Biology. [Online]. Available: http://precedings.nature.com/documents/4322/version/2 [Accessed 18 January 2017].

Wang, X. & DeFranco, D. B. 2005. Alternative effects of the ubiquitin-proteasome pathway on glucocorticoid receptor down-regulation and transactivation are mediated by CHIP, an E3 ligase. *Mol Endocrinol,* 19**,** 1474-82.

Watson, M. S., Carroll, A. J., Shuster, J. J., Steuber, C. P., Borowitz, M. J., Behm, F. G., Pullen, D. J. & Land, V. J. 1993. Trisomy 21 in childhood acute lymphoblastic leukemia: a Pediatric Oncology Group study (8602). *Blood,* 82**,** 3098-102.

Webster, J. C., Huber, R. M., Hanson, R. L., Collier, P. M., Haws, T. F., Mills, J. K., Burn, T. C. & Allegretto, E. A. 2002. Dexamethasone and tumor necrosis factor-alpha act together to induce the cellular inhibitor of apoptosis-2 gene and prevent apoptosis in a variety of cell types. *Endocrinology,* 143**,** 3866-74.

WHO. 2015. Cancer [Online]. World Health Organisation. Available: http://www.who.int/mediacentre/factsheets/fs297/en/ [Accessed 05 January 2017].

Wiemels, J. 2012. Perspectives on the Causes of Childhood Leukemia. *Chem Biol Interact,* 196.

Woolley, A. & Kostopoulou, O. 2013. Clinical Intuition in Family Medicine: More Than First Impressions. *The Annals of Family Medicine,* 11**,** 60-66.

Wu, W., Liu, P. & Li, J. 2012. Necroptosis: an emerging form of programmed cell death. *Crit Rev Oncol Hematol,* 82**,** 249-58.

Wyszomierski, S. L., Yeh, J. & Rosen, J. M. 1999. Glucocorticoid receptor/signal transducer and activator of transcription 5 (STAT5) interactions enhance STAT5 activation by prolonging STAT5 DNA binding and tyrosine phosphorylation. *Mol Endocrinol,* 13**,** 330-43.

Yu, L., Wan, F., Dutta, S., Welsh, S., Liu, Z., Freundt, E., Baehrecke, E. H. & Lenardo, M. 2006. Autophagic programmed cell death by selective catalase degradation. *Proc Natl Acad Sci U S A,* 103**,** 4952-7.

Zhang, J. P., Wong, C. K. & Lam, C. W. K. 2000. Role of caspases in dexamethasone-induced apoptosis and activation of c-Jun NH(2)-terminal kinase and p38 mitogen-activated protein kinase in human eosinophils. *Clinical and Experimental Immunology,* 122**,** 20-27.

Zhou, J. & Cidlowski, J. A. 2005. The human glucocorticoid receptor: one gene, multiple proteins and diverse responses. *Steroids,* 70**,** 407-17.